Part 6
Coupled Spins

14 Spin-1/2 Pairs

In all real samples, the nuclear spins interact with each other. In the previous chapters, these spin–spin interactions were either completely ignored or absorbed into phenomenological relaxation parameters, which describe the damping of the coherences or the drift of the populations towards their thermal equilibrium values.

Most samples consist of more complex molecules which contain more than one spin. In general, the spin–spin couplings cannot be ignored. In this chapter, I discuss the simplest possible situation: a large number of identical molecules, each containing only two spins-1/2. In this case, the set of nuclear spins comprises an *ensemble of spin-1/2 pairs*:

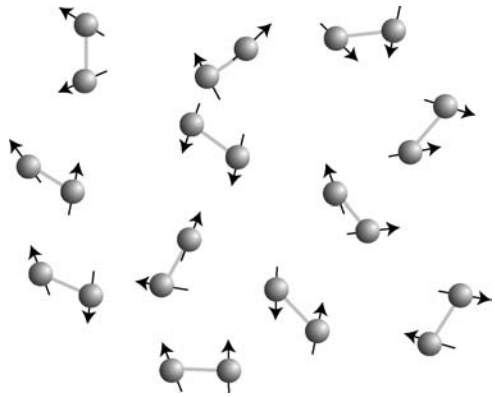

Figure 14.1
Ensemble of spin-1/2 pairs.

If the members of the pair are of the same isotopic type, then the spin system consists of a *homonuclear spin pair*. If the members of the pair are of different isotopic types, then the term *heteronuclear spin pair* is used.

I now examine the behaviour of spin-1/2 pairs in the presence of dipole–dipole couplings as well as J-couplings, allowing the treatment of spin-1/2 pairs in isotropic liquids, liquid crystals, and solids. The pairs are assumed to be *homonuclear* for most of this chapter.

14.1 Coupling Regimes

The behaviour of homonuclear spin-1/2 pairs depends strongly on the difference in chemical shifts between the spins, as compared to the spin-spin coupling.

Spin Dynamics: Basics of Nuclear Magnetic Resonance, Second Edition Malcolm H. Levitt

Weakly coupled pairs. If the *difference* in chemical shift frequencies is much larger than the spin–spin coupling, then the spin pair is said to be weakly coupled. A weakly coupled spin pair is denoted by the symbol AX (this 'alphabet notation' is discussed in more detail in Chapter 17).

Strongly coupled pairs. If the chemical shift frequency difference has roughly the same magnitude as the spin–spin coupling, then the spin system is said to be *strongly coupled*. The spin pair is denoted AB in this case.

Identical chemical shifts. If the chemical shifts of the two spins are the same,[1] then the two spins are said to be *magnetically equivalent*. The spin system in each molecule is denoted by the symbol A_2. An example is given by the protons in water.

The behaviour of strongly coupled spin systems is examined in Appendix A.8. The following discussion concentrates on the magnetically equivalent and weakly coupled cases.

14.2 Zeeman Product States and Superposition States

The pair of coupled spins-1/2 form a single quantum system. The state of the spin pair is described by a single ket, which has the following general form:

$$|\psi\rangle = c_{\alpha\alpha}|\alpha\alpha\rangle + c_{\alpha\beta}|\alpha\beta\rangle + c_{\beta\alpha}|\beta\alpha\rangle + c_{\beta\beta}|\beta\beta\rangle \tag{14.1}$$

The states $|\alpha\alpha\rangle$, $|\alpha\beta\rangle$ ... are called *Zeeman product states* of the two spin-1/2 particles. In the notation $|\alpha\beta\rangle$, the α symbol indicates that the z-angular momentum of spin I_1 has the definite value $+1/2$, and the β symbol indicates that the z-angular momentum of spin I_2 has the definite value $-1/2$. The four Zeeman product states of the spin-1/2 pair obey the following eigenequations:

$$\begin{aligned}
\hat{I}_{1z}|\alpha\alpha\rangle &= +\tfrac{1}{2}|\alpha\alpha\rangle \quad & \hat{I}_{2z}|\alpha\alpha\rangle &= +\tfrac{1}{2}|\alpha\alpha\rangle \\
\hat{I}_{1z}|\alpha\beta\rangle &= +\tfrac{1}{2}|\alpha\beta\rangle & \hat{I}_{2z}|\alpha\beta\rangle &= -\tfrac{1}{2}|\alpha\beta\rangle \\
\hat{I}_{1z}|\beta\alpha\rangle &= -\tfrac{1}{2}|\beta\alpha\rangle & \hat{I}_{2z}|\beta\alpha\rangle &= +\tfrac{1}{2}|\beta\alpha\rangle \\
\hat{I}_{1z}|\beta\beta\rangle &= -\tfrac{1}{2}|\beta\beta\rangle & \hat{I}_{2z}|\beta\beta\rangle &= -\tfrac{1}{2}|\beta\beta\rangle
\end{aligned}$$

⚠The use of the Zeeman product states $|\alpha\alpha\rangle$, $|\beta\alpha\rangle$ ... does *not* imply that the spin pair may *only* adopt such states, any more than the use of $|\alpha\rangle$ and $|\beta\rangle$ for a single spin-1/2 implies that the spin polarization may only be 'up' or 'down'. The single spin-1/2 may be, and usually is, in a superposition of the 'up' or 'down' states, and the spin-1/2 pair may be, and usually is, in a superposition of the four Zeeman product states.

Physically, the state in Equation 14.1 describes a spin pair with both polarizations pointing in some arbitrary direction:

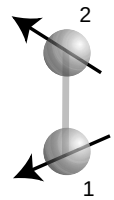

Figure 14.2
A pair of coupled spins.

The coefficients $c_{\alpha\alpha}$, $c_{\beta\alpha}$ ... are complex numbers. As usual, they must be normalized:

$$|c_{\alpha\alpha}|^2 + |c_{\alpha\beta}|^2 + |c_{\beta\alpha}|^2 + |c_{\beta\beta}|^2 = 1$$

The superposition state in Equation 14.1 is conveniently written as a column vector:

$$|\psi\rangle = \begin{pmatrix} c_{\alpha\alpha} \\ c_{\alpha\beta} \\ c_{\beta\alpha} \\ c_{\beta\beta} \end{pmatrix}$$

The normalization condition may then be written as

$$\langle\psi|\psi\rangle = \begin{pmatrix} c_{\alpha\alpha}{}^*, & c_{\alpha\beta}{}^*, & c_{\beta\alpha}{}^*, & c_{\beta\beta}{}^* \end{pmatrix} \cdot \begin{pmatrix} c_{\alpha\alpha} \\ c_{\alpha\beta} \\ c_{\beta\alpha} \\ c_{\beta\beta} \end{pmatrix} = 1$$

Once again, note the use of the complex conjugate when transforming the 'ket' column vector to the 'bra' row vector.

14.3 Spin-Pair Hamiltonian

The behaviour of an individual spin pair is treated by constructing the Hamiltonian and solving the Schrödinger equation.

Start with the most general case. Each of the spins I_1 and I_2 has a different chemical shift δ_1 and δ_2, leading to chemically shifted Larmor frequencies given by

$$\begin{aligned} \omega_1^0 &= -\gamma B^0(1+\delta_1) \\ \omega_2^0 &= -\gamma B^0(1+\delta_2) \end{aligned} \tag{14.2}$$

The spins have a mutual J-coupling J_{12}, and also a secular dipole–dipole coupling d_{12}, as described in Sections 9.3 and 9.4.

The secular spin Hamiltonian is equal to

$$\widehat{\mathcal{H}}^0 = \omega_1^0 \hat{I}_{1z} + \omega_2^0 \hat{I}_{2z} + 2\pi J_{12} \hat{\mathbf{I}}_1 \cdot \hat{\mathbf{I}}_2 + d_{12}(3\hat{I}_{1z}\hat{I}_{2z} - \hat{\mathbf{I}}_1 \cdot \hat{\mathbf{I}}_2) \tag{14.3}$$

Our first task is to form the matrix representation of this Hamiltonian in the basis of Zeeman product states $\{|\alpha\alpha\rangle, |\alpha\beta\rangle, |\beta\alpha\rangle, |\beta\beta\rangle\}$. To do this, first expand the scalar product $\hat{\mathbf{I}}_1 \cdot \hat{\mathbf{I}}_2$ into the explicit angular momentum operators:

$$\hat{\mathbf{I}}_1 \cdot \hat{\mathbf{I}}_2 = \hat{I}_{1x}\hat{I}_{2x} + \hat{I}_{1y}\hat{I}_{2y} + \hat{I}_{1z}\hat{I}_{2z}$$

The products of the x- and y-operators may be expanded into shift operators (see Section 7.8.5), as follows:

$$\hat{I}_{1x}\hat{I}_{2x} + \hat{I}_{1y}\hat{I}_{2y} = \frac{1}{2}\left(\hat{I}_1^+\hat{I}_2^- + \hat{I}_1^-\hat{I}_2^+\right)$$

The spin Hamiltonian in Equation 14.3 may be split into two terms:

$$\widehat{\mathcal{H}}^0 = \widehat{\mathcal{H}}^0_{\mathrm{A}} + \widehat{\mathcal{H}}^0_{\mathrm{B}} \tag{14.4}$$

where the two parts are

$$\begin{aligned} \widehat{\mathcal{H}}^0_{\mathrm{A}} &= \omega^0_1 \hat{I}_{1z} + \omega^0_2 \hat{I}_{2z} + \omega^{\mathrm{A}}_{12} 2\hat{I}_{1z}\hat{I}_{2z} \\ \widehat{\mathcal{H}}^0_{\mathrm{B}} &= \omega^{\mathrm{B}}_{12} \frac{1}{2}\left(\hat{I}^+_1 \hat{I}^+_2 + \hat{I}^-_1 \hat{I}^-_2\right) \end{aligned} \tag{14.5}$$

The spin–spin coupling terms are defined as follows:

$$\begin{aligned} \omega^{\mathrm{A}}_{12} &= \pi J_{12} + d_{12} \\ \omega^{\mathrm{B}}_{12} &= 2\pi J_{12} - d_{12} \end{aligned} \tag{14.6}$$

The term $\widehat{\mathcal{H}}^0_{\mathrm{A}}$ is called the *diagonal part* of the spin Hamiltonian. The term $\widehat{\mathcal{H}}^0_{\mathrm{B}}$ is called the *off-diagonal part* of the spin Hamiltonian, or sometimes the *flip-flop term*. Equation 14.6 shows that the J-coupling and the dipole–dipole coupling contribute to both terms, but with different pre-factors and different signs.

The matrix representations of the two parts of the Hamiltonian in the Zeeman product basis $\{|\alpha\alpha\rangle, |\alpha\beta\rangle, |\beta\alpha\rangle, |\beta\beta\rangle\}$ are given by

$$\widehat{\mathcal{H}}^0_{\mathrm{A}} = \frac{1}{2}\begin{pmatrix} \omega^0_1 + \omega^0_2 + \omega^{\mathrm{A}}_{12} & 0 & 0 & 0 \\ 0 & \omega^0_1 - \omega^0_2 - \omega^{\mathrm{A}}_{12} & 0 & 0 \\ 0 & 0 & -\omega^0_1 + \omega^0_2 - \omega^{\mathrm{A}}_{12} & 0 \\ 0 & 0 & 0 & -\omega^0_1 - \omega^0_2 + \omega^{\mathrm{A}}_{12} \end{pmatrix} \tag{14.7}$$

and

$$\widehat{\mathcal{H}}^0_{\mathrm{B}} = \frac{1}{2}\begin{pmatrix} 0 & 0 & 0 & 0 \\ 0 & 0 & \omega^{\mathrm{B}}_{12} & 0 \\ 0 & \omega^{\mathrm{B}}_{12} & 0 & 0 \\ 0 & 0 & 0 & 0 \end{pmatrix} \tag{14.8}$$

For example, the element in the second row and third column of the matrix representation of $\widehat{\mathcal{H}}^0_{\mathrm{B}}$ may be calculated as follows:

$$\begin{aligned} \langle\alpha\beta|\widehat{\mathcal{H}}^0_{\mathrm{B}}|\beta\alpha\rangle &= \frac{1}{2}\omega^{\mathrm{B}}_{12} \langle\alpha\beta|\left(\hat{I}^+_1\hat{I}^-_2 + \hat{I}^-_1\hat{I}^+_2\right)|\beta\alpha\rangle \\ &= \frac{1}{2}\omega^{\mathrm{B}}_{12}\left(\langle\alpha\beta|\hat{I}^+_1\hat{I}^-_2|\beta\alpha\rangle + \langle\alpha\beta|\hat{I}^-_1\hat{I}^+_2|\beta\alpha\rangle\right) \\ &= \frac{1}{2}\omega^{\mathrm{B}}_{12}\left(\langle\alpha\beta|\alpha\beta\rangle + 0\right) \\ &= \frac{1}{2}\omega^{\mathrm{B}}_{12} \end{aligned}$$

I now consider the cases of magnetic equivalence and weak coupling separately.

14.4 Pairs of Magnetically Equivalent Spins

14.4.1 Singlets and triplets

If the two chemical shifts are the same $\omega_1^0 = \omega_2^0 = \omega^0$, the spins are magnetically equivalent. The matrix representation of the spin Hamiltonian is given by

$$\widehat{\mathcal{H}}^0 = \frac{1}{2}\begin{pmatrix} 2\omega^0 + \omega_{12}^{\mathrm{A}} & 0 & 0 & 0 \\ 0 & -\omega_{12}^{\mathrm{A}} & \omega_{12}^{\mathrm{B}} & 0 \\ 0 & \omega_{12}^{\mathrm{B}} & -\omega_{12}^{\mathrm{A}} & 0 \\ 0 & 0 & 0 & -2\omega^0 + \omega_{12}^{\mathrm{A}} \end{pmatrix} \quad \text{(in the Zeeman product basis)} \tag{14.9}$$

This matrix is not diagonal, which indicates that the Zeeman product states $\{|\alpha\alpha\rangle, |\alpha\beta\rangle, |\beta\alpha\rangle, |\beta\beta\rangle\}$ are not all eigenstates of the Hamiltonian.

The Hamiltonian matrix may be *diagonalized* by choosing a different set of four basis states, called the *singlet–triplet basis*. Choose three *triplet states*, defined as follows:

$$\begin{aligned} |T_{+1}\rangle &= |\alpha\alpha\rangle \\ |T_0\rangle &= \frac{1}{\sqrt{2}}\left(|\alpha\beta\rangle + |\beta\alpha\rangle\right) \\ |T_{-1}\rangle &= |\beta\beta\rangle \end{aligned} \tag{14.10}$$

and one *singlet state*, defined as follows:

$$|S_0\rangle = \frac{1}{\sqrt{2}}\left(|\alpha\beta\rangle - |\beta\alpha\rangle\right) \tag{14.11}$$

The triplet states $|T_{+1}\rangle$ and $|T_{-1}\rangle$ are the same as the Zeeman product states $|\alpha\alpha\rangle$ and $|\beta\beta\rangle$ respectively. The states $|T_0\rangle$ and $|S_0\rangle$ are normalized superpositions of the states $|\alpha\beta\rangle$ and $|\beta\alpha\rangle$, but with opposite signs.

The matrix elements of the Hamiltonian in the singlet–triplet basis may be derived according to the following example:

$$\begin{aligned} \langle S_0|\widehat{\mathcal{H}}^0|T_0\rangle &= \frac{1}{2}\left(\langle\alpha\beta| - \langle\beta\alpha|\right)\widehat{\mathcal{H}}^0\left(|\alpha\beta\rangle + |\beta\alpha\rangle\right) \\ &= \frac{1}{2}\left(\langle\alpha\beta|\widehat{\mathcal{H}}^0|\alpha\beta\rangle - \langle\beta\alpha|\widehat{\mathcal{H}}^0|\alpha\beta\rangle + \langle\alpha\beta|\widehat{\mathcal{H}}^0|\beta\alpha\rangle - \langle\beta\alpha|\widehat{\mathcal{H}}^0|\beta\alpha\rangle\right) \\ &= \frac{1}{4}\left(-\omega_{12}^{\mathrm{A}} - \omega_{12}^{\mathrm{B}} + \omega_{12}^{\mathrm{B}} - (-\omega_{12}^{\mathrm{A}})\right) = 0 \end{aligned}$$

Repetition for all elements generates the following matrix representation in the singlet–triplet basis:

$$\widehat{\mathcal{H}}^0 = \frac{1}{2}\begin{pmatrix} \omega^0 + \frac{1}{2}\pi J_{12} + \frac{1}{2}d_{12} & 0 & 0 & 0 \\ 0 & -d_{12} + \frac{1}{2}\pi J_{12} & 0 & 0 \\ 0 & 0 & -\omega^0 + \frac{1}{2}\pi J_{12} + \frac{1}{2}d_{12} & 0 \\ 0 & 0 & 0 & -\frac{3}{2}\pi J_{12} \end{pmatrix}$$

(in the singlet–triplet basis) (14.12)

Since this matrix is diagonal, the singlet–triplet basis states $\{|T_{+1}\rangle, |T_0\rangle, |T_{-1}\rangle, |S_0\rangle\}$ are the energy eigenstates of the magnetically equivalent spin pair.

The three triplet states of the spin-1/2 pair behave in a similar way to the three states of a *single* nuclear spin with $I = 1$. The analogy may be emphasized by constructing *total* angular momentum operators by adding together the angular momentum operators of the two spins:

$$\begin{aligned} \hat{I}_x &= \hat{I}_{1x} + \hat{I}_{2x} \\ \hat{I}_y &= \hat{I}_{1y} + \hat{I}_{2y} \\ \hat{I}_z &= \hat{I}_{1z} + \hat{I}_{2z} \end{aligned} \tag{14.13}$$

The *total square angular momentum* operator may be constructed as follows:

$$\hat{I}^2 = \hat{I}_x^2 + \hat{I}_y^2 + \hat{I}_z^2 \tag{14.14}$$

The three triplet states obey the following eigenequations:

$$\begin{aligned} \hat{I}_z|T_M\rangle &= M|T_M\rangle \\ \hat{I}^2|T_M\rangle &= 2|T_M\rangle \end{aligned} \tag{14.15}$$

where M is equal to $+1$, 0, or -1. Equation 14.15 is exactly the same as the eigenequations for the three states $|1, M\rangle$ of a spin-1 nucleus (see Equation 13.1).

Similarly, the singlet state $|S_0\rangle$ behaves in the same way as the state of a spin $I = 0$ nucleus:

$$\begin{aligned} \hat{I}_z|S_0\rangle &= 0 \\ \hat{I}^2|S_0\rangle &= 0 \end{aligned} \tag{14.16}$$

The magnetically equivalent pairs of spins-1/2 behave like a set of independent spin-0 and spin-1 nuclei.[2]

14.4.2 Energy levels

The energy levels are equal to the diagonal elements of Equation 14.12. The corresponding eigenequations are as follows:

$$\begin{aligned} \widehat{\mathcal{H}}^0|T_{+1}\rangle &= (\omega^0 + \frac{1}{2}\pi J_{12} + \frac{1}{2}d_{12})\,|T_{+1}\rangle \\ \widehat{\mathcal{H}}^0|T_0\rangle &= (\frac{1}{2}\pi J_{12} - d_{12})\,|T_0\rangle \\ \widehat{\mathcal{H}}^0|T_{-1}\rangle &= (-\omega^0 + \frac{1}{2}\pi J_{12} + \frac{1}{2}d_{12})\,|T_{-1}\rangle \\ \widehat{\mathcal{H}}^0|S_0\rangle &= (-\frac{3}{2}\pi J_{12})\,|S_0\rangle \end{aligned}$$

The energy contributions of the different terms are sketched in Figure 14.3. The Zeeman interaction of one spin with the magnetic field creates a splitting ω^0. Each level is split again by the Zeeman interaction of the second spin with the field. This leads to a three-level structure, with the central level being doubly degenerate. The J-coupling breaks the degeneracy by shifting three levels in one direction, with one of the central levels being shifted by three times as much in the opposite direction. Finally, the dipole–dipole

coupling shifts two of the levels up and one level down. Note that the energy of the singlet state (shown in grey) is not affected by the dipole–dipole coupling.

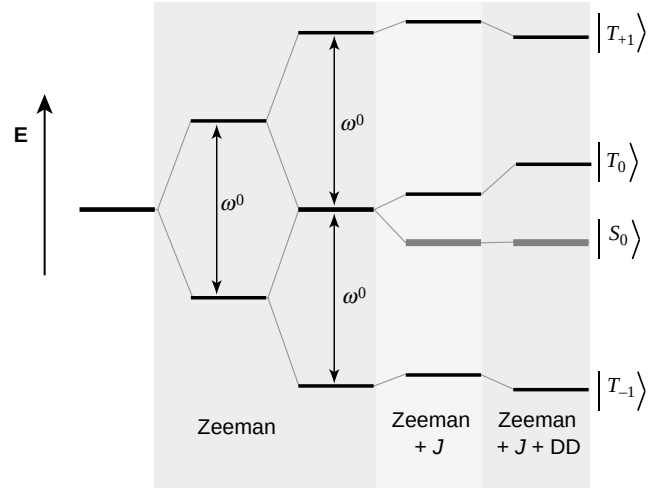

Figure 14.3
Energy levels for a pair of magnetically equivalent spins-1/2. The singlet state is shown in grey. The energy level shifts due to the spin–spin couplings are greatly exaggerated. The J-coupling and dipole–dipole (DD) coupling are assumed to have opposite signs.

If the energy levels of the singlet and triplet states are separated, then we get the picture shown in Figure 14.4. The energy level differences between adjacent triplet states are $\omega^0 \pm \frac{3}{2}d_{12}$. The J-coupling shifts the energy of the singlet state relative to the triplet states, but does not influence the triplet splittings.

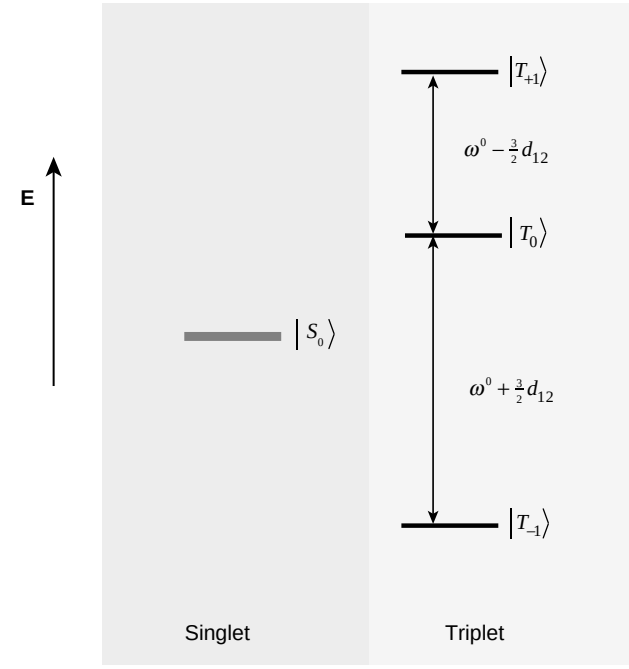

Figure 14.4
Singlet and triplet energy levels for a pair of magnetically equivalent spins-1/2.

The energy levels of the triplet states, therefore, are the same as for a spin-1 nucleus (see Figure 13.1), but with the first-order quadrupolar coupling $\omega_Q^{(1)}$ replaced by three times the dipole–dipole coupling d_{12}.

14.4.3 NMR spectra

A pair of magnetically equivalent spins-1/2 has four energy eigenstates: three triplet states and one singlet state. The singlet state has total spin $I = 0$ and is non-magnetic. It may usually be completely ignored in the context of NMR experiments.[2] All NMR signals are associated with the three triplet states, which behave in exactly the same way as the three Zeeman states of a spin-1 nucleus, except that the first-order quadrupolar interaction is substituted by three times the dipole–dipole coupling. The treatment of spin-1 dynamics given in Section 13.1 may therefore be recycled, with only minor changes.

Since there are two (-1)-quantum coherences within the triplet manifold, the spectrum consists of a doublet, in the general case:

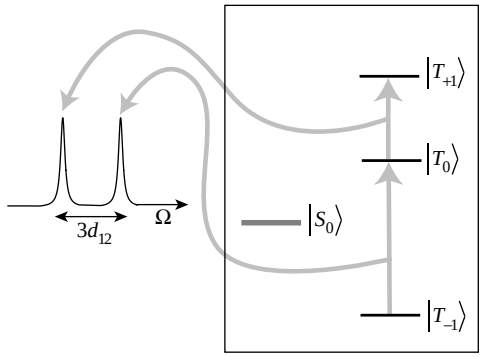

Figure 14.5
Doublet NMR spectrum generated by magnetically equivalent spin-1/2 pairs.

The splitting is given by $3d_{12}$, where d_{12} is the secular part of the dipole–dipole coupling. Compare with the spin-1 case depicted in Figure 13.5, in which the splitting is equal to the first-order quadrupolar coupling $\omega_{\mathrm{Q}}^{(1)}$.

Pairs of magnetically equivalent spins-1/2 generate the following types of NMR spectra in the different phases of matter.

Isotropic liquids. Since the secular dipole–dipole coupling d_{12} vanishes in isotropic liquids, the two peaks coincide. This is why the NMR spectrum of liquid water is a singlet (see Figure 14.6a).

Liquid crystals. A dipolar splitting $3d_{12}$ is observed in anisotropic liquids[3] (see Figure 14.6b). The magnitude of this splitting depends on the secular dipole–dipole coupling, averaged over the anisotropic molecular motion (see Equation 9.40).

Powders. In solids, the dipolar splitting $3d_{12}$ depends on the orientation of the internuclear vector with respect to the external magnetic field (see Equation 9.40). As in the spin-1 case, this orientation dependence leads to a Pake doublet spectrum for pairs of magnetically equivalent spins-1/2 in a solid powder (see Figure 14.6c).

The splitting between the prominent peaks of the Pake doublet is equal to $3b_{12}$, in units of radians per second. Here, b_{12} is the dipole–dipole coupling constant in radians per second (see Equation 9.32), which is inversely proportional to the distance r_{12} between the nuclei I_1 and I_2:

$$b_{12} = -\frac{\mu_0}{4\pi}\frac{\gamma^2\hbar}{r_{12}^3} \tag{14.17}$$

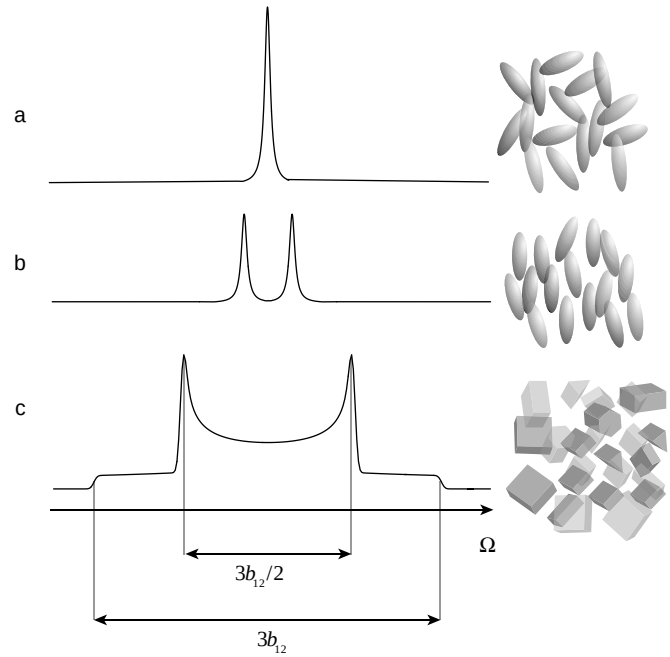

Figure 14.6
Typical spectra of magnetically equivalent spin-1/2 pairs in. (a) isotropic liquids; (b) nematic liquid crystals; (c) solid powders.

The powder NMR spectra of spin-1/2 pairs may, therefore, be used to estimate the distance between the nuclei (see Exercise 14.1).

14.4.4 Dipolar echo

Since the triplet manifold of equivalent spin-1/2 pairs behaves exactly like a spin-1, except with the dipole–dipole coupling replacing the quadrupole coupling, the two-pulse echo technique described in Section 13.1.10 also works in the spin-pair case. In this context, the echo involves the refocusing of homonuclear dipole–dipole interactions and is called a *dipolar echo*.[4]

14.5 Weakly Coupled Spin Pairs

14.5.1 Weak coupling

The spin-pair system is said to be weakly coupled if the following general condition is satisfied:[5]

$$\frac{1}{2}|\omega_{12}^{\mathrm{B}}| << |\omega_1^0 - \omega_2^0| \tag{14.18}$$

where the flip-flop coupling term is $\omega_{12}^{\mathrm{B}} = 2\pi J_{12} - d_{12}$.

In the case of isotropic liquids, the secular dipole–dipole coupling vanishes. The weak-coupling condition in isotropic phase is therefore

$$|\pi J_{12}| << |\omega_1^0 - \omega_2^0|$$

or equivalently

$$\left|\frac{1}{2}J_{12}\right| << \left|(\delta_1 - \delta_2)\frac{\omega^0}{2\pi}\right| \qquad \text{(in isotropic liquids)} \tag{14.19}$$

This is the most commonly used version of the weak-coupling condition. Half the J-coupling (in hertz) must be much less than the chemical shift frequency difference (also in hertz).

⚠ Equation 14.19 is the weak-coupling condition in the *isotropic phase*. In solids or liquid crystals, the more general form of Equation 14.18 must be used.

14.5.2 AX spin systems

Actual compounds containing homonuclear AX spin systems are rather uncommon. An example of a ^{1}H AX system is dichloroacetaldehyde in isotropic solution:

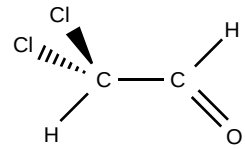

Figure 14.7
Dichloroacetaldehyde.

The isotopomers of this molecule potentially contain five types of magnetic spin: ^{1}H, ^{35}Cl, ^{37}Cl, ^{13}C and ^{2}H. The abundant ^{35}Cl and ^{37}Cl nuclei have a large electric quadrupole moment and relax rapidly. As discussed in Section 17.3, these quadrupolar spins may be ignored. The isotopes ^{13}C and ^{2}H occur in low natural abundance. By far the most common isotopomer of dichloroacetaldehyde contains only two magnetic nuclei, both protons. The two protons have very different chemical shifts due to the strong electronegativity of the Cl atoms. The chemical shift difference between the two protons is $\delta_1 - \delta_2 = 3.28$ ppm and their isotropic J-coupling is $J_{12} = 2.9$ Hz.

The weak-coupling condition (Equation 14.19) is satisfied at all reasonable magnetic fields. For example, if the proton Larmor frequency is $|\omega^0/2\pi| = 500$ MHz, then the chemical shift frequency difference is $3.28\text{ ppm} \times 500\text{ MHz} = 1.64$ kHz, which is three orders of magnitude larger than $\frac{1}{2}J_{12} = 1.45$ Hz.

A liquid sample of dichloroacetaldehyde, therefore, may be considered, to a good approximation, to consist of an ensemble of identical ^{1}H AX spin systems. The minor isotopomers containing ^{13}C or ^{2}H spins give rise to small additional spectral peaks, which are ignored here.[6]

14.5.3 Energy levels

If the general form of the weak-coupling condition (Equation 14.18) is satisfied, then the *secular approximation* (see Appendix A.6) may be used to discard the flip-flop Hamiltonian term $\widehat{\mathcal{H}}^0_{\mathrm{B}}$. The spin Hamiltonian may be approximated by the $\widehat{\mathcal{H}}^0_{\mathrm{A}}$ part alone:

$$\widehat{\mathcal{H}}^0_{\mathrm{A}} = \omega^0_1 \hat{I}_{1z} + \omega^0_2 \hat{I}_{2z} + \omega^{\mathrm{A}}_{12} 2\hat{I}_{1z}\hat{I}_{2z} \tag{14.20}$$

where $\omega^{\mathrm{A}}_{12} = \pi J_{12} + d_{12}$. An immediate consequence of weak coupling is that the Zeeman product states $\{|\alpha\alpha\rangle, |\alpha\beta\rangle, |\beta\alpha\rangle, |\beta\beta\rangle\}$ are also eigenstates of the spin Hamiltonian. The matrix representation of the weak-

coupling Hamiltonian is given in Equation 14.7. The corresponding eigenequations are

$$\widehat{\mathcal{H}}_{\mathrm{A}}^{0}|\alpha\alpha\rangle = \omega_{\alpha\alpha}|\alpha\alpha\rangle \quad \widehat{\mathcal{H}}_{\mathrm{A}}^{0}|\alpha\beta\rangle = \omega_{\alpha\beta}|\alpha\beta\rangle$$
$$\widehat{\mathcal{H}}_{\mathrm{A}}^{0}|\beta\alpha\rangle = \omega_{\beta\alpha}|\beta\alpha\rangle \quad \widehat{\mathcal{H}}_{\mathrm{A}}^{0}|\beta\beta\rangle = \omega_{\beta\beta}|\beta\beta\rangle$$

where the energies of the states are given by

$$\begin{aligned}
\omega_{\alpha\alpha} &= +\frac{1}{2}\omega_1^0 + \frac{1}{2}\omega_2^0 + \frac{1}{2}\omega_{12}^{\mathrm{A}} \\
\omega_{\alpha\beta} &= +\frac{1}{2}\omega_1^0 - \frac{1}{2}\omega_2^0 - \frac{1}{2}\omega_{12}^{\mathrm{A}} \\
\omega_{\beta\alpha} &= -\frac{1}{2}\omega_1^0 + \frac{1}{2}\omega_2^0 - \frac{1}{2}\omega_{12}^{\mathrm{A}} \\
\omega_{\beta\beta} &= -\frac{1}{2}\omega_1^0 - \frac{1}{2}\omega_2^0 + \frac{1}{2}\omega_{12}^{\mathrm{A}}
\end{aligned} \tag{14.21}$$

The contributions to the energy levels of the weakly coupled spin pair are sketched in Figure 14.8. The Zeeman interactions of the two spins with the magnetic field create a three-level structure, with the central level being doubly degenerate. The different chemical shifts of the two spins, followed by the J-coupling and the dipole–dipole coupling, break the degeneracy. In contrast to the magnetically equivalent case, the J-coupling and the dipole–dipole coupling work in exactly the same way, and either reinforce each other or partially cancel, depending on the relative signs.

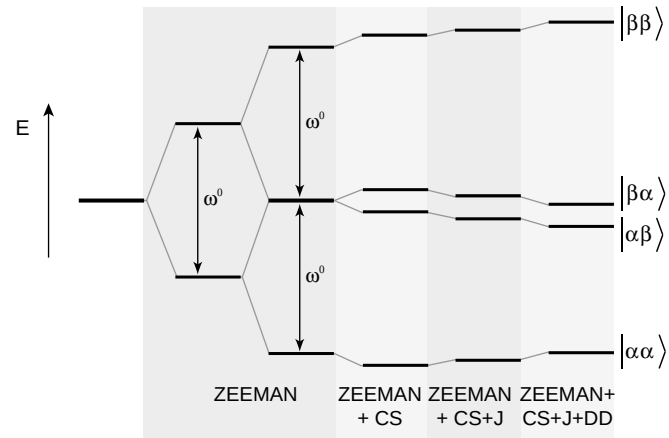

Figure 14.8
Energy levels for a weakly coupled spin-1/2 pair.

The figure above is not to scale; in reality, the splitting between the two central levels is far smaller than the Zeeman splitting.

14.5.4 AX spectrum

The NMR spectrum of an AX system contains four peaks, corresponding to the four different (−1)-quantum coherences in the AX spin ensemble, as shown in Figure 14.9. In general, the splitting between the components of each doublet is $2\omega_{12}^{\mathrm{A}} = 2\pi J_{12} + 2d_{12}$. The splitting, therefore, contains a contribution from both the J-coupling and the secular dipole–dipole coupling.

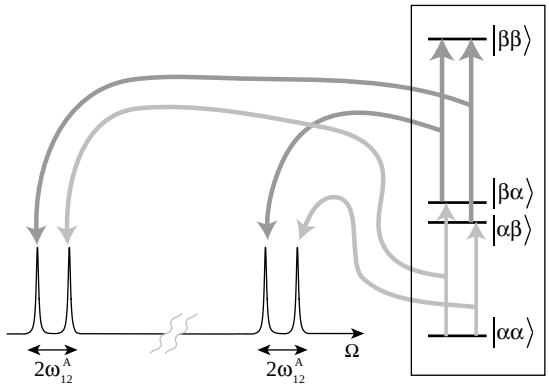

Figure 14.9
NMR spectrum containing two doublets, generated by weakly coupled spin-1/2 pairs.

In isotropic liquids, the secular dipole–dipole coupling vanishes. The splitting in this case is equal to $2\pi J_{12}$ in radians per second. When written in hertz, the splitting is simply J_{12}. This is the origin of the doublet multiplet structure introduced in Section 3.8.

The proton spectrum of dichloroacetaldehyde in solution is shown below. Note the splitting of 2.9 Hz in each doublet:

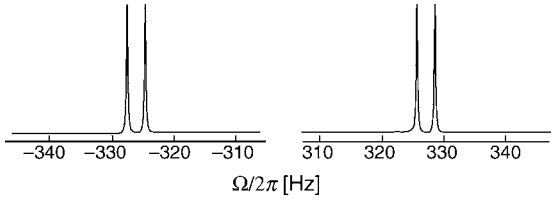

Figure 14.10
Proton spectrum of dichloroacetaldehyde, in a field of 4.7 T.

14.5.5 Heteronuclear spin pairs

Heteronuclear spin pairs contain two nuclei of different isotopic types, e.g. a ^{13}C nucleus coupled to a ^{1}H nucleus. Since the Larmor frequency difference between different isotopes is very large, heteronuclear spin pairs are always weakly coupled.

Notes

1. In general, two spins with the same chemical shift are only magnetically equivalent if the couplings to *other* spins fulfil additional symmetry requirements. This subject is discussed in detail in Section 17.5. The current chapter considers isolated pairs of spins, and neglects couplings to spins outside the pair. In this context, spins with the same chemical shift are also magnetically equivalent.

2. Since the singlet states of spin-1/2 pairs behave as if they are spin-0 nuclei, they are non-magnetic and have some unusual properties. In particular, these states are immune to many of the common relaxation mechanisms and have very long lifetimes in some circumstances. Rather surprisingly, the long lifetimes of singlet states may be exploited even if the spins are not magnetically equivalent. For example, see M. Carravetta, O. G. Johannessen and M. H. Levitt, *Phys. Rev. Lett.* **92**, 153003 (2004) and M. Carravetta and M. H. Levitt, *J. Am. Chem. Soc.* **126**, 6228–6229 (2004).

3. See Chapter 13 Note 6.

4. The dipolar echo induced by a two-pulse sequence is sometimes called a *solid echo*. The terms *dipolar echo* and *solid echo* are both rather misleading, since the echo formation is specific to well-separated pairs of magnetically equivalent spins-1/2.

5. Equation 14.19 does not ensure the validity of neglecting $\widehat{\mathcal{H}}_{\mathrm{B}}^{0}$ under *all* experimental situations (see Section 18.14).

6. Small additional peaks due to minor isotopomers are sometimes termed *satellites*. The same term has a completely different meaning in the context of quadrupolar nuclei (see Chapter 13).

Exercises

14.1 In the original paper by G. E. Pake *(J. Chem. Phys.* **16**, 327 (1948)), the distance between the protons in water was estimated by measuring the ^{1}H powder spectrum of gypsum (calcium sulfate dihydrate). The splitting between the strong peaks in the Pake doublet was found to be 10.8 G (1.08 mT), in an old-fashioned swept-field experiment.
(i) Show that the Pake splitting corresponds to 45.98 kHz in a modern NMR protocol.
(ii) Use this number to estimate the distance between the two protons in a water molecule.

15 Homonuclear AX System

I now examine the dynamics of a homonuclear AX system in more detail.

Each molecule contains two spins-1/2, I_1 and I_2, which are of the same isotopic type but with different chemical shifts. The sketches below use different symbols to denote the inequivalence of the sites:

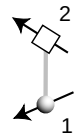

Figure 15.1
A pair of coupled spins with different chemical shifts.

In the following discussion, the spins are assumed to have a positive gyromagnetic ratio γ. The chemical shifts of the two sites are arranged in the order $\delta_1 < \delta_2$. This implies that the resonances of spin I_1 appear to the right of those of spins I_2, in a conventionally presented spectrum. The chemically shifted Larmor frequencies ω_1^0 and ω_2^0 are defined in Equation 14.2, and are both negative, with $\omega_1^0 > \omega_2^0$.

For simplicity, an isotropic liquid phase is assumed. The diagonal part of the coupling term is therefore given by $\omega_{12}^{\mathrm{A}} = \pi J_{12}$ (see Equation 14.6).

The spin system is assumed to satisfy Equation 14.19 and is therefore weakly coupled. The off-diagonal coupling term $\widehat{\mathcal{H}}_{\mathrm{B}}^0$ is neglected, as described in Section 14.5.

15.1 Eigenstates and Energy Levels

The weakly coupled spin Hamiltonian for a spin-1/2 pair in isotropic liquids is given by

$$\widehat{\mathcal{H}}^0 \cong \omega_1^0 \hat{I}_{1z} + \omega_2^0 \hat{I}_{2z} + 2\pi J_{12} \hat{I}_{1z} \hat{I}_{2z} \tag{15.1}$$

The Zeeman product states $\{|\alpha\alpha\rangle, |\alpha\beta\rangle, |\beta\alpha\rangle, |\beta\beta\rangle\}$ are eigenstates of the weakly coupled spin Hamiltonian, as follows:

$$\widehat{\mathcal{H}}^0|\alpha\alpha\rangle = \omega_{\alpha\alpha}|\alpha\alpha\rangle \quad \widehat{\mathcal{H}}^0|\alpha\beta\rangle = \omega_{\alpha\beta}|\alpha\beta\rangle$$
$$\widehat{\mathcal{H}}^0|\beta\alpha\rangle = \omega_{\beta\alpha}|\beta\alpha\rangle \quad \widehat{\mathcal{H}}^0|\beta\beta\rangle = \omega_{\beta\beta}|\beta\beta\rangle$$

where the energies of the states are given in isotropic phase by

Spin Dynamics: Basics of Nuclear Magnetic Resonance, Second Edition Malcolm H. Levitt

$$\omega_{\alpha\alpha} = +\frac{1}{2}\omega_1^0 + \frac{1}{2}\omega_2^0 + \frac{1}{2}\pi J_{12}$$
$$\omega_{\alpha\beta} = +\frac{1}{2}\omega_1^0 - \frac{1}{2}\omega_2^0 - \frac{1}{2}\pi J_{12}$$
$$\omega_{\beta\alpha} = -\frac{1}{2}\omega_1^0 + \frac{1}{2}\omega_2^0 - \frac{1}{2}\pi J_{12}$$
$$\omega_{\beta\beta} = -\frac{1}{2}\omega_1^0 - \frac{1}{2}\omega_2^0 + \frac{1}{2}\pi J_{12} \qquad (15.2)$$

The energy level structure is sketched in Figure 14.8.

The four Zeeman product states are eigenstates of the total z-angular momentum operator $\hat{I}_z$, with eigenvalues denoted M. The corresponding eigenequations are

$$\begin{aligned}
\hat{I}_z|\alpha\alpha\rangle &= |\alpha\alpha\rangle \quad (M_{\alpha\alpha} = +1)\\
\hat{I}_z|\alpha\beta\rangle &= 0 \quad (M_{\alpha\beta} = 0)\\
\hat{I}_z|\beta\alpha\rangle &= 0 \quad (M_{\beta\alpha} = 0)\\
\hat{I}_z|\beta\beta\rangle &= -|\beta\beta\rangle \quad (M_{\beta\beta} = -1)
\end{aligned}$$

The two central energy levels have total z-angular momentum $M = 0$, and the two extreme energy levels have $M = \pm 1$.

15.2 Density Operator

In a real sample, such as dichloroacetaldehyde, there is a very large number of independent spin-pair systems. The collection of independent, non-interacting spin pairs forms an *ensemble of AX spin systems*:

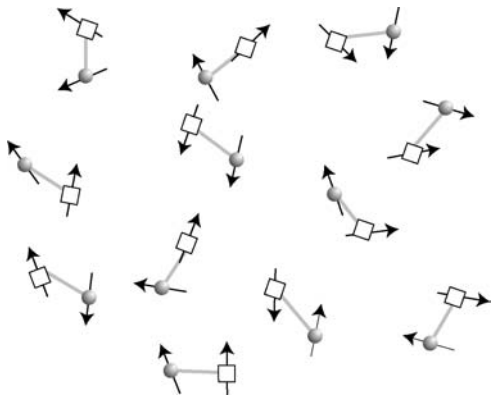

Figure 15.2
Ensemble of AX spin systems.

The quantum state of a spin-pair ensemble is constructed in just the same way as for non-interacting spins. The density operator $\hat{\rho}$ is defined as

$$\hat{\rho} = \overline{|\psi\rangle\langle\psi|} \qquad (15.3)$$

where the overbar denotes an average over all ensemble members.

The density matrix for the spin-pair ensemble may be constructed by multiplying the column and row vectors in the usual way:

$$\hat{\rho} = \overline{\begin{pmatrix} c_{\alpha\alpha} \\ c_{\alpha\beta} \\ c_{\beta\alpha} \\ c_{\beta\beta} \end{pmatrix} \begin{pmatrix} c_{\alpha\alpha}^*, & c_{\alpha\beta}^*, & c_{\beta\alpha}^*, & c_{\beta\beta}^* \end{pmatrix}} = \begin{pmatrix} \overline{c_{\alpha\alpha}c_{\alpha\alpha}^*} & \overline{c_{\alpha\alpha}c_{\alpha\beta}^*} & \overline{c_{\alpha\alpha}c_{\beta\alpha}^*} & \overline{c_{\alpha\alpha}c_{\beta\beta}^*} \\ \overline{c_{\alpha\beta}c_{\alpha\alpha}^*} & \overline{c_{\alpha\beta}c_{\alpha\beta}^*} & \overline{c_{\alpha\beta}c_{\beta\alpha}^*} & \overline{c_{\alpha\beta}c_{\beta\beta}^*} \\ \overline{c_{\beta\alpha}c_{\alpha\alpha}^*} & \overline{c_{\beta\alpha}c_{\alpha\beta}^*} & \overline{c_{\beta\alpha}c_{\beta\alpha}^*} & \overline{c_{\beta\alpha}c_{\beta\beta}^*} \\ \overline{c_{\beta\beta}c_{\alpha\alpha}^*} & \overline{c_{\beta\beta}c_{\alpha\beta}^*} & \overline{c_{\beta\beta}c_{\beta\alpha}^*} & \overline{c_{\beta\beta}c_{\beta\beta}^*} \end{pmatrix}$$

As for non-interacting spins, I now introduce the 'box notation', and write the density matrix as follows:

$$\hat{\rho} = \begin{pmatrix} \rho_{\boxed{\alpha\alpha}} & \rho_{\boxed{\alpha+}} & \rho_{\boxed{+\alpha}} & \rho_{\boxed{++}} \\ \rho_{\boxed{\alpha-}} & \rho_{\boxed{\alpha\beta}} & \rho_{\boxed{+-}} & \rho_{\boxed{+\beta}} \\ \rho_{\boxed{-\alpha}} & \rho_{\boxed{-+}} & \rho_{\boxed{\beta\alpha}} & \rho_{\boxed{\beta+}} \\ \rho_{\boxed{--}} & \rho_{\boxed{-\beta}} & \rho_{\boxed{\beta-}} & \rho_{\boxed{\beta\beta}} \end{pmatrix} \tag{15.4}$$

The four elements on the diagonal represent the populations of the four energy eigenstates. The 12 off-diagonal elements represent coherences between pairs of states.

Although there are 16 elements in the density operator, they are not all independent of each other. The four populations sum to unity, since the state of each spin pair is normalized:

$$\rho_{\boxed{\alpha\alpha}} + \rho_{\boxed{\beta\alpha}} + \rho_{\boxed{\alpha\beta}} + \rho_{\boxed{\beta\beta}} = 1$$

The coherences appear in complex conjugate pairs:

$$\rho_{\boxed{\beta-}} = \rho_{\boxed{\beta+}}^* \qquad \rho_{\boxed{+-}} = \rho_{\boxed{-+}}^*$$

and so on. There are nine independent quantities in the density operator of the ensemble of spin-1/2 pairs.

The coherences are classified according to the difference in the quantum number M for the connected states.

Coherences connecting states whose total z-angular momentum quantum numbers differ by one are called (± 1)-quantum coherences, or *single-quantum coherences*. Such coherences also arise for isolated spins-1/2, as discussed in Chapter 11.

Coherences connecting states whose total z-angular momentum quantum numbers differ by two are called (± 2)-quantum coherences, or *double-quantum coherences*. Such coherences cannot arise for isolated spins-1/2, but may exist for nuclei with $I \geq 1$ (see Chapter 13).

Coherences connecting states whose total z-angular momentum quantum numbers are the same are called *zero-quantum coherences*. These coherences are a feature of coupled spin systems, and cannot arise for isolated nuclei.

The term *multiple-quantum coherence* is used for coherences with orders not equal to ± 1. Zero-quantum coherences are also classed as multiple-quantum coherences.

The 'box notation' allows the coherence order to be determined by inspection. The order is the sum of contributions from each symbol in the box, a '$-$' contributing -1, a '$+$' contributing $+1$, and 'α' and 'β' both contribute zero. For example, populations such as $\rho_{\boxed{\alpha\alpha}}$ have order zero, whereas $\rho_{\boxed{++}}$ is a ($+2$)-quantum coherence.

It is sometimes convenient to use a pictorial representation of the populations and coherences. For example, the term $\rho_{\boxed{\alpha\alpha}}$ is defined as

$$\rho_{\boxed{\alpha\alpha}} = \overline{c_{\alpha\alpha}c_{\alpha\alpha}^*}$$

and represents the (fractional) population of state $|\alpha\alpha\rangle$. It may be depicted by 'little balls' sitting on the $|\alpha\alpha\rangle$ energy level:

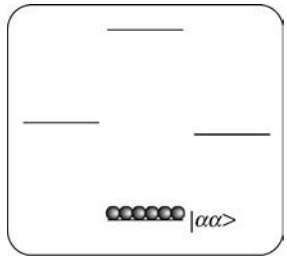

Figure 15.3
The population of state $|\alpha\alpha\rangle$.

The (-1)-quantum coherence $\rho_{\boxed{-\alpha}}$ is defined as

$$\rho_{\boxed{-\alpha}} = \overline{c_{\beta\alpha} c_{\alpha\alpha}{}^*} \tag{15.5}$$

It represents the coherent superposition of states $|\alpha\alpha\rangle$ and $|\beta\alpha\rangle$. It may be represented on a diagram as an arrow leading from state $|\alpha\alpha\rangle$ to state $|\beta\alpha\rangle$:

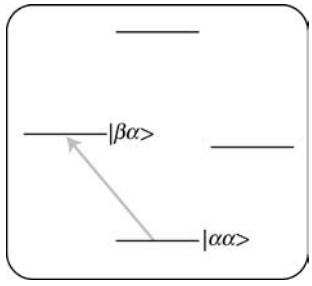

Figure 15.4
The coherence $\rho_{\boxed{-\alpha}}$.

The arrow for a (-1)-quantum coherence points *up* for spins of positive γ.

⚠To understand the correspondence between the two sides of Equation 15.5, read the product $\overline{c_{\beta\alpha} c_{\alpha\alpha}{}^*}$ from *right to left*. The quantum number for the first spin changes in the negative direction on going from right to left (from $+1/2$ to $-1/2$), hence the '$-$' label. The quantum number for the second spin remains unchanged at $+1/2$, hence the 'α' label. This is the significance of the box notation $\rho_{\boxed{-\alpha}}$. Similar arguments apply to the box notation for the other populations and coherences.

Loosely speaking, the coherence $\rho_{\boxed{-\alpha}}$ may be referred to as a '(-1)-quantum coherence of spin I_1, with spin I_2 in the state $|\alpha\rangle$'. This language is misleading, since almost all spins in the ensemble are in superposition states under ordinary circumstances. Nevertheless, the above terminology is a useful shorthand.

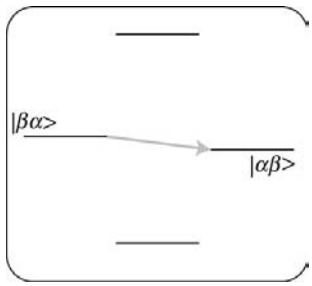

Figure 15.5
The coherence $\rho_{\boxed{+-}}$.

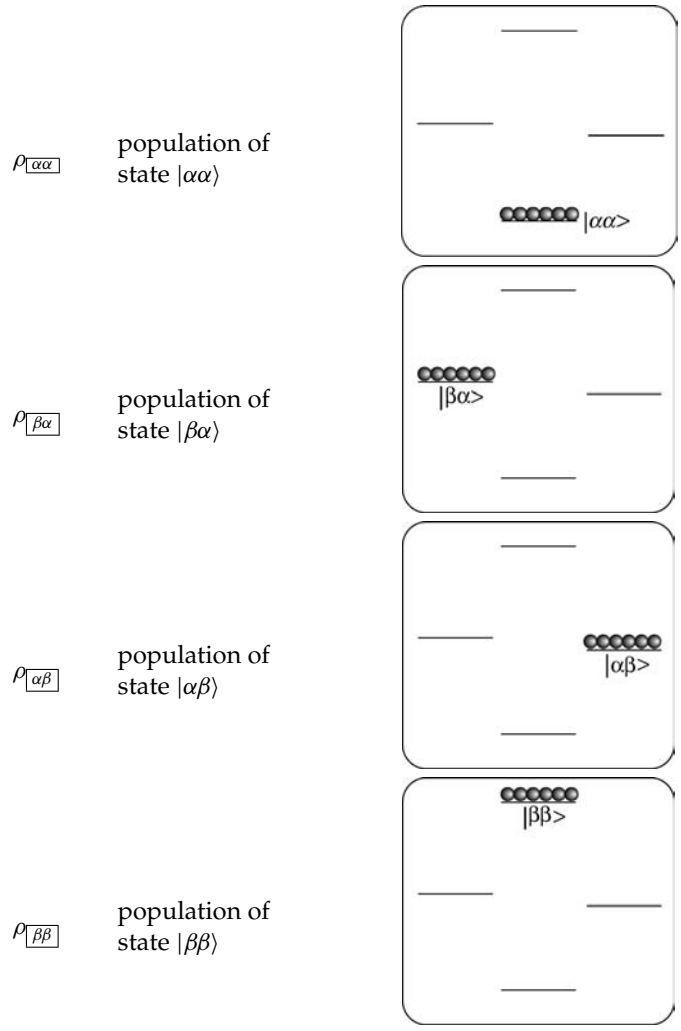

Figure 15.6 Representations of populations in an AX spin ensemble.

To continue: the zero-quantum coherence $\rho_{\boxed{+-}}$ is defined as

$$\rho_{\boxed{+-}} = \overline{c_{\alpha\beta} c_{\beta\alpha}{}^*}$$

It represents a coherent superposition of states $|\beta\alpha\rangle$ and $|\alpha\beta\rangle$. Its diagrammatic representation is shown in Figure 15.5. Diagrammatic representations of all populations and coherences are shown in Figures 15.6 and 15.7.

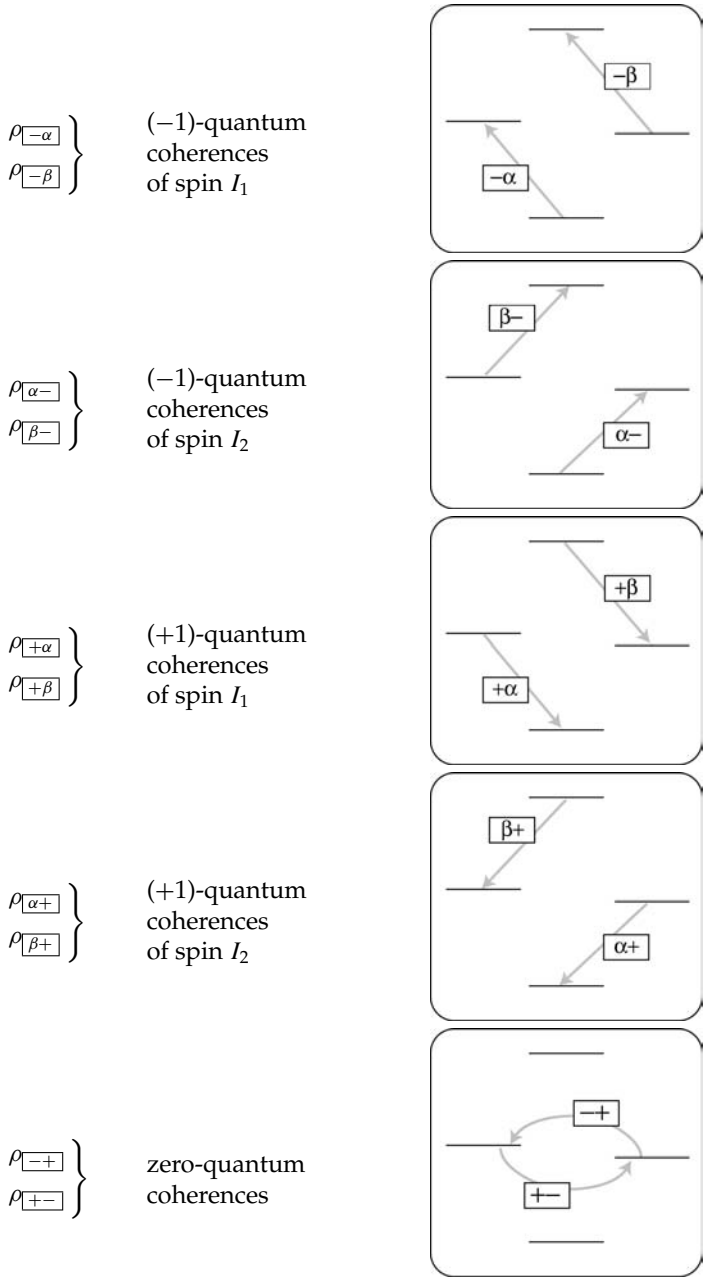

Figure 15.7 Representations of coherences in an AX spin ensemble.

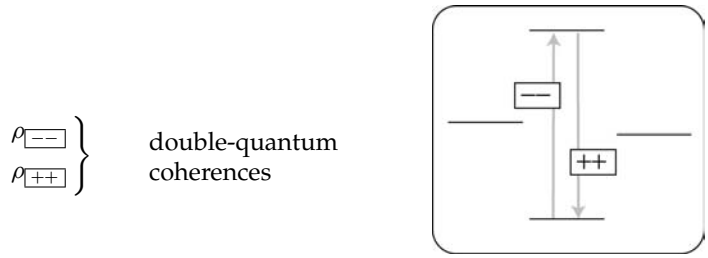

Figure 15.7 (*Continued*).

15.3 Rotating Frame

The behaviour of the spin-pair system is analysed most conveniently in a rotating reference frame, in which the action of the r.f. fields appears as simple as possible. The theory of the rotating frame may be developed by extending the arguments given in Section 10.6 for non-interacting spins.

A rotating-frame spin density operator is defined as follows:

$$\hat{\tilde{\rho}} = \hat{R}_z(-\Phi(t))\hat{\rho}\hat{R}_z(+\Phi(t))$$

where the rotating-frame transformation operator is

$$\hat{R}_z(\Phi) = \exp\{-\mathrm{i}\Phi\hat{I}_z\} = \exp\{-\mathrm{i}\Phi(\hat{I}_{1z} + \hat{I}_{2z})\}$$

The rotation angle of the frame is given, as before, by

$$\Phi(t) = \omega_{\mathrm{ref}}t + \phi_{\mathrm{ref}}$$

where the appropriate choices for ω_{ref} and ϕ_{ref} are discussed in Section 10.6.

The spin density operator evolves under the rotating-frame Hamiltonian $\hat{\tilde{\mathcal{H}}}$, given by

$$\hat{\tilde{\mathcal{H}}} = \hat{R}_z(-\Phi)\hat{\mathcal{H}}\hat{R}_z(\Phi) - \omega_{\mathrm{ref}}\hat{I}_z \tag{15.6}$$

In the absence of an r.f. pulse, the rotating-frame spin Hamiltonian for the weakly coupled spin pair is

$$\hat{\tilde{\mathcal{H}}}^0 = \hat{R}_z(-\Phi)\hat{\mathcal{H}}^0\hat{R}_z(\Phi) - \omega_{\mathrm{ref}}\hat{I}_z$$

This evaluates to

$$\hat{\tilde{\mathcal{H}}}^0 = \Omega_1^0\hat{I}_{1z} + \Omega_2^0\hat{I}_{2z} + 2\pi J_{12}\hat{I}_{1z}\hat{I}_{2z} \tag{15.7}$$

where the offset frequencies Ω_1^0 and Ω_2^0 represent differences between the chemically shifted Larmor frequencies and the spectrometer reference frequency:

$$\Omega_1^0 = \omega_1^0 - \omega_{\mathrm{ref}} = -\gamma B^0(\delta_1 - \delta_{\mathrm{ref}})$$
$$\Omega_2^0 = \omega_2^0 - \omega_{\mathrm{ref}} = -\gamma B^0(\delta_2 - \delta_{\mathrm{ref}})$$

As usual, δ_{ref} is the chemical shift corresponding to the spectrometer reference frequency, i.e. the exact centre of the spectrum.

The rotating-frame Hamiltonian $\hat{\tilde{\mathcal{H}}}^0$ is exactly the same as the fixed-frame Hamiltonian, except with the offset frequencies Ω_1^0 and Ω_2^0 replacing the absolute Larmor frequencies ω_1^0 and ω_2^0. The eigenvalues of the rotating-frame spin Hamiltonian are given by

$$\begin{aligned} \Omega_{\alpha\alpha} &= +\frac{1}{2}\Omega_1^0 + \frac{1}{2}\Omega_2^0 + \frac{1}{2}\pi J_{12} \qquad & \Omega_{\beta\alpha} &= -\frac{1}{2}\Omega_1^0 + \frac{1}{2}\Omega_2^0 - \frac{1}{2}\pi J_{12} \\ \Omega_{\alpha\beta} &= +\frac{1}{2}\Omega_1^0 - \frac{1}{2}\Omega_2^0 - \frac{1}{2}\pi J_{12} \qquad & \Omega_{\beta\beta} &= -\frac{1}{2}\Omega_1^0 - \frac{1}{2}\Omega_2^0 + \frac{1}{2}\pi J_{12} \end{aligned} \tag{15.8}$$

The matrix representation of the weakly coupled spin Hamiltonian, in the absence of an r.f. field, is

$$\hat{\tilde{\mathcal{H}}}^0 = \begin{pmatrix} \Omega_{\alpha\alpha} & & & \\ & \Omega_{\alpha\beta} & & \\ & & \Omega_{\beta\alpha} & \\ & & & \Omega_{\beta\beta} \end{pmatrix}$$

The rotating frame is assumed for the rest of this chapter. The tilde symbols are dropped.

15.4 Free Evolution

Suppose that the spin-pair ensemble has a certain state at time point ②. The system is allowed to evolve freely over an interval τ, up to time point ③. We now investigate the relationship between the spin density operators at these two time points.

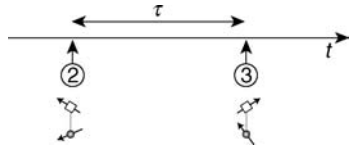

Figure 15.8
Free precession of a spin pair.

In the following discussion, I ignore relaxation.

15.4.1 Evolution of a spin pair

Consider a single spin pair, with a state $|\psi\rangle_②$ at the beginning of the free evolution interval. In general, the spin pair is in a superposition of the four energy eigenstates:

$$|\psi\rangle_② = \begin{pmatrix} c_{\alpha\alpha}② \\ c_{\alpha\beta}② \\ c_{\beta\alpha}② \\ c_{\beta\beta}② \end{pmatrix}$$

where the superposition coefficients $c_{\alpha\alpha}② \ldots$, etc., are complex numbers.

The Schrödinger equation for the spin pair is

$$\frac{\mathrm{d}}{\mathrm{d}t}|\psi\rangle = -\mathrm{i}\widehat{\mathcal{H}}^0|\psi\rangle$$

where the rotating-frame Hamiltonian $\widehat{\mathcal{H}}^0$ is given by Equation 15.7.

The Schrödinger equation has the solution

$$|\psi\rangle_③ = \widehat{U}(\tau)|\psi\rangle_②$$

where the operator $\widehat{U}(\tau)$ is called the *free evolution propagator*, and is defined by

$$\widehat{U}(\tau) = \exp\{-\mathrm{i}\widehat{\mathcal{H}}^0\tau\}$$

The free evolution propagator has the following matrix representation:

$$\widehat{U}(\tau) = \exp\{-\mathrm{i}\widehat{\mathcal{H}}^0\tau\} = \begin{pmatrix} \exp\{-\mathrm{i}\Omega_{\alpha\alpha}\tau\} & & & \\ & \exp\{-\mathrm{i}\Omega_{\alpha\beta}\tau\} & & \\ & & \exp\{-\mathrm{i}\Omega_{\beta\alpha}\tau\} & \\ & & & \exp\{-\mathrm{i}\Omega_{\beta\beta}\tau\} \end{pmatrix}$$

Each superposition coefficient oscillates with a frequency equal to the energy of the corresponding eigenstate:

$$c_{\alpha\alpha}③ = c_{\alpha\alpha}② \exp\{-\mathrm{i}\Omega_{\alpha\alpha}\tau\}$$
$$c_{\alpha\beta}③ = c_{\alpha\beta}② \exp\{-\mathrm{i}\Omega_{\alpha\beta}\tau\}$$
$$\vdots$$

15.4.2 Evolution of the coherences

Now consider the ensemble of very many spin pairs.

The evolution of the populations and coherences may be treated by reproducing the discussion in Section 11.7. In the absence of relaxation, the populations of the spin system remain unchanged over the interval τ. The coherences rotate in the complex plane, according to the energy difference between the participating states. In general, the following equation of motion applies:

$$\rho_{rs}③ \cong \rho_{rs}② \exp\{-\mathrm{i}(\Omega_r - \Omega_s)\tau\} \tag{15.9}$$

where Ω_r and Ω_s are the eigenvalues of $\widehat{\mathcal{H}}^0$.

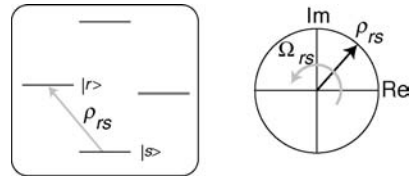

Figure 15.9
Free evolution of a coherence.

For example, the coherence $\rho_{\boxed{-\beta}}$ involves the states $|r\rangle = |\beta\beta\rangle$ and $|s\rangle = |\alpha\beta\rangle$. The coherence, therefore, evolves according to

$$\rho_{\boxed{-\beta}}③ = \rho_{\boxed{-\beta}}② \exp\{i\Omega_{\boxed{-\beta}}\tau\}$$

where the characteristic frequency $\Omega_{\boxed{-\beta}}$ is

$$\Omega_{\boxed{-\beta}} = -(\Omega_{\beta\beta} - \Omega_{\alpha\beta}) = \Omega_1^0 - \pi J_{12}$$

Similar equations apply for the other coherences. For completeness, the characteristic frequencies of all coherences are listed here:

$$\begin{aligned}
\Omega_{\boxed{--}} &= -(\Omega_{\beta\beta} - \Omega_{\alpha\alpha}) = \Omega_1^0 + \Omega_2^0 \\
\Omega_{\boxed{-\beta}} &= -(\Omega_{\beta\beta} - \Omega_{\alpha\beta}) = \Omega_1^0 - \pi J_{12} \\
\Omega_{\boxed{-\alpha}} &= -(\Omega_{\beta\alpha} - \Omega_{\alpha\alpha}) = \Omega_1^0 + \pi J_{12} \\
\Omega_{\boxed{\beta-}} &= -(\Omega_{\beta\beta} - \Omega_{\beta\alpha}) = \Omega_2^0 - \pi J_{12} \\
\Omega_{\boxed{\alpha-}} &= -(\Omega_{\alpha\beta} - \Omega_{\alpha\alpha}) = \Omega_2^0 + \pi J_{12} \\
\Omega_{\boxed{-+}} &= -(\Omega_{\beta\alpha} - \Omega_{\alpha\beta}) = \Omega_1^0 - \Omega_2^0 \\
\Omega_{\boxed{+-}} &= -(\Omega_{\alpha\beta} - \Omega_{\beta\alpha}) = -\Omega_1^0 + \Omega_2^0 \\
\Omega_{\boxed{+\beta}} &= -(\Omega_{\alpha\beta} - \Omega_{\beta\beta}) = -\Omega_1^0 + \pi J_{12} \\
\Omega_{\boxed{+\alpha}} &= -(\Omega_{\alpha\alpha} - \Omega_{\beta\alpha}) = -\Omega_1^0 - \pi J_{12} \\
\Omega_{\boxed{\beta+}} &= -(\Omega_{\beta\alpha} - \Omega_{\beta\beta}) = -\Omega_2^0 + \pi J_{12} \\
\Omega_{\boxed{\alpha+}} &= -(\Omega_{\alpha\alpha} - \Omega_{\alpha\beta}) = -\Omega_2^0 - \pi J_{12} \\
\Omega_{\boxed{++}} &= -(\Omega_{\alpha\alpha} - \Omega_{\beta\beta}) = -\Omega_1^0 - \Omega_2^0
\end{aligned} \tag{15.10}$$

Relaxation may be included in the evolution equations in a phenomenological way by adding a damping term. The evolution of a (-1)-quantum coherence is written as

$$\rho_{\boxed{-\beta}}③ = \rho_{\boxed{-\beta}}② \exp\{(i\Omega_{\boxed{-\beta}} - \lambda)\tau\}$$

where λ is the damping rate constant (inverse of T_2 for that particular coherence). In general, each of the six independent coherences in the spin-pair ensemble has a different damping rate constant. For simplicity, I assume here that all the damping rate constants are the same.[1]

The relaxation of the *populations* in a spin-pair ensemble is an important but complicated subject, which is tackled in Chapter 20.

15.5 Spectrum of the AX System: Spin–Spin Splitting

Assume that an r.f. pulse sequence is applied to the spin-pair ensemble, and the NMR signal detected afterwards. As always, the time point $t = 0$ is defined as the start of signal detection, i.e. just after the end of the pulse sequence. The pulse sequence leads to a spin density operator $\hat{\rho}(0)$, which then evolves freely over the subsequent time interval. The complex NMR signal emerging from the quadrature receiver is collected and digitized. In this section, I consider the form of the NMR signal generated by the spin-pair ensemble, and its relationship with the coherences existing at time $t = 0$.

By repeating the arguments given in Appendix A.5, one gets the following relationship between the quadrature NMR signal and the (−1)-quantum coherences of the spin system:

$$s(t) = 2\mathrm{i}(\rho_{\boxed{-\beta}}(t) + \rho_{\boxed{-\alpha}}(t) + \rho_{\boxed{\beta-}}(t) + \rho_{\boxed{\alpha-}}(t)) \exp\{-\mathrm{i}\phi_{\mathrm{rec}}\} \tag{15.11}$$

Here, ϕ_{rec} is the overall signal phase shift in the receiver and digitizer, as discussed in Section 4.5.4.

For an ensemble of spin-1/2 pairs, there are four (−1)-quantum coherences, and hence four independent contributions to the NMR signal.

The four (−1)-quantum coherences evolve in the rotating frame according to the following equations:

$$\begin{aligned}
\rho_{\boxed{-\beta}}(t) &= \rho_{\boxed{-\beta}}(0) \exp\{(\mathrm{i}\Omega_{\boxed{-\beta}} - \lambda)t\} \\
\rho_{\boxed{-\alpha}}(t) &= \rho_{\boxed{-\alpha}}(0) \exp\{(\mathrm{i}\Omega_{\boxed{-\alpha}} - \lambda)t\} \\
\rho_{\boxed{\beta-}}(t) &= \rho_{\boxed{\beta-}}(0) \exp\{(\mathrm{i}\Omega_{\boxed{\beta-}} - \lambda)t\} \\
\rho_{\boxed{\alpha-}}(t) &= \rho_{\boxed{\alpha-}}(0) \exp\{(\mathrm{i}\Omega_{\boxed{\alpha-}} - \lambda)t\}
\end{aligned}$$

where $\Omega_{\boxed{-\beta}} \ldots$ are the characteristic frequencies, given in Equation 15.10.

After FT, the NMR spectrum from the spin-pair ensemble contains *four* peaks:

$$\begin{aligned}
S(\Omega) = a_{\boxed{-\beta}} \mathcal{L}(\Omega; \Omega_{\boxed{-\beta}}, \lambda) + a_{\boxed{\beta-}} \mathcal{L}(\Omega; \Omega_{\boxed{\beta-}}, \lambda) + \\
a_{\boxed{-\alpha}} \mathcal{L}(\Omega; \Omega_{\boxed{-\alpha}}, \lambda) + a_{\boxed{\alpha-}} \mathcal{L}(\Omega; \Omega_{\boxed{\alpha-}}, \lambda)
\end{aligned}$$

where the complex amplitude of each peak depends on the amplitude of the corresponding coherence at the beginning of the detection period:

$$\begin{aligned}
a_{\boxed{-\beta}} &= 2\mathrm{i}\rho_{\boxed{-\beta}}(0) \exp\{-\mathrm{i}\phi_{\mathrm{rec}}\} \qquad a_{\boxed{\beta-}} = 2\mathrm{i}\rho_{\boxed{\beta-}}(0) \exp\{-\mathrm{i}\phi_{\mathrm{rec}}\} \\
a_{\boxed{-\alpha}} &= 2\mathrm{i}\rho_{\boxed{-\alpha}}(0) \exp\{-\mathrm{i}\phi_{\mathrm{rec}}\} \qquad a_{\boxed{\alpha-}} = 2\mathrm{i}\rho_{\boxed{\alpha-}}(0) \exp\{-\mathrm{i}\phi_{\mathrm{rec}}\}
\end{aligned} \tag{15.12}$$

Just as for the spin-1/2 case, the appearance of the spectral peaks depends on the phase of the complex amplitudes. For example, if $a_{\boxed{-\beta}}$ is real and positive, then the real part of $S(\Omega)$ contains a positive absorption Lorentzian centred at $\Omega = \Omega_{\boxed{-\beta}}$, and so on.

The peak frequencies correspond to the precession frequencies of the (−1)-quantum coherences in the rotating frame, given by Equation 15.10. These frequencies may be deduced by inspection from the 'box notation'. The spin with a '−' symbol contributes the chemical shift offset frequency, and the spin with an 'α' or 'β' symbol contributes plus or minus one-half of the J-coupling. For example, the coherence $\rho_{\boxed{-\beta}}$ generates a peak at the frequency $\Omega_{\boxed{-\beta}} = \Omega_1^0 - \pi J_{12}$, whereas the coherence $\rho_{\boxed{\alpha-}}$ generates a peak at the frequency $\Omega_{\boxed{\alpha-}} = \Omega_2^0 + \pi J_{12}$.

The spectrum, therefore, contains four peaks, two of which are near the chemical shift frequency Ω_1^0 and two of which are near the chemical shift frequency Ω_2^0, with a 'splitting' given by the J-coupling $2\pi J_{12}$.

The assignment of the peaks to particular coherences depends on the sign of the gyromagnetic ratio and the sign of the J-coupling. In Figures 15.10 and 15.11, it is assumed that the gyromagnetic ratio γ is positive, so that the frequency axis increases from left to right.

In the case $J_{12} > 0$, the peak assignments are as follows:

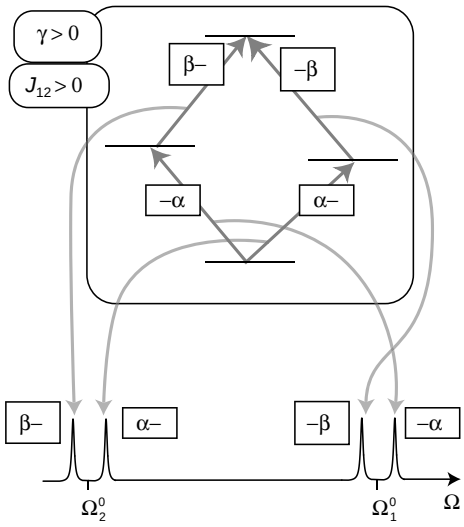

Figure 15.10
Relationship between the coherences and the spectrum for $\gamma > 0$ and $J_{12} > 0$.

The α-components are displaced towards positive frequency if the J-coupling is positive.

For $J_{12} < 0$, the peaks are assigned as follows:

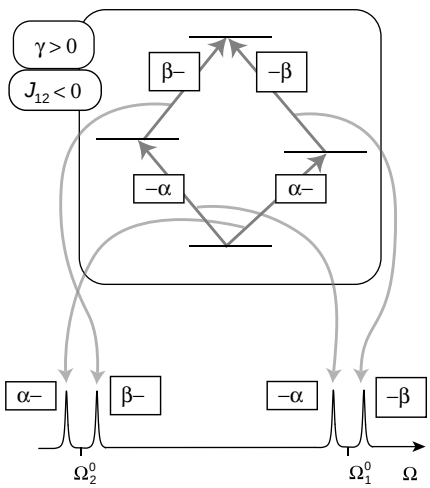

Figure 15.11
Relationship between the coherences and the spectrum for $\gamma > 0$ and $J_{12} < 0$.

The α-components are displaced towards negative frequency if the J-coupling is negative.

If the gyromagnetic ratio γ is negative, then the frequency axis increases from right to left (see Section 3.5). The peak assignments are as follows:

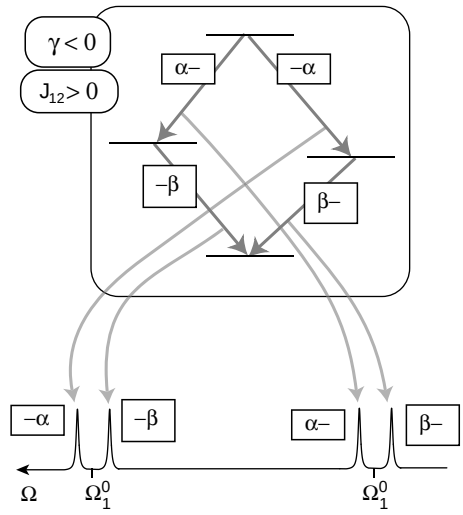

Figure 15.12
Relationship between the coherences and the spectrum for $\gamma > 0$ and $J_{12} < 0$.

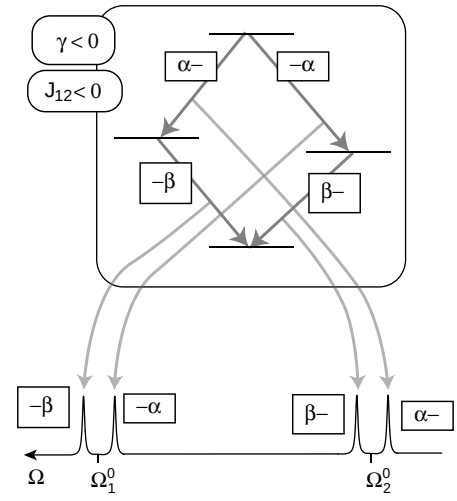

Figure 15.13
Relationship between the coherences and the spectrum for $\gamma < 0$ and $J_{12} < 0$.

As before, the α-components are displaced towards positive frequency if the J-coupling is positive, but are displaced towards negative frequency if the J-coupling is negative.

This is the origin of the spectral splittings by J-couplings, described in Section 3.8.[2]

15.6 Product Operators

We now calculate the evolution of the spin-pair density operator through some r.f. pulse sequences.

Recall the treatment of non-interacting spins-1/2. In that case, spin dynamical calculations are performed most conveniently by rotating the angular momentum operators $\hat{I}_x$, $\hat{I}_y$ and $\hat{I}_z$ in three-dimensional space, as summarized in Section 11.8. During strong r.f. pulses, the spin angular momentum is rotated about axes in the xy-plane of the rotating frame, according to the flip angles and phases of the pulses. During intervals of free precession, the spin angular momentum is rotated about the z-axis, at the chemical shift frequency in the rotating frame.

For coupled spin systems, this technique is extended. Instead of rotating single angular momentum operators, one must rotate *products* of angular momentum operators. The effect of spin–spin couplings must be considered alongside the action of strong r.f. pulses and chemical shifts.

The *product operator formalism* is a calculation method for weakly coupled spin systems. It is most useful for pulse sequences consisting of only two sorts of elements, i.e. very short r.f. pulses and free precession intervals in which the r.f. field is turned completely off. In such cases, the product operator method often allows the dynamics of coupled spin systems to be calculated by simple geometrical arguments and employing minimal mathematics.

In this section, the product operator method is applied to the homonuclear AX system.

15.6.1 Construction of product operators

The subject of product operators may be introduced through their matrix representations.

For an isolated spin-1/2, the four operators $\frac{1}{2}\widehat{1}$, $\hat{I}_x$, $\hat{I}_y$ and $\hat{I}_z$ have the following matrix representations in the basis $\{|\alpha\rangle, |\beta\rangle\}$:

$$\tfrac{1}{2}\widehat{1} = \frac{1}{2}\begin{pmatrix} 1 & 0 \\ 0 & 1 \end{pmatrix} \quad \hat{I}_z = \frac{1}{2}\begin{pmatrix} 1 & 0 \\ 0 & -1 \end{pmatrix}$$

$$\hat{I}_x = \frac{1}{2}\begin{pmatrix} 0 & 1 \\ 1 & 0 \end{pmatrix} \quad \hat{I}_y = \frac{1}{2\mathrm{i}}\begin{pmatrix} 0 & 1 \\ -1 & 0 \end{pmatrix}$$

For the two-spin system, 16 product operators may be constructed through the following recipe:

$$\boxed{\text{product operator}} = 2 \times \boxed{\begin{array}{l}\text{operator for}\\ \text{spin } I_1\\ \text{(4 choices)}\end{array}} \times \boxed{\begin{array}{l}\text{operator for}\\ \text{spin } I_2\\ \text{(4 choices)}\end{array}}$$

Examples of valid product operators for the two-spin system are $2\hat{I}_{1z}\hat{I}_{2x}$ and $2\hat{I}_{1x}\hat{I}_{2x}$.

When $\frac{1}{2}\widehat{1}$ operators are involved, the product operator may be abbreviated; for example:

$$2\,\frac{1}{2}\widehat{1}_1\,\frac{1}{2}\widehat{1}_2 = \frac{1}{2}\widehat{1}$$

$$2\,\frac{1}{2}\,\hat{I}_{1z}\widehat{1}_2 = \hat{I}_{1z}$$

The operators $\widehat{1}_1$, $\widehat{1}_2$ and $\widehat{1}$ are entirely equivalent:

$$\widehat{1}_1 = \widehat{1}_2 = \widehat{1}$$

The subscripts 1 and 2 are useful for bookkeeping, but have no other significance in this context. Note carefully that the implied summation

$$\widehat{1} = \widehat{1}_1 + \widehat{1}_2 \qquad \text{(incorrect!)}$$

does *not* hold for the unity operators.

It is advisable to retain the factors of two in product operators such as $2\hat{I}_{1z}\hat{I}_{2z}$, $2\hat{I}_{1x}\hat{I}_{2y}$. Do not group the factors of two with any other numerical factors. Always use a consistent order for indices 1 and 2.

The matrix representations of the product operators may be constructed by taking the *direct product* of the matrix representations of the individual operators:

Example 1

$$2\hat{I}_{1x}\hat{I}_{2z} = 2\,\frac{1}{2}\begin{pmatrix}0 & 1\\ 1 & 0\end{pmatrix}\otimes\frac{1}{2}\begin{pmatrix}1 & 0\\ 0 & -1\end{pmatrix} = \frac{1}{2}\begin{pmatrix}0 & 1\\ 1 & 0\end{pmatrix}\otimes\begin{pmatrix}1 & 0\\ 0 & -1\end{pmatrix}$$

$$= \frac{1}{2}\begin{pmatrix} 0\begin{pmatrix}1 & 0\\ 0 & -1\end{pmatrix} & 1\begin{pmatrix}1 & 0\\ 0 & -1\end{pmatrix} \\ 1\begin{pmatrix}1 & 0\\ 0 & -1\end{pmatrix} & 0\begin{pmatrix}1 & 0\\ 0 & -1\end{pmatrix}\end{pmatrix}$$

$$= \frac{1}{2}\begin{pmatrix}0 & 0 & 1 & 0\\ 0 & 0 & 0 & -1\\ 1 & 0 & 0 & 0\\ 0 & -1 & 0 & 0\end{pmatrix}$$

Example 2

$$\hat{I}_{2y} = 2\,\frac{1}{2}\widehat{1}_1\hat{I}_{2y} = \frac{1}{2\mathrm{i}}\begin{pmatrix}1 & 0\\ 0 & 1\end{pmatrix}\otimes\begin{pmatrix}0 & 1\\ -1 & 0\end{pmatrix}$$

$$= \frac{1}{2\mathrm{i}}\begin{pmatrix} 1\begin{pmatrix}0 & 1\\ -1 & 0\end{pmatrix} & 0\begin{pmatrix}0 & 1\\ -1 & 0\end{pmatrix} \\ 0\begin{pmatrix}0 & 1\\ -1 & 0\end{pmatrix} & 1\begin{pmatrix}0 & 1\\ -1 & 0\end{pmatrix}\end{pmatrix}$$

$$= \frac{1}{2\mathrm{i}}\begin{pmatrix}0 & 1 & 0 & 0\\ -1 & 0 & 0 & 0\\ 0 & 0 & 0 & 1\\ 0 & 0 & -1 & 0\end{pmatrix}$$

The construction of the direct product should be self-explanatory from these examples: copies of the *second* matrix are multiplied by the elements of the *first* matrix, and assembled into a larger matrix.

15.6.2 Populations and coherences

In general, the spin density operator may be expressed as a sum of product operator terms, i.e.

$$\hat{\rho} = a\widehat{1} + b\hat{I}_{1z} + c2\hat{I}_{1x}\hat{I}_{2y} + \ldots \tag{15.13}$$

where a, b, c, etc. are real numbers. The presence of a particular product operator term in the density operator implies a certain configuration of the populations and the coherences.

Example 1. The operator $\hat{I}_{1z}$ has a matrix representation of

$$\hat{I}_{1z} = \frac{1}{2}\begin{pmatrix} 1 & & & \\ & 1 & & \\ & & -1 & \\ & & & -1 \end{pmatrix}$$

(omitting zero elements). If $\hat{\rho}$ contains a (positive) term $\hat{I}_{1z}$, then the populations of states $|\beta\alpha\rangle$ and $|\beta\beta\rangle$ are *depleted* with respect to the populations of states $|\alpha\beta\rangle$ and $|\alpha\alpha\rangle$. The product operator $\hat{I}_{1z}$ indicates a *population differential* across the single-quantum transitions of spin I_1:

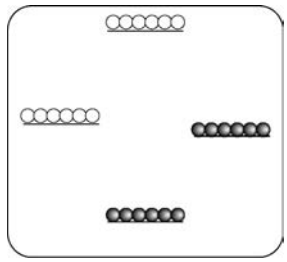

Figure 15.14
Population distribution corresponding to a density operator term $\hat{I}_{1z}$.

In this diagram, 'hollow balls' represent 'negative populations', and 'filled balls' represent 'positive populations'. The concept of a negative population is possible because we are only considering the contribution of a single term to the density operator; when all terms are taken into account, the *total* population of each state is always positive.

Example 2. The operator $2\hat{I}_{1z}\hat{I}_{2z}$ has a matrix representation of

$$2\hat{I}_{1z}\hat{I}_{2z} = \frac{1}{2}\begin{pmatrix} 1 & & & \\ & -1 & & \\ & & -1 & \\ & & & 1 \end{pmatrix}$$

If $\hat{\rho}$ contains a (positive) term $2\hat{I}_{1z}\hat{I}_{2z}$, then the two central states $|\alpha\beta\rangle$ and $|\beta\alpha\rangle$ are depleted in population with respect to the outer states $|\alpha\alpha\rangle$ and $|\beta\beta\rangle$:

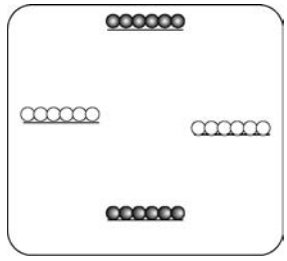

Figure 15.15
Population distribution corresponding to a density operator term $2\hat{I}_{1z}\hat{I}_{2z}$.

This population pattern is called *two-spin Zeeman order*.

Example 3. The operator $-\hat{I}_{1y}$ has a matrix representation of

$$-\hat{I}_{1y} = \frac{1}{2\mathrm{i}} \begin{pmatrix} 0 & 0 & -1 & 0 \\ 0 & 0 & 0 & -1 \\ 1 & 0 & 0 & 0 \\ 0 & 1 & 0 & 0 \end{pmatrix}$$

If $\hat{\rho}$ contains a term $-\hat{I}_{1y}$, then the spin ensemble contains single-quantum coherences belonging to spin I_1:

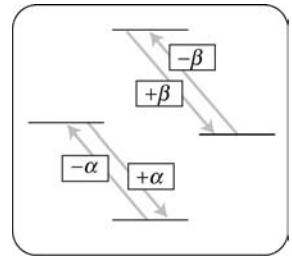

Figure 15.16
Coherences corresponding to a density operator term $-\hat{I}_{1y}$.

Single-quantum coherences are capable of inducing an NMR signal, so the presence of a term $-\hat{I}_{1y}$ in the density operator $\hat{\rho}(0)$ is associated with observable spectral peaks. For example, suppose that the receiver phase shift ϕ_{rec} is zero. If the density operator at the start of signal detection $\hat{\rho}(0)$ contains a component proportional to $-\hat{I}_{1y}$, then the (-1)-quantum coherences $\rho_{\boxed{-\beta}}(0)$ and $\rho_{\boxed{-\alpha}}(0)$ are proportional to $(1/2\mathrm{i})$. From Equation 15.12, FT of the signal generates a spectrum with two absorption peaks near the chemical shift of spin I_1:

Figure 15.17
In-phase spectral multiplet corresponding to a density operator term $-\hat{I}_{1y}$.

(This sketch is shown for the case of positive γ and positive J_{12}.) This spectral configuration is called an *in-phase multiplet* of spin I_1.

Example 4. The operator $-2\hat{I}_{1y}\hat{I}_{2z}$ has a matrix representation of

$$-2\hat{I}_{1y}\hat{I}_{2z} = \frac{1}{2\mathrm{i}} \begin{pmatrix} 0 & 0 & -1 & 0 \\ 0 & 0 & 0 & 1 \\ 1 & 0 & 0 & 0 \\ 0 & -1 & 0 & 0 \end{pmatrix}$$

If $\hat{\rho}$ contains a term $-2\hat{I}_{1y}\hat{I}_{2z}$, then the (-1)-quantum coherences $\rho_{\boxed{-\beta}}$ and $\rho_{\boxed{-\alpha}}$ have opposite sign. The spectrum obtained by Fourier transforming the signal displays two absorption peaks near the chemical shift of spin I_1, with the $\rho_{\boxed{-\beta}}$ peak inverted in sign with respect to the $\rho_{\boxed{-\alpha}}$ peak:

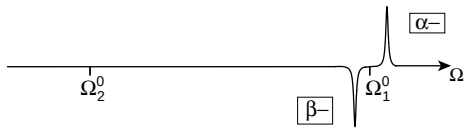

Figure 15.18
Antiphase spectral multiplet corresponding to a density operator term $-2\hat{I}_{1y}\hat{I}_{2z}$.

This spectral configuration is called an *antiphase multiplet* of spin I_1.
An antiphase multiplet of spin I_2 is produced by a density operator term $-2\hat{I}_{1z}\hat{I}_{2y}$.
Example 5. The operator $2\hat{I}_{1x}\hat{I}_{2y}$ has a matrix representation of

$$2\hat{I}_{1x}\hat{I}_{2y} = \frac{1}{2\mathrm{i}}\begin{pmatrix} & & & 1 \\ & & -1 & \\ & 1 & & \\ -1 & & & \end{pmatrix}$$

The presence of this operator as a component of $\hat{\rho}$ indicates that the spin ensemble contains zero- and double-quantum coherences:

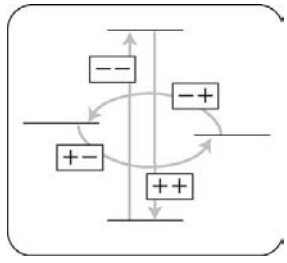

Figure 15.19
Coherences corresponding to a density operator term $2\hat{I}_{1x}\hat{I}_{2y}$.

Unlike single-quantum coherences, zero- and double-quantum coherences do not induce NMR signals, and hence cannot be associated with a particular configuration of peaks in the spectrum. These coherences are important, nevertheless because they may be converted by r.f. pulses into single-quantum coherences, which *do* induce signals.

It is also possible to use shift and projection operators to determine the configuration of populations and coherences in a product operator term, without writing out the matrices. For example, suppose that the density operator is

$$\hat{\rho} = \ldots + r\,2\hat{I}_{1y}\hat{I}_{2x} + \ldots$$

where r is a real number. The amplitude of the zero-quantum coherence $\rho_{\boxed{-+}}$ may be calculated as follows:

$$\begin{aligned}\hat{\rho} &= \ldots + r\,2\frac{1}{2\mathrm{i}}\left(\hat{I}_1^+ - \hat{I}_1^-\right)\frac{1}{2}\left(\hat{I}_2^+ + \hat{I}_2^-\right) + \ldots \\ &= \ldots - \frac{r}{2\mathrm{i}}\hat{I}_1^-\hat{I}_2^+ + \ldots\end{aligned}$$

The coherence $\rho_{\boxed{-+}}$ is the coefficient of $\hat{I}_1^-\hat{I}_2^+$ in the density operator, and is equal to $-r/(2\mathrm{i})$ in this case.
Similar calculations may be made for any other population or coherence.

15.6.3 Spin orientations

What do the product operator terms mean physically?

In this section, I draw schematic pictures of microscopic spin orientations for a few different members of the ensemble. I distinguish between the two sets of spins by using a 'ball' for spins 1 and a 'square' for spins 2. To bring out the features of each product operator, I have greatly exaggerated the preference of the spins for particular configurations, which is sometimes misleading. In practice, the statistical tendencies are exceedingly small (around 10^{-5}), and would be invisible if drawn realistically.

Example 1. The operator $\hat{I}_{1z}$. If the spin density operator contains a term $\hat{I}_{1z}$, there is a net polarization of spins I_1 along the magnetic field direction (z-axis). The polarizations of spins I_2 are isotropically distributed:

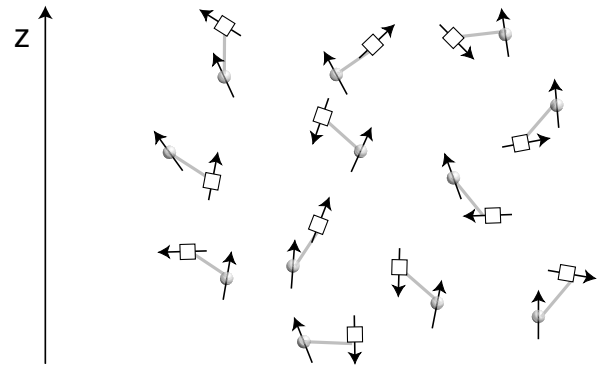

Figure 15.20
Microscopic spin polarizations corresponding to a density operator term $\hat{I}_{1z}$. Spins I_1 are shown as spheres; spins I_2 are shown as squares.

Example 2. The operator $\hat{I}_{2z}$. The presence of a term $\hat{I}_{2z}$ in the density operator implies that there is a net polarization of spins I_2 along the magnetic field, and the polarizations of spins I_1 are isotropically distributed:

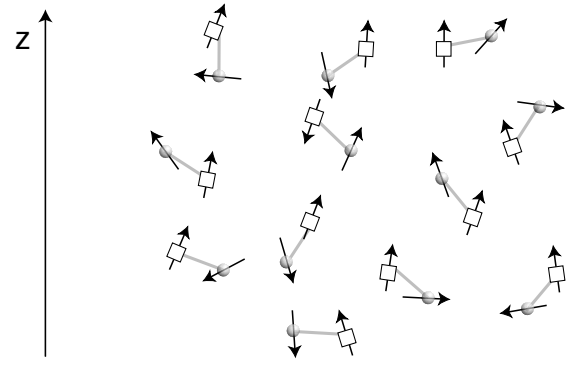

Figure 15.21
Microscopic spin polarizations corresponding to a density operator term $\hat{I}_{2z}$.

Example 3. The operator $\hat{I}_{1x}$. The presence of a term $\hat{I}_{1x}$ in the density operator implies that the polarization vectors of spins I_1 tend to be aligned along the x-axis. The polarization vectors of spins I_2 have no preferential orientation (see Figure 15.22).

The following examples introduce the new concept of *correlations* between the polarizations of the two spins.

Example 4. The operator $2\hat{I}_{1z}\hat{I}_{2z}$. The presence of the two-spin Zeeman order term $2\hat{I}_{1z}\hat{I}_{2z}$ in the density operator implies that there is *no* net tendency for either of the spin species to be polarized along the z-axis. Nevertheless, there is a *correlation* between the spin polarizations. Although the polarization direction for a given spin I_1 is unpredictable, its neighbour I_2 is likely to have the *same* direction of polarization along the magnetic field, as shown in Figure 15.23. Note that the correlation only applies to the z-components of the spin polarization vectors.

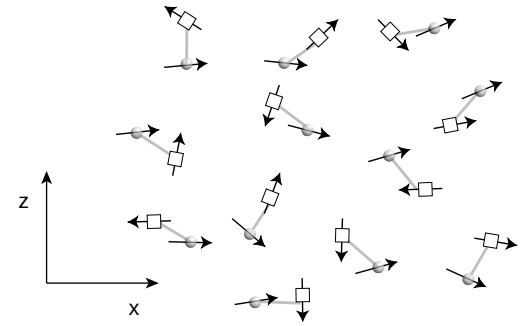

Figure 15.22
Microscopic spin polarizations corresponding to a density operator term $\hat{I}_{1x}$.

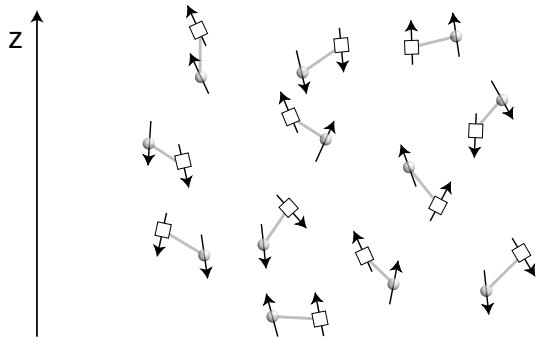

Figure 15.23
Microscopic spin polarizations corresponding to a density operator term $2\hat{I}_{1z}\hat{I}_{2z}$.

The concept of correlation is subtle but important. The following analogy might help. Choose at random a large number of married couples. Now pick blindly one married pair from this 'ensemble'. There is no way of predicting in advance whether the man is shorter or taller than the average. The same goes for the woman. However, one may state with some confidence that if the man is shorter than the average, then so is the woman. Similarly, if the chosen man is taller than the average, then the woman also tends to be taller. This is because height is strongly *correlated* within married couples.

Something analogous is going on for a spin-pair ensemble in a density operator state containing the term $2\hat{I}_{1z}\hat{I}_{2z}$. The z-components of the polarizations are randomly distributed, but correlated within each spin pair.

Example 5. The operator $2\hat{I}_{1x}\hat{I}_{2x}$. The presence of the product operator term $2\hat{I}_{1x}\hat{I}_{2x}$ implies a correlation in the x-components of the spin polarizations:

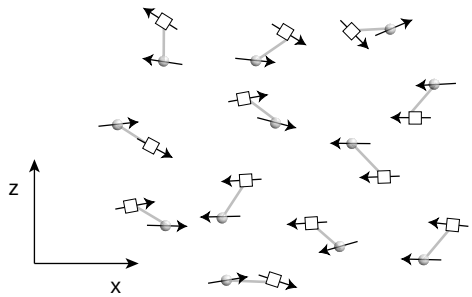

Figure 15.24
Microscopic spin polarizations corresponding to a density operator term $2\hat{I}_{1x}\hat{I}_{2x}$.

There is no *individual* tendency for either set of spins to be polarized in a particular direction. However, if a given spin is polarized along $+x$, then its neighbour tends also to be polarized along $+x$. Similarly, if a given spin is polarized along $-x$, then its neighbour tends also to be polarized along $-x$.

There are also more complicated possibilites. For example, the presence of a term $2\hat{I}_{1z}\hat{I}_{2x}$ implies a correlation of the z-components of the polarizations of spins I_1 with the x-components of the polarizations of spins I_2, i.e. if a spin I_1 is polarized along the z-axis, then its neighbour tends to be polarized along the x-axis, and so on. It is difficult to convey these properties accurately in a simple diagram, and I will not attempt it.

The presence of a *negative* term $-2\hat{I}_{1z}\hat{I}_{2z}$ in the spin density operator implies *anticorrelation*. The two members of a spin pair tend to have *opposite* spin polarizations along the z-axis.

The above diagrams shed light on the physical significance of zero- and double-quantum coherences. It is sometimes stated that multiple-quantum coherences are intrinsically quantum mechanical. This conclusion is false. Zero- and double-quantum coherences are contained in product operator terms like $2\hat{I}_{1x}\hat{I}_{2x}$, which merely indicate certain modes of correlation of the transverse spin polarizations. Correlation is by no means a quantum-mechanical concept, as illustrated by the married couple analogy given above.

In general, the spin density operator contains a sum of product operator terms, as in Equation 15.13. The statistical distribution of the microscopic spin polarizations is therefore a superposition of the elemental distributions described above. This is quite difficult to visualize, and an analogy may help again. A random selection of people from a crowd includes single people as well as married couples. The married couples display a correlation of characteristics, such as height (the two-spin terms, such as $2\hat{I}_{1x}\hat{I}_{2y}$); the single people are, for the moment, uncorrelated with anyone else (the one-spin terms, such as $\hat{I}_{1z}$). A statistical measurement of the entire population, without knowledge of marital status, displays a superposition of the statistical properties of these two independent segments of the population. As time goes by, the interactions between single people lead to the development of new correlated states, and also their destruction. These phenomena also have their analogy in the world of the spins (see below).

15.7 Thermal Equilibrium

When the spin ensemble is left undisturbed for a sufficient amount of time, it adopts a state of thermal equilibrium with respect to the molecular environment. The thermal equilibrium spin density operator may be estimated by making use of the same assumptions as in Section 11.3, namely: (1) no coherences; (2) populations determined by the Boltzmann distribution at the temperature of the molecular environment.

For example, the population of state $|\alpha\alpha\rangle$ in thermal equilibrium at temperature T is given by

$$\rho^{\mathrm{eq}}_{[\alpha\alpha]} = \frac{\exp\{-\hbar\omega_{\alpha\alpha}/k_{\mathrm{B}}T\}}{\sum_s \exp\{-\hbar\omega_s/k_{\mathrm{B}}T\}}$$

where k_{B} is the Boltzmann constant and the sum is over all four eigenstates. Employing the high-temperature appoximation ($k_{\mathrm{B}}T$ much greater than 1Q spin energy differences), the exponentials in this expression may be written as

$$\exp\{-\hbar\omega_{\alpha\alpha}/k_{\mathrm{B}}T\} \cong 1 - \frac{\hbar\omega_{\alpha\alpha}}{k_{\mathrm{B}}T}$$

Since the sum of the fixed-frame energies is zero (see Equation 15.2):

$$\omega_{\alpha\alpha} + \omega_{\beta\alpha} + \omega_{\alpha\beta} + \omega_{\beta\beta} = 0$$

the sum in the denominator reduces to

$$\sum_s \exp\{-\hbar\omega_s/k_{\mathrm{B}}T\} \cong 4$$

within the same level of approximation. The population of state $|\alpha\alpha\rangle$ is therefore given by

$$\rho^{\mathrm{eq}}_{\boxed{\alpha\alpha}} \cong \frac{1}{4}\left(1 - \frac{\hbar\omega_{\alpha\alpha}}{k_{\mathrm{B}}T}\right)$$

Now, from Equation 15.2, the energy of state $|\alpha\alpha\rangle$ is

$$\begin{aligned}\omega_{\alpha\alpha} &= \frac{1}{2}\omega_1^0 + \frac{1}{2}\omega_2^0 + \frac{1}{2}\pi J_{12} \\ &= -\gamma B^0 + \left\{-\frac{1}{2}\gamma B^0(\delta_1 + \delta_2) + \frac{1}{2}\pi J_{12}\right\}\end{aligned}$$

Under ordinary circumstances, the second term is around five orders of magnitude smaller than the first, and may be ignored for the purposes of estimating the thermal equilibrium populations. This is called the *high-field approximation*. Within the twin approximations of high field and high temperature, the thermal equilibrium population of state $|\alpha\alpha\rangle$ may be expressed as

$$\rho^{\mathrm{eq}}_{\boxed{\alpha\alpha}} \cong \frac{1}{4} + \frac{1}{4}\mathbb{B}$$

where the Boltzmann factor is defined as

$$\mathbb{B} = \frac{\hbar\gamma B^0}{k_{\mathrm{B}}T} \tag{15.14}$$

as before.

Repetition of these arguments gives the following values for the thermal equilibrium populations:

$$\begin{aligned}\rho^{\mathrm{eq}}_{\boxed{\alpha\alpha}} &\cong \frac{1}{4} + \frac{1}{4}\mathbb{B} & \rho^{\mathrm{eq}}_{\boxed{\beta\alpha}} &\cong \frac{1}{4} \\ \rho^{\mathrm{eq}}_{\boxed{\alpha\beta}} &\cong \frac{1}{4} & \rho^{\mathrm{eq}}_{\boxed{\beta\beta}} &\cong \frac{1}{4} - \frac{1}{4}\mathbb{B}\end{aligned}$$

which has the following form:

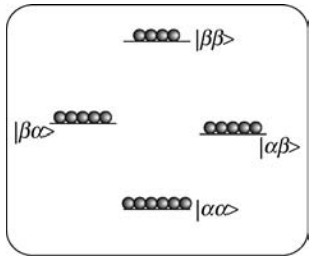

Figure 15.25
Thermal equilibrium populations in the AX spin ensemble.

The lowest energy state $|\alpha\alpha\rangle$ is the most populated; the highest energy state $|\beta\beta\rangle$ is the least populated. The two central energy states $|\alpha\beta\rangle$ and $|\beta\alpha\rangle$ are approximately degenerate and have the same populations in thermal equilibrium.

The thermal equilibrium density matrix, for an ensemble of spin-1/2 pairs, is therefore

$$\hat{\rho}^{\mathrm{eq}} \cong \frac{1}{4}\begin{pmatrix} 1+\mathbb{B} & & & \\ & 1 & & \\ & & 1 & \\ & & & 1-\mathbb{B} \end{pmatrix}$$

or in operator form:

$$\begin{aligned} \hat{\rho}^{\mathrm{eq}} &\cong \frac{1}{4}\widehat{1} + \frac{1}{4}\mathbb{B}\hat{I}_z \\ &= \frac{1}{4}\widehat{1} + \frac{1}{4}\mathbb{B}\hat{I}_{1z} + \frac{1}{4}\mathbb{B}\hat{I}_{2z} \end{aligned} \tag{15.15}$$

This density operator may now be used as a starting point for product operator calculations of the spin dynamics.

15.8 Radio-Frequency Pulses

Suppose that a strong, short, r.f. pulse is applied to the spin-pair ensemble:

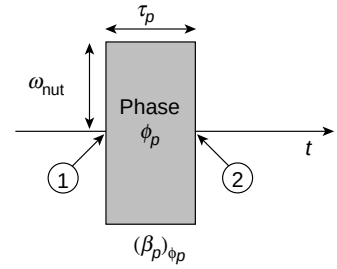

Figure 15.26
An r.f. pulse.

The flip angle of the pulse is $\beta_{\mathrm{p}} = \omega_{\mathrm{nut}}\tau_{\mathrm{p}}$, where the nutation frequency ω_{nut} is the amplitude of the r.f. field, measured in frequency units, and τ_{p} is the duration of the pulse.

The pulse duration τ_{p} is assumed to be short enough that the resonance offsets and J-coupling cause negligible evolution during the pulse.

If these conditions are satisfied, then only the effect of the r.f. field during the pulse is important. The r.f. field affects the two spins equally. For a pair of spins-1/2, the rotating-frame spin Hamiltonian during the pulse is

$$\widehat{\mathcal{H}}_{\mathrm{p}} \cong \omega_{\mathrm{nut}}\left(\hat{I}_x \cos\phi_{\mathrm{p}} + \hat{I}_y \sin\phi_{\mathrm{p}}\right)$$

where

$$\begin{aligned} \hat{I}_x &= \hat{I}_{1x} + \hat{I}_{2x} \\ \hat{I}_y &= \hat{I}_{1y} + \hat{I}_{2y} \end{aligned}$$

I first consider the effect of the pulse on a single spin pair, and then on an ensemble of spin pairs.

15.8.1 Rotations of a single spin pair

Consider a single spin pair in a rotating-frame state $|\psi\rangle_{①}$ before the pulse. During the pulse, the spin state evolves according to the time-dependent Schrödinger equation:

$$\frac{\mathrm{d}}{\mathrm{d}t}|\psi\rangle(t) = -\mathrm{i}\widehat{\mathcal{H}}_{\mathrm{p}}|\psi\rangle(t)$$

with the solution

$$|\psi\rangle_{②} = \widehat{R}_{\phi_{\mathrm{p}}}(\beta_{\mathrm{p}})|\psi\rangle_{①}$$

where the rotation operator is

$$\widehat{R}_{\phi_{\mathrm{p}}}(\beta_{\mathrm{p}}) = \exp\{-\mathrm{i}\widehat{\mathcal{H}}_{\mathrm{p}}\tau_{\mathrm{p}}\}$$

Since all operators of spin I_1 commute with the operators of spin I_2, the spin-pair rotation operator may be factorized:

$$\widehat{R}_{\phi_{\mathrm{p}}}(\beta_{\mathrm{p}}) = \widehat{R}_{1,\phi_{\mathrm{p}}}(\beta_{\mathrm{p}})\widehat{R}_{2,\phi_{\mathrm{p}}}(\beta_{\mathrm{p}})$$

where the rotation operators for the individual spins are

$$\widehat{R}_{1,\phi_{\mathrm{p}}}(\beta_{\mathrm{p}}) = \exp\{-\mathrm{i}\beta_{\mathrm{p}}\left(\hat{I}_{1x}\cos\phi_{\mathrm{p}} + \hat{I}_{1y}\sin\phi_{\mathrm{p}}\right)\}$$

$$\widehat{R}_{2,\phi_{\mathrm{p}}}(\beta_{\mathrm{p}}) = \exp\{-\mathrm{i}\beta_{\mathrm{p}}\left(\hat{I}_{2x}\cos\phi_{\mathrm{p}} + \hat{I}_{2y}\sin\phi_{\mathrm{p}}\right)\}$$

Repeating the discussion in Section 10.8, these rotation operators may be written as

$$\widehat{R}_{1,\phi_{\mathrm{p}}}(\beta_{\mathrm{p}}) = \widehat{R}_{1z}(\phi_{\mathrm{p}})\widehat{R}_{1x}(\beta_{\mathrm{p}})\widehat{R}_{1z}(-\phi_{\mathrm{p}})$$

where

$$\widehat{R}_{1z}(\phi_{\mathrm{p}}) = \exp\{-\mathrm{i}\phi_{\mathrm{p}}\hat{I}_{1z}\}$$

$$\widehat{R}_{1x}(\beta_{\mathrm{p}}) = \exp\{-\mathrm{i}\beta_{\mathrm{p}}\hat{I}_{1x}\}$$

and similarly for the operators of spin I_2.

It is possible to examine the effect of the pulse on an individual spin pair by using the matrix representations of the rotation operators. The matrix representation of $\widehat{R}_{\phi_{\mathrm{p}}}(\beta_{\mathrm{p}})$ is given by the direct product of the individual rotation operators:

$$\widehat{R}_{\phi_{\mathrm{p}}}(\beta_{\mathrm{p}}) = \widehat{R}_{1,\phi_{\mathrm{p}}}(\beta_{\mathrm{p}})\widehat{R}_{2,\phi_{\mathrm{p}}}(\beta_{\mathrm{p}}) = \begin{pmatrix} c & -\mathrm{i}se_{-} \\ -\mathrm{i}se_{+} & c \end{pmatrix} \otimes \begin{pmatrix} c & -\mathrm{i}se_{-} \\ -\mathrm{i}se_{+} & c \end{pmatrix}$$

$$= \begin{pmatrix} c^2 & -\mathrm{i}sce_{-} & -\mathrm{i}sce_{-} & -s^2e_{-}^2 \\ -\mathrm{i}sce_{+} & c^2 & -s^2 & -\mathrm{i}sce_{-} \\ -\mathrm{i}sce_{+} & -s^2 & c^2 & -\mathrm{i}sce_{-} \\ -s^2e_{-}^2 & -\mathrm{i}sce_{+} & -\mathrm{i}sce_{+} & c^2 \end{pmatrix}$$

using the abbreviations

$$c = \cos\tfrac{1}{2}\beta_{\mathrm{p}}$$

$$s = \sin\tfrac{1}{2}\beta_{\mathrm{p}}$$

$$e_{\pm} = \exp\{\pm\mathrm{i}\phi_{\mathrm{p}}\}$$

For example, suppose that the spin pair is in the state $|\alpha\alpha\rangle$ and a pulse $(\pi/2)_x$ is applied. The spin state after the pulse may be calculated as follows:

$$|\psi\rangle_{②} = \frac{1}{2}\begin{pmatrix} 1 & -\mathrm{i} & -\mathrm{i} & -1 \\ -\mathrm{i} & 1 & -1 & -\mathrm{i} \\ -\mathrm{i} & -1 & 1 & -\mathrm{i} \\ -1 & -\mathrm{i} & -\mathrm{i} & 1 \end{pmatrix}\begin{pmatrix} 1 \\ 0 \\ 0 \\ 0 \end{pmatrix} = \frac{1}{2}\begin{pmatrix} 1 \\ -\mathrm{i} \\ -\mathrm{i} \\ -1 \end{pmatrix}$$

The pulse transforms the stationary state $|\alpha\alpha\rangle$ into a superposition of all four stationary states:

$$|\psi\rangle_{②} = \frac{1}{2}\{|\alpha\alpha\rangle - \mathrm{i}|\alpha\beta\rangle - \mathrm{i}|\beta\alpha\rangle - |\beta\beta\rangle\}$$

15.8.2 Rotations of the spin density operator

The transformation of the spin density operator by the r.f. pulse is easily calculated by the 'sandwich equation':

$$\hat{\rho}_{②} = \widehat{R}_{\phi_\mathrm{p}}(\beta_\mathrm{p})\hat{\rho}_{①}\widehat{R}_{\phi_\mathrm{p}}(-\beta_\mathrm{p})$$

Consider, for example, the case where the spin density operator is initially in thermal equilibrium:

$$\hat{\rho}_{①} = \frac{1}{4}\widehat{1} + \frac{1}{4}\mathbb{B}\left(\hat{I}_{1z} + \hat{I}_{2z}\right)$$

If a strong $(\pi/2)_x$ pulse is applied, then the state after the pulse may be calculated from the matrix representations:

$$\begin{aligned}\hat{\rho}_{②} &= \widehat{R}_x(\beta_\mathrm{p})\hat{\rho}_{①}\widehat{R}_x(-\beta_\mathrm{p}) \\ &= \frac{1}{2}\begin{pmatrix} 1 & -\mathrm{i} & -\mathrm{i} & -1 \\ -\mathrm{i} & 1 & -1 & -\mathrm{i} \\ -\mathrm{i} & -1 & 1 & -\mathrm{i} \\ -1 & -\mathrm{i} & -\mathrm{i} & 1 \end{pmatrix} \times \frac{1}{4}\begin{pmatrix} 1+\mathbb{B} & & & \\ & 1 & & \\ & & 1 & \\ & & & 1-\mathbb{B} \end{pmatrix} \times \frac{1}{2}\begin{pmatrix} 1 & \mathrm{i} & \mathrm{i} & -1 \\ \mathrm{i} & 1 & -1 & \mathrm{i} \\ \mathrm{i} & -1 & 1 & \mathrm{i} \\ -1 & \mathrm{i} & \mathrm{i} & 1 \end{pmatrix} \\ &= \frac{1}{4}\begin{pmatrix} 1 & \frac{1}{2}\mathrm{i}\mathbb{B} & \frac{1}{2}\mathrm{i}\mathbb{B} & 0 \\ -\frac{1}{2}\mathrm{i}\mathbb{B} & 1 & 0 & \frac{1}{2}\mathrm{i}\mathbb{B} \\ -\frac{1}{2}\mathrm{i}\mathbb{B} & 0 & 1 & \frac{1}{2}\mathrm{i}\mathbb{B} \\ 0 & \frac{1}{2}\mathrm{i}\mathbb{B} & \frac{1}{2}\mathrm{i}\mathbb{B} & 1 \end{pmatrix}\end{aligned}$$

This may be identified as a representation of the operator:

$$\hat{\rho}_{②} = \frac{1}{4}\widehat{1} - \frac{1}{4}\mathbb{B}\left(\hat{I}_{1y} + \hat{I}_{2y}\right)$$

The pulse rotates both z-operators by $\pi/2$ around the x-axis, transforming them into $-y$-operators:

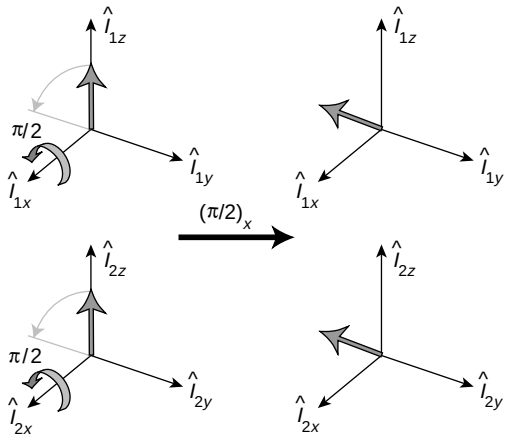

Figure 15.27
A $(\pi/2)_x$ pulse transforms the thermal equilibrium AX density operator.

In a second example, consider an initial density operator of the form

$$\hat{\rho}_{①} = \ldots + r2\hat{I}_{1x}\hat{I}_{2y} + \ldots$$

where r is a real number. The matrix representation of $2\hat{I}_{1x}\hat{I}_{2y}$ may be found in the usual way:

$$2\hat{I}_{1x}\hat{I}_{2y} = 2\,\frac{1}{2}\begin{pmatrix}0 & 1\\ 1 & 0\end{pmatrix} \otimes \frac{1}{2\mathrm{i}}\begin{pmatrix}0 & 1\\ -1 & 0\end{pmatrix} = \frac{1}{2\mathrm{i}}\begin{pmatrix}0 & 0 & 0 & 1\\ 0 & 0 & -1 & 0\\ 0 & 1 & 0 & 0\\ -1 & 0 & 0 & 0\end{pmatrix}$$

The density operator contains zero- and double-quantum coherences.

The action of the pulse on the multiple-quantum coherences may be calculated as follows:

$$\widehat{R}_x(\pi/2)2\hat{I}_{1x}\hat{I}_{2y}\widehat{R}_x(-\pi/2) =$$

$$\frac{1}{8\mathrm{i}}\begin{pmatrix}1 & -\mathrm{i} & -\mathrm{i} & -1\\ -\mathrm{i} & 1 & -1 & -\mathrm{i}\\ -\mathrm{i} & -1 & 1 & -\mathrm{i}\\ -1 & -\mathrm{i} & -\mathrm{i} & 1\end{pmatrix} \times \begin{pmatrix}0 & 0 & 0 & 1\\ 0 & 0 & -1 & 0\\ 0 & 1 & 0 & 0\\ -1 & 0 & 0 & 0\end{pmatrix} \times \begin{pmatrix}1 & \mathrm{i} & \mathrm{i} & -1\\ \mathrm{i} & 1 & -1 & \mathrm{i}\\ \mathrm{i} & -1 & 1 & \mathrm{i}\\ -1 & \mathrm{i} & \mathrm{i} & 1\end{pmatrix}$$

$$= \frac{1}{2}\begin{pmatrix}0 & 0 & 1 & 0\\ 0 & 0 & 0 & -1\\ 1 & 0 & 0 & 0\\ 0 & -1 & 0 & 0\end{pmatrix} = 2\,\frac{1}{2}\begin{pmatrix}0\,1\\ 1\,0\end{pmatrix} \otimes \frac{1}{2}\begin{pmatrix}1 & 0\\ 0 & -1\end{pmatrix} = 2\hat{I}_{1x}\hat{I}_{2z}$$

The multiple-quantum coherences are transformed by the pulse into antiphase single-quantum coherences. A 'rotation picture' again clarifies this transformation:

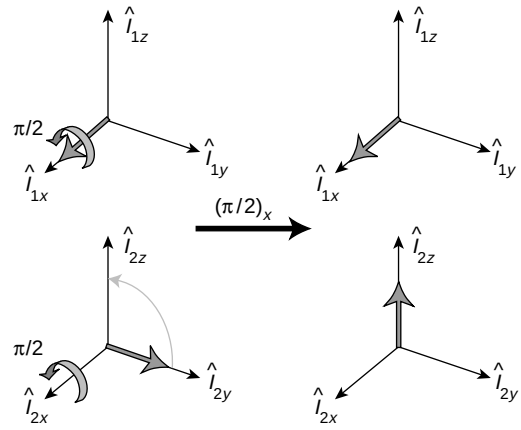

Figure 15.28
A $(\pi/2)_x$ pulse transforms the density operator term $2\hat{I}_{1x}\hat{I}_{2y}$.

15.8.3 Operator transformations

The matrix multiplication scheme described above is straightforward, but clumsy. Much work is saved by using the *commutation relationships* of the operators, rather than their matrix representations.

Consider, for example, the transformation of multiple-quantum coherences, as analysed above. The same relationship may also be deduced in the following way:

$$\begin{aligned}\widehat{R}_x(\pi/2)2\hat{I}_{1x}\hat{I}_{2y}\widehat{R}_x(-\pi/2) &= \widehat{R}_{1x}(\pi/2)\widehat{R}_{2x}(\pi/2)\cdot 2\hat{I}_{1x}\hat{I}_{2y}\cdot\widehat{R}_{1x}(-\pi/2)\widehat{R}_{2x}(-\pi/2)\\ &= 2\,\widehat{R}_{1x}(\pi/2)\hat{I}_{1x}\widehat{R}_{1x}(-\pi/2)\cdot\widehat{R}_{2x}(\pi/2)\hat{I}_{2y}\widehat{R}_{2x}(-\pi/2)\end{aligned}$$

The last step follows because all operators that act on spins I_1 commute with all operators acting on spins I_2.

The first term in the product is given by

$$\widehat{R}_{1x}(\pi/2)\hat{I}_{1x}\widehat{R}_{1x}(-\pi/2) = \hat{I}_{1x}$$

since the operator for a rotation around the x-axis commutes with $\hat{I}_{1x}$.

The second term $\widehat{R}_{2x}(\pi/2)\hat{I}_{2y}\widehat{R}_{2x}(-\pi/2)$ may be analysed using the *cyclic commutation relationships* of the angular momentum operators for spin I_2:

$$\left[\hat{I}_{2x}, \hat{I}_{2y}\right] = \mathrm{i}\hat{I}_{2z} \qquad \circlearrowleft$$

As shown in Section 6.6.2, cyclic commutation leads to the following property:

$$\widehat{R}_{2x}\left(\beta_\mathrm{p}\right)\hat{I}_{2y}\widehat{R}_{2x}\left(-\beta_\mathrm{p}\right) = \hat{I}_{2y}\cos\beta_\mathrm{p} + \hat{I}_{2z}\sin\beta_\mathrm{p}$$

The transformation

$$2\hat{I}_{1x}\hat{I}_{2y} \xrightarrow{(\pi/2)_x} 2\hat{I}_{1x}\hat{I}_{2z}$$

follows easily.

The transformation rules for a pulse with phase $\phi_\mathrm{p} = 0$ ('x-pulse') may be depicted as

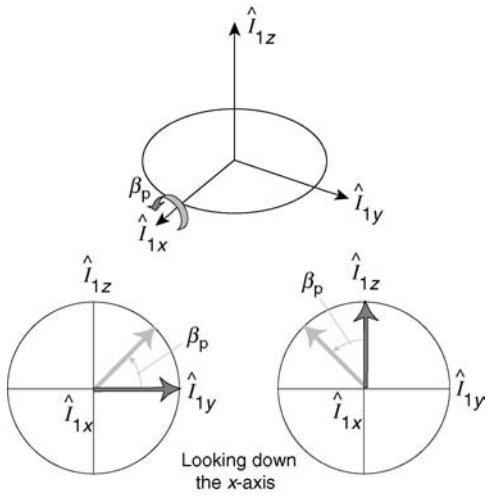

Figure 15.29
Transformation rules for a pulse with phase $\phi_p = 0$.

and summarized as follows:

$$
\begin{aligned}
\tfrac{1}{2}\widehat{1}_1 &\rightarrow \tfrac{1}{2}\widehat{1}_1 \\
\hat{I}_{1x} &\rightarrow \hat{I}_{1x} \\
\hat{I}_{1y} &\rightarrow \hat{I}_{1y}\cos\beta_p + \hat{I}_{1z}\sin\beta_p \\
\hat{I}_{1z} &\rightarrow \hat{I}_{1z}\cos\beta_p - \hat{I}_{1y}\sin\beta_p
\end{aligned}
\tag{15.16}
$$

and similarly for spin I_2.

The transformation rules for a pulse with phase $\phi_p = \pi/2$ ('y-pulse') may be depicted as:

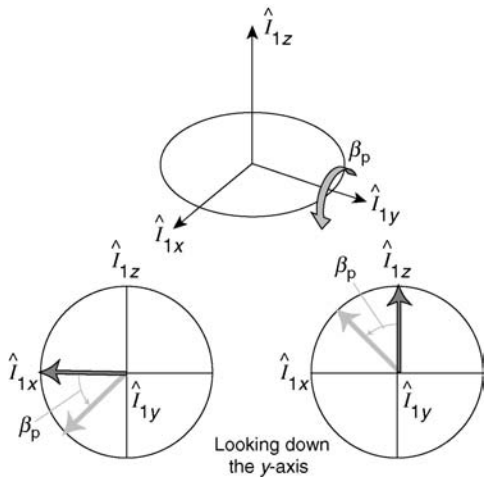

Figure 15.30
Transformation rules for a pulse with phase $\phi_p = \pi/2$.

and summarized as follows:

$$\begin{aligned} \tfrac{1}{2}\widehat{1}_1 &\rightarrow \tfrac{1}{2}\widehat{1}_1 \\ \hat{I}_{1x} &\rightarrow \hat{I}_{1x}\cos\beta_{\mathrm{p}} - \hat{I}_{1z}\sin\beta_{\mathrm{p}} \\ \hat{I}_{1y} &\rightarrow \hat{I}_{1y} \\ \hat{I}_{1z} &\rightarrow \hat{I}_{1z}\cos\beta_{\mathrm{p}} + \hat{I}_{x}\sin\beta_{\mathrm{p}} \end{aligned} \tag{15.17}$$

and similarly for spin I_2.

These transformations have a straightforward physical interpretation in terms of the microscopic polarization states of the spins. For example, a density operator term proportional to $\hat{I}_{1z}$ indicates a preferential polarization of spins I_1 along the z-axis, uncorrelated with the states of spins I_2. A $(\pi/2)_y$ pulse rotates all spin polarizations around the y-axis through an angle of $\pi/2$, so that spins I_1 become preferentially polarized along the x-axis after the pulse, but are still uncorrelated with spins I_2.

The transformation properties of the individual spin operators, for pulses of any phase, are summarized in Section 11.8.

15.9 Free Evolution of the Product Operators

Now consider the free evolution of the spin density operator between the pulses. It is possible to perform this calculation using the individual populations and coherences, as discussed in Section 15.4. However, in many cases, the calculations are made more comfortable by using the cyclic commutation properties of the product operators.

Assume that the spin density operator $\hat{\rho}_{②}$ is known at a time point ②, and that we want to calculate it at a later time ③. The two time points are separated by an interval τ of free evolution in the absence of applied r.f. fields.

If relaxation is ignored, the evolution may be calculated by the 'sandwich equation':

$$\hat{\rho}_{③} = \widehat{U}(\tau)\hat{\rho}_{①}\,\widehat{U}(\tau)^{-1}$$

where

$$\widehat{U} = \exp\{-\mathrm{i}\widehat{\mathcal{H}}^0\tau\}$$

and $\widehat{\mathcal{H}}^0$ is the weakly coupled spin Hamiltonian in the rotating frame (Equation 15.7).

The spin Hamiltonian is the sum of three terms, all of which commute with each other:

$$\widehat{\mathcal{H}}^0 = \widehat{\mathcal{H}}_1^0 + \widehat{\mathcal{H}}_2^0 + \widehat{\mathcal{H}}_{12}^0$$

where

$$\widehat{\mathcal{H}}_1^0 = \Omega_1^0\hat{I}_{1z}$$

$$\widehat{\mathcal{H}}_2^0 = \Omega_2^0\hat{I}_{2z}$$

$$\widehat{\mathcal{H}}_{12}^0 = \pi J_{12}\,2\hat{I}_{1z}\hat{I}_{2z}$$

and

$$\left[\widehat{\mathcal{H}}_1^0, \widehat{\mathcal{H}}_2^0\right] = \left[\widehat{\mathcal{H}}_1^0, \widehat{\mathcal{H}}_{12}^0\right] = \left[\widehat{\mathcal{H}}_2^0, \widehat{\mathcal{H}}_{12}^0\right] = 0$$

From Equation 6.32, the evolution operator may be factorized into three commuting terms:

$$\widehat{U}(\tau) = \widehat{U}_1(\tau)\widehat{U}_2(\tau)\widehat{U}_{12}(\tau) \tag{15.18}$$

where

$$\left[\widehat{U}_1, \widehat{U}_2\right] = \left[\widehat{U}_1, \widehat{U}_{12}\right] = \left[\widehat{U}_2, \widehat{U}_{12}\right] = 0$$

The mutual commutation of these terms implies that the product in Equation 15.18 may be written in any order.
The term $\widehat{U}_1$ is the *chemical shift propagator for spins* I_1:

$$\widehat{U}_1 = \exp\{-\mathrm{i}\Omega_1^0\tau\ \hat{I}_{1z}\} = \widehat{R}_{1z}\left(\Omega_1^0\tau\right) \tag{15.19}$$

The term $\widehat{U}_2$ is the *chemical shift propagator for spins* I_2:

$$\widehat{U}_2 = \exp\{-\mathrm{i}\Omega_2^0\tau\ \hat{I}_{2z}\} = \widehat{R}_{2z}\left(\Omega_2^0\tau\right) \tag{15.20}$$

The term $\widehat{U}_{12}$ is the *J-coupling propagator*:

$$\widehat{U}_{12} = \exp\{-\mathrm{i}\pi J_{12}\tau\ 2\hat{I}_{1z}\hat{I}_{2z}\} \tag{15.21}$$

The spin density operator at time point ③ may be calculated using any order for the three operations:

$$\hat{\rho}_{③} = \underbrace{\underbrace{\underbrace{\widehat{U}_{12}(\tau)\ \widehat{U}_2(\tau)\ \underbrace{\widehat{U}_1(\tau)\hat{\rho}_{②}\ \widehat{U}_1(\tau)^{-1}}_{\text{chemical shift of spin } I_1}\ \widehat{U}_2(\tau)^{-1}}_{\text{chemical shift of spin } I_2}\ \widehat{U}_{12}(\tau)^{-1}}_{\text{spin–spin coupling}}}$$

or

$$\hat{\rho}_{③} = \underbrace{\underbrace{\underbrace{\widehat{U}_{12}(\tau)\ \widehat{U}_1(\tau)\ \underbrace{\widehat{U}_2(\tau)\hat{\rho}_{②}\ \widehat{U}_2(\tau)^{-1}}_{\text{chemical shift of spin } I_2}\ \widehat{U}_1(\tau)^{-1}}_{\text{chemical shift of spin } I_1}\ \widehat{U}_{12}(\tau)^{-1}}_{\text{spin–spin coupling}}}$$

or

$$\hat{\rho}_{③} = \underbrace{\underbrace{\underbrace{\widehat{U}_2(\tau)\ \ \widehat{U}_1(\tau)\ \underbrace{\widehat{U}_{12}(\tau)\hat{\rho}_{②}\ \widehat{U}_{12}(\tau)^{-1}}_{\text{spin–spin coupling}}\ \widehat{U}_1(\tau)^{-1}}_{\text{chemical shift of spin } I_1}\ \ \widehat{U}_2(\tau)^{-1}}_{\text{chemical shift of spin } I_2}}$$

and so on. The order of the operations may be chosen according to the circumstances of the calculation.

Using an obvious notation, these calculation methods may be denoted as follows:

$$\hat{\rho}_{②} \xrightarrow{\Omega_1^0\tau} \xrightarrow{\Omega_2^0\tau} \xrightarrow{\pi J_{12}\tau} \hat{\rho}_{③}$$

or alternatively:

$$\hat{\rho}_{②} \xrightarrow{\Omega_2^0\tau} \xrightarrow{\Omega_1^0\tau} \xrightarrow{\pi J_{12}\tau} \hat{\rho}_{③}$$

and so on.

15.9.1 Chemical shift evolution

The transformation of the density operator under the terms $\widehat{U}_1$ and $\widehat{U}_2$ is very similar to their transformations under r.f. pulses. The only differences are: (1) the rotations occur around the z-axis, rather than around axes in the xy-plane; (2) the rotation angles are different for the two spins.

The transformation rules may be summarized as

$$\begin{aligned}
\tfrac{1}{2}\widehat{1}_1 &\xrightarrow{\Omega_1^0\tau} \tfrac{1}{2}\widehat{1}_1 \\
\hat{I}_{1x} &\longrightarrow \hat{I}_{1x}\cos\Omega_1^0\tau + \hat{I}_{1y}\sin\Omega_1^0\tau \\
\hat{I}_{1y} &\longrightarrow \hat{I}_{1y}\cos\Omega_1^0\tau - \hat{I}_{1x}\sin\Omega_1^0\tau \\
\hat{I}_{1z} &\longrightarrow \hat{I}_{1z}
\end{aligned} \qquad (15.22)$$

and depicted as follows:

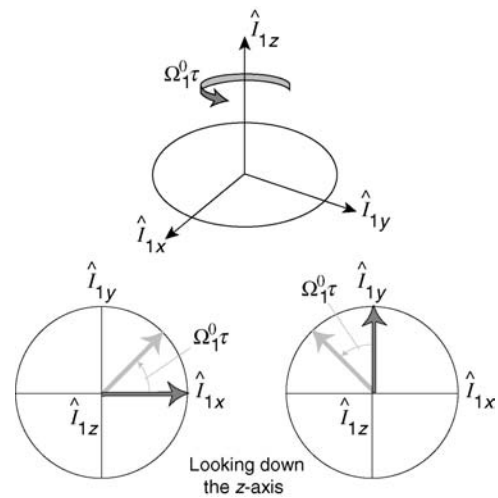

Figure 15.31
Transformation rules for the chemical shift evolution of spins I_1.

Similar relationships apply for spin I_2.

For example, the chemical shift evolution of a density operator term $\hat{I}_{1x}$ may be calculated as follows:

$$\hat{I}_{1x}$$
$$\downarrow \Omega_2^0\tau$$
$$\hat{I}_{1x}$$
$$\downarrow \Omega_1^0\tau$$
$$\hat{I}_{1x}\cos\Omega_1^0\tau + \hat{I}_{1y}\sin\Omega_1^0\tau$$

or written more formally:

$$\widehat{U}_1(\tau)\widehat{U}_2(\tau)\hat{I}_{1x}\widehat{U}_2(\tau)^{-1}\widehat{U}_1(\tau)^{-1} = \hat{I}_{1x}\cos\Omega_1^0\tau + \hat{I}_{1y}\sin\Omega_1^0\tau$$

The result is the same if the operations are taken the other way round.

Similarly, the chemical shift evolution of the product operator term $2\hat{I}_{1x}\hat{I}_{2y}$ may be calculated as follows:

$$2\hat{I}_{1x}\hat{I}_{2y}$$
$$\downarrow \Omega_1^0\tau$$
$$2\left(\hat{I}_{1x}\cos\Omega_1^0\tau + \hat{I}_{1y}\sin\Omega_1^0\tau\right)\hat{I}_{2y}$$
$$\downarrow \Omega_2^0\tau$$
$$2\hat{I}_{1x}\left(\hat{I}_{2y}\cos\Omega_2^0\tau - \hat{I}_{2x}\sin\Omega_2^0\tau\right)\cos\Omega_1^0\tau$$
$$+2\hat{I}_{1y}\left(\hat{I}_{2y}\cos\Omega_2^0\tau - \hat{I}_{2x}\sin\Omega_2^0\tau\right)\sin\Omega_1^0\tau$$

or more formally:

$$\begin{aligned}\widehat{U}_1(\tau)\widehat{U}_2(\tau)2\hat{I}_{1x}\hat{I}_{2y}\widehat{U}_2(\tau)^{-1}\widehat{U}_1(\tau)^{-1} = {} & 2\hat{I}_{1x}\hat{I}_{2y}\cos\Omega_1^0\tau\,\cos\Omega_2^0\tau - 2\hat{I}_{1x}\hat{I}_{2x}\cos\Omega_1^0\tau\,\sin\Omega_2^0\tau \\ & +2\hat{I}_{1y}\hat{I}_{2y}\sin\Omega_1^0\tau\,\cos\Omega_2^0\tau - 2\hat{I}_{1y}\hat{I}_{2x}\sin\Omega_1^0\tau\,\sin\Omega_2^0\tau\end{aligned}$$

Remember that the action of the J-coupling is not yet included.

These transformations correspond to the independent precession of the spins around the z-axis at their individual chemical shift offset frequencies.

15.9.2 J-coupling evolution

The action of the J-coupling introduces some new features. Density operator terms proportional to single-spin operators such as $\hat{I}_{1x}$ are converted into two-spin terms such as $2\hat{I}_{1y}\hat{I}_{2z}$, and vice versa. This indicates

the creation, and destruction, of correlations between the spin polarizations, under the influence of the spin–spin couplings.

The transformations of the product operator terms may be calculated from the following cyclic commutation relationships, which apply to the spin-1/2 matrix representations:

$$\begin{aligned}
\left[2\hat{I}_{1z}\hat{I}_{2z},\, \hat{I}_{1x}\right] &= \mathrm{i}2\hat{I}_{1y}\hat{I}_{2z} \circlearrowleft \\
\left[2\hat{I}_{1z}\hat{I}_{2z},\, \hat{I}_{2x}\right] &= \mathrm{i}2\hat{I}_{1z}\hat{I}_{2y} \circlearrowleft \\
\left[2\hat{I}_{1x}\hat{I}_{2z},\, \hat{I}_{1y}\right] &= \mathrm{i}2\hat{I}_{1z}\hat{I}_{2z} \circlearrowleft \\
\left[2\hat{I}_{1z}\hat{I}_{2x},\, \hat{I}_{2y}\right] &= \mathrm{i}2\hat{I}_{1z}\hat{I}_{2z} \circlearrowleft
\end{aligned} \tag{15.23}$$

The cyclic commutation relationships may be depicted geometrically:

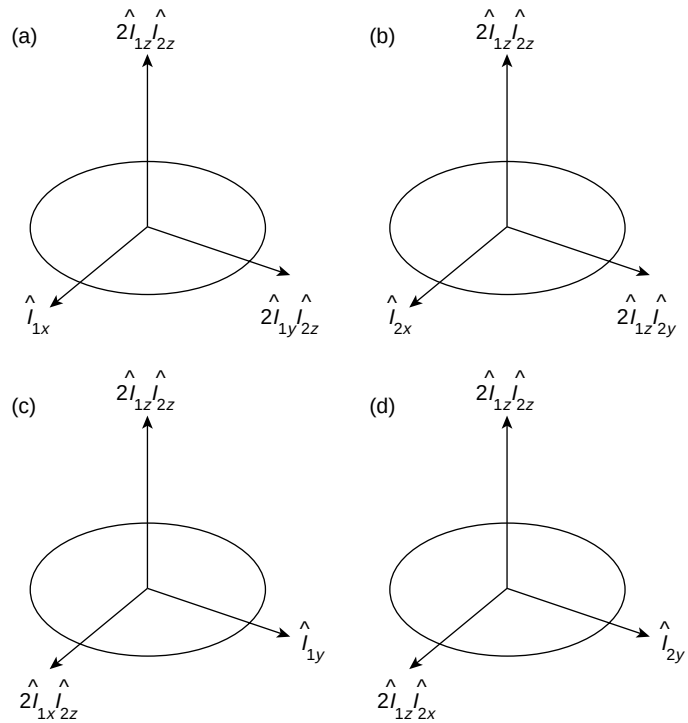

Figure 15.32
Cyclic commutation relationships of product operators.

Note the common pattern. In the right-handed axis system, with a z-operator along the vertical axis, an x-operator is always placed on the left and a y-operator on the right. If the x-operator occurs in a product with a z-operator on the left, then the z-operator is missing on the right. If the z-operator is missing on the left, then the y-operator occurs in a product with a z-operator on the right. Note also that the operators are always written with the indices 1 and 2 in the same order. This is not essential, but it simplifies the bookkeeping.

Each of the diagrams above implies a geometrical representation of the product operator transformations. For example, Figures 15.32a indicates the following transformations:

$$\widehat{U}_{12}(\tau)\hat{I}_{1x}\widehat{U}_{12}(\tau)^{-1} = \hat{I}_{1x}\cos\pi J_{12}\tau + 2\hat{I}_{1y}\hat{I}_{2z}\sin\pi J_{12}\tau$$

$$\widehat{U}_{12}(\tau)2\hat{I}_{1y}\hat{I}_{2z}\widehat{U}_{12}(\tau)^{-1} = 2\hat{I}_{1y}\hat{I}_{2z}\cos\pi J_{12}\tau - \hat{I}_{1x}\sin\pi J_{12}\tau$$

which are conveniently notated as

$$\begin{aligned} \hat{I}_{1x} &\xrightarrow{\pi J_{12}\tau} \hat{I}_{1x}\cos\pi J_{12}\tau + 2\hat{I}_{1y}\hat{I}_{2z}\sin\pi J_{12}\tau \\ 2\hat{I}_{1y}\hat{I}_{2z} &\longrightarrow 2\hat{I}_{1y}\hat{I}_{2z}\cos\pi J_{12}\tau - \hat{I}_{1x}\sin\pi J_{12}\tau \end{aligned}$$

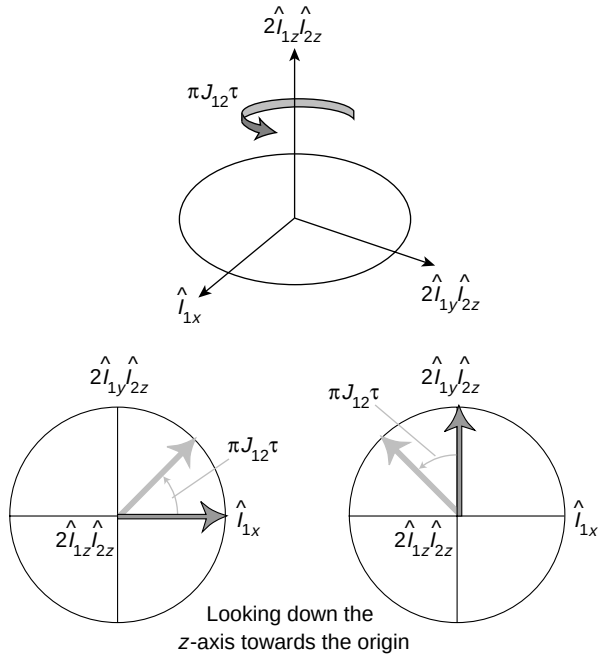

Figure 15.33
Transformation rules for the J-coupling (part 1).

Similarly, Figure 15.32c indicates the following transformations:

$$\begin{aligned} 2\hat{I}_{1x}\hat{I}_{2z} &\xrightarrow{\pi J_{12}\tau} 2\hat{I}_{1x}\hat{I}_{2z}\cos\pi J_{12}\tau + \hat{I}_{1y}\sin\pi J_{12}\tau \\ \hat{I}_{1y} &\longrightarrow \hat{I}_{1y}\cos\pi J_{12}\tau - 2\hat{I}_{1x}\hat{I}_{2z}\sin\pi J_{12}\tau \end{aligned}$$

These diagrams are shown for the case of positive J_{12}; if J_{12} is negative, the rotation is in the opposite sense.

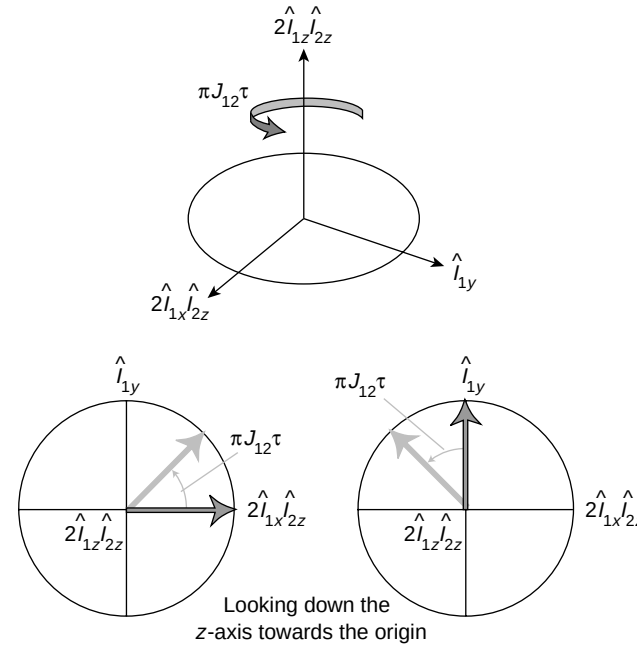

Figure 15.34
Transformation rules for the J-coupling (part 2).

These relationships indicate the creation and destruction of spin correlations by evolution in the presence of the couplings. This works as follows on the microscopic level. In the presence of couplings, the magnetic fields at the sites of spins I_1 depend on the instantaneous polarizations of the spins I_2. The angle through which spins I_1 precess over a certain interval depends, therefore, on the states of spins I_2. Over a period of time, the *transverse* polarizations of spins I_1 develop a correlation with the *longitudinal* polarizations of spins I_2. The correlated spin state that develops corresponds to the presence of a density operator term $2\hat{I}_{1y}\hat{I}_{2z}$. The same correlation may also be destroyed by a continuation of the same mechanism.

To complete the picture of evolution under the J-coupling, one also needs the following commutation relationships:[3]

$$\begin{aligned}
\left[2\hat{I}_{1z}\hat{I}_{2z}, \hat{I}_{1z}\right] &= \left[2\hat{I}_{1z}\hat{I}_{2z}, \hat{I}_{2z}\right] = 0 \\
\left[2\hat{I}_{1z}\hat{I}_{2z}, 2\hat{I}_{1z}\hat{I}_{2z}\right] &= \left[2\hat{I}_{1z}\hat{I}_{2z}, \hat{1}\right] = 0 \\
\left[2\hat{I}_{1z}\hat{I}_{2z}, 2\hat{I}_{1x}\hat{I}_{2x}\right] &= \left[2\hat{I}_{1z}\hat{I}_{2z}, 2\hat{I}_{1x}\hat{I}_{2y}\right] = 0 \\
\left[2\hat{I}_{1z}\hat{I}_{2z}, 2\hat{I}_{1y}\hat{I}_{2x}\right] &= \left[2\hat{I}_{1y}\hat{I}_{2z}, 2\hat{I}_{1x}\hat{I}_{2y}\right] = 0
\end{aligned} \tag{15.24}$$

This implies that the J-coupling does not cause any evolution of density operator terms such as $2\hat{I}_{1y}\hat{I}_{2x}$:

$$\begin{aligned}
2\hat{I}_{1y}\hat{I}_{2x} &\xrightarrow{\pi J_{12}\tau} 2\hat{I}_{1y}\hat{I}_{2x} \\
2\hat{I}_{1x}\hat{I}_{2x} &\longrightarrow 2\hat{I}_{1x}\hat{I}_{2x}
\end{aligned}$$

Double- and zero-quantum coherences do not evolve under the coupling between the two involved spins.

We are now ready to complete the calculation of the free evolution of the density operator term $\hat{I}_{1x}$:

$$\hat{I}_{1x}$$
$$\downarrow \Omega_2^0\tau$$
$$\hat{I}_{1x}$$
$$\downarrow \Omega_1^0\tau$$
$$\hat{I}_{1x}\cos\Omega_1^0\tau + \hat{I}_{1y}\sin\Omega_1^0\tau$$
$$\downarrow \pi J_{12}\tau$$
$$\begin{aligned}&\hat{I}_{1x}\cos\Omega_1^0\tau\,\cos\pi J_{12}\tau + \hat{I}_{1y}\sin\Omega_1^0\tau\,\cos\pi J_{12}\tau\\ &+2\hat{I}_{1y}\hat{I}_{2z}\cos\Omega_1^0\tau\,\sin\pi J_{12}\tau - 2\hat{I}_{1x}\hat{I}_{2z}\sin\Omega_1^0\tau\,\sin\pi J_{12}\tau\end{aligned}$$

If the initial term is instead $2\hat{I}_{1x}\hat{I}_{2y}$, the free evolution transformations are instead:

$$2\hat{I}_{1x}\hat{I}_{2y}$$
$$\downarrow \pi J_{12}\tau$$
$$2\hat{I}_{1x}\hat{I}_{2y}$$
$$\downarrow \Omega_1^0\tau$$
$$2\hat{I}_{1x}\hat{I}_{2y}\cos\Omega_1^0\tau + 2\hat{I}_{1y}\hat{I}_{2y}\sin\Omega_1^0\tau$$
$$\downarrow \Omega_2^0\tau$$
$$\begin{aligned}&2\hat{I}_{1x}\hat{I}_{2y}\cos\Omega_1^0\tau\,\cos\Omega_2^0\tau + 2\hat{I}_{1y}\hat{I}_{2y}\sin\Omega_1^0\tau\,\cos\Omega_2^0\tau\\ &-2\hat{I}_{1x}\hat{I}_{2x}\cos\Omega_1^0\tau\,\sin\Omega_2^0\tau - 2\hat{I}_{1y}\hat{I}_{2x}\sin\Omega_1^0\tau\,\sin\Omega_2^0\tau\end{aligned}$$

Note that the term $2\hat{I}_{1x}\hat{I}_{2y}$ is unchanged by the spin–spin coupling. This follows from the commutation properties in Equation 15.24.

15.9.3 Relaxation

The free evolution of the product operators also involves relaxation.

The relaxation of product operators that involve *populations*, such as $\hat{I}_{1z}$ and $2\hat{I}_{1z}\hat{I}_{2z}$, is rather complicated in a coupled spin system. This subject is discussed further in Chapter 20.

The relaxation of product operators involving *coherences* is very simple if one assumes that all coherences in the product operator relax with the same rate constant. One simply multiplies each product operator by a decay factor of the form $\exp\{-\lambda\tau\}$.

The simple assumption of identical coherence decay rate constants breaks down in some circumstances. For example, this happens if the relaxation mechanisms are *cross-correlated*, as described in Section 20.8. A more sophisticated treatment of the product operator evolution is necessary in that case.

In this book, I generally neglect the relaxation of the product operators in the intervals between pulses.

15.10 Spin Echo Sandwich

As indicated above, free evolution of product operators usually leads to an increase in complexity. Each term splits up into many other terms. In addition, the final state is often strongly dependent on the chemical shift values.

These features are often undesirable, but may be avoided by building pulse sequences around the following element:

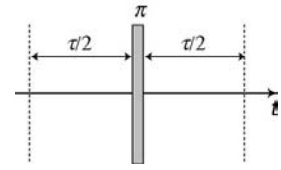

Figure 15.35
A spin echo sandwich of duration τ.

i.e. two intervals of free evolution, both of duration $\tau/2$, 'sandwiching' a strong, short, pulse of flip angle π (in practice, the pulse is many orders of magnitude shorter than the precession intervals). This pulse sequence element is called a *spin echo sandwich* (SES).

To a good approximation,[4] the state of the spins after the spin echo sandwich is the same as that produced by the following fictitious sequence:

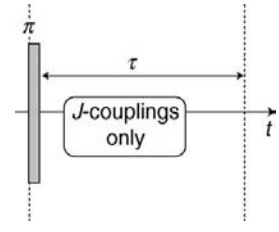

Figure 15.36
A short-cut for calculating the evolution under a spin-echo sandwich.

i.e. a π pulse, followed by a full interval τ of evolution *under the J-couplings only*.

Mathematically, this implies that the spin echo sandwich propagator, given by

$$\widehat{U}_{\mathrm{SES}} = \widehat{U}(\tau/2)\widehat{R}_x(\pi)\widehat{U}(\tau/2)$$

may be written as

$$\widehat{U}_{\mathrm{SES}} \cong \widehat{U}_{12}(\tau)\widehat{R}_x(\pi) \qquad (15.25)$$

This property is proved in Appendix A.10.

By basing a pulse sequence upon spin echo sandwich elements, it is possible to make use of the J-couplings without worrying about the precise values of the chemical shifts. The calculation of the spin dynamics is easier, and the pulse sequences are more effective.

A further simplification may often be made. In many cases, the values of the J-couplings are rather well known beforehand. For example, three-bond ^{1}H–^{1}H J-couplings are often around ~7.5 Hz in conformationally mobile systems, and one-bond ^{1}H–^{13}C J-couplings are around ~135 Hz. Suppose that the total duration of the spin echo sandwich τ is set equal to the value

$$\tau = |(2J_{12})^{-1}|$$

(The magnitude symbol is necessary, because J_{12} may be negative, while τ is always positive.) This implies that τ should be set close to the value 67 ms in the case of three-bond ^{1}H–^{1}H J-couplings, and close to the value 3.7 ms in the case of one-bond ^{1}H–^{13}C J-couplings.

If τ is set to the value $|(2J_{12})^{-1}|$ and J_{12} is positive, then $\pi J_{12}\tau$ is equal to $+\pi/2$, and the transformations of product operators by the J-coupling part of the propagator become simple:

$$\left.\begin{aligned}
\hat{I}_{1x} &\xrightarrow{\pi J_{12}\tau} 2\hat{I}_{1y}\hat{I}_{2z}\\
2\hat{I}_{1y}\hat{I}_{2z} &\xrightarrow{\pi J_{12}\tau} -\hat{I}_{1x}\\
\hat{I}_{2x} &\xrightarrow{\pi J_{12}\tau} 2\hat{I}_{1z}\hat{I}_{2y}\\
2\hat{I}_{1z}\hat{I}_{2y} &\xrightarrow{\pi J_{12}\tau} -\hat{I}_{2x}\\
2\hat{I}_{1x}\hat{I}_{2z} &\xrightarrow{\pi J_{12}\tau} \hat{I}_{1y}\\
\hat{I}_{1y} &\xrightarrow{\pi J_{12}\tau} -2\hat{I}_{1x}\hat{I}_{2z}\\
2\hat{I}_{1z}\hat{I}_{2x} &\xrightarrow{\pi J_{12}\tau} \hat{I}_{2y}\\
\hat{I}_{2y} &\xrightarrow{\pi J_{12}\tau} -2\hat{I}_{1z}\hat{I}_{2x}
\end{aligned}\right\} \text{for } J_{12} > 0$$

All other product operators are unchanged. To calculate the full effect of the spin echo sandwich, the π pulse should be taken into account as well. If the π pulse has phase $\phi_{\mathrm{P}} = 0$, we get

$$\left.\begin{array}{rcrcl}
\hat{I}_{1x} & \xrightarrow{\pi_x} & \hat{I}_{1x} & \xrightarrow{\pi J_{12}\tau} & 2\hat{I}_{1y}\hat{I}_{2z} \\
2\hat{I}_{1y}\hat{I}_{2z} & \xrightarrow{\pi_x} & 2\hat{I}_{1y}\hat{I}_{2z} & \xrightarrow{\pi J_{12}\tau} & -\hat{I}_{1x} \\
\hat{I}_{2x} & \xrightarrow{\pi_x} & \hat{I}_{2x} & \xrightarrow{\pi J_{12}\tau} & 2\hat{I}_{1z}\hat{I}_{2y} \\
2\hat{I}_{1z}\hat{I}_{2y} & \xrightarrow{\pi_x} & 2\hat{I}_{1z}\hat{I}_{2y} & \xrightarrow{\pi J_{12}\tau} & -\hat{I}_{2x} \\
2\hat{I}_{1x}\hat{I}_{2z} & \xrightarrow{\pi_x} & -2\hat{I}_{1x}\hat{I}_{2z} & \xrightarrow{\pi J_{12}\tau} & -\hat{I}_{1y} \\
\hat{I}_{1y} & \xrightarrow{\pi_x} & -\hat{I}_{1y} & \xrightarrow{\pi J_{12}\tau} & 2\hat{I}_{1x}\hat{I}_{2z} \\
2\hat{I}_{1z}\hat{I}_{2x} & \xrightarrow{\pi_x} & -2\hat{I}_{1z}\hat{I}_{2x} & \xrightarrow{\pi J_{12}\tau} & -\hat{I}_{2y} \\
\hat{I}_{2y} & \xrightarrow{\pi_x} & -\hat{I}_{2y} & \xrightarrow{\pi J_{12}\tau} & 2\hat{I}_{1z}\hat{I}_{2x}
\end{array}\right\} \text{for } J_{12} > 0$$

A spin echo sandwich with an appropriately chosen duration may, therefore, be used for the *complete conversion of uncorrelated spin states into correlated spin states*, and vice versa. Spin echo sandwiches are ubiquitous in liquid-state NMR. Some examples are given in Chapter 16.

If $\tau = |(2J_{12})^{-1}|$ and J_{12} is negative, then $\pi J_{12}\tau$ is equal to $-\pi/2$, and the transformations by the spin echo sandwich have the opposite sign; for example:

$$\left.\begin{array}{rcrcl}
\hat{I}_{1x} & \xrightarrow{\pi_x} & \hat{I}_{1x} & \xrightarrow{\pi J_{12}\tau} & -2\hat{I}_{1y}\hat{I}_{2z} \\
2\hat{I}_{1y}\hat{I}_{2z} & \xrightarrow{\pi_x} & 2\hat{I}_{1y}\hat{I}_{2z} & \xrightarrow{\pi J_{12}\tau} & +\hat{I}_{1x}
\end{array}\right\} \text{for } J_{12} < 0$$

Notes

1. Cross-correlation effects (see Section 20.8) may cause coherences such as $\rho_{\boxed{-\alpha}}$ and $\rho_{\boxed{-\beta}}$ to relax with different rate constants.

2. It is tempting to make the following 'physical interpretation' of the splitting associated with the J-coupling: the peak at frequency $\Omega_{\boxed{-\alpha}} = \Omega_1^0 + \pi J_{12}$ is associated with the precession of spins I_1, with spins I_2 in the $|\alpha\rangle$ state, whereas the peak at frequency $\Omega_{\boxed{-\beta}} = \Omega_1^0 - \pi J_{12}$ is associated with the precession of spins I_1, with spins I_2 being in the $|\beta\rangle$ state. Spins in the $|\alpha\rangle$ state shift the magnetic field experienced by their neighbours in one direction, and spins in the $|\beta\rangle$ state shift the magnetic field of their neighbours in the opposite direction.

   Although this argument is tempting, it must be wrong, since most of the spin pairs in the ensemble are actually in superposition states, with spin polarization vectors pointing in arbitrary directions. The discussion given in this chapter explains the appearance of the spectral splittings from the Schrödinger equation while avoiding the unrealistic assumption that the spins are only in states $|\alpha\rangle$ or $|\beta\rangle$.

3. The last two cyclic commutation relationships in Equation 15.24 only apply to spins-1/2 and may be derived by multiplying out the matrix representations.

4. See Appendix A.10 for a general treatment of spin echo sandwiches.

Further Reading

- For more product operator theory, see: R. R. Ernst, G. Bodenhausen and A. Wokaun, *Principles of Nuclear Magnetic Resonance in One and Two Dimensions*, Clarendon Press, Oxford, 1987; M. Goldman, *Quantum Description of High-Resolution NMR in Liquids*, Clarendon Press, Oxford, 1988; J. Cavanagh, W. J. Fairbrother, A. G. Palmer and N. J. Skelton, *Protein NMR Spectroscopy. Principles and Practice*, Academic, New York, 1996; and J. Keeler, *Understanding NMR Spectroscopy*, Wiley, Chichester, 2005.

Exercises

15.1 This exercise concerns the transformation of a single population $\rho_{\boxed{\alpha\alpha}}$ in an AX spin system. Suppose that the spin ensemble is only populated in the single state $|\alpha\alpha\rangle$, i.e.

$$\hat{\rho} = \begin{pmatrix} 1 & 0 & 0 & 0 \\ 0 & 0 & 0 & 0 \\ 0 & 0 & 0 & 0 \\ 0 & 0 & 0 & 0 \end{pmatrix}$$

(i) What is the density operator after a strong $(\pi/2)_y$ pulse?
(ii) What is the density operator after a pulse with phase $\pi/2$ and an arbitrary flip angle β?
(iii) Suppose that the flip angle β is very small, and ignore all terms that have a power of 3 or higher in β after the pulse. Which coherences are excited by the pulse to *first order* in β? Which coherences are excited by the pulse to *second order* in β? Suggest a pattern for these observations.

16 Experiments on AX Systems

This chapter discusses some practical NMR experiments on coupled spins in isotropic liquids. For simplicity, I assume that the experiments are conducted on weakly coupled AX systems.

16.1 COSY

16.1.1 The assignment problem

Suppose that the sample contains a mixture of two different compounds, each with a different AX spin system, but with identical J-couplings. The NMR spectrum would have the following appearance:

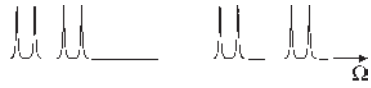

Figure 16.1
An ambiguous one-dimensional spectrum.

Clearly, this spectrum has a number of different interpretations. The peaks might belong to the different spin systems as follows:

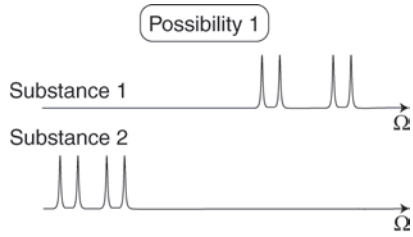

Figure 16.2
One interpretation.

or

Spin Dynamics: Basics of Nuclear Magnetic Resonance, Second Edition Malcolm H. Levitt

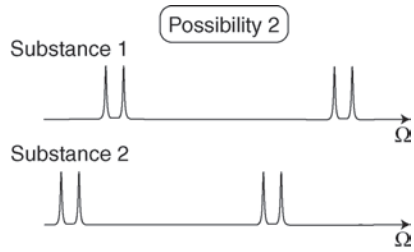

Figure 16.3
A second interpretation.

or perhaps:

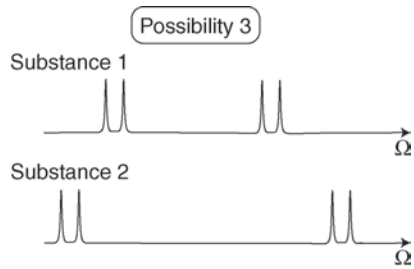

Figure 16.4
A third interpretation.

It is not possible to distinguish between these interpretations by examining the one-dimensional NMR spectrum alone.

If the compounds are known, then chemical shift values may provide some clues. However, in many cases, chemical shifts do not provide an unambiguous answer.

The above example illustrates the *assignment problem*. The one-dimensional NMR spectrum provides no indication as to which NMR peaks originate in the same spin system, and which originate in different spin systems.

Ideally, one would like a 'correlation map', indicating pictorially which peaks 'belong together'. The 'correlation maps' for the three possible peak assignments all look different:

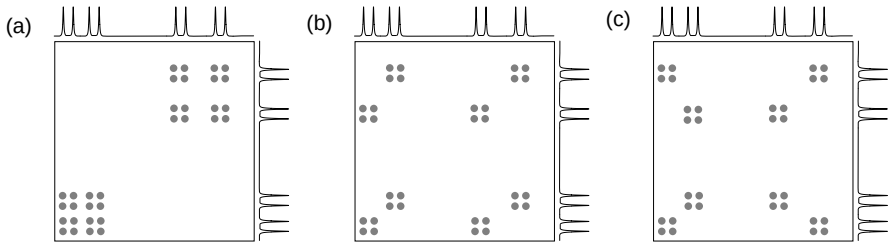

Figure 16.5 Correlation maps for (a) the first interpretation, (b) the second interpretation and (c) the third interpretation.

In this section, we investigate a simple two-dimensional NMR technique, called *correlation spectroscopy* (COSY), that provides such experimental correlation maps, indicating the correct assignment of peaks. COSY is now an essential tool in the NMR of complex molecules.

16.1.2 COSY pulse sequence

COSY was the first two-dimensional NMR experiment, described by the Belgian scientist Jean Jeener in 1971, but never published in a scientific journal. Fortunately, a graduate student of R. R. Ernst took detailed notes of Jeener's sketchy conference report. Ernst's group took up the idea and developed multidimensional spectroscopy into an immensely powerful and versatile range of methods (while giving full credit to Jeener!). Ernst was awarded the Nobel Prize in 1991.

The pulse sequence for COSY is very simple. It contains just two $\pi/2$ pulses, separated by a variable delay t_1. The experiment is conducted in the usual arrayed fashion:

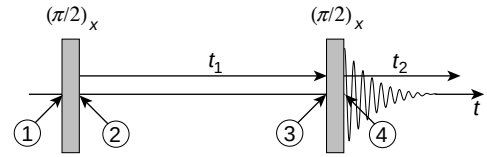

Figure 16.6
COSY pulse sequence: 'cosine' version.

This two-dimensional pulse sequence provides the 'cosine' two-dimensional data matrix $s^{\cos}(t_1, t_2)$ in the States procedure (see Section 5.9.4). The 'sine' data matrix is obtained by using the same pulse sequence, but with a $-\pi/2$ phase shift of the first pulse:[1]

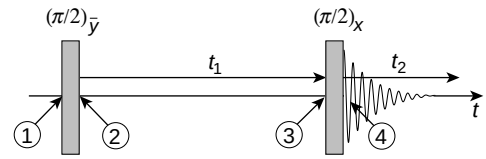

Figure 16.7
COSY pulse sequence: 'sine' version.

The two data matrices are combined and Fourier transformed as in Section 5.9.4 to obtain the two-dimensional spectrum $S(\Omega_1, \Omega_2)$.

16.1.3 Theory of COSY: coherence interpretation

Consider an ensemble of AX spin systems, subjected to the 'cosine' pulse sequence, in which the phases of the pulses are both zero.

The density operator is transformed by the first $\pi/2$ pulse as follows:

$$\hat{\rho}_{①} = \hat{\rho}^{\text{eq}} = \hat{I}_{1z} + \hat{I}_{2z}$$

$$\downarrow \quad (\pi/2)_x$$

$$\hat{\rho}_{②} = -\hat{I}_{1y} - \hat{I}_{2y}$$

omitting the unity operator and unnecessary constants.

The density operator after the first pulse $\hat{\rho}_{②}$ may be written in terms of shift and projection operators as follows:

$$\hat{\rho}_{②} = \frac{1}{2\text{i}}\hat{I}_1^-\hat{I}_2^\alpha + \frac{1}{2\text{i}}\hat{I}_1^-\hat{I}_2^\beta + \ldots$$

The (-1)-quantum coherences immediately after the first pulse are therefore given by:

$$\rho_{\boxed{-\alpha}②} = \frac{1}{2\mathrm{i}} \qquad \rho_{\boxed{\alpha-}②} = \frac{1}{2\mathrm{i}}$$
$$\rho_{\boxed{-\beta}②} = \frac{1}{2\mathrm{i}} \qquad \rho_{\boxed{\beta-}②} = \frac{1}{2\mathrm{i}}$$

The first pulse may be thought of as generating a branching 'tree' of (± 1)-quantum coherences:

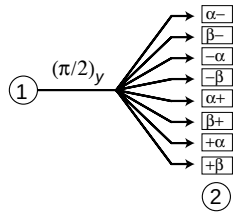

Figure 16.8
Generation of coherences by the first pulse in COSY.

During the interval t_1, the coherences evolve at their characteristic frequencies. At time point ③, just before the second $\pi/2$ pulse, the (-1)-quantum coherences have the following amplitudes:

$$\rho_{\boxed{-\alpha}③} = \frac{1}{2\mathrm{i}} \exp\{\left(\mathrm{i}\Omega_{\boxed{-\alpha}} - \lambda\right) t_1\} \qquad \rho_{\boxed{\alpha-}③} = \frac{1}{2\mathrm{i}} \exp\{\left(\mathrm{i}\Omega_{\boxed{\alpha-}} - \lambda\right) t_1\}$$
$$\rho_{\boxed{-\beta}③} = \frac{1}{2\mathrm{i}} \exp\{(\mathrm{i}\Omega_{\boxed{-\beta}} - \lambda) t_1\} \qquad \rho_{\boxed{\beta-}③} = \frac{1}{2\mathrm{i}} \exp\{(\mathrm{i}\Omega_{\boxed{\beta-}} - \lambda) t_1\}$$

where the characteristic frequencies of the coherences are given in Equation 15.10. I have assumed that all the decay constants λ are the same, for the sake of simplicity.

The spin density operator at time point ③ is therefore given by

$$\hat{\rho}_③ = \frac{1}{2\mathrm{i}} \exp\{\left(\mathrm{i}\Omega_{\boxed{-\alpha}} - \lambda\right) t_1\} \hat{I}_1^- \hat{I}_2^\alpha + \frac{1}{2\mathrm{i}} \exp\{(\mathrm{i}\Omega_{\boxed{-\beta}} - \lambda) t_1\} \hat{I}_1^- \hat{I}_2^\beta + \ldots$$

i.e. one term for each of the excited coherences. In the 'tree' picture, the t_1 evolution causes each branch to 'grow', without branching any further:

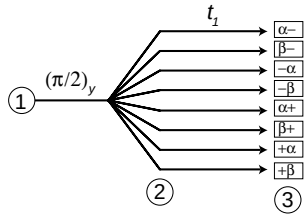

Figure 16.9
Evolution of coherences during t_1.

Let us take just one of these branches and examine how it gives rise to an NMR signal in the period after the second $\pi/2$ pulse.

The fate of the coherence $\rho_{\boxed{-\alpha}③}$ may be examined by evaluating the following transformation:

$$\hat{R}_x(\pi/2) \hat{I}_1^- \hat{I}_2^\alpha \hat{R}_x(-\pi/2)$$

This is conveniently evaluated by using the matrix representations. The matrix representation of the rotation operator $\widehat{R}_x(\pi/2)$ is

$$\widehat{R}_x(\pi/2) = \frac{1}{\sqrt{2}}\begin{pmatrix} 1 & -\mathrm{i} \\ -\mathrm{i} & 1 \end{pmatrix} \otimes \frac{1}{\sqrt{2}}\begin{pmatrix} 1 & -\mathrm{i} \\ -\mathrm{i} & 1 \end{pmatrix} = \frac{1}{2}\begin{pmatrix} 1 & -\mathrm{i} & -\mathrm{i} & -1 \\ -\mathrm{i} & 1 & -1 & -\mathrm{i} \\ -\mathrm{i} & -1 & 1 & -\mathrm{i} \\ -1 & -\mathrm{i} & -\mathrm{i} & 1 \end{pmatrix}$$

The transformation of the coherence $\rho_{\boxed{-\alpha}}$ by the second $\pi/2$ pulse is therefore

$$\widehat{R}_x(\pi/2)\hat{I}_1^- \hat{I}_2^{\alpha}\widehat{R}_x(-\pi/2) = \frac{1}{2}\begin{pmatrix} 1 & -\mathrm{i} & -\mathrm{i} & -1 \\ -\mathrm{i} & 1 & -1 & -\mathrm{i} \\ -\mathrm{i} & -1 & 1 & -\mathrm{i} \\ -1 & -\mathrm{i} & -\mathrm{i} & 1 \end{pmatrix}\begin{pmatrix} 0 & 0 & 0 & 0 \\ 0 & 0 & 0 & 0 \\ 1 & 0 & 0 & 0 \\ 0 & 0 & 0 & 0 \end{pmatrix}$$

$$\times\frac{1}{2}\begin{pmatrix} 1 & \mathrm{i} & \mathrm{i} & -1 \\ \mathrm{i} & 1 & -1 & \mathrm{i} \\ \mathrm{i} & -1 & 1 & \mathrm{i} \\ -1 & \mathrm{i} & \mathrm{i} & 1 \end{pmatrix} = \frac{1}{4}\begin{pmatrix} -\mathrm{i} & 1 & 1 & \mathrm{i} \\ -1 & -\mathrm{i} & -\mathrm{i} & 1 \\ 1 & \mathrm{i} & \mathrm{i} & -1 \\ -\mathrm{i} & 1 & 1 & \mathrm{i} \end{pmatrix}$$

This indicates that the pulse transforms the single coherence $\rho_{\boxed{-\alpha}}$ into *every other* population and coherence in the spin system:

$$\rho_{\boxed{-\alpha}} \xrightarrow{(\pi/2)_x} \frac{1}{4}\rho_{\boxed{-\alpha}} + \frac{1}{4}\rho_{\boxed{-\beta}} - \frac{1}{4}\rho_{\boxed{\alpha-}} + \frac{1}{4}\rho_{\boxed{\beta-}} + \ldots$$

Each 'branch' of the 'tree' forks again into many different 'twigs':

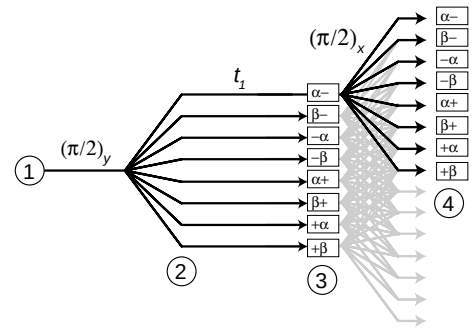

Figure 16.10
Branching of coherences induced by the second pulse in COSY.

The process by which a single coherence is converted by an r.f. pulse into one or more different coherences is called *coherence transfer*.

Let us concentrate for the moment on a single 'twig' of the 'tree', corresponding to the following coherence transfer history:

$$\hat{\rho}^{\mathrm{eq}} \xrightarrow{(\pi/2)_y} \rho_{\boxed{-\alpha}} \xrightarrow{(\pi/2)_x} \rho_{\boxed{\alpha-}}$$

The NMR signal component from this single 'twig' will be denoted

$$s_{\boxed{-\alpha}\rightarrow\boxed{\alpha-}}(t_1, t_2)$$

The signal generated by this single *coherence transfer pathway* is proportional to (1) the efficiency with which the coherence $\rho_{\boxed{-\alpha}}$ is excited by the first r.f. pulse, (2) the amplitude factor accumulated by the coherence $\rho_{\boxed{-\alpha}}$ during its evolution in the t_1 period, (3) the amplitude for conversion of the coherence $\rho_{\boxed{-\alpha}}$ into $\rho_{\boxed{\alpha-}}$ by the second $\pi/2$ pulse, (4) the amplitude factor accumulated by the coherence $\rho_{\boxed{\alpha-}}$ during its evolution in the t_2 period, and (5) a factor 2i coming from the quadrature detection process.[2] By combining all these factors we get the following result:

$$s_{\boxed{-\alpha}\rightarrow\boxed{\alpha-}}(t_1, t_2) = \left(\frac{1}{2\mathrm{i}}\right) \times \exp\{\left(\mathrm{i}\Omega_{\boxed{-\alpha}} - \lambda\right) t_1\} \times \left(-\frac{1}{4}\right) \times \exp\{\left(\mathrm{i}\Omega_{\boxed{\alpha-}} - \lambda\right) t_2\} \times (2\mathrm{i})$$

giving

$$s_{\boxed{-\alpha}\rightarrow\boxed{\alpha-}}(t_1, t_2) = -\frac{1}{4} \exp\{\left(\mathrm{i}\Omega_{\boxed{-\alpha}} - \lambda\right) t_1 + \left(\mathrm{i}\Omega_{\boxed{\alpha-}} - \lambda\right) t_2\}$$

We have seen this type of two-dimensional signal in Section 5.9. After two-dimensional FT, we get a two-dimensional spectrum with a peak at the frequency coordinates $(\Omega_1, \Omega_2) = (\Omega_{\boxed{-\alpha}}, \Omega_{\boxed{\alpha-}})$. Since the frequency of coherence $\rho_{\boxed{-\alpha}}$ is $\Omega_{\boxed{-\alpha}} = \Omega_1^0 + \pi J_{12}$, and the frequency of coherence $\rho_{\boxed{\alpha-}}$ is $\Omega_{\boxed{\alpha-}} = \Omega_2^0 + \pi J_{12}$, this contribution to the two-dimensional spectrum has the following appearance:

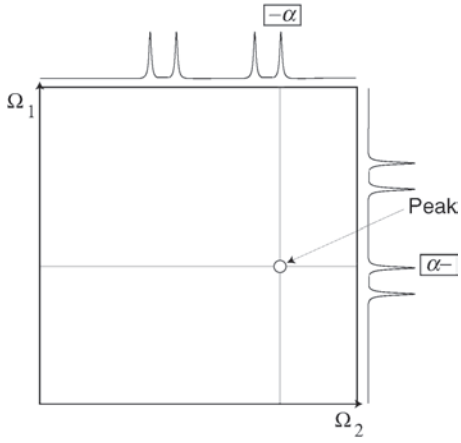

Figure 16.11
A single peak in a COSY spectrum.

This is only one 'twig' of the 'tree'. In fact, every coherence in the spin system is converted into every other coherence by the second $\pi/2$ pulse. When the signal is summed over all 'twigs', we get a two-dimensional spectrum with a peak in every possible place, as shown in Figure 16.12.

Peaks with the same frequency in the two dimensions are called *diagonal peaks* (they lie on the dashed line in the plot above). Peaks with different frequency in the two dimensions are called *cross-peaks*. In general, diagonal peaks are not particularly informative, whereas cross-peaks carry useful information.

The phases of the COSY peaks (indicated by the shading) are discussed below.

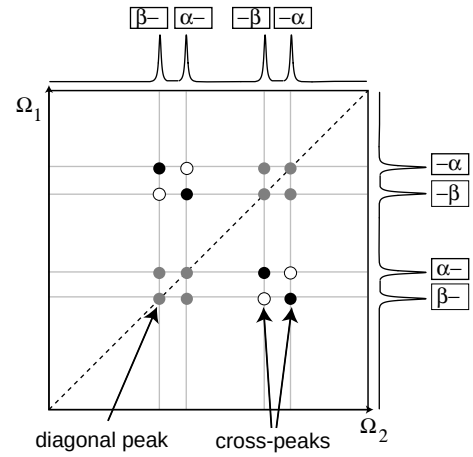

Figure 16.12
All peaks in the COSY spectrum of an AX ensemble.

Now consider the situation in which there are two different types of AX system in the sample. Each type of AX system generates its own 'tree' and its own two-dimensional correlation map. But since coherences are not transferred between different molecules, it is not possible to generate two-dimensional peaks connecting signals belonging to different spin systems. If 'possibility 1' is the correct assignment, as in Figure 16.2, then the two-dimensional COSY spectrum of a mixture of two AX spin systems has the following form:

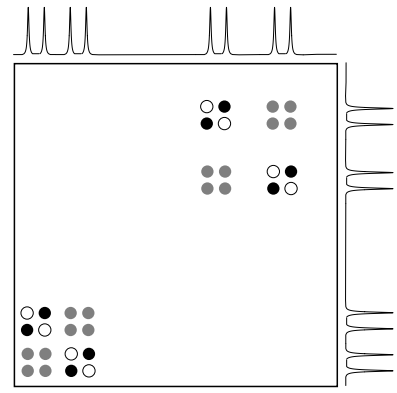

Figure 16.13
The form of the COSY spectrum for two AX systems.

This is precisely the sort of two-dimensional correlation map that I tried to motivate at the beginning of this section.

16.1.4 Product operator interpretation

It is possible to calculate the details of the COSY spectrum by repeating the calculation above for every coherence in the system. However, a more economical interpretation of COSY is obtained using product operators. Consider again the 'cosine' pulse sequence (Figure 16.6). The spin density operator after the first pulse is given by

$$\hat{\rho}_{②}^{\cos} = -\hat{I}_{1y} - \hat{I}_{2y}$$

omitting the unity operator and the numerical factors. The product operator evolution rules in Section 15.9 may be used to write down the density operator at the end of the t_1 interval, time point ③:

$$\begin{aligned}\hat{\rho}_{③}^{\cos} = &-\hat{I}_{1y}\cos(\Omega_1^0 t_1)\cos(\pi J_{12} t_1) + 2\hat{I}_{1x}\hat{I}_{2z}\cos(\Omega_1^0 t_1)\sin(\pi J_{12} t_1)\\ &+\hat{I}_{1x}\sin(\Omega_1^0 t_1)\cos(\pi J_{12} t_1) + 2\hat{I}_{1y}\hat{I}_{2z}\sin(\Omega_1^0 t_1)\sin(\pi J_{12} t_1)\\ &-\hat{I}_{2y}\cos(\Omega_2^0 t_1)\cos(\pi J_{12} t_1) + 2\hat{I}_{1z}\hat{I}_{2x}\cos(\Omega_2^0 t_1)\sin(\pi J_{12} t_1)\\ &+\hat{I}_{2x}\sin(\Omega_2^0 t_1)\cos(\pi J_{12} t_1) + 2\hat{I}_{1z}\hat{I}_{2y}\sin(\Omega_2^0 t_1)\sin(\pi J_{12} t_1)\end{aligned} \tag{16.1}$$

This is a superposition of in-phase single-quantum terms ($\hat{I}_{1x}$, $\hat{I}_{1y}$, $\hat{I}_{2x}$ and $\hat{I}_{2y}$) and antiphase single-quantum terms ($2\hat{I}_{1y}\hat{I}_{2z}$, $2\hat{I}_{1x}\hat{I}_{2z}$, $2\hat{I}_{1z}\hat{I}_{2y}$ and $2\hat{I}_{1z}\hat{I}_{2x}$).

This density operator is transformed by the $(\pi/2)_x$ pulse according to the rules given in Section 15.8:

$$\begin{aligned}\hat{\rho}_{④}^{\cos} = &-\hat{I}_{1z}\cos(\Omega_1^0 t_1)\cos(\pi J_{12} t_1) - 2\hat{I}_{1x}\hat{I}_{2y}\cos(\Omega_1^0 t_1)\sin(\pi J_{12} t_1)\\ &+\hat{I}_{1x}\sin(\Omega_1^0 t_1)\cos(\pi J_{12} t_1) - 2\hat{I}_{1z}\hat{I}_{2y}\sin(\Omega_1^0 t_1)\sin(\pi J_{12} t_1)\\ &-\hat{I}_{2z}\cos(\Omega_2^0 t_1)\cos(\pi J_{12} t_1) - 2\hat{I}_{1y}\hat{I}_{2x}\cos(\Omega_2^0 t_1)\sin(\pi J_{12} t_1)\\ &+\hat{I}_{2x}\sin(\Omega_2^0 t_1)\cos(\pi J_{12} t_1) - 2\hat{I}_{1y}\hat{I}_{2z}\sin(\Omega_2^0 t_1)\sin(\pi J_{12} t_1)\end{aligned}$$

In order to analyse the NMR signal, we need only consider the single-quantum terms:

$$\begin{aligned}\hat{\rho}_{④}^{\cos} = &+\hat{I}_{1x}\sin(\Omega_1^0 t_1)\cos(\pi J_{12} t_1) - 2\hat{I}_{1z}\hat{I}_{2y}\sin(\Omega_1^0 t_1)\sin(\pi J_{12} t_1)\\ &+\hat{I}_{2x}\sin(\Omega_2^0 t_1)\cos(\pi J_{12} t_1) - 2\hat{I}_{1y}\hat{I}_{2z}\sin(\Omega_2^0 t_1)\sin(\pi J_{12} t_1) + \ldots\end{aligned} \tag{16.2}$$

If we repeat the calculation for the 'sine' pulse sequence (Figure 16.7), we get

$$\begin{aligned}\hat{\rho}_{④}^{\sin} = &-\hat{I}_{1x}\cos(\Omega_1^0 t_1)\cos(\pi J_{12} t_1) + 2\hat{I}_{1z}\hat{I}_{2y}\cos(\Omega_1^0 t_1)\sin(\pi J_{12} t_1)\\ &-\hat{I}_{2x}\cos(\Omega_2^0 t_1)\cos(\pi J_{12} t_1) + 2\hat{I}_{1y}\hat{I}_{2z}\cos(\Omega_2^0 t_1)\sin(\pi J_{12} t_1) + \ldots\end{aligned} \tag{16.3}$$

Examine in detail the second terms in Equations 16.2 and 16.3:

$$\begin{aligned}\hat{\rho}_{④}^{\cos} &= -2\hat{I}_{1z}\hat{I}_{2y}\sin(\Omega_1^0 t_1)\sin(\pi J_{12} t_1) + \ldots\\ \hat{\rho}_{④}^{\sin} &= +2\hat{I}_{1z}\hat{I}_{2y}\cos(\Omega_1^0 t_1)\sin(\pi J_{12} t_1) + \ldots\end{aligned}$$

Standard trigonometric identities may be used to write these terms as follows:

$$\begin{aligned}\hat{\rho}_{④}^{\cos} &= -2\hat{I}_{1z}\hat{I}_{2y} \times \frac{1}{2}\left\{\cos\left((\Omega_1^0 - \pi J_{12})t_1\right) - \cos\left((\Omega_1^0 + \pi J_{12})t_1\right)\right\} + \ldots\\ \hat{\rho}_{④}^{\sin} &= -2\hat{I}_{1z}\hat{I}_{2y} \times \frac{1}{2}\left\{\sin\left((\Omega_1^0 - \pi J_{12})t_1\right) - \sin\left((\Omega_1^0 + \pi J_{12})t_1\right)\right\} + \ldots\end{aligned} \tag{16.4}$$

These terms display the appropriate cosine and sine amplitude modulations for the two pulse sequences, as required in the States procedure (Section 5.9.4). The frequency of these modulations is $\Omega_1^0 \pm \pi J_{12}$, with the two components having opposite sign. In addition, the density operator term $-2\hat{I}_{1z}\hat{I}_{2y}$ implies an antiphase absorption peak, centred around frequency Ω_2^0 in the Ω_2 dimension. Equation 16.4, therefore, signifies a *doubly antiphase cross-peak*, in which each component has pure absorption phase, after States data processing. An expansion of the cross-peak is shown on the following page:

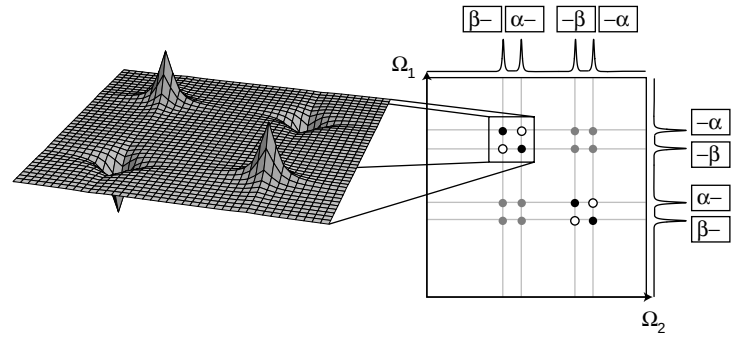

Figure 16.14
The form of a COSY cross-peak multiplet.

If one examines the fourth terms in Equations 16.2 and 16.3, one finds another doubly antiphase pure absorption cross-peak, but this time centred at frequency coordinates $(\Omega_1, \Omega_2) = (\Omega_2^0, \Omega_1^0)$.

The first and third terms in Equations 16.2 and 16.3 do not work out so comfortably. These terms describe diagonal and near-diagonal peaks, and are given by

$$\hat{\rho}_{④}^{\cos} = \hat{I}_{1x} \sin(\Omega_1^0 t_1) \cos(\pi J_{12} t_1) + \ldots$$
$$\hat{\rho}_{④}^{\sin} = -\hat{I}_{1x} \cos(\Omega_1^0 t_1) \cos(\pi J_{12} t_1) + \ldots$$

Trigonometric identities give

$$\hat{\rho}_{④}^{\cos} = \hat{I}_{1x} \times \frac{1}{2} \left\{ \sin((\Omega_1^0 + \pi J_{12}) t_1) + \sin((\Omega_1^0 - \pi J_{12}) t_1) \right\} + \ldots$$
$$\hat{\rho}_{④}^{\sin} = \hat{I}_{2x} \times \frac{1}{2} \left\{ -\cos((\Omega_1^0 + \pi J_{12}) t_1) - \cos((\Omega_1^0 - \pi J_{12}) t_1) \right\} + \ldots \quad (16.5)$$

Everything is wrong here. We have sine modulations with respect to t_1 in the 'cosine' data set, and we have cosine modulations with respect to t_1 in the 'sine' data set. Furthermore, the $\hat{I}_{1x}$ terms in the density operator indicate dispersion peaks in the Ω_2 dimension, instead of absorption peaks. As a result, the States procedure does not work at all for these peaks. States data processing, as described in Section 5.9.4, gives the following shape for the diagonal peak:

$$\begin{aligned} \mathrm{Re}\{S_{\mathrm{States}}(\Omega_1, \Omega_2)\} = & \frac{1}{2} \mathcal{D}(\Omega_1; \Omega_1^0 - \pi J_{12}, \lambda) \mathcal{D}(\Omega_2; \Omega_1^0 - \pi J_{12}, \lambda) \\ & + \frac{1}{2} \mathcal{D}(\Omega_1; \Omega_1^0 + \pi J_{12}, \lambda) \mathcal{D}(\Omega_2; \Omega_1^0 - \pi J_{12}, \lambda) \\ & + \frac{1}{2} \mathcal{D}(\Omega_1; \Omega_1^0 - \pi J_{12}, \lambda) \mathcal{D}(\Omega_2; \Omega_1^0 + \pi J_{12}, \lambda) \\ & + \frac{1}{2} \mathcal{D}(\Omega_1; \Omega_1^0 + \pi J_{12}, \lambda) \mathcal{D}(\Omega_2; \Omega_1^0 + \pi J_{12}, \lambda) \end{aligned}$$

which appears as follows:

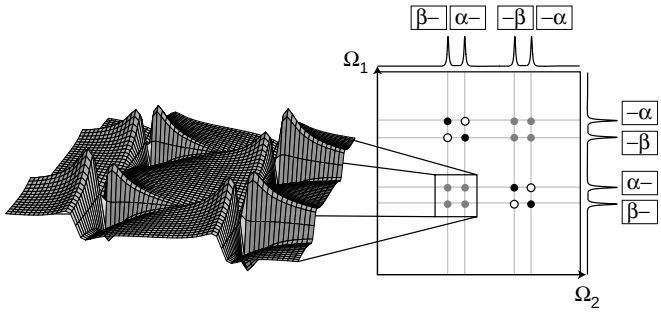

Figure 16.15
The form of a COSY diagonal-peak multiplet.

The ugly double-dispersion appearance of the diagonal peaks is a drawback of the original COSY pulse sequence. The long dispersion tails of the diagonal peaks tend to obscure any nearby cross-peaks.

A variant called *double-quantum-filtered COSY* provides absorption lineshapes for both the diagonal peaks and the cross-peaks, and is usually used in practice (see Exercise 16.2).

16.1.5 Experimental examples

Figure 16.16 shows an experimental COSY spectrum of an organic molecule in solution. It would be an exceedingly difficult task to assign all of the NMR peaks in such a complex spectrum without the aid of two-dimensional spectra.

Apart from being more informative, two-dimensional spectra have the advantage of being much *less crowded* than one-dimensional spectra. There is much more room in a two-dimensional spectral plane compared with the one-dimensional frequency axis of a one-dimensional NMR spectrum. The chance of peaks landing on top of each other is greatly reduced in two dimensions. Figure 16.17 shows the ^{1}H double-quantum-filtered COSY spectrum of a medium-sized protein molecule in aqueous solution (the huge water resonance is visible as an ugly vertical stripe). The protein contains approximately 1000 non-equivalent proton sites.

Although the use of two-dimensional spectroscopy greatly reduces the problems caused by overlapping peaks, the spectra of biological molecules are still often too crowded. Figure 16.17 displays several spectral regions in which the peaks assignments remain problematic. In the NMR of large molecules, it is fairly usual to record three- or higher-dimensional NMR spectra in order to reduce the spectral crowding further.

16.2 INADEQUATE

The pulse sequence INADEQUATE was designed by Ad Bax and co-workers in 1980. The ironical acronym stands for 'Incredible Natural Abundance Double Quantum Technique'. The aim of this pulse sequence is to suppress signals from isolated ^{13}C spins, allowing the selective detection of NMR signals from very rare molecules containing natural pairs of ^{13}C atoms.

16.2.1 ^{13}C isotopomers

As background to this method, consider a sample of ordinary ethanol (CH_3CH_2OH). There are two C sites in each molecule, which are occupied by either ^{13}C or ^{12}C nuclei, according to their natural abundances. The natural abundance of ^{12}C (spin = 0) is ~98.9%; the natural abundance of ^{13}C (spin-1/2) is ~1.1%. An ethanol molecule has four carbon isotopomers:

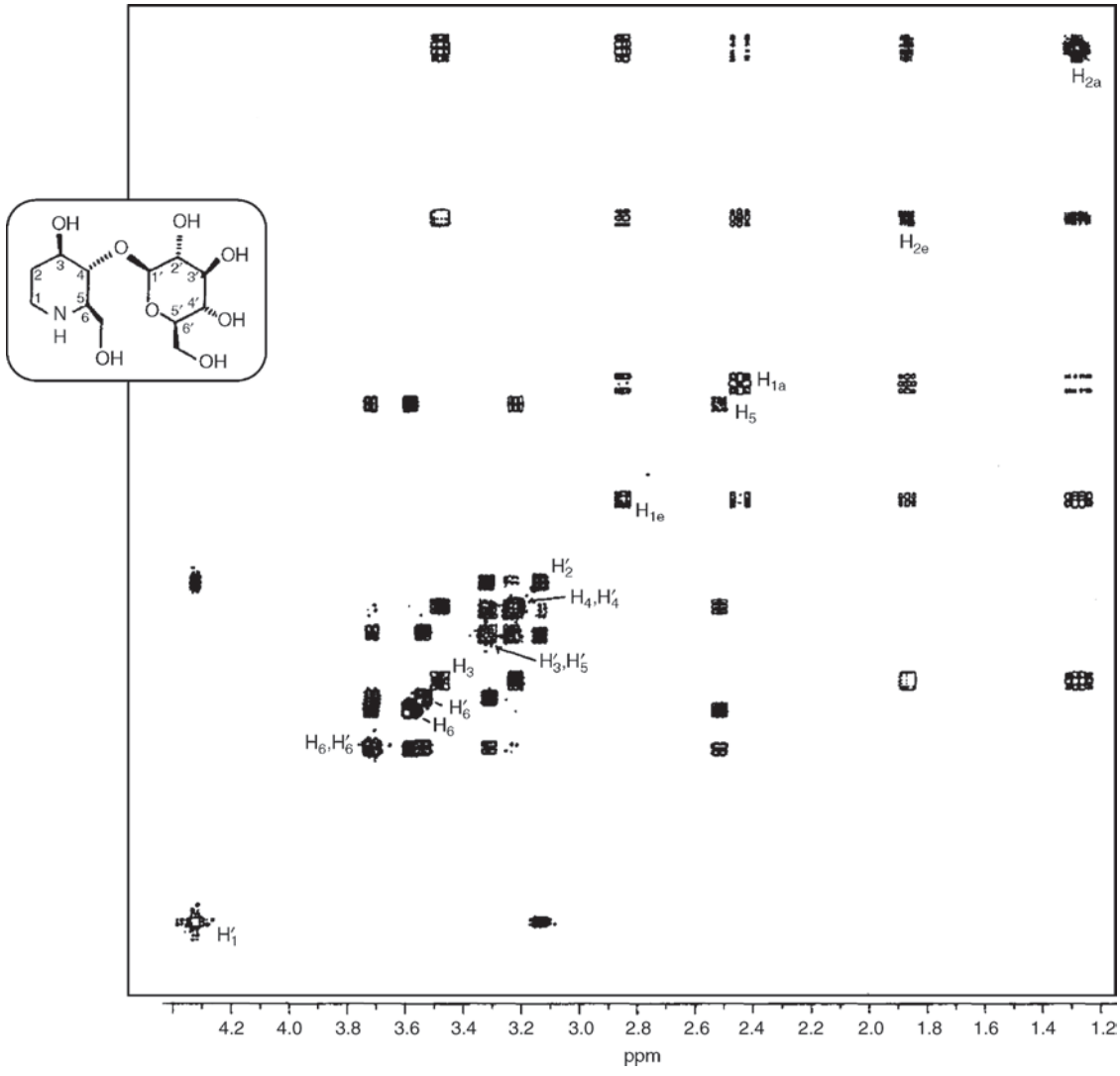

Figure 16.16 Experimental ^{1}H COSY spectrum of an organic molecule in solution. Adapted from A. E. Derome, *Modern NMR Techniques in Chemistry Research*, Pergamon Press, Oxford, 1990, p. 192. Copyright 1990, Elsevier Science.

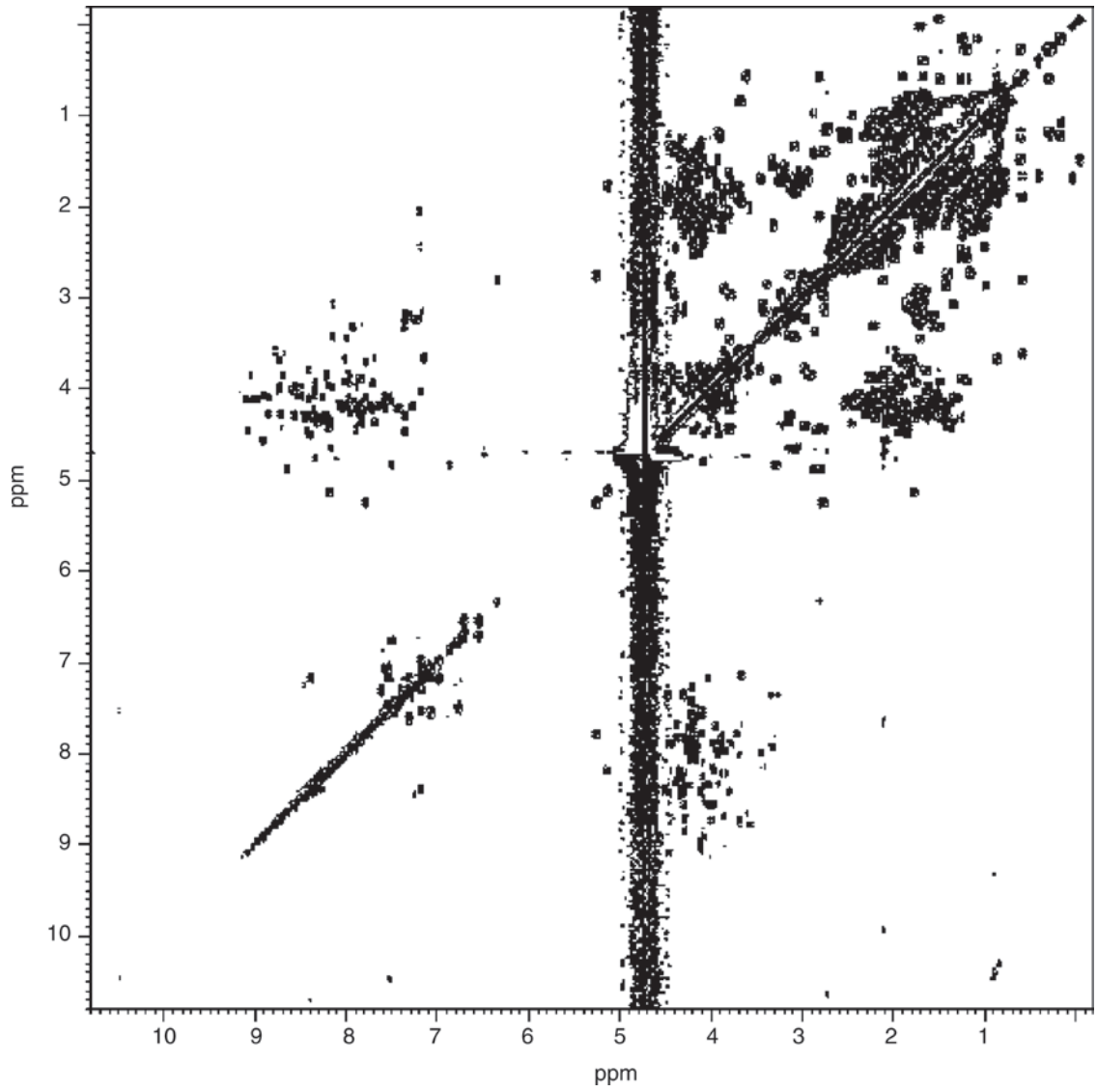

Figure 16.17 Experimental ^{1}H COSY spectrum of a medium-sized biomolecule in solution (the C-terminal domain of rat ERp29 protein). The protein contains 120 amino acid residues. A long interval of weak r.f. irradiation at the water proton Larmor frequency ('presaturation') was applied before the start of the pulse sequence to suppress the water proton signals. The residual water signal is visible as a strong vertical band in the centre of the spectrum. Thanks to E. Liepinsh and G. Otting for supplying this spectrum.

- *Species I*. $^{12}CH_3{}^{12}CH_2OH$; both C sites are occupied by ^{12}C nuclei.
- *Species II*. $^{13}CH_3{}^{12}CH_2OH$; the CH_3 site is occupied by ^{13}C and the CH_2 site is occupied by ^{12}C.
- *Species III*. $^{12}CH_3{}^{13}CH_2OH$; the CH_3 site is occupied by ^{12}C and the CH_2 site is occupied by ^{13}C.
- *Species IV*. $^{13}CH_3{}^{13}CH_2OH$; both C sites are occupied by ^{13}C nuclei.

The relative abundances of these isotopomers may be calculated as follows. Suppose that the fractional abundance of ^{13}C is x, and that of ^{12}C is $1 - x$. The fractional abundance of species I is equal to the probability that the CH_3 site is occupied by ^{12}C, multiplied by the probability that the CH_2 site is *also* occupied by ^{12}C. This probability is

$$\mathrm{P_I} = (1 - x)(1 - x) \cong 97.81\%$$

using the value $x \cong 1.1\%$.

Similarly, the fractional abundance of species II is equal to the probability that the CH_3 site is occupied by ^{13}C, multiplied by the probability that the CH_2 site is occupied by ^{12}C:

$$\mathrm{P_{II}} = (1 - x)x \cong 1.09\%$$

and likewise for the fractional abundance of species III:

$$\mathrm{P_{III}} = x(1 - x) \cong 1.09\%$$

The fractional abundance of the $^{13}C_2$ species IV is equal to:

$$\mathrm{P_{IV}} = x^2 \cong 0.012\%$$

This means that only around 1 out of every 10 000 ethanol molecules contains two ^{13}C spins.

Since the dominant isotopomer I contains no ^{13}C spins, the ^{13}C spectrum of ethanol is dominated by signals from the isotopomers II and III. If the ^{1}H spins are decoupled by an r.f. field at the proton Larmor frequency, each of these isotopomers contributes a single spectral peak, at the chemical shift of the ^{13}C site. Isotopomer II gives a peak at the chemical shift of spins in the ethanol CH_3 site, and isotopomer III gives a peak at the chemical shift of spins in the ethanol CH_2 site:

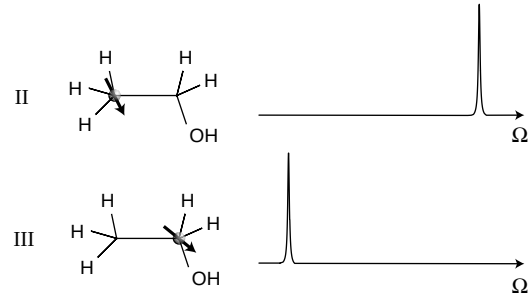

Figure 16.18
Ethanol isotopomers II and III and their ^{1}H-decoupled ^{13}C spectra.

The rare isotopomer IV contains two ^{13}C spins, which form a homonuclear AX system in the presence of proton decoupling. The J-coupling between the ^{13}C spins is around 50 Hz. This isotopomer contributes a four-line spectral pattern:

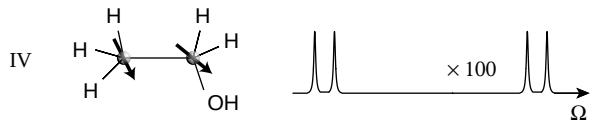

Figure 16.19
Ethanol isotopomer IV and its ^{1}H-decoupled ^{13}C spectrum.

(The spectrum is shown at 100 times magnification). The total spectrum therefore consists of two large peaks from the relatively common isotopomers II and III, and four very small *satellite* peaks generated by the rare isotopomer IV:

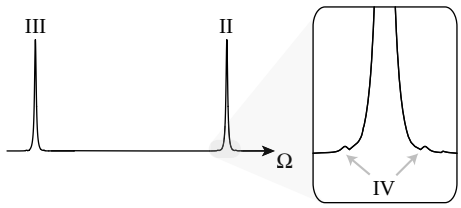

Figure 16.20
Total ^{1}H-decoupled ^{13}C spectrum of ethanol.

In practice, the satellite peaks are extremely difficult to observe, since the main peaks are ~200 times larger. (A factor of 100 comes from the relative abundances of the isotopomers, and a further factor of 2 comes from the fact that the $^{13}C_2$ peaks are split by the J-coupling.)

INADEQUATE is a method that supresses the main peaks, which come from non-interacting spins-1/2. Only 'satellite' signals from the rare spin-1/2 pairs appear in the final spectrum.

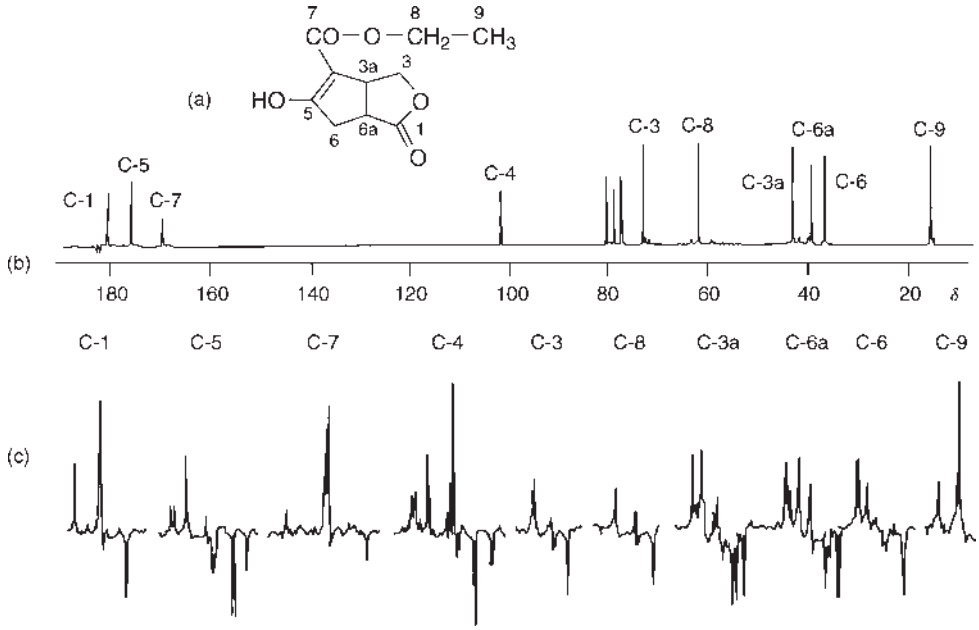

Figure 16.21 ^{13}C spectra of the compound shown in (a) (a small amount of a paramagnetic relaxation agent was added to the solution in order to decrease the waiting interval between transients). (b) Proton-decoupled ^{13}C spectrum. (c) Expanded sections of the ^{13}C INADEQUATE spectrum, showing the antiphase $^{13}C_2$ satellites. The data were taken over 16 h on 1.2 g of material in a field of 9.4 T. Adapted from J. Buddrus and H. Bauer, *Angew. Chem. Int. Ed. Engl.* **26**, 625 (1987). (Reproduced by permission of Wiley–VCH.)

An experimental example is given in Figure 16.21, which shows the INADEQUATE spectrum of a sample in which each molecule has 10 inequivalent carbon sites. In this case, there are 45 possible $^{13}C_2$ isotopomers ($_{10}C_2 = 10!/(2!\,8!) = 45$), each giving four satellite signals. The experimental INADEQUATE spectrum at the top of the figure displays many such $^{13}C_2$ signals. The satellite signals are invisible in the conventional ^{13}C spectrum in Figure 16.21b.

The satellite peaks produced by INADEQUATE have a characteristic antiphase configuration. We will see why soon.

Why is the observation of satellite signals useful? First, the observation of $^{13}C_2$ satellites allows the measurement of ^{13}C–^{13}C J-couplings. These couplings, especially longer-range couplings, often provide useful information as to the geometry of the molecules. Second, the examination of $^{13}C_2$ satellite spectra assists greatly in the *assignment* of the ^{13}C spectrum: molecules with many carbon sites provide a spectrum with many ^{13}C peaks, and it is not always possible to decide which peak belongs to which site. By observing the ^{13}C–^{13}C couplings, one may figure out which carbon site is a neighbour to which other site.

16.2.2 Pulse sequence

The INADEQUATE pulse sequence is as follows:

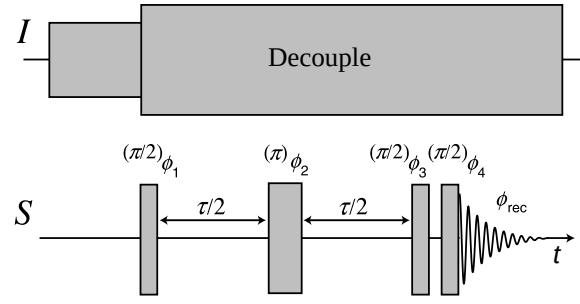

Figure 16.22
INADEQUATE pulse sequence.

The ^1H r.f. fields are denoted I, and the ^{13}C r.f. fields are denoted S.

The pulse sequence on the ^{13}C spins consists of three pulses of flip angle $\pi/2$ and one pulse of flip angle π. The last two $\pi/2$ pulses follow each other almost immediately; it is only necessary to wait a few microseconds for the r.f. phase shift to be implemented.

The first part of the pulse sequence involves a spin echo sandwich with duration τ. The interval τ is chosen to match the ^{13}C–^{13}C coupling constant, according to

$$\tau = |(2J_{12})^{-1}|$$

One-bond ^{13}C–^{13}C couplings are often around $+50$ Hz, so the value of τ is approximately 10 ms. The pulse sequence intervals, therefore, are $\tau/2 \cong 5$ ms. However, one should be aware that the values of one-bond ^{13}C–^{13}C coupling constants vary considerably from compound to compound, so that the figure of 5 ms is only a rough estimate.

Irradiation is applied at the ^1H Larmor frequency throughout the sequence and the observation interval, in order to decouple the ^{13}C spins from the protons. In addition, one normally applies low-level ^1H irradiation for several seconds before the start of the ^{13}C pulse sequence. This enhances the ^{13}C magnetization through the *NOE*, as discussed in Section 20.5.

As usual, the pulse sequence is not drawn to scale along the time axis. In practice, the durations of the pulses are much smaller than the intervals between the pulses, and the ^1H irradiation before the sequence lasts much longer than anything else.

Table 16.1 A four-step phase cycle ($\mathfrak{n} = 4$) appropriate for the INADEQUATE experiment.

Cycle counter $\mathfrak{m}$	ϕ_1	ϕ_2	ϕ_3	ϕ_4	ϕ_{rec}
0	0	0	0	$\pi/2$	0
1	0	0	0	π	$3\pi/2$
2	0	0	0	$3\pi/2$	π
3	0	0	0	0	$\pi/2$

The phases of the ^{13}C pulses are denoted ϕ_1, ϕ_2, ϕ_3 and ϕ_4. The signal is detected using a receiver phase shift ϕ_{rec}. These phases are subject to a phase cycle, as described in Section 5.3. A series of independent experiments is performed, with different values for the pulse phases $\phi_1 \ldots \phi_4$ and receiver phase ϕ_{rec}. The signals from these different experiments are added together.

A simple phase cycle suitable for the INADEQUATE experiment is shown in Table 16.1. The symbol $\mathfrak{n}$ is used for the number of steps in the phase cycle ($\mathfrak{n} = 4$ in this case) and the symbol $\mathfrak{m}$ is used for the phase cycle counter. This may be calculated from the transient counter $\mathfrak{M} = 0, 1, 2, 3, 4, 5 \ldots$ through the following formula:

$$\mathfrak{m} = \text{mod}(\mathfrak{M}, 4)$$

The phase cycle counter, therefore, runs $\mathfrak{m} = 0, 1, 2, 3, 0, 1, 2 \ldots$, implying that the phase cycle is to be read from top-to-bottom, top-to-bottom, etc., until a complete number of phase cycle steps is completed. The number of acquired transients must be a multiple of 4.

In the cycle shown, only the phase ϕ_4 of the last pulse and the receiver phase ϕ_{rec} change during the phase cycle. Some longer and more sophisticated phase cycles are presented in Appendix A.11.

16.2.3 Theory of INADEQUATE

We now calculate the spectral peak amplitudes generated by the INADEQUATE pulse sequence. For simplicity, the effects of relaxation are ignored.

As described in Section 15.10, the operation of the pulse sequence may be analysed using the simplified form shown in Figure 16.23, which uses phases given in the first row of Table 16.1. Conceptually, the π pulse in the centre of the spin echo sandwich is shifted to the beginning of that period, where it merges with the first $\pi/2$ pulse to form one pulse of flip angle $3\pi/2$, followed by an interval τ, in which only the J-couplings are active.

The calculation is conducted in two parts: First for isolated spin signals and then for two-spin signals. We wish to demonstrate that isolated spin signals are destroyed, whereas the signals from spin pairs build up.

1. *Isolated spin signals.* Consider, first, the signals from the one-spin systems (the dominant $^{13}C_1$ isotopomers). The initial density operator is given by

$$\hat{\rho}_{①} = \frac{1}{2}\hat{1} + \epsilon_{\text{NOE}}\frac{1}{2}\mathbb{B}\hat{I}_z$$

where ϵ_{NOE} is the nuclear Overhauser enhancement factor brought about by ^{1}H irradiation before the start of each experiment (see Section 20.5). Typically, $\epsilon_{\text{NOE}} \sim 2$.

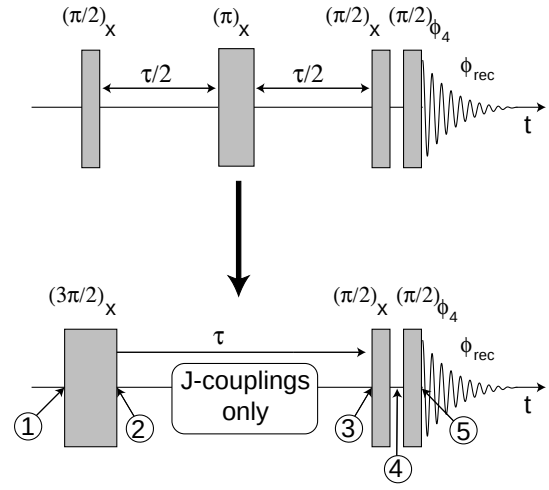

Figure 16.23
Conceptual simplification of the INADEQUATE pulse sequence.

The density operator may be written in a simplified form, leaving out the unity operator and numerical factors:

$$\hat{\rho}_{①} \sim \hat{I}_z$$

This notation is loose but convenient.

The evolution of the density operator up to time point ⑤ runs as follows:

$$\hat{\rho}_{①} = \hat{\rho}^{\mathrm{eq}} = \hat{I}_z$$

$$\downarrow (3\pi/2)_x$$

$$\hat{\rho}_{②} = +\hat{I}_y$$

$$\downarrow \tau \text{ (chemical shifts suppressed)}$$

$$\hat{\rho}_{③} = +\hat{I}_y$$

$$\downarrow (\pi/2)_x$$

$$\hat{\rho}_{④} = \hat{I}_z$$

The τ interval has no effect for isolated spins-1/2, since there are no J-couplings.

The phase of the next pulse depends on the step in the phase cycle. Let $\hat{\rho}_{⑤}^{[\mathfrak{m}]}$ denote the density operator at time point ⑤, for phase cycle step $\mathfrak{m}$.

For $\mathfrak{m} = 0$, the phase of the last pulse is $\phi_4 = \pi/2$, leading to

$$\hat{\rho}_{④} = \hat{I}_z \xrightarrow{(\pi/2)_y} \hat{\rho}_{⑤}^{[0]} = \hat{I}_x$$

For the other phase cycle steps, we get different final states:

$$\hat{\rho}_{④} \xrightarrow{(\pi/2)_{\bar{x}}} \hat{\rho}_{⑤}^{[1]} = \hat{I}_y$$

$$\hat{\rho}_{④} \xrightarrow{(\pi/2)_{\bar{y}}} \hat{\rho}_{⑤}^{[2]} = -\hat{I}_x$$

$$\hat{\rho}_{④} \xrightarrow{(\pi/2)_{x}} \hat{\rho}_{⑤}^{[3]} = -\hat{I}_y$$

Time point ⑤ is the start of signal detection, defined as usual $t = 0$. The amplitudes of the (-1)-quantum coherence at this time are deduced from the density operator in the usual way:

$$\rho_{\boxed{-}⑤}^{[0]} = \frac{1}{2} \qquad \rho_{\boxed{-}⑤}^{[2]} = -\frac{1}{2}$$
$$\rho_{\boxed{-}⑤}^{[1]} = -\frac{1}{2\mathrm{i}} \qquad \rho_{\boxed{-}⑤}^{[3]} = +\frac{1}{2\mathrm{i}}$$

The amplitude of the spectral peak is given by the equation:

$$a = 2\mathrm{i}\rho_{\boxed{-}⑤} \exp\{-\mathrm{i}\phi_{\mathrm{rec}}\}$$

The receiver phase ϕ_{rec} depends on the step in the phase cycle, according to Table 16.1. The peak amplitude for each step in the phase cycle must be worked out individually. For example, for the phase cycle step $\mathfrak{m} = 1$, the signal amplitude works out as

$$a^{[1]} = 2\mathrm{i}\rho_{\boxed{-}⑤}^{[1]} \exp\{-\mathrm{i}3\pi/2\} = -\mathrm{i}$$

The results for all the phase cycle steps are

$$a^{[0]} = \mathrm{i} \qquad a^{[2]} = \mathrm{i}$$
$$a^{[1]} = -\mathrm{i} \qquad a^{[3]} = -\mathrm{i}$$

The average phase-cycled peak amplitude is therefore identically zero:

$$a^{\mathrm{av}} = \frac{1}{4}\sum_{\mathfrak{m}=0}^{3} a^{[\mathfrak{m}]} = 0$$

This is the expected result. *The signals from isolated spins cancel out.*

2. *Two-spin signals.* Turning now to the calculation of the two-spin signals, the initial density operator may be written strictly as

$$\hat{\rho}_{①} = \frac{1}{4}\hat{1} + \epsilon_{\mathrm{NOE}}\frac{1}{4}\mathbb{B}\left(\hat{I}_{1z} + \hat{I}_{2z}\right)$$

where ϵ_{NOE} is the nuclear Overhauser enhancement factor. For simplicity, use the loose form:

$$\hat{\rho}_{①} \sim \hat{I}_{1z} + \hat{I}_{2z}$$

The propagation of the spin-pair density operator up to time point ④ runs as follows:

$$\begin{aligned}
\hat{\rho}_{①} &= \hat{\rho}^{\mathrm{eq}} = \hat{I}_{1z} + \hat{I}_{2z} \\
&\downarrow (3\pi/2)_x \\
\hat{\rho}_{②} &= \hat{I}_{1y} + \hat{I}_{2y} \\
&\downarrow \pi J_{12}\tau \\
\hat{\rho}_{③} &= -2\hat{I}_{1x}\hat{I}_{2z} - 2\hat{I}_{1z}\hat{I}_{2x} \\
&\downarrow (\pi/2)_x \\
\hat{\rho}_{④} &= 2\hat{I}_{1x}\hat{I}_{2y} + 2\hat{I}_{1y}\hat{I}_{2x}
\end{aligned}$$

This assumes that the interval τ is exactly matched to the J-coupling, $\tau = |(2J_{12})^{-1}|$, and $J_{12} > 0$.

For the spin-pair system, the density operator at time point ④ corresponds to a state of correlated spin polarizations. If the last two terms are expanded in terms of shift operators, we get

$$2\hat{I}_{1x}\hat{I}_{2y} + 2\hat{I}_{1y}\hat{I}_{2x} = -\mathrm{i}\hat{I}_1^+\hat{I}_2^+ + \mathrm{i}\hat{I}_1^-\hat{I}_2^- \tag{16.6}$$

This indicates the presence of double-quantum coherences at time point ④:

$$\begin{aligned}
\rho_{\boxed{++}}④ &= -\mathrm{i} \\
\rho_{\boxed{--}}④ &= \mathrm{i}
\end{aligned}$$

The presence of double-quantum coherences at the junction of the last two pulses is crucial for the operation of the pulse sequence.

For the moment, we proceed by calculating the individual result of each step in the phase cycle. The state of the spin-pair ensemble after the last pulse, for each of the phase cycle steps, is

$$\begin{aligned}
\hat{\rho}_{④} &\xrightarrow{(\pi/2)_{y}} \hat{\rho}^{[0]}_{⑤} = -2\hat{I}_{1z}\hat{I}_{2y} - 2\hat{I}_{1y}\hat{I}_{2z} \\
\hat{\rho}_{④} &\xrightarrow{(\pi/2)_{\bar{x}}} \hat{\rho}^{[1]}_{⑤} = -2\hat{I}_{1x}\hat{I}_{2z} - 2\hat{I}_{1z}\hat{I}_{2x} \\
\hat{\rho}_{④} &\xrightarrow{(\pi/2)_{\bar{y}}} \hat{\rho}^{[2]}_{⑤} = 2\hat{I}_{1z}\hat{I}_{2y} + 2\hat{I}_{1y}\hat{I}_{2z} \\
\hat{\rho}_{④} &\xrightarrow{(\pi/2)_{x}} \hat{\rho}^{[3]}_{⑤} = 2\hat{I}_{1x}\hat{I}_{2z} + 2\hat{I}_{1z}\hat{I}_{2x}
\end{aligned} \tag{16.7}$$

All of these density operators correspond to states of antiphase transverse magnetization, as discussed in Section 15.6.

Each spin-pair ensemble has four (−1)-quantum coherences and generates four spectral peaks. Consider for the moment the peak associated with the coherence $\rho_{\boxed{-\beta}}$. The amplitude of this coherence at the end of the pulse sequence, for each of the four steps of the phase cycle, is given by

$$\begin{aligned}
\rho^{[0]}_{\boxed{-\beta}}⑤ &= \frac{1}{2}\mathrm{i} & \rho^{[2]}_{\boxed{-\beta}}⑤ &= -\frac{1}{2}\mathrm{i} \\
\rho^{[1]}_{\boxed{-\beta}}⑤ &= \frac{1}{2} & \rho^{[3]}_{\boxed{-\beta}}⑤ &= -\frac{1}{2}
\end{aligned} \tag{16.8}$$

The amplitude of this peak, in the successive experiments, is given by

$$a^{[0]}_{\boxed{-\beta}} = a^{[1]}_{\boxed{-\beta}} = a^{[2]}_{\boxed{-\beta}} = a^{[3]}_{\boxed{-\beta}} = -1 \tag{16.9}$$

taking into account the changing values of ϕ_{rec} on the different steps of the cycle.

This peak has the same amplitude for the four different experiments, despite the fact that the phases of the pulses and the receiver are different. The average phase-cycled amplitude is therefore:

$$a^{\mathrm{av}}_{\boxed{-\beta}} = \frac{1}{4}\sum_{\mathfrak{m}=0}^{3} a^{[\mathfrak{m}]}_{\boxed{-\beta}} = -1 \tag{16.10}$$

The arguments may be repeated for the other three coherences, which have phase-cycled amplitudes:

$$\begin{aligned}
a^{\mathrm{av}}_{\boxed{-\alpha}} &= +1 \\
a^{\mathrm{av}}_{\boxed{\beta-}} &= -1 \\
a^{\mathrm{av}}_{\boxed{\alpha-}} &= +1
\end{aligned} \tag{16.11}$$

The INADEQUATE spectrum from the two-spin systems, therefore, has a characteristic antiphase appearance:

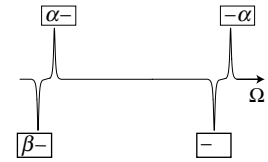

Figure 16.24
Appearance of the INADEQUATE spectrum of a two-spin system.

These antiphase doublets are very visible in experimental spectra, such as that shown in Figure 16.21.

16.2.4 Coherence transfer pathways and phase cycling

The participation of double-quantum coherences at time point ④ is very important for the operation of INADEQUATE. The history of coherence orders during the pulse sequence may be emphasized by drawing a *coherence transfer pathway diagram*, as introduced in Section 12.2.6. For INADEQUATE, this diagram appears as follows:

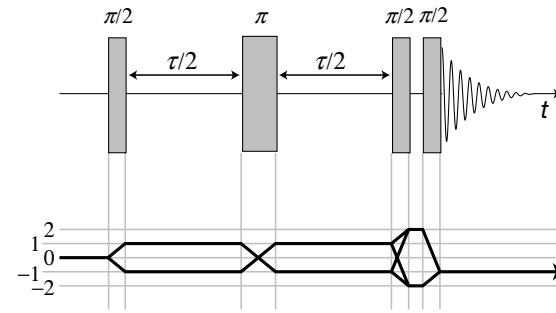

Figure 16.25
Coherence transfer pathway diagram for INADEQUATE.

The pathway starts at order 0, corresponding to thermal equilibrium. The first $\pi/2$ pulse excites (± 1)-quantum coherences, which evolve in the first $\tau/2$ interval. The π pulse inverts the coherence orders, as may be seen through properties such as

$$\widehat{R}_x(\pi)\hat{I}_1^-\hat{I}_2^\alpha\widehat{R}_x(-\pi) = \hat{I}_1^+\hat{I}_2^\beta$$

The second $\pi/2$ pulse converts the single-quantum coherences into double-quantum coherences. The branching of the pathway indicates that both (± 2)-quantum coherences are generated, and that each of the (± 1)-quantum coherences contributes to each of the double-quantum orders. The double-quantum coherences are immediately converted back into single-quantum coherences by the last $\pi/2$ pulse. All pathways terminate at level -1, to indicate quadrature detection of the NMR signal.

As proved in Appendix A.11, the *only* signals that survive the phase cycle given in Table 16.1 pass through (± 2)-quantum coherence during the short interval between the last two $\pi/2$ pulses. This allows the theory of the experiment to be greatly abbreviated, since one only needs to calculate the first step in the phase cycle. The theory in Appendix A.11 proves that (i) the signals from the other phase cycle

steps are the same, providing that the density operator elements correspond to (±2)-quantum coherences at time point ④, and (ii) signals passing through all other density operator components at time point ④ vanish.

Using this point of view, the calculation up to time point ④ may be repeated for the spin-pair signals:

$$
\begin{aligned}
\hat{\rho}_{①} &= \hat{\rho}^{\mathrm{eq}} = \hat{I}_{1z} + \hat{I}_{2z} \\
&\downarrow\ (3\pi/2)_x \\
\hat{\rho}_{②} &= \hat{I}_{1y} + \hat{I}_{2y} \\
&\downarrow\ \pi J_{12}\tau \\
\hat{\rho}_{③} &= -2\hat{I}_{1x}\hat{I}_{2z} - 2\hat{I}_{1z}\hat{I}_{2x} \\
&\downarrow\ (\pi/2)_x \\
\hat{\rho}_{④} &= 2\hat{I}_{1x}\hat{I}_{2y} + 2\hat{I}_{1y}\hat{I}_{2x} \\
&\downarrow\ \text{allow only } (\pm 2)\text{-quantum coherences} \\
\hat{\rho}_{④} &= 2\hat{I}_{1x}\hat{I}_{2y} + 2\hat{I}_{1y}\hat{I}_{2x}
\end{aligned}
\tag{16.12}
$$

The density operator term $2\hat{I}_{1x}\hat{I}_{2y} + 2\hat{I}_{1y}\hat{I}_{2x}$ passes through the final step unscathed, since it contains only (±2)-quantum coherences (Equation 16.6).

The first step of the phase cycle may be used to continue the calculation:

$$
\begin{aligned}
\hat{\rho}_{④} &= 2\hat{I}_{1x}\hat{I}_{2y} + 2\hat{I}_{1y}\hat{I}_{2x} \\
&\downarrow\ (\pi/2)_y \\
\hat{\rho}_{⑤} &= -2\hat{I}_{1z}\hat{I}_{2y} - 2\hat{I}_{1y}\hat{I}_{2z}
\end{aligned}
$$

As described in Section 15.6, these terms represent antiphase absorption peaks for both spins. The form of the INADEQUATE spectrum may, therefore, be deduced without the laborious step-by-step calculations of Equations 16.7–16.11.

This approach is even more powerful for the single-spin signals. Since isolated spins-1/2 cannot support double-quantum coherences, those signals are completely destroyed by the phase cycle. Formally, we get

$$\hat{\rho}_{①} = \hat{\rho}^{\mathrm{eq}} = \hat{I}_z$$

$$\downarrow (3\pi/2)_x$$

$$\hat{\rho}_{②} = \hat{I}_y$$

$$\downarrow \tau \text{ (chemical shifts suppressed)}$$

$$\hat{\rho}_{③} = \hat{I}_y$$

$$\downarrow (\pi/2)_x$$

$$\hat{\rho}_{④} = \hat{I}_z$$

$$\downarrow \text{allow only } (\pm 2)\text{-quantum coherences}$$

$$0$$

This conclusion remains valid even if the r.f. pulses are imperfect or if there is relaxation in the intervals between pulses.

16.2.5 Two-dimensional INADEQUATE

The INADEQUATE experiment is easily extended to a very useful two-dimensional form by inserting a variable evolution interval t_1 between the last two $\pi/2$ pulses. In spin-pair systems, the double-quantum coherences evolve during this interval, before being converted into observable (-1)-quantum coherences by the last $\pi/2$ pulse:

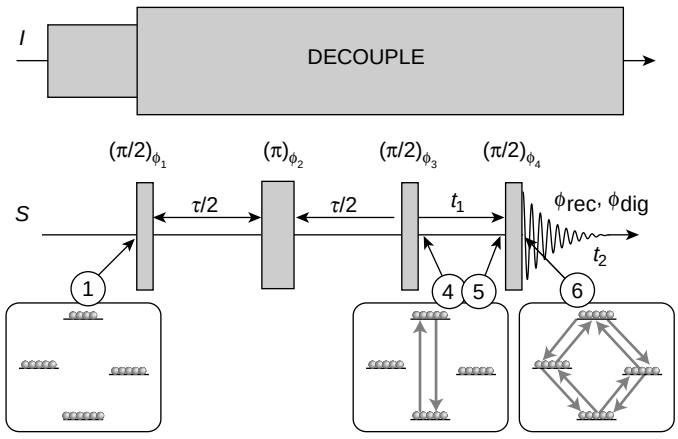

Figure 16.26
Two-dimensional INADEQUATE pulse sequence and the transformations of populations and coherences.

A phase cycle suitable for the two-dimensional INADEQUATE experiment is given in Table 16.2. It is the same as in the one-dimensional experiment, except for an additional phase shift of the first three pulses, which is used in the States procedure for obtaining pure absorption two-dimensional lineshapes (see Section 5.9.4).

The operation of the first part of the 'cosine' pulse sequence is as follows:

$$\hat{\rho}_{①} = \hat{\rho}^{\mathrm{eq}} = \hat{I}_{1z} + \hat{I}_{2z}$$

$$\downarrow (3\pi/2)_x$$

$$\downarrow \pi J_{12}\tau$$

$$\downarrow (\pi/2)_x$$

$$\hat{\rho}^{\mathrm{cos}}_{④} = 2\hat{I}_{1x}\hat{I}_{2y} + 2\hat{I}_{1y}\hat{I}_{2x}$$

where the superscript 'cos' refers to the 'cosine' pulse sequence ($\Psi = 0$ in Table 16.2).

The phase cycling selects only (± 2)-quantum coherences at this point, which leaves this particular density operator unscathed. All signals from isolated spins-1/2 are suppressed.

Table 16.2 A four-step phase cycle ($\mathfrak{n} = 4$) appropriate for the two-dimensional INADEQUATE experiment. The phase Ψ is equal to zero for the 'cosine' data set in the States procedure, whereas $\Psi = -\pi/4$ for the 'sine' data set in the States procedure.[1]

Cycle counter $\mathfrak{m}$	ϕ_1	ϕ_2	ϕ_3	ϕ_4	ϕ_{rec}
0	Ψ	Ψ	Ψ	$\pi/2$	0
1	Ψ	Ψ	Ψ	π	$3\pi/2$
2	Ψ	Ψ	Ψ	$3\pi/2$	π
3	Ψ	Ψ	Ψ	0	$\pi/2$

The evolution during the t_1 interval may be calculated according to the principles in Section 15.9:

$$\hat{\rho}^{\cos}_{\textcircled{4}} = 2\hat{I}_{1x}\hat{I}_{2y} + 2\hat{I}_{1y}\hat{I}_{2x}$$

$$\downarrow t_1$$

$$\begin{aligned}\hat{\rho}^{\cos}_{\textcircled{5}} &= \left(2\hat{I}_{1x}\hat{I}_{2y} + 2\hat{I}_{1y}\hat{I}_{2x}\right)\cos\left((\Omega_1^0 + \Omega_2^0)t_1\right) \\ &\quad - \left(2\hat{I}_{1x}\hat{I}_{2x} - 2\hat{I}_{1y}\hat{I}_{2y}\right)\sin\left((\Omega_1^0 + \Omega_2^0)t_1\right)\end{aligned}$$

Note that the double-quantum evolution proceeds as the sum of the two chemical shift frequencies and is independent of the J-coupling.

The final $\pi/2$ pulse transforms the spin-pair density operator as follows:

$$\begin{aligned}\hat{\rho}^{\cos}_{\textcircled{5}} &= \left(2\hat{I}_{1x}\hat{I}_{2y} + 2\hat{I}_{1y}\hat{I}_{2x}\right)\cos\left((\Omega_1^0 + \Omega_2^0)t_1\right) \\ &\quad - \left(2\hat{I}_{1x}\hat{I}_{2x} - 2\hat{I}_{1y}\hat{I}_{2y}\right)\sin\left((\Omega_1^0 + \Omega_2^0)t_1\right)\end{aligned}$$

$$\downarrow (\pi/2)_y$$

$$\begin{aligned}\hat{\rho}^{\cos}_{\textcircled{6}} &= -\left(2\hat{I}_{1z}\hat{I}_{2y} + 2\hat{I}_{1y}\hat{I}_{2z}\right)\cos\left((\Omega_1^0 + \Omega_2^0)t_1\right) \\ &\quad - \left(2\hat{I}_{1z}\hat{I}_{2z} - 2\hat{I}_{1y}\hat{I}_{2y}\right)\sin\left((\Omega_1^0 + \Omega_2^0)t_1\right)\end{aligned}$$

Only the first term in $\hat{\rho}^{\cos}_{\textcircled{6}}$ contains observable single-quantum coherences. For the purpose of the final NMR signal, the density operator may therefore be simplified as follows:

$$\hat{\rho}^{\cos}_{\textcircled{6}} = -\left(2\hat{I}_{1z}\hat{I}_{2y} + 2\hat{I}_{1y}\hat{I}_{2z}\right)\cos\left((\Omega_1^0 + \Omega_2^0)t_1\right) + \ldots \tag{16.13}$$

The observable operators generate antiphase multiplets, as in the one-dimensional experiment. Note the cosine modulation of the signal with respect to the evolution interval t_1.

If the calculation is repeated for the 'sine' pulse sequence in the States procedure[1] ($\Psi = -\pi/4$ in Table 16.2), we get

$$\hat{\rho}^{\sin}_{\textcircled{6}} = -\left(2\hat{I}_{1z}\hat{I}_{2y} + 2\hat{I}_{1y}\hat{I}_{2z}\right)\sin\left((\Omega_1^0 + \Omega_2^0)t_1\right) + \ldots \tag{16.14}$$

In this case, the signal has a sine modulation with respect to the evolution interval t_1.

For a single AX system, States data processing (Section 5.9.4) of the cosine and sine two-dimensional data sets gives a two-dimensional spectrum of the following form:

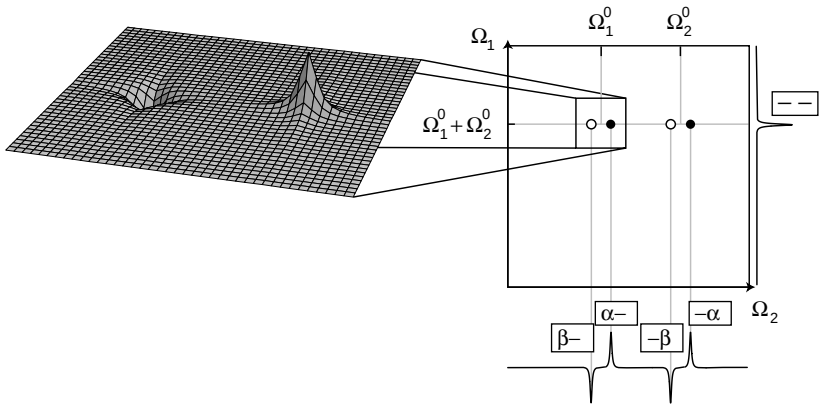

Figure 16.27
Two-dimensional INADEQUATE spectrum of a single AX spin ensemble.

The peaks are in positive and negative pure absorption, and appear at the double-quantum frequency $\Omega_1^0 + \Omega_2^0$ in the Ω_1-dimension.

Note that the double-quantum coherences are not *directly* observable, but are observed *indirectly* in the two-dimensional experiment by transforming them into observable (-1)-quantum coherences using a $\pi/2$ pulse. The modulations of the observable signals reveal the existence of the 'hidden' (± 2)-quantum coherences during the t_1 interval.

If the two-dimensional INADEQUATE experiment is performed on a sample containing many AX systems (e.g. the natural ^{13}C–^{13}C isotopomers of an organic compound containing more than two carbon sites), then the two-dimensional spectrum has the following appearance:
The two-dimensional peaks are symmetrically disposed about the 'double-quantum diagonal' (the dashed line $\Omega_1 = 2\Omega_2$ in Figure 16.28). A practical example of a two-dimensional ^{13}C INADEQUATE spectrum of an organic compound is given in Figure 16.29. Such two-dimensional INADEQUATE spectra are extremely useful for assigning ^{13}C spectra and deducing the molecular structure.

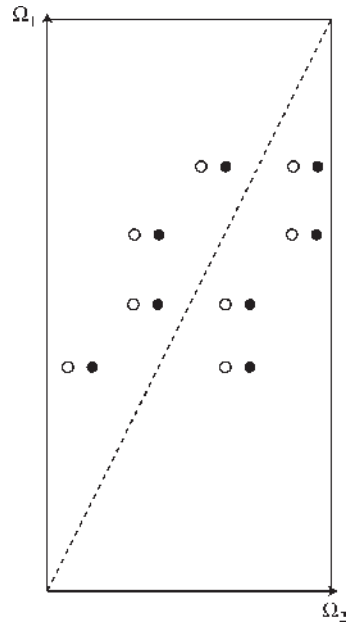

Figure 16.28
Form of the two-dimensional INADEQUATE spectrum for many $^{13}C_2$ pairs.

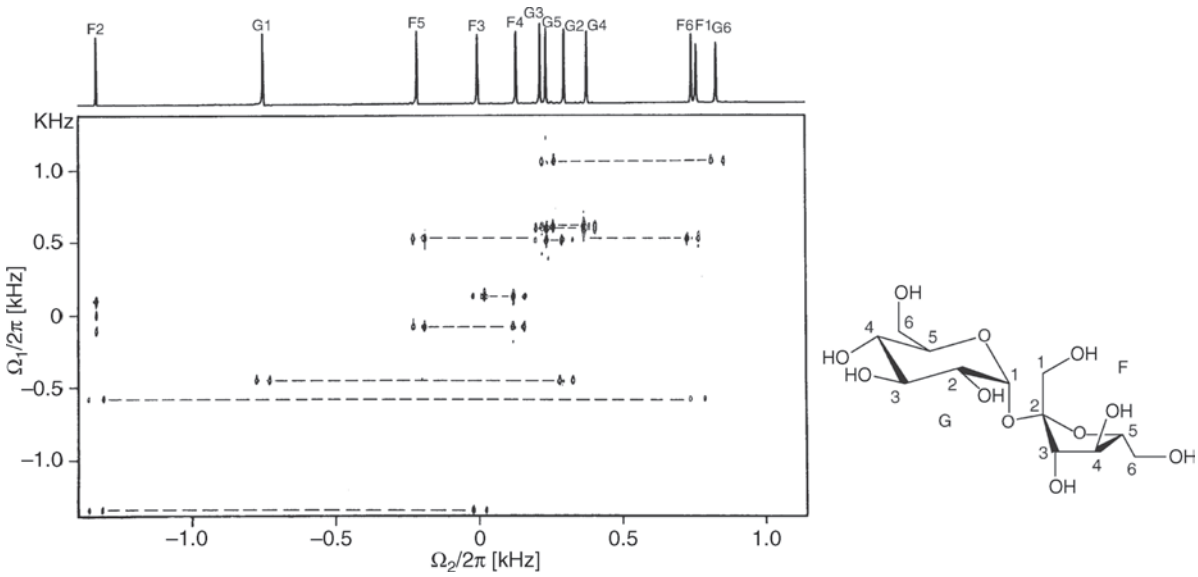

Figure 16.29 Two-dimensional INADEQUATE ^{13}C spectrum of a sucrose solution. The conventional ^{13}C spectrum at the top of the plot was assigned by noting which resonances are linked in the double-quantum ^{13}C spectrum. Adapted from A. Bax, R. Freeman, T. A. Frenkiel and M. H. Levitt, *J. Magn. Reson.* **43**, 478 (1981). Copyright, Academic Press.

The main drawback of the INADEQUATE experiment, as applied to ^{13}C in natural abundance, is its very low sensitivity, due to the extreme rarity of the natural $^{13}C_2$ isotopomers. In most cases, the experiment requires large quantities of material in order to obtain sufficient signal.

16.3 INEPT

16.3.1 The sensitivity of nuclear isotopes

In general, nuclear isotopes with high gyromagnetic ratio γ are easier to observe than those with small γ values. There are several reasons for this:

1. The nuclear magnetic moment is proportional to γ. A large value of γ implies strongly magnetic spins, a large macroscopic magnetic moment, and a strong NMR signal.

2. The magnitude of the nuclear Larmor frequency is proportional to γ. The induced current in the coil is proportional to the *rate of change* of the magnetic moment, so the strength of the NMR signal is proportional to the Larmor frequency (see Appendix A.5).

3. At thermal equilibrium, the Boltzmann polarization of the spins in the magnetic field is proportional to the Zeeman energy level splitting, which is also proportional to γ.

4. Strongly magnetic spins couple strongly to the molecular environment, and tend to have shorter values of T_1. This allows experiments to be repeated more quickly, in order to enhance the signal-to-noise ratio (see Section 5.2).[3]

One factor that works in the *opposite sense* is:

5. Empirically, the noise generated by electrons in the coil is approximately proportional to the square root of the frequency.

Overall, these factors lead to the following rough dependence of signal-to-noise ratio on γ and field B^0 (see Note 4):

$$\text{signal/noise} \propto |\gamma|^{5/2}(B^0)^{3/2} \tag{16.15}$$

For example, a certain number of ^1H nuclei provide a signal-to-noise ratio that is about 300 times larger than an equal number of ^{15}N nuclei, at the same magnetic field. This implies that one needs about 100 000 times longer to acquire a ^{15}N spectrum with the same signal-to-noise ratio as a ^1H spectrum, even if the number of spins is the same in the two cases.

In this section, I discuss a method for transferring polarization from the strongly magnetic proton spins to the weakly magnetic ^{15}N nuclei, using the J-couplings between the spins. This gets around factors 3 and 4 in the list above. After polarization transfer, the magnetization of the ^{15}N nuclei depends not on the ^{15}N γ-value but on that of the bonded protons. For ^{15}N, polarization transfer from neighbouring ^1H nuclei enhances the NMR signal by a factor of up to $|\gamma(^1H)/\gamma(^{15}N)| \cong 10$. In addition, experiments may be repeated at a rate set by the T_1 values of the protons, rather than those of the ^{15}N spins, which are usually longer.

This corresponds to more than a 100-fold decrease in the experimental time required to obtain the same signal-to-noise ratio.

One of the most popular pulse sequences for achieving this signal enhancement is called INEPT (Insensitive Nuclei Enhanced by Polarization Transfer).[5]

16.3.2 INEPT pulse sequence

The basic INEPT pulse sequence is as follows:

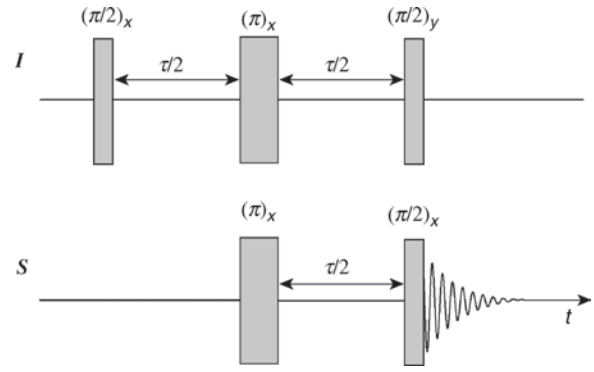

Figure 16.30
Pulse sequence for INEPT.

This is a heteronuclear pulse sequence involving synchronized r.f. irradiation on two spectrometer channels. We use the convention that I denotes the high-γ species and S denotes the low γ-species. In the case of ^{1}H and ^{15}N, the I-spins are protons and the S-spins are ^{15}N nuclei.

Several of the pulses are shown as simultaneous on the two channels. In practice, it does not matter if the pulses are really simultaneous or if one pulse slightly precedes the other (in any order).

The first part of the pulse sequence is a spin echo sandwich. The sandwich looks a little different here, because it is applied to a heteronuclear system. Nevertheless, as shown in Appendix A.10.4, it is possible to apply the conclusions of Section 15.10, as long as the π pulses are applied to *both* channels. The INEPT pulse sequence may, therefore, be analysed by using the following simplified form:

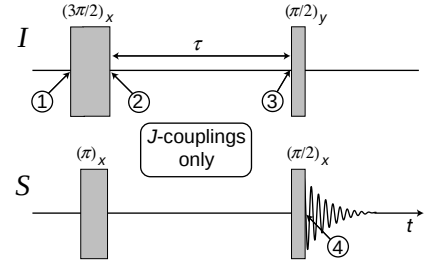

Figure 16.31
Equivalent pulse sequence for INEPT.

The interval τ is chosen to be equal to

$$\tau = |(2J_{IS})^{-1}|$$

where J_{IS} is the J-coupling (in hertz) between the two spins. In the case of directly bonded ^{1}H and ^{15}N spins in biomolecules, the J-coupling is usually around $J_{IS} \cong -93$ Hz, so the pulse sequence intervals $\tau/2$ should be set to a value around 2.7 ms.

The spin density operator at time point ① corresponds to thermal equilibrium. For a heteronuclear two-spin system, this is given by

$$\hat{\rho}_{①} = \frac{1}{4}\widehat{1} + \frac{1}{4}\mathbb{B}_I \hat{I}_z + \frac{1}{4}\mathbb{B}_S \hat{S}_z \tag{16.16}$$

where $\mathbb{B}_I$ and $\mathbb{B}_S$ are the Boltzmann factors of the two spin species:

$$\mathbb{B}_I = \frac{\gamma_I B^0}{k_B T} \qquad \mathbb{B}_S = \frac{\gamma_S B^0}{k_B T} \tag{16.17}$$

and γ_I and γ_S are the gyromagnetic ratios. In the case of $I = {}^1\mathrm{H}$ and $S = {}^{15}\mathrm{N}$, the Boltzmann factors are related by $\mathbb{B}_I \cong -10\mathbb{B}_S$.

The density operator may be propagated through the pulse sequence, using the fact that pulses on the I-channel only rotate the polarizations of the I-spins, and similarly for the pulses on the S-channel. For example, the effect of the first two pulses is as follows:

$$\begin{aligned}
\hat{\rho}_{①} &= \frac{1}{4}\widehat{1} + \frac{1}{4}\mathbb{B}_I \hat{I}_z + \frac{1}{4}\mathbb{B}_S \hat{S}_z \\
&\downarrow\ (3\pi/2)_x^I \\
\hat{\rho}_{②} &= \frac{1}{4}\widehat{1} + \frac{1}{4}\mathbb{B}_I \hat{I}_y + \frac{1}{4}\mathbb{B}_S \hat{S}_z \\
&\downarrow\ \pi_x^S \\
\hat{\rho}_{②} &= \frac{1}{4}\widehat{1} + \frac{1}{4}\mathbb{B}_I \hat{I}_y - \frac{1}{4}\mathbb{B}_S \hat{S}_z
\end{aligned}$$

The effect of the spin echo sandwich may be calculated using the results of Section 15.10. If J_{IS} is negative (the usual situation for ^{1}H and ^{15}N spins) and the delay τ is set to the value $|2J_{IS}|^{-1}$, then the angle πJ_{IS} is equal to $-\pi/2$. The calculation continues as follows:

$$\begin{aligned}
\hat{\rho}_{②} &= \frac{1}{4}\widehat{1} + \frac{1}{4}\mathbb{B}_I \hat{I}_y - \frac{1}{4}\mathbb{B}_S \hat{S}_z \\
&\downarrow\ \pi J_{IS}\tau\ (J\text{-couplings only}) \\
\hat{\rho}_{③} &= \frac{1}{4}\widehat{1} + \frac{1}{4}\mathbb{B}_I 2\hat{I}_x \hat{S}_z - \frac{1}{4}\mathbb{B}_S \hat{S}_z
\end{aligned}$$

The last two $\pi/2$ pulses rotate the spin species about different axes. The result is

$$\hat{\rho}_{③} = \frac{1}{4}\widehat{1} + \frac{1}{4}\mathbb{B}_I 2\hat{I}_x\hat{S}_z - \frac{1}{4}\mathbb{B}_S\hat{S}_z$$

$$\downarrow (\pi/2)_y^I$$

$$\frac{1}{4}\widehat{1} - \frac{1}{4}\mathbb{B}_I 2\hat{I}_z\hat{S}_z - \frac{1}{4}\mathbb{B}_S\hat{S}_z$$

$$\downarrow (\pi/2)_x^S$$

$$\hat{\rho}_{④} = \frac{1}{4}\widehat{1} + \underbrace{\frac{1}{4}\mathbb{B}_I 2\hat{I}_z\hat{S}_y}_{\text{transferred}} + \underbrace{\frac{1}{4}\mathbb{B}_S\hat{S}_y}_{\text{non-transferred}} \qquad (16.18)$$

The 'transferred' term corresponds to antiphase S-spin magnetization, and is proportional to the Boltzmann factor of spin I. The 'non-transferred' term corresponds to negative in-phase S-spin magnetization, and is proportional to the Boltzmann factor of spin S. The resulting ^{15}N spectrum is a superposition of both of these components, and appears as follows for the directly bonded ^{1}H–^{15}N case (see Note 6):

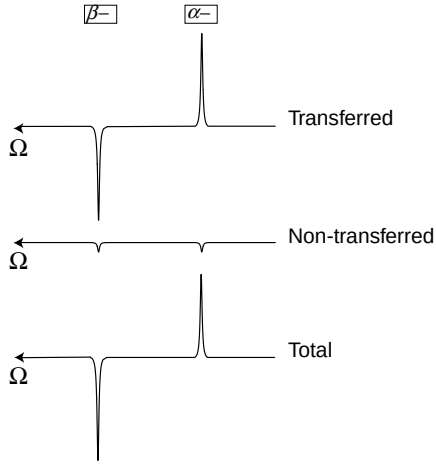

Figure 16.32
Components of the INEPT spectrum for the case of a ^{1}H–^{15}N system.

Note that the transferred signal is much larger than the non-transferred signal, and is in antiphase. Figure 16.33 shows some experimental INEPT spectra, which display the expected enhancement.

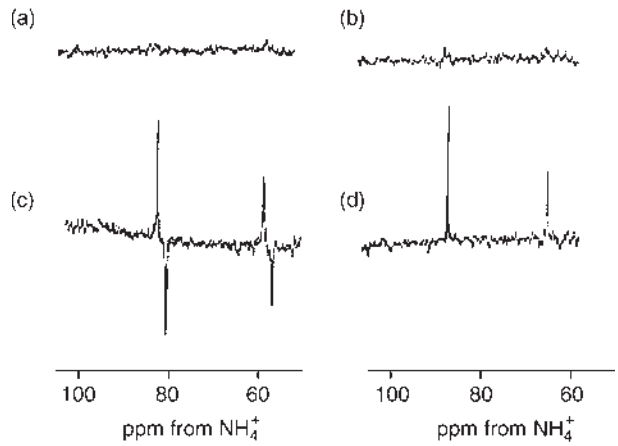

Figure 16.33 Experimental natural-abundance ^{15}N spectra of a small peptide in solution; the same instrument time was used for each spectrum. (a) The ^{15}N signals were excited using a single $\pi/2$ pulse and observed without a proton decoupling field. (b) The ^{15}N signals were excited using a single $\pi/2$ pulse and observed with a proton decoupling field. In both cases, the ^{15}N signals are almost invisible. (c) The INEPT pulse sequence was used to enhance the ^{15}N magnetization by polarization transfer from the J-coupled protons. (d) The refocused INEPT pulse sequence was used and the signals were observed with ^1H decoupling. Adapted from G. A. Morris, *J. Am. Chem. Soc.* **102**, 428 (1980), copyright, the American Chemical Society.

16.3.3 Refocused INEPT

In many cases, it is desirable to observe the S-spin signal in the presence of decoupling irradiation of the I-spins. As described in Section 3.9, this simplifies the spectrum and further enhances the signal, by collapsing split signal components into a single resonance.

It is not possible to decouple the INEPT-enhanced signal simply by applying an I-spin decoupling field under the acquisition interval, starting at time point ④. The decoupling field would simply collapse the J-splitting and cause the enhanced antiphase signals to cancel out. The only part of the spectrum that survives the decoupling is the in-phase non-transferred component:

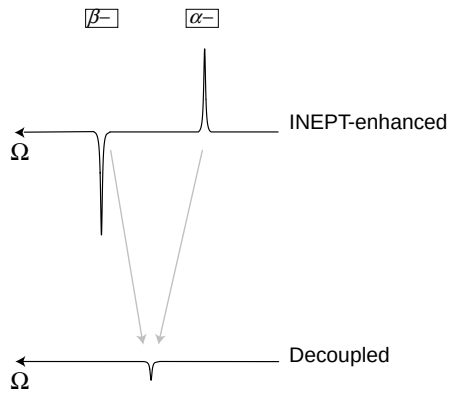

Figure 16.34
^1H decoupling of an INEPT spectrum destroys the transferred antiphase component.

In order to allow decoupling, it is necessary to *refocus* the enhanced antiphase components, so that they are brought back into phase again. This may be done by adding another spin echo sandwich to the pulse sequence. The *refocused INEPT* pulse sequence is as follows:

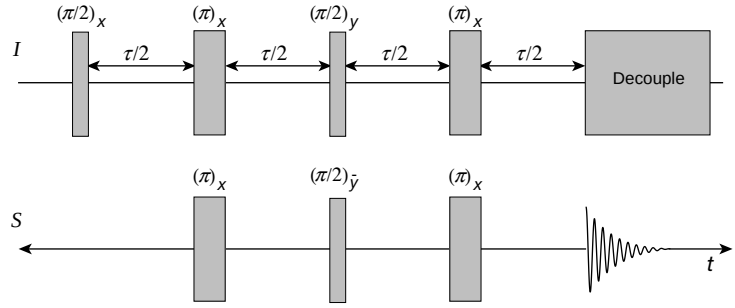

Figure 16.35
Refocused INEPT pulse sequence.

Apart from the additional spin echo sandwich, the phase of one of the S-spin pulses has been changed. This modification allows one to produce enhanced spectra in absorption phase.

The pulse sequence may be analysed by using the standard simplifications for the spin echo sandwiches:

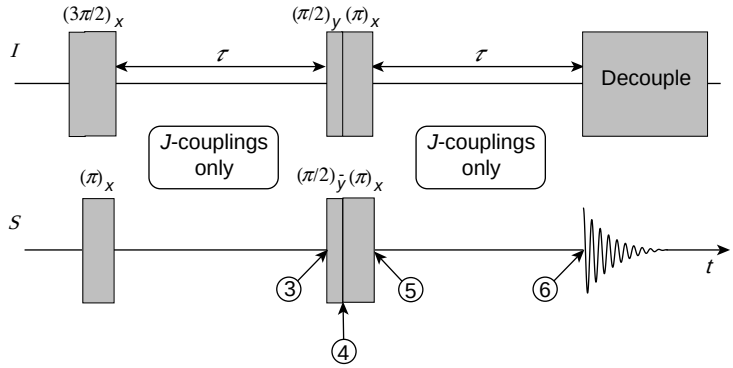

Figure 16.36
Equivalent refocused INEPT pulse sequence.

The propagation of the density operator through the last part of the pulse sequence is as follows:

$$\hat{\rho}_{③} = \frac{1}{4}\widehat{1} + \frac{1}{4}\mathbb{B}_I 2\hat{I}_x\hat{S}_z - \frac{1}{4}\mathbb{B}_S\hat{S}_z$$

$$\downarrow \quad (\pi/2)_y^I, (\pi/2)_{\bar{y}}^S$$

$$\hat{\rho}_{④} = \frac{1}{4}\widehat{1} + \frac{1}{4}\mathbb{B}_I 2\hat{I}_z\hat{S}_x + \frac{1}{4}\mathbb{B}_S\hat{S}_x$$

$$\downarrow \quad \pi_x^I, \pi_x^S$$

$$\hat{\rho}_{⑤} = \frac{1}{4}\widehat{1} - \frac{1}{4}\mathbb{B}_I 2\hat{I}_z\hat{S}_x + \frac{1}{4}\mathbb{B}_S\hat{S}_x$$

$$\downarrow \pi J_{IS}\tau \text{ } (J\text{-couplings only})$$

$$\hat{\rho}_{⑥} = \frac{1}{4}\widehat{1} + \underbrace{\frac{1}{4}\mathbb{B}_I\hat{S}_y}_{\text{transferred}} - \underbrace{\frac{1}{4}\mathbb{B}_S 2\hat{I}_z\hat{S}_y}_{\text{non-transferred}}$$

The 'transferred' term corresponds to in-phase S-spin magnetization and is proportional to the Boltzmann factor of spin I. It gives rise to a positive in-phase signal (see Note 6). The 'non-transferred' term corresponds to antiphase S-spin magnetization. Upon decoupling, the non-transferred term cancels out, leaving only a greatly enhanced signal from the in-phase transferred term (see Figure 16.37). An experimental spectrum obtained with refocused-INEPT is shown in Figure 16.38.

The behaviour of INEPT in systems with more than two spins is discussed in Section 18.12.

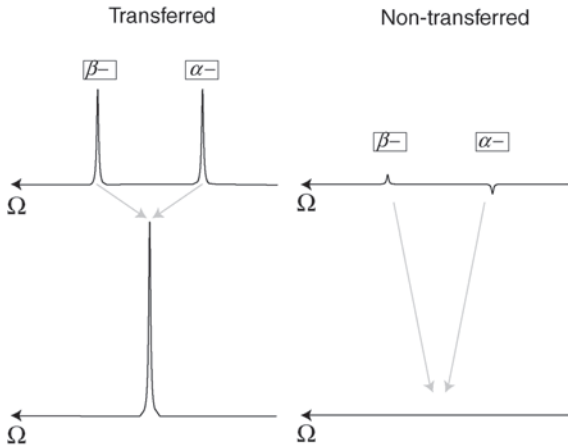

Figure 16.37 Subspectral components for refocused INEPT.

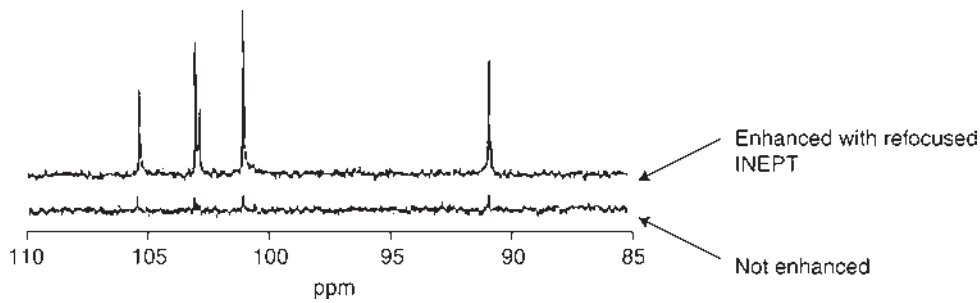

Figure 16.38 Experimental ^{15}N spectra of gramicidin in aqueous solution, using a single $\pi/2$ pulse to excite the ^{15}N spectrum (bottom) and using refocused INEPT (top). Adapted from *Encyclopedia of Nuclear Magnetic Resonance*, Vol. 4, D. M. Grant and R. K. Harris (eds), Wiley, Chichester, p. 2533 (Reproduced by permission of Wiley & Sons, Inc.)

16.4 Residual Dipolar Couplings

So far, all the experiments in this chapter have dealt with spin systems in an isotropic liquid phase, in which the molecular orientations are uniformly distributed. In this section, I discuss the use of *weakly oriented liquids* in biomolecular NMR. In these phases, the molecules tumble freely, but there is a very slight preference for some particular orientation, or set of orientations (see Section 1.6).

For simplicity, I will discuss these effects in the context of an ensemble of heteronuclear two-spin systems, such as ^{13}C–^{1}H or ^{15}N–^{1}H pairs in an isotopically labelled biomolecule. However, experiments of this type are also applicable to the NMR of inorganic substances.

16.4.1 Angular information

Consider a ^{13}C–^{1}H pair in a weakly oriented biomolecule. For simplicity, suppose that the molecule is shaped like an ellipsoid, and denote the angle between the ^{13}C–^{1}H vector and the molecular long axis by the symbol θ_{IS}:

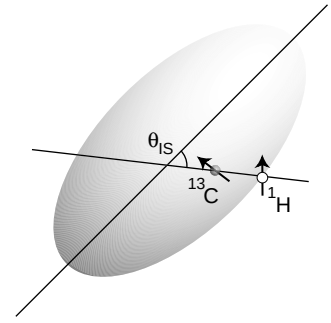

Figure 16.39
The angle θ_{IS} between the internuclear vector and the molecular long axis.

By dissolving the biomolecules in an anisotropic liquid phase, it becomes possible to estimate the angle θ_{IS}, which determines which way the ^{13}C–^{1}H vector 'points' with respect to the rest of the molecule. This important angular information complements nicely the internuclear distance information revealed by the NOESY or ROESY experiments (see Sections 20.6 and 20.7). By measuring the angles θ_{IS} for many different heteronuclear spin pairs, and combining this information with internuclear distances from NOESY or ROESY, it is possible to build up a very detailed picture of the molecular structure (see *Further Reading*).

16.4.2 Spin Hamiltonian

Denote the angle between the long axis of the molecule and the magnetic field as Θ. In a liquid, Θ fluctuates rapidly as the molecules tumble. The distribution of molecular orientations is not uniform, if the liquid is anisotropic. Denote the angle between the ^{13}C–^{1}H vector and the *field* by the symbol Θ_{IS} (see Figure 16.40). The angle Θ_{IS} depends in a complicated way on the molecular orientation and the angle θ_{IS}, and fluctuates strongly in a liquid.

From Equations 9.40 and 14.20the spin Hamiltonian for the pair is

$$\hat{\mathcal{H}} = \omega_I^0 \hat{I}_z + \omega_S^0 \hat{S}_z + \omega_{IS} 2\hat{I}_z \hat{S}_z \tag{16.19}$$

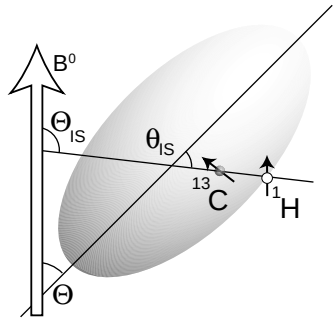

Figure 16.40
The angle Θ between the molecular long axis and the field, and the angle Θ_{IS} between the internuclear vector and the field.

where the ^{1}H nucleus is denoted I and the ^{13}C nucleus is denoted S, and the Larmor frequencies in the anisotropic phase are

$$\omega_I^0 = -\gamma_I B^0 \left(1 + \overline{\delta_{zz}^I(\Theta)}\right)$$

$$\omega_S^0 = -\gamma_S B^0 \left(1 + \overline{\delta_{zz}^S(\Theta)}\right)$$

The spin–spin coupling in the anisotropic phase is

$$\omega_{IS} = d_{IS} + \pi J_{IS} \tag{16.20}$$

where the secular part of the dipole–dipole coupling is

$$d_{IS} = b_{IS}\,\frac{1}{2}\overline{(3\cos^2\Theta_{IS} - 1)} \tag{16.21}$$

The overbars denote averages over all molecular orientations Θ, weighted by their probability, and b_{IS} is the dipole–dipole coupling constant:

$$b_{IS} = -\frac{\mu_0}{4\pi}\frac{\gamma_I\gamma_S\hbar}{r_{IS}^3}$$

where r_{IS} is the distance between the spins. The symbols $\delta_{zz}^I(\Theta)$ and $\delta_{zz}^S(\Theta)$ denote the secular parts of the chemical shift tensors for the ^{1}H and ^{13}C sites respectively (see Section 9.1.9).

In general, the angles Θ, Θ_{IS} and θ_{IS} are linked with each other in rather a complicated way. As the molecule tumbles, Θ changes, and this changes in turn the value of Θ_{IS}, in a way that depends on the angle θ_{IS}.

The term d_{IS} in Equation 16.19 is called the *residual dipolar coupling*. In a fully isotropic liquid, d_{IS} vanishes. In a weakly anisotropic liquid, on the other hand, d_{IS} is small but finite. Measurement of d_{IS} allows one to estimate the angle θ_{IS}, which describes the orientation of the heteronuclear vector with respect to the molecular long axis.

16.4.3 Orienting media

There are many different physical media that generate weakly oriented liquid solvents. These include suspensions of virus particles, suspensions of cell membrane fragments, polyacrylamide gels that have been slightly squeezed in one direction, and *bicelles*, which are aggregates of *lipid* molecules. The area is under intense current development (see *Further Reading*). In this section, I discuss the specific case of bicelles, which were one of the first media to be used for this purpose.[7]

Lipids are amphiphilic organic molecules, with a polar headgroup attached to hydrophobic aliphatic chains. In water, the lipid molecules tend to aggregate spontaneously into *bilayers*, in which the hydrophobic tails are in contact and shielded from the water by the hydrophilic headgroups. For certain mixtures of lipids, the bilayers form disk-shaped aggregates called bicelles, which swim around freely in the aqueous solution.[7] Often, the bicelles are circular in profile, and, under suitable conditions, the bicelle disks orient spontaneously in a strong external magnetic field, because they have an anisotropic magnetic susceptibility (see Section 2.2). In many cases, the disks tend to orient so that the external magnetic field is approximately in the plane of each disk:

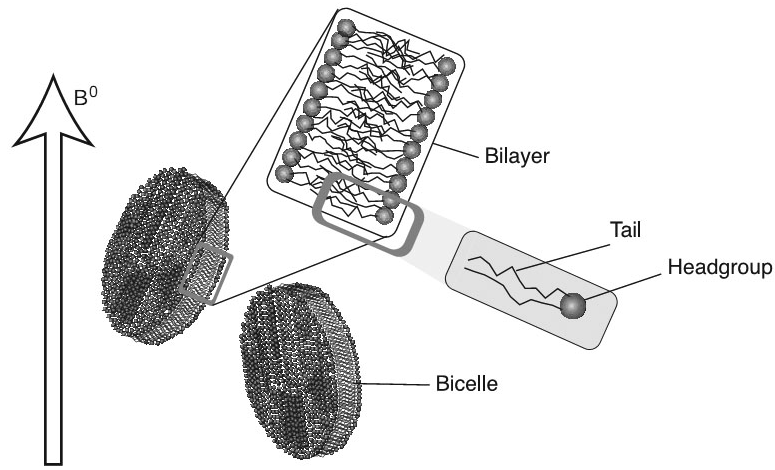

Figure 16.41
A bicelle is composed of a lipid bilayer.

In addition, steric interference between the bicelle disks causes them to stack up like coins. The bicelle disks, therefore, are oriented with respect to each other as well as with respect to the magnetic field. Locally, the director for the bicelle phase is *perpendicular* to the magnetic field:

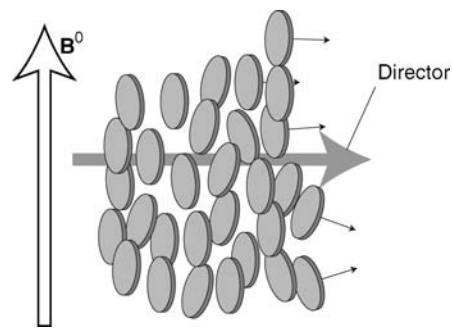

Figure 16.42
The bicelle director is perpendicular to the field. The normals to the bicelle planes (indicated by arrows) are aligned with the director.

If biomolecules are dissolved in the liquid between the bicelles, then the orientation of the bicelles is transferred weakly to the orientation of the biomolecules. One simple mechanism for this *orientation transfer* process is sketched here. In practice, the process may be complex and involves a superposition of several different mechanisms.

Biomolecules in solution acquire a partial orientation by collisions with the bicelle disks. The usual tendency is for the long axes of the molecules to become slightly oriented *parallel* to the bicelle planes – one can imagine the molecules being squeezed between the bicelles, and there is more room for the molecules if they are oriented this way:

In reality, the tendency for orientation is very small (only around 10^{-3}), but this is enough to lead to useful effects on the NMR spectrum.

Note carefully that the long axes of the molecules are not oriented *along* the magnetic field. The long axes of the molecules are uniformly distributed around the director, which is itself perpendicular to the magnetic field. Any orientation of the molecular long axis that is perpendicular to the director is equally likely.

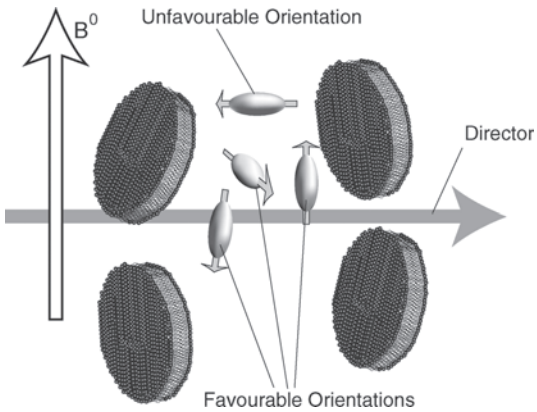

Figure 16.43
Molecules in solution tend to be oriented so that their long axes are in the plane of the bicelles, i.e. perpendicular to the director.

16.4.4 Doublet splittings

The spin Hamiltonian for the weakly oriented heteronuclear spin pair, Equation 16.19, is identical to that in an isotropic phase, except that (i) the chemical shift terms are different and (ii) that the J-coupling term πJ_{IS} is replaced by a term ω_{IS} including both the J-coupling and the residual dipolar coupling (see Equation 16.19).

The ^{13}C spectrum, therefore, consists of a doublet with splitting $2\omega_{IS} = 2\pi J_{IS} + 2d_{IS}$ in units of radians per second, or $J_{IS} + d_{IS}/\pi$ in units of hertz. The doublet splitting is either slightly larger than the J-coupling or slightly smaller, depending on the orientation of the ^{13}C–^{1}H vector with respect to the molecule.

If the ^{13}C–^{1}H vector is *parallel* to the long axis of the molecule, then the doublet splitting is slightly *smaller*. This may be seen as follows. Suppose, for simplicity, that the orientation of the molecules by the bicelles is extreme, so that all molecular long axes are forced to be parallel to the bicelle planes. View the system along the bicelle director, so that the bicelle planes appear to be in the plane of the paper:

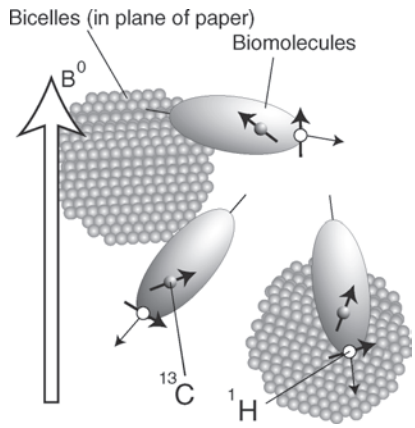

Figure 16.44
Case where the ^{13}C–^{1}H vectors are along the long axis of the molecules, and the molecular long axes are parallel to the bicelle planes.

In this case, the angle Θ_{IS} between the ^{13}C–^{1}H vector and the field takes all possible angles with equal probability, even though the molecules are partially ordered. The relevant orientational average is therefore

$$\frac{1}{2}\overline{(3\cos^2\Theta_{IS}-1)} = (2\pi)^{-1}\int_0^{2\pi} \mathrm{d}\Theta_{IS}\,\frac{1}{2}\left(3\cos^2\Theta_{IS}-1\right) = \frac{1}{4}$$

(Note the subtle difference between this *planar* average and the *spherical* average calculated in Equation 9.38.) It follows that, in this extreme situation of perfect orientation by the bicelles, with the ^{13}C–^{1}H vectors along the long axes of the molecules, the doublet splitting is given in units of radians per second by

$$2\omega_{IS} = 2\pi J_{IS} + \frac{1}{2}b_{IS} \tag{16.22}$$

In practice, the degree of orientation by the bicelles is very small, so the relevant factor is much less than 1/2. Nevertheless, the residual dipolar coupling retains the same sign as in the idealized calculation. Since the dipolar coupling constant b_{IS} is *negative* for ^{13}C–^{1}H interactions, whereas the one-bond J-coupling is *positive*, the effect of the orientation by the bicelles is to *reduce* the doublet splitting slightly, compared with its value in isotropic liquids:

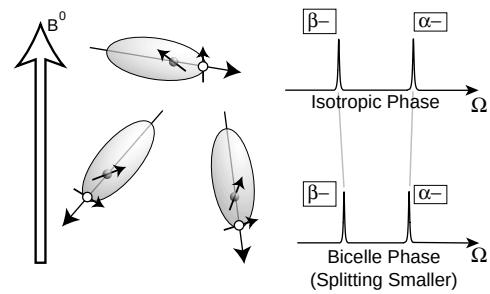

Figure 16.45
If the ^{13}C-^{1}H vectors are parallel to the molecular long axes, then the ^{13}C–^{1}H splitting is slightly smaller in the oriented bicelle phase.

The calculation for ^{13}C–^{1}H vectors which are perpendicular to the molecular long axis is more complicated, since there are two degrees of freedom in this case. The molecules may tumble around their own long axes, and the long axes may themselves rotate in the plane of the bicelles. A detailed calculation (not reproduced here) gives the following result:

$$\frac{1}{2}\overline{(3\cos^2\Theta_{IS}-1)} = -\frac{1}{8}$$

The doublet splitting, in the case that the ^{13}C–^{1}H vectors are perpendicular to the molecular long axes, is given in this extreme case by

$$2\omega_{IS} = 2\pi J_{IS} - \frac{1}{4}b_{IS} \tag{16.23}$$

Since b_{IS} is negative, the doublet splitting in the oriented phase is slightly larger than its value in isotropic phase:

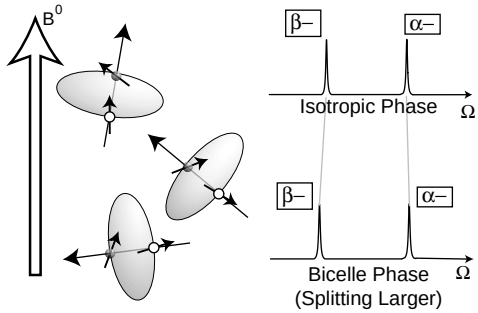

Figure 16.46
If the ^{13}C-^{1}H vectors are perpendicular to the molecular long axes, the ^{13}C–^{1}H splitting is slightly larger in the oriented bicelle phase.

By studying the small changes in the doublet splittings, when a biomolecule is dissolved in a bicelle solution, it is possible to deduce the orientations of the ^{13}C–^{1}H vectors with respect to the molecular long axes. An experimental example is shown in Figure 16.47.

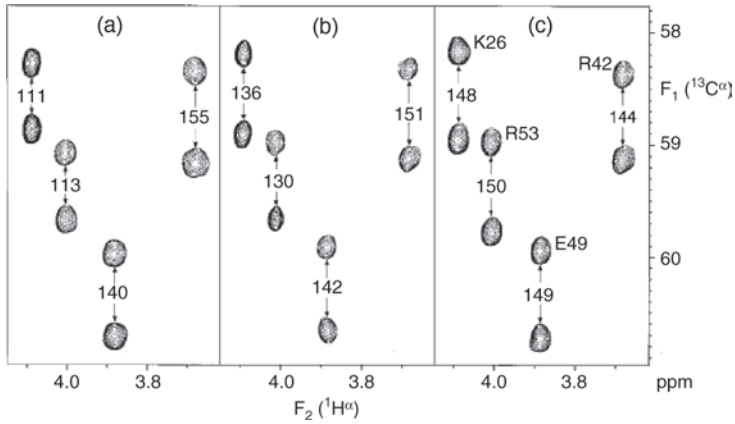

Figure 16.47 Experimental measurements of residual dipolar couplings in a weakly oriented liquid. The plots show extracts from the C^{α}–H^{α} regions of two-dimensional ^{1}H–^{13}C correlation spectra, for solutions of the small protein called bovine pancreatic trypsin inhibitor (BPTI). The ^{13}C resonances are split into doublets through the coupling to the directly bonded proton. Plots (a) and (b) are taken in two different weakly oriented phases, containing different concentrations of the bicelle-forming agents DMPC (dimyristoyl-phosphatidylcholine) and DHPC (dihexanoyl-phosphatidylcholine). Plot (c) is taken in isotropic solution. The splittings in (c) are equal to the ^{1}H–^{13}C J-couplings, and the splittings in (a) and (b) contain contributions from the dipole–dipole couplings. Most splittings increase when going from (a) to (c), but one decreases. This is because of the different relative angles of the ^{1}H–^{13}C internuclear vectors relative to the order axis. Adapted from M. Ottiger and A. Bax, *J. Biomol. NMR* **12**, 361–372 (1998), copyright, Springer Science and Business Media.

Similar studies are possible for other heteronuclear pairs of nuclei, such as ^{15}N and ^{1}H, and also homonuclear spin pairs, such as protons. The splittings for directly bonded ^{15}N–^{1}H pairs behave in the same way as for directly bonded ^{13}C–^{1}H pairs. The splitting becomes smaller in the oriented bicelle solution if the ^{15}N–^{1}H vector is parallel to the molecular long axis, and it becomes slightly larger in the oriented phase if the ^{15}N–^{1}H vector is perpendicular to the molecular long axis. This may be seen from Equations 16.22 and 16.23, using the fact that b_{IS} is positive for the ^{15}N–^{1}H interaction and that J_{IS} is negative for directly bonded ^{15}N–^{1}H pairs.

There are also many other media that may be used to induce a weak molecular orientation, giving rise to a similar dependence of the spectral splittings on the directions of the internuclear vectors. In some cases,

the magnetic susceptibility of the biomolecules itself causes weak orientational effects, without assistance from agents such as bicelles (see *Further Reading*).

It might be expected that increasing the degree of orientation of the molecules would make these effects larger and, hence, improve the quality of the geometrical information. However, in most cases, increasing the molecular alignment sharply degrades the resolution, sensitivity, and simplicity of the spectra. This is because almost all realistic molecules contain many coupled spins. If the molecules are oriented too strongly, then all of the dipolar couplings in the system become finite. The spin system becomes strongly coupled, and the spectrum becomes intractable. The beauty of the bicelle work is that the molecules are oriented so slightly that the system remains weakly coupled. The largest dipolar couplings only act as weak perturbations of the J-couplings, and the huge number of additional dipolar couplings only give rise to a slight broadening.

Notes

1. The pulse sequence phases are consistent with the 'sign-corrected' version of the States procedure discussed in Section 5.9.4. The use of $\Phi = -\pi/4$ for the 'sine' signal derives from the fact that double-quantum coherences are twice as sensitive to r.f. phase shifts as single-quantum coherences (see Appendix A.11.3).

2. In strongly coupled systems, the signal induced by a coherence transfer pathway incurs an additional factor representing the coupling strength of the coherence to the receiver coil (see Appendix A.8). In the case of the weakly coupled systems discussed in the current chapter, the signal coupling strengths are the same for all observable (-1)-quantum coherences.

3. There are cases in which nuclei with large values of γ relax more *slowly* than nuclei with small values of γ. For example, consider an ensemble of isolated ^{13}C–^{1}H systems, and assume that the relaxation is caused predominantly by the intramolecular dipole–dipole interaction of the two spins, as discussed in Chapter 20. The mutual dipole–dipole interactions of the two spins are exactly equal: the ^{13}C spin experiences a strong local field generated by the strongly magnetic ^{1}H neighbour, but interacts weakly with that field since the γ-value of ^{13}C is relatively low. Similarly, the ^{1}H spin experiences a weak local field generated by the weakly magnetic ^{13}C neighbour, but interacts strongly with that field since the γ-value of ^{1}H is relatively high. Since the mutual dipole–dipole interactions are equal, one might expect that the spin–lattice relaxation time constants of the ^{1}H and ^{13}C spins should also be the same. However, there is another effect involved. As described in Chapter 20, the values of T_1 depend on the spectral density of the dipole–dipole fluctuations at the nuclear Larmor frequency. Since the ^{13}C spins have a lower Larmor frequency than ^{1}H spins in the same field, and since the spectral density function is peaked at zero frequency, the ^{13}C spins have *shorter* values of T_1 than ^{1}H spins in this particular case. This is actually observed experimentally in heavily deuterated biomolecules. More commonly, ^{1}H spins have more rapid longitudinal relaxation than ^{13}C spins, because each ^{1}H couples strongly to local fields generated by *other* protons.

4. The formula in Equation 16.15, which relates the signal-to-noise ratio to γ and B^0, is very rough and assumes comparable linewidths and probe performance.

5. The INEPT pulse sequence was invented by Gareth Morris (see G. A. Morris and R. Freeman, *J. Am. Chem. Soc.* **101**, 760 (1979)). Non-native English speakers may not be aware that INEPT is another ironical NMR acronym. The word means 'clumsy' or 'incompetent'.

6. Estimating the spectral appearance in Figures 16.32 and 16.37 requires great care. Equation 16.18 indicates the presence of a non-transferred term proportional to $+\frac{1}{4}\mathbb{B}_S\hat{S}_y$ and a transferred term proportional to $+\frac{1}{4}\mathbb{B}_I 2\hat{I}_z\hat{S}_y$. Taking the non-transferred term first, one should remember that the thermal equilibrium density operator contains a term proportional to $+\frac{1}{4}\mathbb{B}_S\hat{S}_z$, which may be converted into a term proportional to $-\frac{1}{4}\mathbb{B}_S\hat{S}_y$ by a $(\pi/2)_x$ pulse. For the case $S = {}^{15}\mathrm{N}$, the Boltzmann factor $\mathbb{B}_S$ is negative (see Equation 16.17), and hence we should interpret a *positive* term proportional to $\hat{S}_y$ as representing a positive absorption signal. The non-transferred term in Equation 16.18, therefore, represents a negative in-phase signal, as shown in Figure 16.32. The transferred term, on the other hand, is proportional to $+\frac{1}{4}\mathbb{B}_I 2\hat{I}_z\hat{S}_y$, which should be interpreted as a *positive* antiphase signal, since $\mathbb{B}_I$ is positive for the case $I = {}^1\mathrm{H}$. Finally, the assignment of the spectral peaks to the coherences $\rho_{\boxed{\alpha-}}$ and $\rho_{\boxed{\beta-}}$ requires taking into account the negative values of γ_S and the one-bond ${}^1\mathrm{H}$–${}^{15}\mathrm{N}$ J-coupling (see Section 15.5). Experimental realizations of this experiment may not reproduce the expected peak pattern because of inconsistencies in the signs of r.f. phase shifts on many NMR spectrometers (see M. H. Levitt, *J. Magn. Reson.* **126**, 164 (1997) and M. H. Levitt and O. G. Johannessen, *J. Magn. Reson.* **142**, 190–194 (2000).

7. It is possible that lipids do not actually form disk-like bicelles under the conditions typically used for biochemical NMR. There is evidence that the lipid bilayers are organized in highly perforated sheet-like structures (the 'Swiss cheese model'), rather than disks. Nevertheless, the precise nature of the lipid phase does not have appreciable consequences for the NMR properties of the partially oriented molecules outside the bilayers.

Further Reading

- For a pedagogical explanation of the experiments in this chapter, use J. Keeler, *Understanding NMR Spectroscopy*, Wiley, Chichester, 2005.
- For a more detailed description of NMR experiments on coupled spin systems, including double-quantum-filtered COSY, see J. Cavanagh, W. J. Fairbrother, A. G. Palmer and N. J. Skelton, *Protein NMR Spectroscopy. Principles and Practice*, Academic Press, New York, 1996.
- For further discussion of INADEQUATE and INEPT, see R. Freeman, *Spin Choreography. Basic Steps in High Resolution NMR*, Spektrum, Oxford, 1997.
- For more on biomolecular NMR experiments in weakly oriented media, see E. de Alba and N. Tjandra, *Prog. NMR Spectrosc.* **40**, 175–197 (2002) and M. Blackledge, *Prog. NMR Spectrosc.* **46**, 23–61 (2005).

Exercises

16.1 This exercise investigates the important *heteronuclear multiple-quantum coherence* (HMQC) experiment, which generates two-dimensional spectra in which the chemical shifts of different spin species appear along the two axes. In this exercise, the HMQC experiment is examined for the simple case of two coupled spins-1/2 of different species I and S.
The pulse sequence for the 'cosine' experiment in the States procedure is shown below:

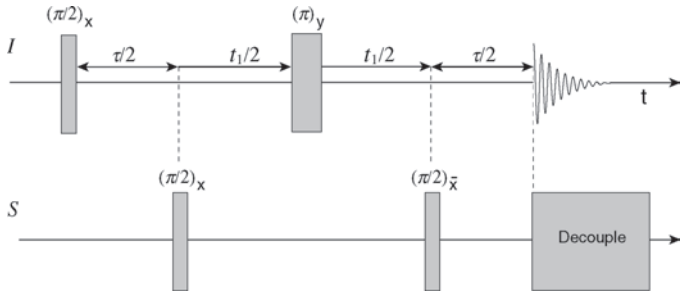

The delays τ are given by $\tau = (2J_{IS})^{-1}$, where J_{IS} is the J-coupling between the two spins. The interval t_1 is incremented in an arrayed fashion (the I-spin π pulse is always kept in the middle of the t_1 interval). The I-spin signal is observed at the end of each pulse sequence.

(i) If the spin density operator before the first pulse is given by $\hat{\rho}(0) = \hat{I}_z$, and relaxation is neglected, what is the spin density operator at the start of the detection period for an arbitrary value of t_1?
(ii) Sketch the form of the two-dimensional spectrum for a single IS spin system.
(iii) How should the pulse sequence be modified in order to provide the 'sine' component in the States procedure?

16.2 This exercise investigates the *double-quantum-filtered COSY* (2QF-COSY) experiment. The 'cosine' pulse sequence is as follows:

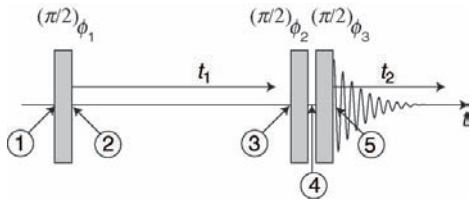

The phase table is as follows:

Cycle counter m	ϕ_1	ϕ_2	ϕ_3	ϕ_{rec}
0	$3\pi/2$	0	$\pi/2$	0
1	$3\pi/2$	0	π	$3\pi/2$
2	$3\pi/2$	0	$3\pi/2$	π
3	$3\pi/2$	0	0	$\pi/2$

Assume a homonuclear AX spin system. The short delay between the last two $\pi/2$ pulses may be ignored.

(i) Take the first step in the phase cycle procedure ($\mathrm{m} = 0$). For simplicity, start with an initial spin density operator $\hat{\rho}_{①} \sim \hat{I}_{1z}$. What is the spin density operator at time point ④?
(ii) Convert the x- and z-operators at time point ④ into shift operators. Which coherence orders are excited at this point?
(iii) The phase cycle has the effect of suppressing all signal components that do not pass through (± 2)-quantum coherences at time point ④. Select the operators that have order ± 2 and apply the final $\pi/2$ pulse. What is the spin density operator at time point ⑤? To bring out the meaning

of the final expression, replace all products of trigonometric functions by single trigonometric functions.

(iv) Repeat the calculation for the 'sine' component of the States procedure, in which the first pulse has phase π instead of phase $3\pi/2$. Use the same initial density operator.

(v) Repeat the calculations using the full form of the initial spin density operator, $\hat{\rho}_{\textcircled{1}} \sim \hat{I}_{1z} + \hat{I}_{2z}$. Sketch the form of the two-dimensional spectrum and remark on the shapes of the diagonal peaks and cross-peaks. What are the favourable properties of the double-quantum-filtered COSY spectrum? Are there any disadvantages of double-quantum-filtered COSY compared with ordinary COSY?

17 Many-Spin Systems

Most molecules contain many more than two coupled nuclear spins. In this chapter, I discuss how to write down the spin Hamiltonian for many-spin systems.

⚠Much of the discussion in this chapter is specific to the NMR of isotropic liquids, and is not generally applicable to solids and liquid crystals.

17.1 Molecular Spin System

In isotropic liquids, the only terms that survive the motional averaging are (i) the isotropic parts of the intramolecular interactions and (ii) the long-range dipole–dipole interactions. If the long-range dipole–dipole interactions are ignored (see Section 8.6.4), the spin Hamiltonian in an isotropic liquid is *purely intramolecular*.

All molecules of the same isotopomeric species, therefore, have the same motionally averaged spin Hamiltonian, given by

$$\widehat{\mathcal{H}} = \widehat{\mathcal{H}}^0 + \widehat{\mathcal{H}}_{\mathrm{RF}}$$

where $\widehat{\mathcal{H}}_{\mathrm{RF}}$ represents the interaction with the r.f. field, and $\widehat{\mathcal{H}}^0$ contains the interaction with the static field, plus the secular parts of the intramolecular chemical shift and J-coupling terms:

$$\widehat{\mathcal{H}}^0 = \underbrace{\sum_j \omega_j^0 \hat{I}_{jz} + \sum_{j<k} 2\pi J_{jk} \hat{\mathbf{I}}_j \cdot \hat{\mathbf{I}}_k}_{\text{all spins in one molecule}} \tag{17.1}$$

The isotropic chemically shifted Larmor frequency ω_j^0 is defined in Equation 9.16.

The term *molecular spin system* refers to the coupled nuclear spins in a single molecule. Often, the term *spin system* is used to imply the molecular spin system.

If all the spins in the molecular spin system are of the same isotopic type, then the spin system is said to be *homonuclear*. If more than one isotope is present, then the spin system is said to be *heteronuclear*.

Suppose, for example, that each molecule contains four spins, of the same isotopic type. The molecular spin system has the following spin Hamiltonian:

Spin Dynamics: Basics of Nuclear Magnetic Resonance, Second Edition Malcolm H. Levitt

$$\begin{aligned}\widehat{\mathcal{H}}^0 &= \omega_1^0 \hat{I}_{1z} + \omega_2^0 \hat{I}_{2z} + \omega_3^0 \hat{I}_{3z} + \omega_4^0 \hat{I}_{4z} \\ &+ 2\pi J_{12} \hat{\mathbf{I}}_1 \cdot \hat{\mathbf{I}}_2 + 2\pi J_{13} \hat{\mathbf{I}}_1 \cdot \hat{\mathbf{I}}_3 + 2\pi J_{14} \hat{\mathbf{I}}_1 \cdot \hat{\mathbf{I}}_4 \\ &+ 2\pi J_{23} \hat{\mathbf{I}}_2 \cdot \hat{\mathbf{I}}_3 + 2\pi J_{24} \hat{\mathbf{I}}_2 \cdot \hat{\mathbf{I}}_4 + 2\pi J_{34} \hat{\mathbf{I}}_3 \cdot \hat{\mathbf{I}}_4 \end{aligned} \tag{17.2}$$

where the chemically shifted Larmor frequencies are given by

$$\omega_j^0 = -\gamma_j B^0 (1 + \delta_j)$$

These four chemically shifted spins, and the six couplings between them, may be depicted by the following icon:

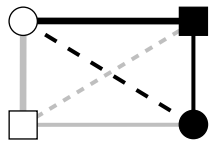

Figure 17.1
A four-spin system.

I have used different symbols to depict the four different chemical shifts and different line types to depict the six different J-couplings.

17.2 Spin Ensemble

The molecules of one isotopomer all have the same motionally averaged spin Hamiltonian. The collection of non-interacting, identical, spin systems is called the *spin system ensemble*:

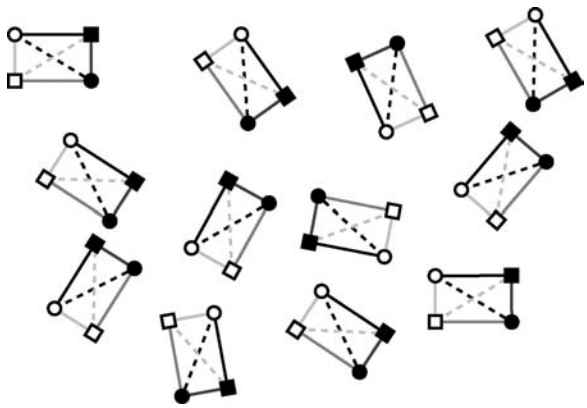

Figure 17.2
An ensemble of four-spin systems.

In a given sample, there are usually several compounds, each with several isotopomers. All the molecules of one isotopomer constitute a single spin ensemble. If there are several isotopomers present, then there are several independent spin ensembles.

17.3 Motionally Suppressed J-Couplings

In some cases, J-couplings are not observed to certain spins, because of a rapid motional process that averages the J-coupling to zero. There are two common situations:

1. Chemical bonds are rapidly forming and reforming, so that a particular nucleus jumps between different molecules;

2. The relevant nuclear spin undergoes very rapid longitudinal relaxation.

In the first case, the rapid dynamics of the nuclear spin is *spatial* – the spin moves physically from molecule to molecule. In the second case, the nucleus remains fixed in a given molecule, but the *polarization* of the spin fluctuates rapidly.

The first case is called *fast chemical exchange*. It is discussed in Section 19.5. A typical case is that of the OH proton in ethanol (CH_3CH_2OH). Unless special precautions are taken, traces of acid or base catalyse the rapid chemical exchange of the hydroxyl proton between different ethanol molecules. As a result, the NMR signals from this proton are usually broad and J-couplings between this proton and the others are not observed.

The second case is typified by *quadrupolar* nuclei. As discussed in Section 8.2.1, most nuclei with spin $> 1/2$ couple strongly to electric field gradients in the molecule. As the molecules rotate, the electric field gradients rotate too, and this causes the magnetic moments of these nuclei to fluctuate relatively strongly. This is manifested in very short spin–lattice relaxation time constants T_1 for most quadrupolar nuclei in a liquid. The rapid spin–lattice relaxation of quadrupolar spins averages out their J-couplings to other spins in the same molecule.

As shown in Section 19.5.3, the J-coupling of a spin I_j to a rapidly relaxing spin I_k may be ignored if the second spin has a longitudinal relaxation time constant T_1^k fulfilling the condition

$$|2\pi J_{jk} T_1^k| << 1$$

The longitudinal relaxation time constants for many quadrupolar spins in solution are as short as microseconds, in which case this condition is easily fulfilled. For example, the ^{1}H spins in ethyl chloride CH_3CH_2Cl experience no noticeable J-couplings to the abundant Cl isotopes ^{35}Cl and ^{37}Cl, since both of these have large quadrupole moments and relax rapidly.

In many cases, the molecular spin Hamiltonian in an isotropic liquid may therefore be written as

$$\hat{\mathcal{H}}^0 \cong \sum_j \omega_j^0 \hat{I}_{jz} + \underbrace{\sum_{j<k} 2\pi J_{jk} \hat{\mathbf{I}}_j \cdot \hat{\mathbf{I}}_k}_{\substack{\text{except spins with} \\ \text{motionally suppressed } J\text{-} \\ \text{couplings}}} \tag{17.3}$$

There are some cases in which couplings to quadrupolar spins must be considered in solution NMR. In particular, the isotope ^{2}H has a relatively small quadrupole moment, and ^{1}H–^{2}H or ^{2}H–^{13}C couplings are sometimes observed. Even isotopes such as ^{14}N, which has a large quadrupole moment, relax slowly if they are in molecular sites with a very small electric field gradient, because of high local symmetry. This is the case, for example, in the tetrahedral ion $^{14}NH_4^+$.

17.4 Chemical Equivalence

Spins are said to be chemically equivalent if the following conditions are both satisfied:

1. The spins are of the same isotopic species.

2. There exists a molecular symmetry operation that exchanges the two spins.

Consider, for example, the molecule 1,1-difluoroethene, which contains two ^{1}H and two ^{19}F spins:

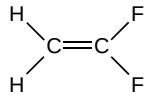

Figure 17.3
1,1-Difluoroethene.

There is clearly a reflection symmetry plane down the centre of the molecule (top to bottom in the diagram above). Reflection in the plane exchanges the two protons, indicating that they are chemically equivalent. The same reflection exchanges the two fluorine atoms, indicating that they are also chemically equivalent. The four-spin system of 1,1-difluoroethene may, therefore, be represented by the following icon:

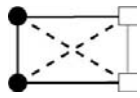

Figure 17.4
The four-spin system of 1,1-difluoroethene.

Chemically equivalent spins have been given the same symbol. Those J-couplings that are interchanged by reflection have been given the same style.

Other familiar examples of chemical equivalence are the six protons in benzene and the two protons in water:

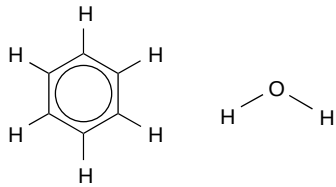

Figure 17.5
Benzene and water.

The corresponding spin systems may be depicted by the following icons:

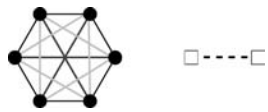

Figure 17.6
Proton spin systems in benzene and water.

Spins with identical chemical shifts are depicted by identical symbols; identical J-couplings are represented by lines of the same style.

Chemically equivalent spins have the same chemical shift. However, the inverse does not always hold. Two spins with the same chemical shift are not necessarily chemically equivalent. The coincidence of the shifts may be purely accidental, having nothing to do with molecular symmetry.

In molecules that have rapid internal mobility, the spin Hamiltonian is averaged over the accessible molecular conformations, weighted by their populations. This often creates additional opportunites for chemical equivalence. Consider, for example, the methyl protons in ethyl chloride (CH_3CH_2Cl). Looking down the C–C bond, we would see the following picture in one of the low-energy staggered conformations:

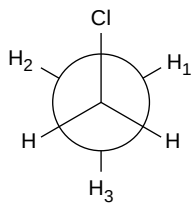

Figure 17.7
Newman projection of CH_3CH_2Cl.

The two CH_2 protons are clearly chemically equivalent, because of the plane of symmetry defined by Cl–C–C–H_3. The two CH_3 protons marked H_1 and H_2 are also chemically equivalent for the same reason. However, the proton H_3 cannot be exchanged with H_1 or H_2 by a symmetry operation, so it is not chemically equivalent to the other two, in this conformation.

However, the methyl group rapidly rotates around the C–C bond, allowing the molecule to explore the other two staggered conformations:

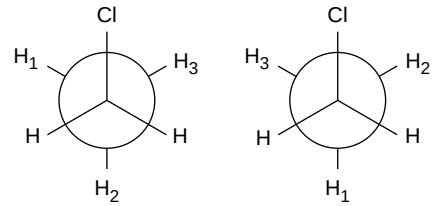

Figure 17.8
Two more staggered conformations of CH_3CH_2Cl.

The three staggered conformations have the same energy, so the molecule spends equal time in each of them. When averaged over all three conformations, each of the three CH_3 protons experiences the same environment, so all three CH_3 protons in ethyl chloride are chemically equivalent. The coupling diagram for the protons in ethyl chloride is as follows:

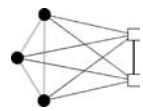

Figure 17.9
Coupling diagram for CH_3CH_2Cl.

There are some subtle traps in this type of system. Consider, for example, the two CH_2 protons in a molecule of the following type:

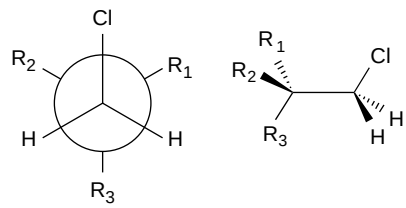

Figure 17.10
A molecule containing diastereotopic CH_2 protons.

where the groups R_1, R_2 and R_3 are all different. Assume, again, that the molecule has full rotational mobility about the C–C bond.

It is tempting to assume that high rotational mobility tends to average out the environments of the two CH_2 protons, leading to chemical equivalence. This is incorrect, as may be seen from the following representations of the three staggered conformations, looking down the C–C bond:

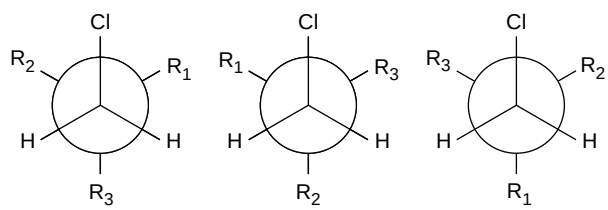

Figure 17.11
Three staggered conformations, all inequivalent.

None of these conformations has a plane of symmetry, so no pair of protons is chemically equivalent in any of the three conformations. Furthermore, no two conformations have the same energy. The three conformations have different populations in thermal equilibrium. The CH_2 protons in this type of system, therefore, are *not* chemically equivalent in general, whatever the degree of internal mobility. The two CH_2 protons have different chemical shifts.

The chemical equivalence of CH_2 protons is even broken by remote influences. Suppose that the groups R_2 and R_3 are identical, but the group R_1 is *chiral* (meaning that it cannot be superimposed on its own mirror image). In this case, the two CH_2 protons are still inequivalent. This situation is common in biological NMR, since most biologically active molecules are chiral.

Although chirality often leads to chemical inequivalence, inequivalent CH_2 protons may also occur in molecules that are not chiral. The case of citric acid is instructive:

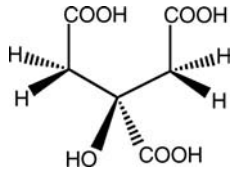

Figure 17.12
Molecular structure of citric acid.

The molecule as a whole has a plane of symmetry (perpendicular to the paper, through the central carbon atom) and is therefore not chiral. Nevertheless, there is no molecular symmetry operation that exchanges the two protons in the same CH_2 group with each other (the mirror reflection exchanges protons in different CH_2 groups). The two protons within each CH_2 group are chemically inequivalent. This remains true even if there is full rotational mobility around the carbon–carbon bonds.

Chemically inequivalent protons in CH_2 groups are called *diastereotopic* protons.

17.5 Magnetic Equivalence

Magnetic equivalence is a strong form of chemical equivalence. A set of spins is magnetically equivalent IF

- Condition 1: the spins have the same chemical shifts

  AND

- (Condition 2a: the spins have identical couplings to all *other* spins in the molecule

  OR

- Condition 2b: there are no other spins in the molecule.)

Consider, for example, the protons in the commonest isotopomer of benzene. The protons are chemically equivalent (Condition 1). Since there are no other spins in the molecule, they are also magnetically equivalent (Condition 2b). The same is true for the usual isotopomer of water. The two protons are chemically equivalent (Condition 1), and there are no other spins in the molecule (Condition 2b). The two protons of water are magnetically equivalent.

As a second example, reconsider the case of ethyl chloride, CH_3CH_2Cl. As discussed before, the two CH_2 protons are chemically equivalent (Condition 1). In addition, each of the two CH_2 protons has the same coupling with each of the three CH_3 protons (Condition 2a). Similarly, the three CH_3 protons are chemically equivalent (Condition 1) and have identical couplings with each of the two CH_2 protons (Condition 2a). The spin system in CH_3CH_2Cl contains one group of three magnetically equivalent protons and one group of two magnetically equivalent protons.

Magnetic equivalence is important because it allows the spin Hamiltonian to be simplified. One example of this was already encountered in Section 14.4, for the case of a spin-1/2 pair. It was shown that the J-coupling between the two spins has no effect on the NMR properties, providing that (i) there are only two spins and (ii) they have the same chemical shift. In this case, the J-coupling term may be omitted from the spin Hamiltonian, without changing any physical predictions.

In the special case of the two-spin system discussed in Section 14.4, chemical equivalence necessarily implies to magnetic equivalence, through Condition 2b above. In the general case of *more than two coupled spins*, chemical equivalence does *not* imply magnetic equivalence.

In Appendix A.9, it is shown that the NMR signal is independent of spin–spin coupling terms *within* magnetically equivalent groups. It is therefore convenient to omit these couplings from the spin Hamiltonian, which then reads

$$\widehat{\mathcal{H}}^0 = \sum_j \omega_j^0 \hat{I}_{jz} + \underbrace{\sum_{j<k}{}' 2\pi J_{jk} \hat{\mathbf{I}}_j \cdot \hat{\mathbf{I}}_k}_{\text{except spins with motionally suppressed } J\text{-couplings}} \tag{17.4}$$

The 'prime' on the summation indicates the exclusion of couplings between magnetically equivalent spins.

For example, consider the spin system specified in Equation 17.2. If spin I_1 is magnetically equivalent to I_2, and I_3 is magnetically equivalent to I_4, then we have

$$\omega_1^0 = \omega_2^0 \qquad \omega_3^0 = \omega_4^0$$
$$J_{13} = J_{14} = J_{23} = J_{24}$$

as depicted in the following coupling diagram:

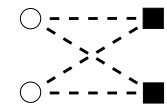

Figure 17.13
A four-spin system with two pairs of magnetically equivalent spins.

Since there are two groups of magnetically equivalent pairs of spins, the following simplified spin Hamiltonian may be used:

$$\widehat{\mathcal{H}}^0 = \omega_1^0(\hat{I}_{1z} + \hat{I}_{2z}) + \omega_3^0(\hat{I}_{3z} + \hat{I}_{4z}) + 2\pi J_{13}(\hat{\mathbf{I}}_1 + \hat{\mathbf{I}}_2) \cdot (\hat{\mathbf{I}}_3 + \hat{\mathbf{I}}_4) \tag{17.5}$$

which may be represented by the following diagram:

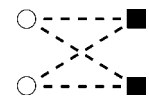

Figure 17.14
The couplings between magnetically equivalent spins may be omitted.

Another example is the spin system of CH_3CH_2Cl, which may be represented as follows:

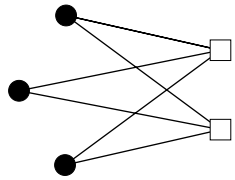

Figure 17.15
Coupling diagram for CH_3CH_2Cl, omitting couplings between magnetically equivalent spins.

Similarly, the spin systems of benzene and water may be depicted thus:

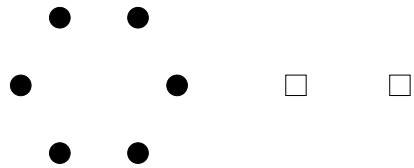

Figure 17.16
Proton spin systems in benzene and water, omitting couplings between magnetically equivalent spins.

indicating that, effectively, there are no active *J*-couplings between any of the spins in these last two molecules.

Reconsider now the 1,1-difluoroethene molecule. As discussed before, the two protons are chemically equivalent, as are the two fluorine spins. Are the two protons magnetically equivalent?

Rather surprisingly, the answer is negative. Each of the two protons has a different coupling with each of the two fluorine nuclei, since one coupling is between spins in trans geometry and the other coupling involves cis geometry:

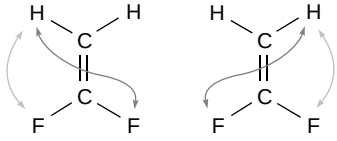

Figure 17.17
Spin-spin couplings in 1,1-Difluoroethene.

It follows that the two protons in this molecule are chemically equivalent, but *not* magnetically equivalent. The same holds for the two fluorine nuclei. The coupling diagram for 1,1-difluoroethene cannot be simplified, and is still as shown below:

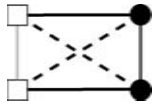

Figure 17.18
The four-spin system of 1,1-Difluoroethene.

It is instructive to contrast this case with the similar molecule 1,1-Difluoropropan-1,2-diene, which has the following molecular geometry:

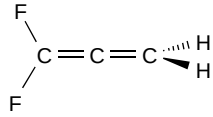

Figure 17.19
1,1-Difluoropropan-1,2-diene.

The two protons nuclei are clearly chemically equivalent, as are the two ^{19}F nuclei. In addition, the geometry of the molecule is such that all four ^{19}F–^{1}H couplings are equal:

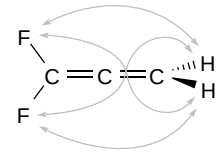

Figure 17.20
Spin-spin couplings in 1,1-difluoropropan-1,2-diene.

The two protons are therefore magnetically equivalent, as are the two ^{19}F nuclei. The spin system for this molecule, therefore, may be simplified:

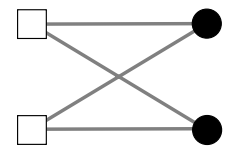

Figure 17.21
The four-spin system of 1,1-difluoropropan-1,2-diene.

The apparent disappearance of J-couplings between magnetically equivalent spins is quite surprising. A physical explanation runs as follows. For magnetically equivalent spins, the local magnetic fields, whatever their source, are exactly the same on the two spins. It follows that the motion of the two spin polarizations is identical. Whatever happens, the polarizations of the two spins are locked in the same relative orientation. There is, therefore, no need to incorporate a term in the spin Hamiltonian that takes into account the dependence of the energy on this relative spin orientation.

17.6 Weak Coupling

The weak-coupling approximation has already been encountered for the case of spin-1/2 pairs in Section 14.5.

The situation is a bit more complicated when more than two spins are involved. A system of many coupled spins is said to be *weakly coupled* if the following condition is satisfied for *all pairs of magnetically inequivalent spins*:

$$|\omega_j^0 - \omega_k^0| >> |\pi J_{jk}| \tag{17.6}$$

In other words, the frequency differences created by chemical shifts must be much larger than the J-couplings between magnetically inequivalent spins. If the weak-coupling approximation is valid, then the following simplified spin Hamiltonian may be used:[1]

$$\hat{\mathcal{H}}_{\text{weak}}^0 = \sum_j \omega_j^0 \hat{I}_{jz} + \underbrace{\sum_{j<k}{}' 2\pi J_{jk} \hat{I}_{jz} \hat{I}_{kz}}_{\text{except spins with motionally suppressed } J\text{-couplings}} \tag{17.7}$$

For example, suppose that the spin system in Equation 17.5 obeys the condition:

$$|\omega_1^0 - \omega_3^0| >> |\pi J_{13}|$$

The approximate spin Hamiltonian

$$\hat{\mathcal{H}}^0_{\text{weak}} = \omega_1^0(\hat{I}_{1z} + \hat{I}_{2z}) + \omega_3^0(\hat{I}_{3z} + \hat{I}_{4z}) + 2\pi J_{13}(\hat{I}_{1z} + \hat{I}_{2z})(\hat{I}_{3z} + \hat{I}_{4z}) \tag{17.8}$$

may be used in this case.

Weak coupling is an example of the *secular approximation* discussed in Appendix A.6. It may be viewed as a form of motional averaging generated by the *differential precession* of the different spins. Since the coupled spins precess at different frequencies, the interactions between the transverse components of the spin polarizations average out to zero. The only coupling terms that are not averaged out involve the longitudinal components of spin polarization, which are unchanged by the spin precession.

Since chemical shift frequency differences are proportional to the applied field, weak coupling is especially common on instruments with large magnetic fields. The development of NMR instrumentation towards ever higher fields has extended the range of the weak coupling approximation. Much NMR methodology in isotropic liquids is based on the reasonable validity of weak coupling.

Spin systems that are not weakly coupled are said to be *strongly coupled*. In these cases, the full form of the spin Hamiltonian shown by Equation 17.4 must be used. Appendix A.8 explores the spectral consequences of strong coupling.

17.7 Heteronuclear Spin Systems

Heteronuclear spin systems contain at least two different isotopic species. The difference in Larmor frequencies between two different isotopes is almost always much larger than the spin–spin couplings. The couplings between spins of different species, therefore, are almost always 'weak', in the sense of the previous section.

Consider, for example, a molecule with four spins, two of species I, called I_1 and I_2, and two of species S, called S_3 and S_4. Suppose that the chemical shifts of all four spins are different. The following spin Hamiltonian may be used:

$$\begin{aligned}\hat{\mathcal{H}}^0 = {} & \omega_1^0\hat{I}_{1z} + \omega_2^0\hat{I}_{2z} + \omega_3^0\hat{S}_{3z} + \omega_4^0\hat{S}_{4z} + 2\pi J_{12}\hat{\mathbf{I}}_1 \cdot \hat{\mathbf{I}}_2 + 2\pi J_{13}\hat{I}_{1z}\hat{S}_{3z} + 2\pi J_{14}\hat{I}_{1z}\hat{S}_{4z} \\ & + 2\pi J_{23}\hat{I}_{2z}\hat{S}_{3z} + 2\pi J_{24}\hat{I}_{2z}\hat{S}_{4z} + 2\pi J_{34}\hat{\mathbf{S}}_3 \cdot \hat{\mathbf{S}}_4\end{aligned} \tag{17.9}$$

where

$$\begin{aligned}\omega_1^0 &= -\gamma_I B^0(1+\delta_1) \qquad & \omega_3^0 &= -\gamma_S B^0(1+\delta_3) \\ \omega_2^0 &= -\gamma_I B^0(1+\delta_2) \qquad & \omega_4^0 &= -\gamma_S B^0(1+\delta_4)\end{aligned}$$

and γ_I and γ_S are the gyromagnetic ratios of the two isotopes.

Now suppose that the two I spins are chemically, but not magnetically, equivalent. Similarly, suppose that the two S spins are chemically, but not magnetically, equivalent (see Figures 17.17 and 17.18). The Larmor frequencies and couplings have the following symmetry:

$$\omega_1^0 = \omega_2^0 \qquad J_{13} = J_{24}$$
$$\omega_3^0 = \omega_4^0 \qquad J_{14} = J_{23}$$

In this case, the spin Hamiltonian may be written as follows:

$$\begin{aligned}\widehat{\mathcal{H}}^0 = {} & \omega_1^0(\hat{I}_{1z} + \hat{I}_{2z}) + \omega_3^0(\hat{S}_{3z} + \hat{S}_{4z}) + 2\pi J_{12}\hat{\mathbf{I}}_1 \cdot \hat{\mathbf{I}}_2 + 2\pi J_{13}(\hat{I}_{1z}\hat{S}_{3z} + \hat{I}_{2z}\hat{S}_{4z}) \\ & + 2\pi J_{14}(\hat{I}_{1z}\hat{S}_{4z} + \hat{I}_{2z}\hat{S}_{3z}) + 2\pi J_{34}\hat{\mathbf{S}}_3 \cdot \hat{\mathbf{S}}_4 \end{aligned} \tag{17.10}$$

Suppose, now, that the two I spins are magnetically equivalent and the two S spins are also magnetically equivalent (see Figures 17.19 and 17.20). The J-couplings now have the symmetry

$$J_{13} = J_{14} = J_{23} = J_{24}$$

and the spin Hamiltonian may be simplified further:

$$\widehat{\mathcal{H}}^0 = \omega_1^0(\hat{I}_{1z} + \hat{I}_{2z}) + \omega_3^0(\hat{S}_{3z} + \hat{S}_{4z}) + 2\pi J_{13}(\hat{I}_{1z}\hat{S}_{3z} + \hat{I}_{2z}\hat{S}_{4z} + \hat{I}_{1z}\hat{S}_{4z} + \hat{I}_{2z}\hat{S}_{3z})$$

Now go back to the case in which the spins are chemically equivalent but not magnetically equivalent (Equation 17.10). Suppose that a strong r.f. decoupling field is applied continuously at the Larmor frequency of species I, in order to effectively remove the couplings to species S (see Section 3.9). In the presence of a heteronuclear decoupling field, all Hamiltonian terms involving the irradiated spins may usually be dropped from the effective spin Hamiltonian, providing caution is used.[2] In the presence of I-spin decoupling, the spin Hamiltonian may therefore be written as follows:

$$\widehat{\mathcal{H}}^0(\text{with } I\text{-spin decoupling}) = \omega_3^0(\hat{S}_{3z} + \hat{S}_{4z}) + 2\pi J_{34}\hat{\mathbf{S}}_3 \cdot \hat{\mathbf{S}}_4$$

The decoupling field effectively renders the S-spins magnetically equivalent, so the spin Hamiltonian may be simplified further:

$$\widehat{\mathcal{H}}^0(\text{with } I\text{-spin decoupling}) = \omega_3^0(\hat{S}_{3z} + \hat{S}_{4z})$$

For this system, the S-spins behave as isolated spins in the presence of I-spin decoupling.

17.8 Alphabet Notation

Molecular spin systems are often denoted using the letters of the alphabet. The idea is that spins with very different chemical shifts are denoted by letters that are remote in the alphabet. This usually implies weak coupling. Spins with similar chemical shifts are denoted by letters which are close in the alphabet. The notation AB implies strong coupling.

Magnetically equivalent groups are denoted by a numerical subscript. Spins that are chemically equivalent, but not magnetically equivalent, are denoted by primes.

For example, the six protons in benzene are magnetically equivalent, so the system is denoted A_6.

The five protons in ethyl chloride divide into two groups of magnetically equivalent spins, one containing three spins and the other containing two spins. Since the chemical shift difference is normally sufficient to ensure weak coupling, the spin system is denoted A_3X_2.

The heteronuclear spin system in 1,1-difluoroethene (Figure 17.3) displays chemical equivalence, but not magnetic equivalence. The ^1H– ^{19}F couplings are 'weak', since two different isotopes are involved, so the spin system is denoted AA' XX'.

The heteronuclear spin system of 1,1-Difluoropropan-1,2-diene (Figure 17.19) displays magnetic equivalence. The appropriate notation for this system is therefore A_2X_2.

The diastereotopic CH_2 protons of amino acid side-chains in proteins are chemically inequivalent, and usually have similar chemical shifts. They often form strongly coupled AB spin systems.

The two pairs of diastereotopic CH_2 protons in citric acid (Figure 17.12) form a strongly coupled AA'BB' spin system, neglecting the rapidly exchanging carboxyl and hydroxyl protons. Each CH_2 group in citric acid contains one A proton and one B proton.

17.9 Spin Coupling Topologies

The Hamiltonian terms in Equation 17.4 may be represented as a diagram, in which each spin is represented as a symbol and couplings between them are represented by lines. This chapter already contains many schematic diagrams of this kind. It is sometimes useful to classify spin systems according to the *topology* of this network. For example, consider the following coupling networks for four-spin-1/2 systems:

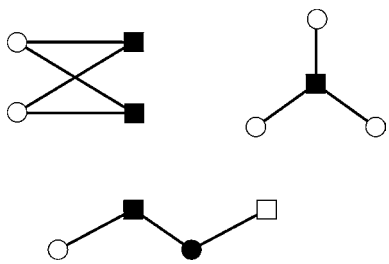

Figure 17.22
Coupling topologies in four-spin systems.

The top-left example represents an A_2X_2 spin system, with a spin Hamiltonian of the form given in Equation 17.5. The coupling network forms a ring.

The 'star-shaped' network at the top right represents an AX_3 spin system. The corresponding spin Hamiltonian for this system has the form

$$\hat{\mathcal{H}}^0 = \omega_1^0 \hat{I}_{1z} + \omega_2^0(\hat{I}_{2z} + \hat{I}_{3z} + \hat{I}_{4z}) + 2\pi J(\hat{I}_{1z}\hat{I}_{2z} + \hat{I}_{1z}\hat{I}_{3z} + \hat{I}_{1z}\hat{I}_{4z})$$

This type of coupling toplogy is encountered, for example, between ^{13}C and ^1H spins in CH_3 groups.

The lower diagram represents a *linear* spin system, in which all J-couplings vanish except between immediate neighbours and no spin has more than two coupling partners. The spin Hamiltonian for an AMXY system of this kind is

$$\widehat{\mathcal{H}}^0 = \omega_1^0 \hat{I}_{1z} + \omega_2^0 \hat{I}_{2z} + \omega_3^0 \hat{I}_{3z} + \omega_4^0 \hat{I}_{4z} + 2\pi J_{12} \hat{I}_{1z} \hat{I}_{2z} + 2\pi J_{23} \hat{I}_{2z} \hat{I}_{3z} + 2\pi J_{34} \hat{I}_{3z} \hat{I}_{4z}$$

Linear spin systems are commonly encountered when the molecular structure has the form of a chain, e.g. in the side chains of some amino acids.

Notes

1. The validity of the weak coupling approximation depends on the r.f. pulse sequence. In particular, the weak coupling Hamiltonian is only valid if Equation 17.6 is satisfied and if the spin system is allowed to evolve in the absence of r.f. fields for an interval τ that is long enough to satisfy the condition

   $$|\omega_j^0 - \omega_k^0|\tau >> 1$$

   Sometimes, densely spaced pulse sequences are applied that deliberately violate this condition, causing a weakly coupled spin system to behave temporarily as if it were strongly coupled (see Section 18.14 and Appendix A.6).

2. It is not always safe to take decoupling into account by cleansing the spin Hamiltonian of those operators which involve the irradiated spins. Although this approach gives correct results for the evolution of the observed spins, it does not give correct results for the evolution of the irradiated spins. One can get away with this if the decoupling field is maintained for the rest of the pulse sequence, but misleading results are obtained if the decoupling field is switched on and off. For a description of the pitfalls, see M. H. Levitt, G. Bodenhausen, and R. R. Ernst, *J. Magn. Reson.*, **53**, 443 (1983).

Further Reading

- For a thorough text on the classification of spin systems, see P. L. Corio, *Structure of High-Resolution NMR Spectra*, Academic Press, New York, 1966. Unfortunately, this book is hard to obtain, and I am unaware of a good alternative.
- For an accessible discussion of heteronuclear spin decoupling, see R. Freeman, *Spin Choreography. Basic Steps in High Resolution NMR.*, Spektrum, Oxford, 1997.

Exercises

17.1 For each of the compounds given below, indicate whether the protons H_a and H_b are chemically equivalent, magnetically equivalent, or both.

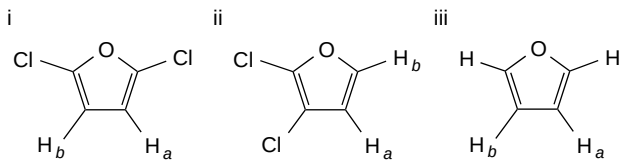

17.2 Give the alphabet notation for the proton spin systems in the following compounds:

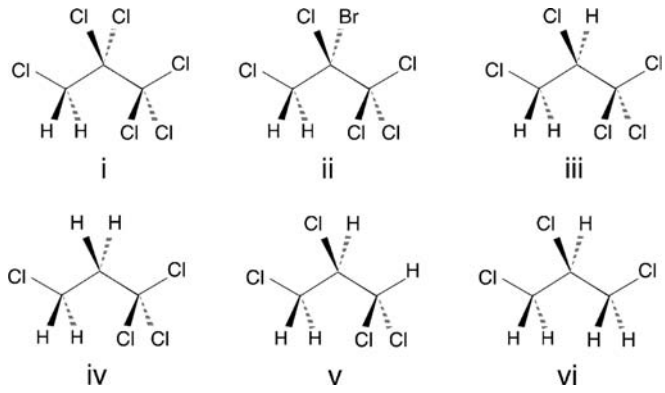

In each case, assume free rotation around the C–C single bonds.

18 Many-Spin Dynamics

The dynamics of many-spin systems can be quite complicated. Nevertheless, matters may still be kept well under control, at least in favourable circumstances.[1]

For simplicity, this chapter deals only with weakly coupled spin-1/2 systems in isotropic liquids.

18.1 Spin Hamiltonian

In the absence of an r.f. field, the spin Hamiltonian for a set of weakly coupled spins in an isotropic liquid is given by Equation 17.7:

$$\widehat{\mathcal{H}}^0 \cong \sum_j \omega_j^0 \hat{I}_{jz} + \sum_{j<k}{}' 2\pi J_{jk} \hat{I}_{jz} \hat{I}_{kz} \tag{18.1}$$

The sum is taken over all magnetically inequivalent spins, ignoring spins undergoing rapid dynamics.

As a first example, consider the three-proton AMX system of 2,3-dibromopropanoic acid:

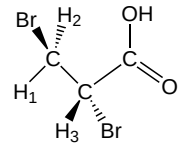

Figure 18.1
2,3-Dibromopropanoic acid

The OH proton is in fast intermolecular exchange and may be ignored. The quadrupolar Br nuclei may also be ignored. The two $-CH_2Br$ protons are diastereotopic and have different chemical shifts (see Section 17.4). The chemical shifts of the three spins are $\delta_1 = 3.70\,\text{ppm}$, $\delta_2 = 3.92\,\text{ppm}$ and $\delta_3 = 4.50\,\text{ppm}$, and the three J-couplings are $J_{12} = -10.1\,\text{Hz}$, $J_{13} = +4.3\,\text{Hz}$ and $J_{23} = +11.3\,\text{Hz}$. In a reasonably high magnetic field, the weak coupling condition (Equation 17.6) is well satisfied for all spin pairs.

If the spectrometer reference frequency is set to $\delta_{\text{ref}} = 4.10\,\text{ppm}$ and the magnetic field is $B^0 = 11.74\,\text{T}$, then the rotating-frame spin Hamiltonian for the three non-exchangeable protons in 2,3-dibromopropanoic acid is given by

$$\widehat{\mathcal{H}}^0 \cong \Omega_1^0 \hat{I}_{1z} + \Omega_2^0 \hat{I}_{2z} + \Omega_3^0 \hat{I}_{3z} + 2\pi J_{12} \hat{I}_{1z} \hat{I}_{2z} + 2\pi J_{13} \hat{I}_{1z} \hat{I}_{3z} + 2\pi J_{23} \hat{I}_{2z} \hat{I}_{3z}$$

where the resonance offset frequencies of the three spins are $\Omega_1^0/2\pi = +200\,\text{Hz}$, $\Omega_2^0/2\pi = +90\,\text{Hz}$ and $\Omega_3^0/2\pi = -200\,\text{Hz}$.

Spin Dynamics: Basics of Nuclear Magnetic Resonance, Second Edition Malcolm H. Levitt

As a second example, consider the five-spin A_2X_3 system of the protons in ethanol CH_3CH_2OH (ignoring the rapidly exchanging hydroxyl proton). As described in Section 17.5, the magnetic equivalence of the CH_2 and CH_3 protons leads to the following coupling topology:

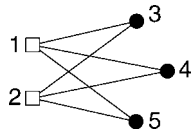

Figure 18.2
Coupling topology for the non-exchangeable protons in ethanol.

If the spectrometer reference frequency set to $\delta_{\text{ref}} = 2.425\,\text{ppm}$ and the magnetic field is $B^0 = 11.74\,\text{T}$, then the rotating-frame spin Hamiltonian for the five non-exchangeable protons in ethanol is given by

$$\widehat{\mathcal{H}}^0 \cong \Omega_1^0(\hat{I}_{1z} + \hat{I}_{2z}) + \Omega_3^0(\hat{I}_{3z} + \hat{I}_{4z} + \hat{I}_{5z}) + 2\pi J(\hat{I}_{1z}\hat{I}_{3z} + \hat{I}_{1z}\hat{I}_{4z} + \hat{I}_{1z}\hat{I}_{5z} + \hat{I}_{2z}\hat{I}_{3z} + \hat{I}_{2z}\hat{I}_{4z} + \hat{I}_{2z}\hat{I}_{5z}) \quad (18.2)$$

where the resonance offset frequencies and J-couplings are $\Omega_1^0/2\pi = -617.5\,\text{Hz}$, $\Omega_3^0/2\pi = +617.5\,\text{Hz}$ and $J = +6.9\,\text{Hz}$.

18.2 Energy Eigenstates

A weakly coupled system of N spins-1/2 has 2^N stationary states, given by the direct products of the Zeeman eigenstates of the individual spins. For example, the eight stationary states of the AMX system are

$$\begin{aligned} |1\rangle &= |\alpha\alpha\alpha\rangle \qquad |2\rangle = |\alpha\alpha\beta\rangle \\ |3\rangle &= |\alpha\beta\alpha\rangle \qquad |4\rangle = |\alpha\beta\beta\rangle \\ |5\rangle &= |\beta\alpha\alpha\rangle \qquad |6\rangle = |\beta\alpha\beta\rangle \\ |7\rangle &= |\beta\beta\alpha\rangle \qquad |8\rangle = |\beta\beta\beta\rangle \end{aligned} \quad (18.3)$$

These are all eigenstates of the z-angular momentum operators of the individual spins; for example:

$$\begin{aligned} \hat{I}_{1z}|\alpha\alpha\alpha\rangle &= +\frac{1}{2}|\alpha\alpha\alpha\rangle \quad \hat{I}_{2z}|\alpha\beta\alpha\rangle = -\frac{1}{2}|\alpha\beta\alpha\rangle \\ \hat{I}_{2z}|\alpha\alpha\alpha\rangle &= +\frac{1}{2}|\alpha\alpha\alpha\rangle \quad \hat{I}_{3z}|\alpha\alpha\beta\rangle = -\frac{1}{2}|\alpha\alpha\beta\rangle \end{aligned}$$

In general, these relationships may be denoted as

$$\hat{I}_{jz}|r\rangle = m_j^{(r)}|r\rangle$$

where $m_j^{(r)} = +1/2$ if the state $|r\rangle$ has an 'α' label in the jth place, and $m_j^{(r)} = -1/2$ if the state $|r\rangle$ has a 'β' label in the jth place. For example, the state $|2\rangle$ in Equation 18.3 has $m_2^{(2)} = +1/2$, $m_2^{(2)} = +1/2$ and $m_3^{(2)} = -1/2$.

It is also convenient to define the *total* z-angular momentum quantum numbers as

$$M_r = \sum_j m_j^{(r)}$$

For example, the state $|1\rangle = |\alpha\alpha\alpha\rangle$ has $M_1 = +3/2$, whereas the states $|6\rangle = |\beta\alpha\beta\rangle$ and $|7\rangle = |\beta\beta\alpha\rangle$ have $M_6 = M_7 = -1/2$.

The direct product Zeeman eigenstates are eigenstates of the weakly coupled spin Hamiltonian in Equation 18.1, according to

$$\widehat{\mathcal{H}}^0|r\rangle = \omega_r|r\rangle$$

The energies of the states are

$$\omega_r = \sum_j \omega_j^0 m_j^{(r)} + \sum_{j<k}{}' 2\pi J_{jk} m_j^{(r)} m_k^{(r)}$$

The diagram below shows these energy levels for systems of $N = 1, 2, 3, 4$ and 5 spins-1/2. The state energies fall into distinct groups, distinguished by the value of M_r:

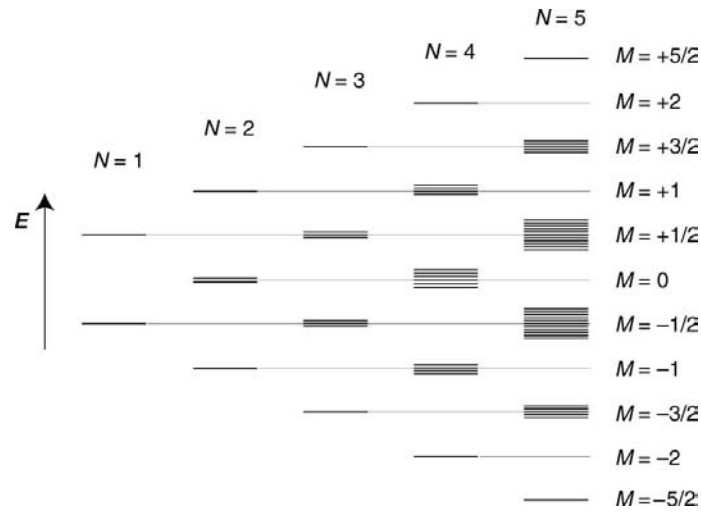

Figure 18.3
Energy levels for coupled spins-1/2.

This diagram greatly exaggerates the small differences in energy between levels in the same group, which are caused by chemical shift differences and J-couplings.

The number of levels in each group follows the binomial distribution. In general, for a system of N spins-1/2, the number of levels with a given value of M is equal to $N!/\{(N/2 - M)!\,(N/2 + M)!\}$.

18.3 Superposition States

In general, each coupled spin system is not in an energy eigenstate. The *superposition states* are defined in the usual way:

$$|\psi\rangle = \sum_{r=1}^{2^N} c_r |r\rangle$$

where the coefficients c_r are normalized complex numbers:

$$\sum_{r=1}^{2^N} |c_r|^2 = 1$$

For example, the state

$$|\psi\rangle = \frac{1}{\sqrt{2}}|\alpha\alpha\alpha\rangle + \frac{1}{2\sqrt{2}}|\alpha\alpha\beta\rangle + \frac{1}{2\sqrt{2}}|\beta\alpha\alpha\rangle + \frac{\mathrm{i}}{2}|\beta\beta\beta\rangle$$

is a valid superposition state for the AMX system.

18.4 Spin Density Operator

The quantum state of an ensemble of multiple-spin systems is described by the spin density operator, defined by

$$\hat{\rho} = \overline{|\psi\rangle\langle\psi|}$$

where $|\psi\rangle$ is the state of an individual spin system and the overbar indicates an ensemble average.

The spin density operator of an ensemble of N-spin-1/2 systems may be written as a $2^N \times 2^N$ density matrix. The 'box notation', described in Section 15.2, is very useful for specifying the density matrix elements. For example, the 8×8 density matrix of an ensemble of AMX spin systems may be written as follows:

$$\hat{\rho} = \begin{pmatrix}
\rho_{\boxed{\alpha\alpha\alpha}} & \rho_{\boxed{\alpha\alpha+}} & \rho_{\boxed{\alpha+\alpha}} & \rho_{\boxed{\alpha++}} & \rho_{\boxed{+\alpha\alpha}} & \rho_{\boxed{+\alpha+}} & \rho_{\boxed{++\alpha}} & \rho_{\boxed{+++}} \\
\rho_{\boxed{\alpha\alpha-}} & \rho_{\boxed{\alpha\alpha\beta}} & \rho_{\boxed{\alpha+-}} & \rho_{\boxed{\alpha+\beta}} & \rho_{\boxed{+\alpha-}} & \rho_{\boxed{+\alpha\beta}} & \rho_{\boxed{++-}} & \rho_{\boxed{++\beta}} \\
\rho_{\boxed{\alpha-\alpha}} & \rho_{\boxed{\alpha-+}} & \rho_{\boxed{\alpha\beta\alpha}} & \rho_{\boxed{\alpha\beta+}} & \rho_{\boxed{+-\alpha}} & \rho_{\boxed{+-+}} & \rho_{\boxed{+\beta\alpha}} & \rho_{\boxed{\alpha\beta+}} \\
\rho_{\boxed{\alpha--}} & \rho_{\boxed{\alpha-\beta}} & \rho_{\boxed{\alpha\beta-}} & \rho_{\boxed{\alpha\beta\beta}} & \rho_{\boxed{+--}} & \rho_{\boxed{+-\beta}} & \rho_{\boxed{+\beta-}} & \rho_{\boxed{+\beta\beta}} \\
\rho_{\boxed{-\alpha\alpha}} & \rho_{\boxed{-\alpha+}} & \rho_{\boxed{-+\alpha}} & \rho_{\boxed{-++}} & \rho_{\boxed{\beta\alpha\alpha}} & \rho_{\boxed{\beta\alpha+}} & \rho_{\boxed{\beta+\alpha}} & \rho_{\boxed{\beta++}} \\
\rho_{\boxed{-\alpha-}} & \rho_{\boxed{-\alpha\beta}} & \rho_{\boxed{-+-}} & \rho_{\boxed{-+\beta}} & \rho_{\boxed{\beta\alpha-}} & \rho_{\boxed{\beta\alpha\beta}} & \rho_{\boxed{\beta+-}} & \rho_{\boxed{\beta+\beta}} \\
\rho_{\boxed{--\alpha}} & \rho_{\boxed{---+}} & \rho_{\boxed{-\beta\alpha}} & \rho_{\boxed{-\beta+}} & \rho_{\boxed{\beta-\alpha}} & \rho_{\boxed{\beta-+}} & \rho_{\boxed{\beta\beta\alpha}} & \rho_{\boxed{\beta\beta+}} \\
\rho_{\boxed{---}} & \rho_{\boxed{--\beta}} & \rho_{\boxed{-\beta-}} & \rho_{\boxed{-\beta\beta}} & \rho_{\boxed{\beta--}} & \rho_{\boxed{\beta-\beta}} & \rho_{\boxed{\beta\beta-}} & \rho_{\boxed{\beta\beta\beta}}
\end{pmatrix}$$

The density matrix of an ensemble of AMX systems contains eight populations $\rho_{\boxed{\alpha\alpha\alpha}}$, $\rho_{\boxed{\alpha\alpha\beta}} \ldots \rho_{\boxed{\beta\beta\beta}}$ (on the top-left to bottom-right diagonal) and 56 coherences $\rho_{\boxed{\alpha\alpha+}}$, $\rho_{\boxed{\alpha+\alpha}} \ldots \rho_{\boxed{\beta\beta-}}$ (off the diagonal).

The procedure for obtaining the 'box notation' for a given element may be illustrated by the following example. Consider the density matrix element $\rho_{67} = \langle 6|\hat{\rho}|7\rangle = \langle\beta\alpha\beta|\hat{\rho}|\beta\beta\alpha\rangle$. This is a coherence between states $|\beta\beta\alpha\rangle$ and $\langle\beta\alpha\beta|$, and since the spin states should be read from *right to left*, the 'coherence arrow' points in this case from to $|\beta\beta\alpha\rangle \rightarrow |\beta\alpha\beta\rangle$.

The state labels for the three spins may now be compared between the two states $|\beta\beta\alpha\rangle$ and $|\beta\alpha\beta\rangle$. Spin I_1 is in state $|\beta\rangle$ for both states, which is indicated by a 'β' label inside the box. Spin I_2 is transformed from state $|\beta\rangle$ to state $|\alpha\rangle$ in making the transformation $|\beta\beta\alpha\rangle \rightarrow |\beta\alpha\beta\rangle$, which is indicated by a '+' label inside the box. Spin I_3 is transformed from state $|\alpha\rangle$ to state $|\beta\rangle$, which is indicated by a '−' label inside the box. The box notation for the element $\langle 6|\hat{\rho}|7\rangle$ is therefore $\rho_{\boxed{\beta+-}}$.

Similarly, the box notation for the element $\rho_{35} = \langle 3|\hat{\rho}|5\rangle = \langle\alpha\beta\alpha|\hat{\rho}|\beta\alpha\alpha\rangle$ is $\rho_{\boxed{+-\alpha}}$.

The box notation is easily extended to larger numbers of spins-1/2. For example, in the five-spin-1/2 system of ethanol, the density matrix element $\langle\beta\alpha\alpha\beta|\hat{\rho}|\alpha\alpha\beta\alpha\beta\rangle$ may be denoted $\rho_{\boxed{-\alpha+\alpha\beta}}$.

Spins with labels '+' or '−' inside the box are termed *active*. Spins with labels 'α' or 'β' inside the box are termed *passive*. For example, in the coherence $\rho_{\boxed{-\alpha+\alpha\beta}}$, spins I_1 and I_3 are active, while spins I_2, I_4 and I_5 are passive.

Table 18.1 Numbers of coherences for N-spin-1/2 systems. There are equal numbers of coherences with order $-p$ and $+p$.

Number of spins N	1	2	3	4	5	6	10	100	500
0-quantum	0	2	12	54	220	860	183 732	9.0×10^{58}	2.7×10^{299}
(+1)-quantum	1	4	15	56	210	792	167 960	8.9×10^{58}	2.7×10^{299}
(+2)-quantum	0	1	6	28	120	495	125 970	8.7×10^{58}	2.7×10^{299}
(+3)-quantum	0	0	1	8	45	220	77 520	8.3×10^{58}	2.7×10^{299}
(+4)-quantum	0	0	0	1	10	66	38 760	7.7×10^{58}	2.6×10^{299}
(+5)-quantum	0	0	0	0	1	12	15 504	7.1×10^{58}	2.6×10^{299}
(+6)-quantum	0	0	0	0	0	1	4845	6.3×10^{58}	2.5×10^{299}
1-spin-(+1)-quantum	1	4	12	32	80	192	5120	6.3×10^{31}	8.2×10^{152}
2-spin-(+2)-quantum	0	1	6	24	80	240	11 520	1.5×10^{33}	1.0×10^{155}
3-spin-(+3)-quantum	0	0	1	8	40	160	15 360	2.6×10^{34}	8.5×10^{156}
4-spin-(+4)-quantum	0	0	0	1	10	60	13 440	3.1×10^{35}	5.3×10^{158}
5-spin-(+5)-quantum	0	0	0	0	1	12	8064	3.0×10^{36}	2.6×10^{160}
6-spin-(+6)-quantum	0	0	0	0	0	1	3360	2.4×10^{37}	1.1×10^{162}

18.5 Populations and Coherences

18.5.1 Coherence orders

The box notation makes it very easy to deduce the *order* of a coherence. Each '+' symbol inside the box contributes +1 to the order, each '−' symbol inside the box contributes −1, and α or β symbols contribute zero. For example, $\rho_{\boxed{\alpha++}}$ is a (+2)-quantum coherence, and $\rho_{\boxed{-+-}}$ is a (−1)-quantum coherence.

The number of coherences of a given order increases very rapidly with the number of coupled spins. The top half of Table 18.1 shows the number of coherences of different order for systems of 1, 2, 3, 4, 5, 6, 10, 100 and 500 coupled spins-1/2.

For a single spin-1/2, there are no zero-quantum coherences, and only one coherence of order +1. For two spins-1/2, there are two zero-quantum coherences, four (+1)-quantum coherence, and one (+2)-quantum coherence. For three spins-1/2, there are 12 zero-quantum coherences, 15 (+1)-quantum coherences, six (+2)-quantum coherences, and one (+3)-quantum coherence.

For 10 coupled spins-1/2, there are 167 960 (+1)-quantum coherences. In a small protein, there are approximately 500 protons, and the number of (+1)-quantum coherences is given by the mind-boggling figure of $\sim 2.7 \times 10^{299}$.

18.5.2 Combination coherences and simple coherences

Consider the coherences $\rho_{\boxed{+-+}}$ and $\rho_{\boxed{\alpha\alpha-}}$ of an AMX spin ensemble. The order of coherence is −1 in both cases. However, the number of active spins is three in the first case and one in the second case. These different types of coherence are distinguished by denoting $\rho_{\boxed{+-+}}$ as a three-spin-(−1)-quantum coherence, while $\rho_{\boxed{\alpha\alpha-}}$ is a one-spin-(−1)-quantum coherence.

Coherences in which the number of active spins is greater than the coherence order are called *combination coherences*. Coherences that are not combination coherences are referred to in this book as *simple coherences*.[2] In the example above, $\rho_{\boxed{+-+}}$ is a combination coherence, whereas $\rho_{\boxed{\alpha\alpha-}}$ is a simple coherence.

The lower half of Table 18.1 shows the number of *simple* coherences in different spin systems. For these coherences, the number of active spins is equal to the coherence order. For example, in a three-spin-1/2 system, there are 15 (+1)-quantum coherences. Twelve of these are simple coherences, and three are combi-

nation coherences (these are $\rho_{\boxed{+-+}}$, $\rho_{\boxed{++-}}$ and $\rho_{\boxed{-++}}$). In a five-spin-1/2 system, there are 45 (+3)-quantum coherences, of which 40 are simple coherences and five are combination coherences.

The number of simple p-quantum coherences in an N-spin-1/2 ensemble is equal to $\{N! \times 2^{N-|p|}\}/\{|p|!\,(N-|p|)!\}$.

By definition, zero-quantum coherences are combination coherences.

18.5.3 Coherence frequencies

In the absence of r.f. fields, and if relaxation is ignored, all coherences evolve as described in Section 15.4. The equation of motion of an individual coherence between time points t_a and t_b is:

$$\rho_{rs}(t_b) = \rho_{rs}(t_a)\exp\{(i\Omega_{rs} - \lambda_{rs})(t_b - t_a)\} \tag{18.4}$$

where Ω_{rs} is the coherence frequency (in the rotating frame) and λ_{rs} is the decay rate constant of the coherence.

The box notation makes it easy to determine the precession frequency Ω_{rs} of a given coherence. As an example, consider the coherence $\rho_{\boxed{+-\alpha}}$ in an AMX spin system. The frequency $\Omega_{\boxed{+-\alpha}}$ of this coherence may be determined as follows:

1. Draw out the coupling topology of the spin system and attach the coherence labels. Draw a lasso around the active spins:

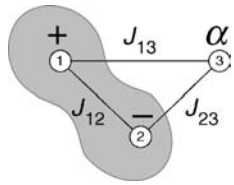

Figure 18.4 Diagram used for calculating the frequency $\Omega_{\boxed{+-\alpha}}$.

2. Calculate the chemical shift contribution to the frequency by assigning $+\Omega_j^0$ to active spins with a '−' label and $-\Omega_j^0$ to active spins with a '+' label. For the coherence $\rho_{\boxed{+-\alpha}}$, the chemical shift frequency contribution comes to

$$\text{chemical shift contribution} = -\Omega_1^0 + \Omega_2^0$$

3. Compute the J-coupling part of the coherence frequency by summing together contributions from all couplings between active spins and passive spins, i.e. from 'inside the lasso' to 'outside the lasso'. Ignore the couplings of active spins with each other, and of passive spins with each other. There are four possible cases:
   (i) The combination of a '−' and an 'α' label contributes $+\pi J_{jk}$.
   (ii) The combination of a '−' and a 'β' label contributes $-\pi J_{jk}$.
   (iii) The combination of a '+' and an 'α' label contributes $-\pi J_{jk}$.
   (iv) The combination of a '+' and a 'β' label contributes $+\pi J_{jk}$.
   In the case of $\rho_{\boxed{+-\alpha}}$, the J-coupling contribution is

$$J\text{-coupling contribution} = -\pi J_{13} + \pi J_{23}$$

The rotating-frame precession frequency of the coherence $\rho_{\boxed{+-\alpha}}$ is therefore

$$\Omega_{\boxed{+-\alpha}} = -\Omega_1^0 + \Omega_2^0 - \pi J_{13} + \pi J_{23}$$

As a more complicated example, consider the three-spin-(−1)-quantum coherence $\rho_{\boxed{-\alpha+\beta-}}$ in the five-spin-1/2 system of ethanol. The 'lasso' picture of this coherence is shown here:

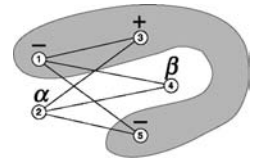

Figure 18.5
Diagram used for calculating the frequency $\Omega_{\boxed{-\alpha+\beta-}}$.

Applying the rules above, and using the magnetic equivalences defined in Equation 18.2, gives the following chemical shift frequency contribution:

$$\text{chemical shift contribution} = +\Omega_1^0 - \Omega_3^0 + \Omega_5^0 = +\Omega_1^0$$

For the J-coupling contribution one gets

$$J\text{-coupling contribution} = -\pi J_{14} - \pi J_{23} + \pi J_{25} = -\pi J$$

The overall precession frequency of this coherence is therefore

$$\Omega_{\boxed{-\alpha+\beta-}} = +\Omega_1^0 - \pi J$$

The frequency of any coherence in a weakly coupled system of spins-1/2 may be deduced in the same way.

18.5.4 Degenerate coherences

Coherences that have the same precession frequency are termed *degenerate*. Degeneracy occurs whenever there is magnetic equivalence, or whenever the J-couplings between any pair of spins is vanishingly small.

For example, in an AMX system, the coherences $\rho_{\boxed{-\alpha\alpha}}$ and $\rho_{\boxed{-\alpha\beta}}$ are degenerate if the coupling J_{13} vanishes, so that the spin system is *linear* (see Section 17.9).

In the A_2X_3 system of the protons in ethanol, the coherences $\rho_{\boxed{-\alpha\alpha\alpha\beta}}$, $\rho_{\boxed{-\alpha\alpha\beta\alpha}}$, $\rho_{\boxed{-\alpha\beta\alpha\alpha}}$, $\rho_{\boxed{\alpha-\alpha\alpha\beta}}$, $\rho_{\boxed{\alpha-\alpha\beta\alpha}}$, $\rho_{\boxed{\alpha-\beta\alpha\alpha}}$, $\rho_{\boxed{-\beta\alpha\alpha\beta}}$, $\rho_{\boxed{-\beta\alpha\beta\alpha}}$, $\rho_{\boxed{-\beta\beta\alpha\alpha}}$, $\rho_{\boxed{\beta-\alpha\alpha\beta}}$, $\rho_{\boxed{\beta-\alpha\beta\alpha}}$ and $\rho_{\boxed{\beta-\beta\alpha\alpha}}$ are all degenerate.

Most large systems of coupled spins-1/2 have a high degree of degeneracy, since it is unlikely that every spin has a finite J-coupling with every other spin.

Degeneracy has important practical consequences: although the number of *coherences* in a small protein molecule is astronomical (see Table 18.1), the number of non-degenerate coherence *frequencies* is relatively manageable. If this were not so, it would be essentially impossible to interpret the NMR spectrum for molecules of a reasonable size.

A very high degree of degeneracy is a characteristic property of weakly coupled spin systems in isotropic liquids. In liquid crystals, the degeneracy is relatively low, and the NMR spectra of molecules containing more than around 10 coupled spins are essentially intractable.[3]

18.5.5 Observable coherences

Only simple (−1)*-quantum coherences generate observable signals in a quadrature receiver*.

This may readily be seen by using the formula for the total spin magnetization along the x-axis:

$$M_x \sim \langle \hat{I}_x \rangle = \mathrm{Tr}\{\hat{\rho}\hat{I}_x\} = \mathrm{Tr}\{\hat{\rho}\hat{I}_{1x}\} + \mathrm{Tr}\{\hat{\rho}\hat{I}_{2x}\} + \ldots$$

In the case of a three-spin-1/2 system we get

$$M_x \sim \mathrm{Tr}\{\hat{\rho}\hat{I}_{1x}\} + \mathrm{Tr}\{\hat{\rho}\hat{I}_{2x}\} + \mathrm{Tr}\{\hat{\rho}\hat{I}_{3x}\}$$

Each individual term may be expanded as follows:

$$\begin{aligned}\mathrm{Tr}\{\hat{\rho}\hat{I}_{1x}\} &= \mathrm{Tr}\{\hat{\rho}\tfrac{1}{2}(\hat{I}_1^+ + \hat{I}_1^-)(\hat{I}_2^\alpha + \hat{I}_2^\beta)(\hat{I}_3^\alpha + \hat{I}_3^\beta)\} \\ &= \tfrac{1}{2}\,\mathrm{Tr}\{\hat{\rho}\hat{I}_1^+\hat{I}_2^\alpha\hat{I}_3^\alpha\} + \tfrac{1}{2}\,\mathrm{Tr}\{\hat{\rho}\hat{I}_1^+\hat{I}_2^\alpha\hat{I}_3^\beta\} + \ldots\end{aligned}$$

Operators such as $\hat{I}_1^+\hat{I}_2^\alpha\hat{I}_3^\beta$ may be written in the following 'ket-bra' form:

$$\hat{I}_1^+\hat{I}_2^\alpha\hat{I}_3^\beta = |\alpha\alpha\beta\rangle\langle\beta\alpha\beta|$$

The properties of the trace (see Section 7.7.4) may be exploited as follows:

$$\mathrm{Tr}\{\hat{\rho}\hat{I}_1^+\hat{I}_2^\alpha\hat{I}_3^\beta\} = \mathrm{Tr}\{\hat{\rho}|\alpha\alpha\beta\rangle\langle\beta\alpha\beta|\} = \langle\beta\alpha\beta|\hat{\rho}|\alpha\alpha\beta\rangle = \rho_{\boxed{-\alpha\beta}}$$

These arguments may be put together to obtain:

$$M_x \sim \langle \hat{I}_x \rangle = \frac{1}{2}\rho_{\boxed{-\alpha\alpha}} + \frac{1}{2}\rho_{\boxed{-\alpha\beta}} + \ldots + \frac{1}{2}\rho_{\boxed{+\alpha\alpha}} + \ldots$$

Only simple (± 1)-quantum coherences appear in the sum.

Although the transverse magnetization M_x contains contributions from the simple ($+1$)-quantum coherences as well as the simple (-1)-quantum coherences, the quadrature-detected NMR signal is purely generated by the simple (-1)-quantum coherences, defined as usual in the rotating frame. The arguments given in Appendix A.5 may be used to derive the following formula for the quadrature NMR signal:

$$s(t) \sim 2\mathrm{i}(\rho_{\boxed{-\alpha\alpha}}(t) + \rho_{\boxed{-\alpha\beta}}(t) + \ldots)\exp\{-\mathrm{i}\phi_{\mathrm{rec}}\}$$

Here, ϕ_{rec} is the receiver phase, as specified in Section 4.5.4.

Although only simple (-1)-quantum coherences generate observable signals directly, the other coherences may be observed *indirectly* by using two-dimensional spectroscopy.

18.6 NMR Spectra

Each of the simple (-1)-quantum coherences is associated with a single spectral peak.

For example, the NMR spectrum of an AMX system has the following mathematical form:

$$S(\Omega) = \alpha_{\boxed{-\alpha\alpha}} \mathcal{L}(\Omega; \Omega_{\boxed{-\alpha\alpha}}, \lambda) + \alpha_{\boxed{-\alpha\beta}} \mathcal{L}(\Omega; \Omega_{\boxed{-\alpha\alpha}}, \lambda) + \ldots$$

There is one term for each of the 12 observable coherences, and the complex amplitudes have the form

$$\alpha_{\boxed{-\alpha\alpha}} = 2\mathrm{i}\rho_{\boxed{-\alpha\alpha}}(0) \exp\{-\mathrm{i}\phi_{\mathrm{rec}}\}$$
$$\alpha_{\boxed{-\alpha\beta}} = 2\mathrm{i}\rho_{\boxed{-\alpha\beta}}(0) \exp\{-\mathrm{i}\phi_{\mathrm{rec}}\}$$

and so on. The time point $t = 0$ corresponds to the beginning of signal detection.

As described in Section 15.5, each peak contributes an absorption Lorentzian if the complex amplitude is a real number, but contributes a dispersion Lorentzian if the complex amplitude is an imaginary number.

If the amplitudes of the simple (-1)-quantum coherences are real and equal at time $t = 0$, then the spectrum of an AMX system has the following appearance:

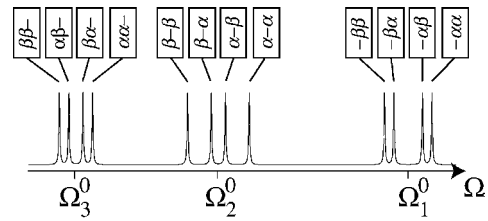

Figure 18.6
Assignment of AMX spectral peaks if all J-couplings and the gyromagnetic ratio are positive.

This spectrum corresponds to the case $\Omega_1^0/2\pi = 300\,\mathrm{Hz}$, $\Omega_2^0/2\pi = 100\,\mathrm{Hz}$, $\Omega_3^0/2\pi = -50\,\mathrm{Hz}$, $J_{12} = 40\,\mathrm{Hz}$, $J_{13} = 10\,\mathrm{Hz}$ and $J_{23} = 25\,\mathrm{Hz}$.

The signs of the J-couplings do not affect the appearance of the spectrum, but do influence the correct labelling of the peaks. For example, if $J_{23} = -25\,\mathrm{Hz}$, while all other parameters are unchanged, the spectrum should be labelled as follows:

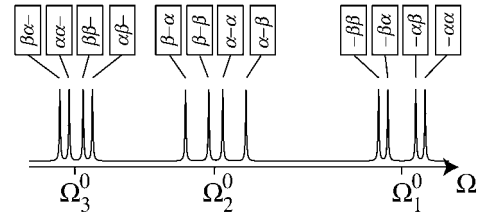

Figure 18.7
Assignment of AMX spectral peaks if J_{23} is negative.

Suppose, now, that the coupling J_{13} vanishes, so that the spin system is linear (see Section 17.9). Several pairs of coherences become degenerate, and the spectrum has the following form:

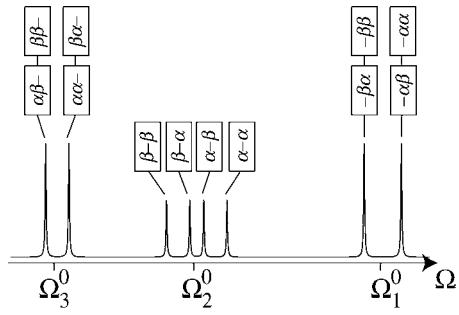

Figure 18.8
Assignment of AMX spectral peaks for a linear three-spin system, showing degeneracy.

This spectrum corresponds to the J-coupling parameters $J_{12} = 40\,\text{Hz}$, $J_{13} = 10\,\text{Hz}$ and $J_{23} = 0$.

If spins I_1 and I_3 are magnetically equivalent, then further degeneracy arises, since the chemical shift frequencies Ω_1^0 and Ω_3^0 are the same, and the J-couplings J_{12} and J_{23} are also identical. The spectrum has the following form in this case:

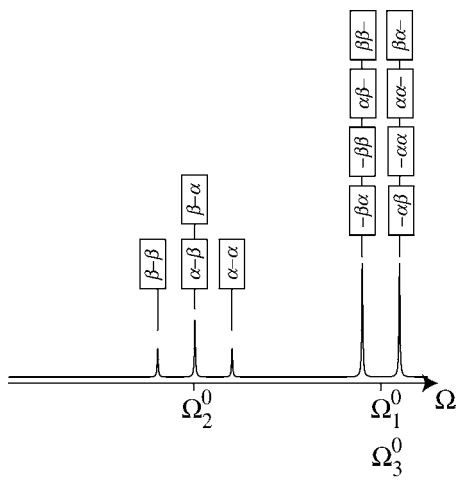

Figure 18.9
Assignment of spectral peaks for an AX_2 spin system.

This corresponds to an AX_2 spectrum with parameters $\Omega_1^0/2\pi = \Omega_3^0/2\pi = 300\,\text{Hz}$, $\Omega_2^0/2\pi = 100\,\text{Hz}$ and $J_{12} = J_{23} = 40\,\text{Hz}$.

This AX_2 spectrum reveals the J-coupled multiplet structure discussed in Section 3.8. The 'A' spin (I_2) is coupled to two magnetically equivalent 'X' spins (I_1 and I_3), providing a triplet multiplet structure, with amplitudes in the ratio 1:2:1. The 'X' spins (I_1 and I_3) are coupled to a single 'A' spin (I_2), so the 'X' spin peak is a doublet.

Note how the amplitude ratios of the multiplet components may be interpreted in terms of the degeneracies of the coherences. The central peak of the 'A' spin triplet is twice as intense as the two outer peaks, because it is generated by twice as many coherences.

The spectrum of the A_2X_3 ethanol spin system appears as follows (the J-coupling is exaggerated for clarity):

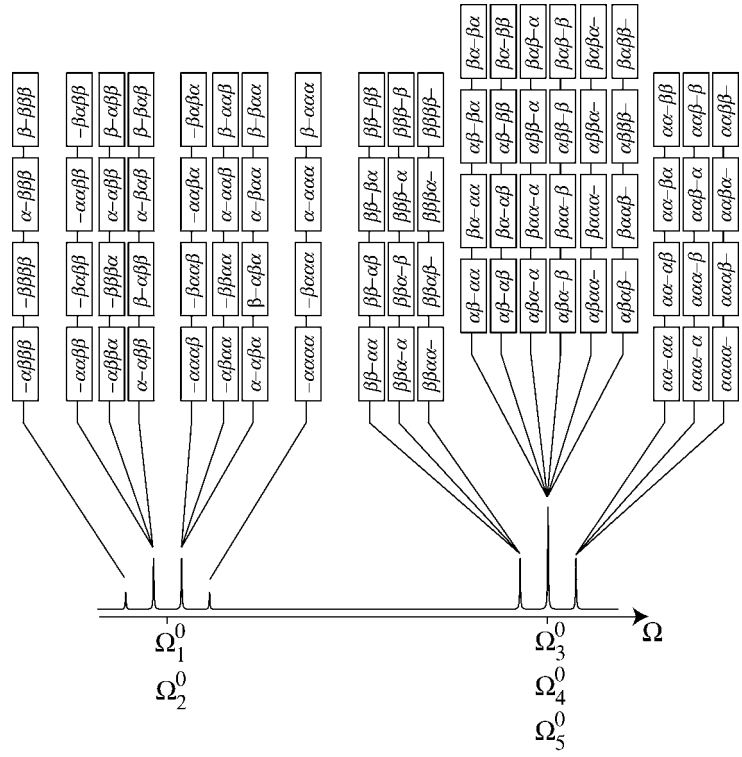

Figure 18.10
Assignment of spectral peaks for an A_2X_3 system.

The magnetic equivalence leads to a high degeneracy of the coherences. Even the smallest peaks in the spectrum contain contributions from four degenerate coherences, and the largest peak in the spectrum is 24-fold degenerate. The A-spin peak is a quartet, since each A spin is coupled to three X spins. The X-spin peak is a triplet, since each X spin is coupled to two A spins.

18.7 Many-Spin Product Operators

Spin dynamical calculations in weakly coupled spin-1/2 systems are greatly facilitated by the product operator formalism, introduced in Section 15.6. The formalism needs to be extended in order to handle systems of more than two coupled spins-1/2.

18.7.1 Construction of product operators

Product operators for an ensemble of N-spin-1/2 systems may be constructed through the following procedure:

product operator	$= 2^{(N-1)} \times$	operator for spin I_1 (4 choices)	$\times$	operator for spin I_2 (4 choices)	$\cdots \times$	operator for spin I_N (4 choices)

The choices for each operator are as follows:

$$\boxed{\begin{array}{l}\text{operator for}\\ \text{spin } I_j\\ \text{(4 choices)}\end{array}} = \begin{cases} \frac{1}{2}\widehat{1}_j \\ \hat{I}_{jx} \\ \hat{I}_{jy} \\ \hat{I}_{jz} \end{cases}$$

Products of unity operators may be eliminated; for example:

$$4 \times \frac{1}{2}\widehat{1}_1 \times \frac{1}{2}\widehat{1}_2 \times \frac{1}{2}\widehat{1}_3 = \frac{1}{2}\widehat{1}$$

$$4 \times \frac{1}{2}\widehat{1}_1 \times \hat{I}_{2z} \times \hat{I}_{3x} = 2\hat{I}_{2z}\hat{I}_{3x}$$

Some valid product operators in a three-spin-1/2 system are $\frac{1}{2}\widehat{1}$, $\hat{I}_{1z}$, $2\hat{I}_{2z}\hat{I}_{3x}$, $4\hat{I}_{1x}\hat{I}_{2z}\hat{I}_{3x}$. Some valid product operators in a five-spin-1/2 system are $\frac{1}{2}\widehat{1}$, $\hat{I}_{1z}$, $2\hat{I}_{2z}\hat{I}_{3x}$, $4\hat{I}_{1x}\hat{I}_{2z}\hat{I}_{3x}$, $8\hat{I}_{1x}\hat{I}_{2z}\hat{I}_{3x}\hat{I}_{4y}$, $16\hat{I}_{1z}\hat{I}_{2z}\hat{I}_{3z}\hat{I}_{4z}\hat{I}_{5z}$.

As usual, it is advisable to keep strict sequential order for the spin indices, and to keep the proper numerical prefactor together with the product operator.

18.7.2 Populations and coherences

In a system of N spins-1/2, each product operator term in the density operator consists of a superposition of 2^N coherences and populations. The use of product operators allows one to keep track of large groups of coherences and populations at the same time, permitting calculations in systems with large numbers of coupled spins.

Consider, for example, an AMX spin system. The product operator $\hat{I}_{1y}$ may be expanded as follows:

$$\begin{aligned}\hat{I}_{1y} &= 4 \times \hat{I}_{1y} \times \frac{1}{2}\widehat{1}_2 \times \frac{1}{2}\widehat{1}_3 \\ &= 4 \times \frac{1}{2\mathrm{i}}(\hat{I}_1^+ - \hat{I}_1^-) \times \frac{1}{2}(\hat{I}_2^\alpha + \hat{I}_2^\beta) \times \frac{1}{2}(\hat{I}_3^\alpha + \hat{I}_3^\beta) \\ &= \frac{1}{2\mathrm{i}}\left(\hat{I}_1^+\hat{I}_2^\alpha\hat{I}_3^\alpha - \hat{I}_1^-\hat{I}_2^\alpha\hat{I}_3^\alpha + \hat{I}_1^+\hat{I}_2^\alpha\hat{I}_3^\beta - \hat{I}_1^-\hat{I}_2^\alpha\hat{I}_3^\beta + \hat{I}_1^+\hat{I}_2^\beta\hat{I}_3^\alpha - \hat{I}_1^-\hat{I}_2^\beta\hat{I}_3^\alpha + \hat{I}_1^+\hat{I}_2^\beta\hat{I}_3^\beta - \hat{I}_1^-\hat{I}_2^\beta\hat{I}_3^\beta\right)\end{aligned}$$

If the density operator contains a term $\hat{I}_{1y}$, this implies the presence of coherences such as $\rho_{\boxed{+\alpha\alpha}}$, $\rho_{\boxed{+\alpha\beta}}$, and also observable (-1)-quantum coherences such as $\rho_{\boxed{-\alpha\alpha}}$ and $\rho_{\boxed{-\alpha\beta}}$.

Product operators such as $\hat{I}_y$, $2\hat{I}_{1y}\hat{I}_{2z}$, $2\hat{I}_{1y}\hat{I}_{3z}$ and $4\hat{I}_{1y}\hat{I}_{2z}\hat{I}_{3z}$ contain the same combinations of coherences, but with different relative phases. Consider again an AMX system, with all couplings resolved. If the AMX density operator contains a term proportional to $-\hat{I}_{1y}$ at the beginning of the detection interval, then the spectrum has the following appearance:

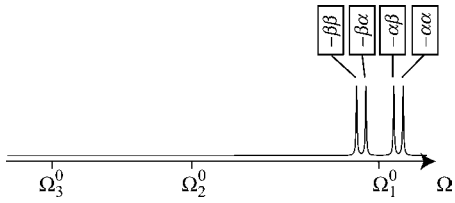

Figure 18.11
Spectrum associated with a product operator term $-\hat{I}_{1y}$, in an AMX system.

If the AMX density operator contains a term proportional to $-2\hat{I}_{1y}\hat{I}_{2z}$ at the beginning of the detection interval, then the spectrum has the following antiphase appearance:

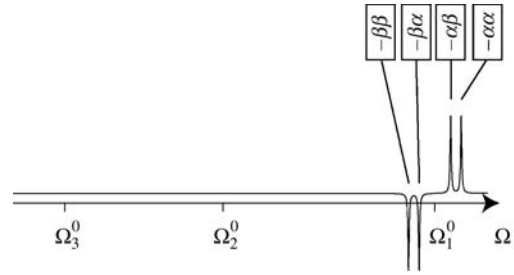

Figure 18.12
Spectrum associated with a product operator term $-2\hat{I}_{1y}\hat{I}_{2z}$, in an AMX system.

Note that peaks from coherences with different labels for spin I_2 have opposite sign.

A term proportional to $-2\hat{I}_{1y}\hat{I}_{3z}$ at the beginning of the detection interval generates a different sort of antiphase spectrum:

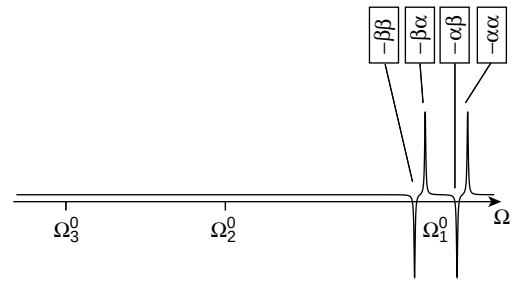

Figure 18.13
Spectrum associated with a product operator term $-2\hat{I}_{1y}\hat{I}_{3z}$, in an AMX system.

This time, the peaks from coherences with different labels for spin I_3 have opposite sign.

A term proportional to $-4\hat{I}_{1y}\hat{I}_{2z}\hat{I}_{3z}$ at the beginning of the detection interval generates a 'doubly antiphase' spectrum:

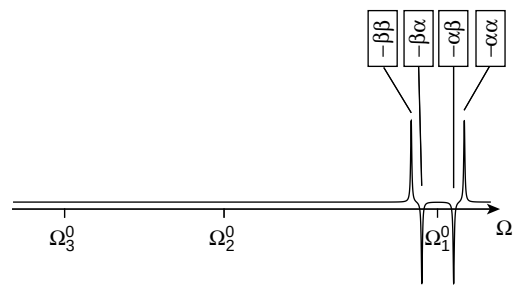

Figure 18.14
Spectrum associated with a product operator term $-4\hat{I}_{1y}\hat{I}_{2z}\hat{I}_{3z}$, in an AMX system.

The peak signs are inverted according to the labels of both spins I_2 and I_3.

In magnetically equivalent systems, the degenerate peaks may either reinforce or cancel each other. For example, consider an AX_2 system, in which I_1 and I_3 are magnetically equivalent. A product operator term $-\hat{I}_{1y}$ generates a spectrum with the following in-phase appearance:

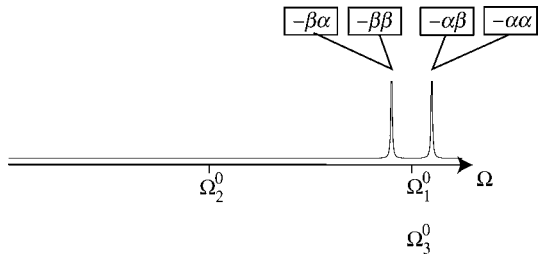

Figure 18.15
Spectrum associated with a product operator term $-\hat{I}_{1y}$, in an AX_2 system.

A product operator term $-2\hat{I}_{1y}\hat{I}_{2z}$ generates an antiphase spectrum:

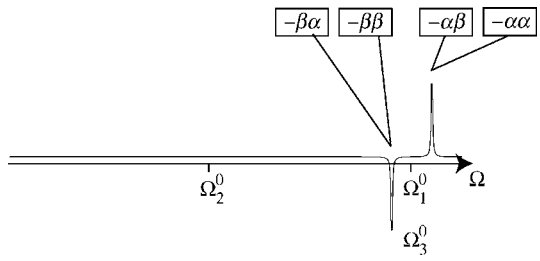

Figure 18.16
Spectrum associated with a product operator term $-2\hat{I}_{1y}\hat{I}_{2z}$, in an AX_2 system.

A product operator term $-2\hat{I}_{1y}\hat{I}_{3z}$, on the other hand, generates no signal at all, since the antiphase peaks from degenerate coherences such as $\rho_{\boxed{-\alpha\alpha}}$ and $\rho_{\boxed{-\alpha\beta}}$ have opposite sign and cancel exactly.[4]

Similarly, the central peak in the A-spin triplet of the AX_2 system vanishes for the antiphase spectrum generated by the term $-2\hat{I}_{1z}\hat{I}_{2y}$:

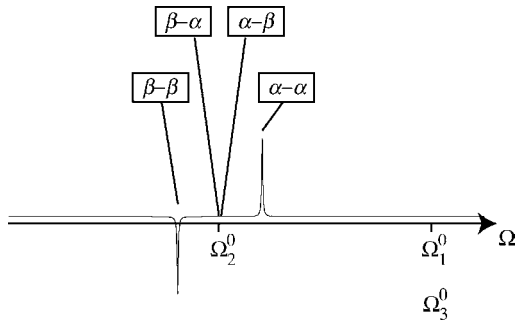

Figure 18.17
Spectrum associated with a product operator term $-2\hat{I}_{1z}\hat{I}_{2y}$, in an AX_2 system.

18.7.3 Physical interpretation of product operators

Product operators in systems of many coupled spins-1/2 have an analogous physical intepretation to that given in Section 15.6 for coupled spin pairs. Density operator terms such as $\hat{I}_{1x}$ indicate a partial alignment of spins I_1 with the x-axis. Density operator terms such as $2\hat{I}_{1x}\hat{I}_{2x}$ indicate that the x-components of the spin angular momenta for spins I_1 and I_2 are correlated.

Density operator terms such as $4\hat{I}_{1x}\hat{I}_{2x}\hat{I}_{3x}$ indicate three-way correlations. The presence of a term $4\hat{I}_{1x}\hat{I}_{2x}\hat{I}_{3x}$ in the density operator indicates that all three spins I_1, I_2 and I_3 tend to have the same polarization along the x-axis. This is depicted (in greatly exaggerated form) in the following diagram:

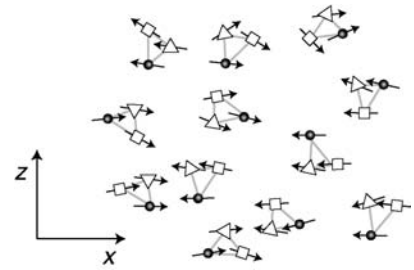

Figure 18.18
Physical interpretation of a density operator term $4\hat{I}_{1x}\hat{I}_{2x}\hat{I}_{3x}$.

18.8 Thermal Equilibrium

Thermal equilibrium in an ensemble of N-spin-1/2 systems corresponds to the usual Boltzmann distribution of populations (see Sections 11.3 and 15.7). In high magnetic field and at normal temperatures, the thermal equilibrium spin density operator of a homonuclear spin system may be approximated as follows:

$$\begin{aligned}\hat{\rho}^{\text{eq}} &\cong 2^{-N}\widehat{1} + 2^{-N}\mathbb{B}\hat{I}_z \\ &= 2^{-N}\widehat{1} + 2^{-N}\mathbb{B}\left(\hat{I}_{1z} + \hat{I}_{2z} + \ldots + \hat{I}_{Nz}\right)\end{aligned}$$

where $\mathbb{B}$ is the Boltzmann factor, $\mathbb{B} = \hbar\gamma B^0/k_B T$.

In many calculations, it is permissible to omit the unity operator and the numerical factors, and simply write

$$\hat{\rho}^{\text{eq}} \sim \hat{I}_z = \hat{I}_{1z} + \hat{I}_{2z} + \ldots + \hat{I}_{Nz}$$

In the case of heteronuclear spin systems, the Boltzmann factors are different for different spins. For example, the thermal equilibrium spin density operator for a heteronuclear I_2S system is written as

$$\hat{\rho}^{\text{eq}} \cong \frac{1}{8}\widehat{1} + \frac{1}{8}\left(\mathbb{B}_I\hat{I}_{1z} + \mathbb{B}_I\hat{I}_{2z} + \mathbb{B}_S\hat{S}_{3z}\right)$$

where $\mathbb{B}_I = \hbar\gamma_I B^0/k_B T$ and $\mathbb{B}_S = \hbar\gamma_S B^0/k_B T$.

18.9 Radio Frequency Pulses

The transformation of a multiple-spin product operator by a strong r.f. pulse is easily calculated by rotating each of the individual operator terms. The technique is exactly the same as for two-spin product operators, as described in Section 15.8. The appropriate transformations for strong pulses with phases $\phi_{\text{p}} = 0$ and $\phi_{\text{p}} = \pi/2$ are summarized in Equations 15.6 and 15.7.

For example, a product operator term $4\hat{I}_{1z}\hat{I}_{2x}\hat{I}_{3y}$ is rotated by a non-selective $(\pi/2)_x$ pulse as follows:

$$4\hat{I}_{1z}\hat{I}_{2x}\hat{I}_{3y} \xrightarrow{(\pi/2)_x} 4(-\hat{I}_{1y})(\hat{I}_{2x})(\hat{I}_{3z}) = -4\hat{I}_{1y}\hat{I}_{2x}\hat{I}_{3z}$$

In heteronuclear spin systems, only the operators that belong to the resonant spin species are rotated; for example:

$$4\hat{I}_{1z}\hat{I}_{2x}\hat{S}_{3y} \xrightarrow{(\pi/2)_x^I} 4(-\hat{I}_{1y})(\hat{I}_{2x})(\hat{S}_{3y}) = -4\hat{I}_{1y}\hat{I}_{2x}\hat{S}_{3y}$$

$$4\hat{I}_{1z}\hat{I}_{2x}\hat{S}_{3y} \xrightarrow{(\pi/2)_x^S} 4\hat{I}_{1z}\hat{I}_{2x}\hat{S}_{3z}$$

18.10 Free Precession

If relaxation is ignored, the evolution of a multiple-spin product operator under an interval of free evolution may be deduced by extending the treatment in Section 15.9.

For weakly coupled systems, the calculation of product operator evolution may be split up into separate sub-calculations for the evolution under each chemical shift frequency, and under each J-coupling. These sub-calculations may be taken in any order, since the corresponding spin propagators commute.

For example, in an AMX system, the evolution of a particular product operator term over an interval τ may be calculated by the following sequence of transformations:

$$\xrightarrow{\Omega_1^0\tau} \xrightarrow{\Omega_2^0\tau} \xrightarrow{\Omega_3^0\tau} \xrightarrow{\pi J_{12}\tau} \xrightarrow{\pi J_{13}\tau} \xrightarrow{\pi J_{23}\tau}$$

18.10.1 Chemical shift evolution

The evolution under a chemical shift term is readily calculated by rotating the appropriate spin operator I_j through the angle $\Omega_j^0\tau$ about the z-axis. The appropriate transformations are given in Equation 15.22.

The calculation is repeated for each spin operator in the product.

For example, the chemical shift evolution of the product operator term $4\hat{I}_{1z}\hat{I}_{2x}\hat{I}_{3y}$ in an AMX system is as follows:

$$4\hat{I}_{1z}\hat{I}_{2x}\hat{I}_{3y}$$

$$\downarrow \Omega_1^0\tau$$

$$4\hat{I}_{1z}\hat{I}_{2x}\hat{I}_{3y}$$

$$\downarrow \Omega_2^0\tau$$

$$4\hat{I}_{1z}(\hat{I}_{2x}\cos\Omega_2^0\tau + \hat{I}_{2y}\sin\Omega_2^0\tau)\hat{I}_{3y}$$

$$\downarrow \Omega_3^0\tau$$

$$4\hat{I}_{1z}(\hat{I}_{2x}\cos\Omega_2^0\tau + \hat{I}_{2y}\sin\Omega_2^0\tau)(\hat{I}_{3y}\cos\Omega_3^0\tau - \hat{I}_{3x}\sin\Omega_3^0\tau)$$

or, to summarize:

$$4\hat{I}_{1z}\hat{I}_{2x}\hat{I}_{3y}$$

$$\downarrow \Omega_1^0\tau$$

$$\downarrow \Omega_2^0\tau$$

$$\downarrow \Omega_3^0\tau$$

$$4\hat{I}_{1z}\hat{I}_{2x}\hat{I}_{3y}\cos\Omega_2^0\tau\ \cos\Omega_3^0\tau + 4\hat{I}_{1z}\hat{I}_{2y}\hat{I}_{3y}\sin\Omega_2^0\tau\ \cos\Omega_3^0\tau$$
$$-4\hat{I}_{1z}\hat{I}_{2x}\hat{I}_{3x}\cos\Omega_2^0\tau\ \sin\Omega_3^0\tau - 4\hat{I}_{1z}\hat{I}_{2y}\hat{I}_{3x}\sin\Omega_2^0\tau\ \sin\Omega_3^0\tau$$

18.10.2 *J*-coupling evolution

The calculation of J-coupling evolution in multiple-spin product operators exploits the commutation relationships summarized in Equations 15.23 and 15.24.

Suppose that we wish to calculate the transformation under the J-coupling between spins I_j and I_k over the interval τ. The product operator does *not* evolve under the coupling J_{jk} in the following cases:

1. If both spins I_j and I_k are missing in the product operator.
2. If only one spin I_j or I_k is present, and that spin carries a z label.
3. If both spins I_j or I_k are present, but *both* spins carry a z label.
4. If both spins I_j or I_k are present, but *neither* spin carries a z label.

Some examples of these cases are as follows:

$$\hat{I}_{3y} \xrightarrow{\pi J_{12}\tau} \hat{I}_{3y} \qquad \text{(case 1)}$$
$$\hat{I}_{2z} \xrightarrow{\pi J_{12}\tau} \hat{I}_{2z} \qquad \text{(case 2)}$$
$$2\hat{I}_{1z}\hat{I}_{3y} \xrightarrow{\pi J_{12}\tau} 2\hat{I}_{1z}\hat{I}_{3y} \qquad \text{(case 2)}$$
$$2\hat{I}_{1z}\hat{I}_{2z} \xrightarrow{\pi J_{12}\tau} 2\hat{I}_{1z}\hat{I}_{2z} \qquad \text{(case 3)}$$
$$2\hat{I}_{2x}\hat{I}_{3x} \xrightarrow{\pi J_{23}\tau} 2\hat{I}_{2x}\hat{I}_{3x} \qquad \text{(case 4)}$$
$$2\hat{I}_{1y}\hat{I}_{3x} \xrightarrow{\pi J_{13}\tau} 2\hat{I}_{1y}\hat{I}_{3x} \qquad \text{(case 4)}$$
$$4\hat{I}_{1y}\hat{I}_{2x}\hat{I}_{3z} \xrightarrow{\pi J_{12}\tau} 4\hat{I}_{1y}\hat{I}_{2x}\hat{I}_{3z} \qquad \text{(case 4)}$$

In all *other* cases, the product operator does evolve under the relevant J-coupling, and the appropriate transformation may be deduced using Equation 15.23.

For example, consider the transformation of $4\hat{I}_{1y}\hat{I}_{2x}\hat{I}_{3z}$ under the coupling J_{23}. The product operator may be written as

$$4\hat{I}_{1y}\hat{I}_{2x}\hat{I}_{3z} = 2\hat{I}_{1y}(2\hat{I}_{2x}\hat{I}_{3z})$$

The following diagram may be used to deduce the J-coupling evolution of the bracketed term:

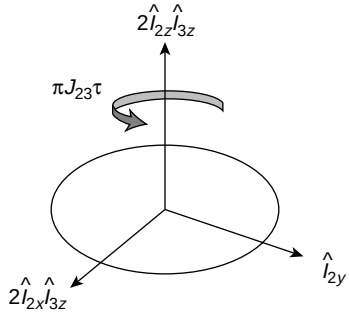

Figure 18.19
Cyclic commutation diagram used for calculating the evolution of $2\hat{I}_{2x}\hat{I}_{3z}$ under J_{23}.

This leads to

$$2\hat{I}_{1y}(2\hat{I}_{2x}\hat{I}_{3z})$$

$$\downarrow \pi J_{23}\tau$$

$$2\hat{I}_{1y}\left(2\hat{I}_{2x}\hat{I}_{3z}\cos\pi J_{23}\tau + \hat{I}_{2y}\sin\pi J_{23}\tau\right)$$

or to summarize:

$$4\hat{I}_{1y}\hat{I}_{2x}\hat{I}_{3z}$$

$$\downarrow \pi J_{23}\tau$$

$$4\hat{I}_{1y}\hat{I}_{2x}\hat{I}_{3z}\cos\pi J_{23}\tau + 2\hat{I}_{1y}\hat{I}_{2y}\sin\pi J_{23}\tau$$

The evolution of the term $4\hat{I}_{1y}\hat{I}_{2x}\hat{I}_{3z}$ under all three J-couplings may be deduced by putting all of these arguments together:

$$4\hat{I}_{1y}\hat{I}_{2x}\hat{I}_{3z}$$

$$\downarrow \pi J_{12}\tau$$

$$4\hat{I}_{1y}\hat{I}_{2x}\hat{I}_{3z}$$

$$\downarrow \pi J_{23}\tau$$

$$4\hat{I}_{1y}\hat{I}_{2x}\hat{I}_{3z}\cos\pi J_{23}\tau + 2\hat{I}_{1y}\hat{I}_{2y}\sin\pi J_{23}\tau$$

$$\downarrow \pi J_{13}\tau$$

$$\begin{aligned}&4\hat{I}_{1y}\hat{I}_{2x}\hat{I}_{3z}\cos\pi J_{23}\tau\ \cos\pi J_{13}\tau - 2\hat{I}_{1x}\hat{I}_{2x}\cos\pi J_{23}\tau\ \sin\pi J_{13}\tau\\ &+2\hat{I}_{1y}\hat{I}_{2y}\sin\pi J_{23}\tau\ \cos\pi J_{13}\tau - 4\hat{I}_{1x}\hat{I}_{2y}\hat{I}_{3z}\sin\pi J_{23}\tau\ \sin\pi J_{13}\tau\end{aligned}$$

18.10.3 Relaxation

In practice, the precession of the coherences is accompanied by decay. In simple cases, the coherence decay may be taken into account by multiplying each product operator term with an exponential decay factor. However, this procedure is invalid if the different coherences that make up a given product operator term have different decay time constants (see Section 20.8).

18.11 Spin Echo Sandwiches

Spin echo sandwiches may be used to simplify the evolution of product operator terms, as described in Section 15.10. Under suitable conditions (see Appendix A.10), chemical shift terms are suppressed, and the propagation may be calculated using a π rotation of all spin operators, followed by an interval of free evolution under the J-couplings alone.

For example, the evolution of the term $4\hat{I}_{1y}\hat{I}_{2x}\hat{I}_{3z}$ under a spin echo sandwich (SES) containing a central π_x pulse is as follows:

$$4\hat{I}_{1y}\hat{I}_{2x}\hat{I}_{3z}$$

$$\downarrow \pi_x$$

$$4(-\hat{I}_{1y})\hat{I}_{2x}(-\hat{I}_{3z}) = 4\hat{I}_{1y}\hat{I}_{2x}\hat{I}_{3z}$$

$$\downarrow \pi J_{12}\tau$$

$$4\hat{I}_{1y}\hat{I}_{2x}\hat{I}_{3z}$$

$$\downarrow \pi J_{13}\tau$$

$$4\hat{I}_{1y}\hat{I}_{2x}\hat{I}_{3z}\cos\pi J_{13} - 2\hat{I}_{1x}\hat{I}_{2x}\sin\pi J_{13}$$

$$\downarrow \pi J_{23}\tau$$

$$4\hat{I}_{1y}\hat{I}_{2x}\hat{I}_{3z}\cos\pi J_{13}\tau\ \cos\pi J_{23}\tau + 2\hat{I}_{1y}\hat{I}_{2y}\cos\pi J_{13}\tau\ \sin\pi J_{23}\tau$$
$$-2\hat{I}_{1x}\hat{I}_{2x}\sin\pi J_{13}\tau\ \cos\pi J_{23}\tau - 4\hat{I}_{1x}\hat{I}_{2y}\hat{I}_{3z}\sin\pi J_{13}\tau\ \sin\pi J_{23}\tau$$

or in summary:

$$4\hat{I}_{1y}\hat{I}_{2x}\hat{I}_{3z}$$

$$\downarrow \text{SES}$$

$$4\hat{I}_{1y}\hat{I}_{2x}\hat{I}_{3z}\cos\pi J_{13}\tau\ \cos\pi J_{23}\tau + 2\hat{I}_{1y}\hat{I}_{2y}\cos\pi J_{13}\tau\ \sin\pi J_{23}\tau$$
$$-2\hat{I}_{1x}\hat{I}_{2x}\sin\pi J_{13}\tau\ \cos\pi J_{23}\tau - 4\hat{I}_{1x}\hat{I}_{2y}\hat{I}_{3z}\sin\pi J_{13}\tau\ \sin\pi J_{23}\tau$$

In the case that all J-couplings between magnetically inequivalent spins have the same magnitude, a particularly simple effect is obtained when the spin echo sandwich has a duration $\tau = |(2J)^{-1}|$. Each product operator is transformed into only one term. Consider, for example, the product operator $4\hat{I}_{1z}\hat{I}_{2x}\hat{I}_{3y}$ in the A_2X_3 system of the protons in ethanol. As shown in Figure 18.20, this term propagates as follows:

$$4\hat{I}_{1z}\hat{I}_{2x}\hat{I}_{3y}$$

$$\downarrow \text{SES}$$

$$8(-\hat{I}_{2x})(-\hat{I}_{3x})(+\hat{I}_{4z})(+\hat{I}_{5z}) = 8\hat{I}_{2x}\hat{I}_{3x}\hat{I}_{4z}\hat{I}_{5z}$$

Note that the final result of this propagation depends strongly on the topology of the coupling network.[5]

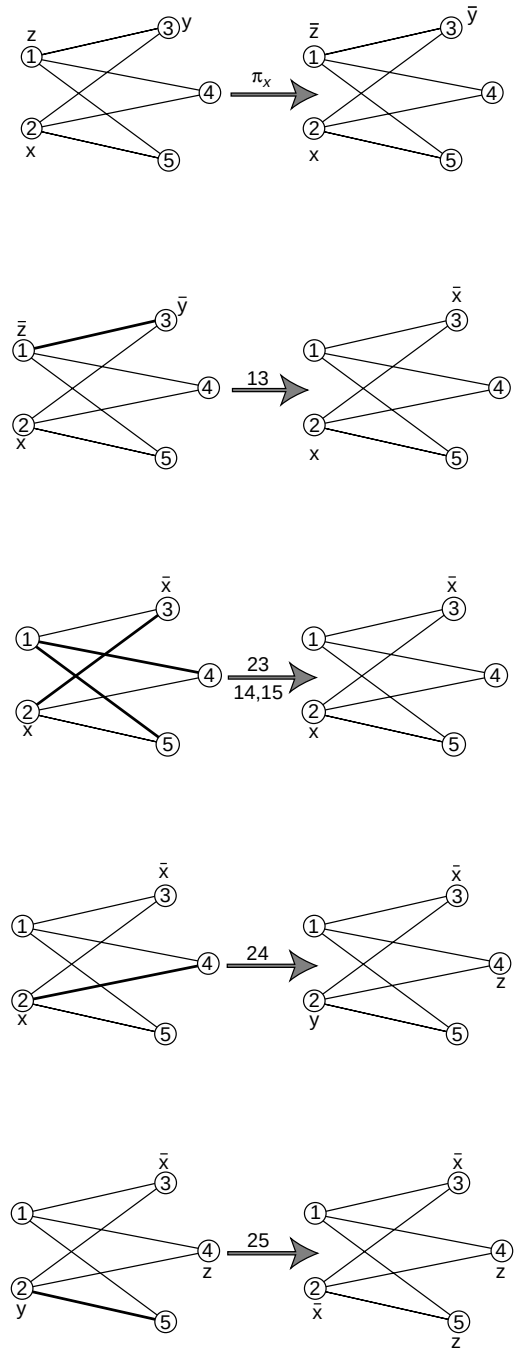

Figure 18.20
Propagation of a product operator in a A_2X_3, system, assuming positive J-couplings.

18.12 INEPT in an I_2S System

Consider the refocused INEPT pulse sequence (see Section 16.3):

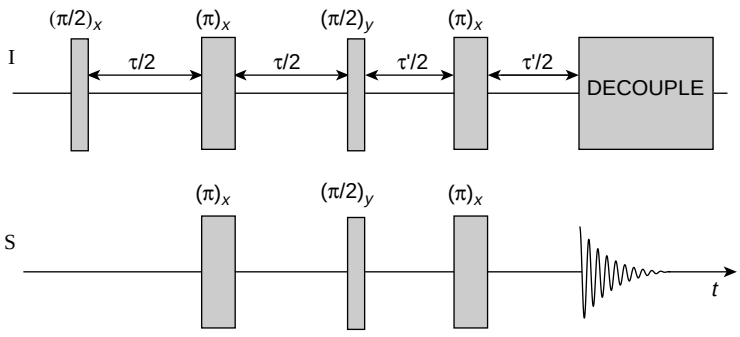

Figure 18.21
Refocused INEPT pulse sequence.

Assume that the two spin echo sandwiches have different durations, denoted τ and τ'. The first spin echo sandwich has duration $\tau = |(2J_{IS})^{-1}|$, and the second interval τ' may be chosen freely. The pulse sequence may be analysed using the following simplified form:

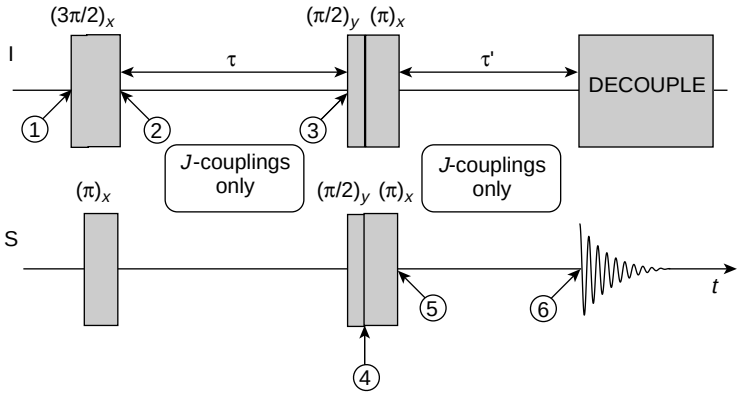

Figure 18.22
Simplification of the refocused INEPT pulse sequence.

Suppose that the pulse sequence is applied to an ensemble of I_2S spin systems, each consisting of three spins I_1, I_2 and S_3. For simplicity, assume that the two I-spins are magnetically equivalent.

The initial spin density operator of the I_2S system is

$$\hat{\rho}_{①} = \frac{1}{8}\hat{1} + \frac{1}{8}\mathbb{B}_I(\hat{I}_{1z} + \hat{I}_{2z}) + \frac{1}{8}\mathbb{B}_S\hat{S}_{3z} \tag{18.5}$$

The thermal equilibrium S-spin magnetization and the unity operator may be dropped for simplicity, leading to the simplified expression

$$\hat{\rho}_{①} = \frac{1}{8}\mathbb{B}_I(\hat{I}_{1z} + \hat{I}_{2z}) + \ldots$$

If relaxation is ignored, then the propagation of the spin density operator during the first half of the pulse sequence is as follows:

$$\hat{\rho}_{①} = \tfrac{1}{8}\mathbb{B}_I(\hat{I}_{1z} + \hat{I}_{2z}) + \ldots$$

$$\downarrow\ (3\pi/2)_x^I; \pi_x^S$$

$$\hat{\rho}_{②} = \tfrac{1}{8}\mathbb{B}_I(\hat{I}_{1y} + \hat{I}_{2y}) + \ldots$$

$$\tau\ \downarrow\ (J\text{-couplings only})$$

$$\hat{\rho}_{③} = -\tfrac{1}{8}\mathbb{B}_I(2\hat{I}_{1x}\hat{S}_{3z} + 2\hat{I}_{2x}\hat{S}_{3z}) + \ldots$$

$$\downarrow\ (\pi/2)_y^I, (\pi/2)_y^S$$

$$\hat{\rho}_{④} = \tfrac{1}{8}\mathbb{B}_I(2\hat{I}_{1z}\hat{S}_{3x} + 2\hat{I}_{2z}\hat{S}_{3x}) + \ldots$$

This shows that the thermal equilibrium I-spin magnetization is converted into antiphase transverse S-spin magnetization.

Each of the product operator terms in $\hat{\rho}_{④}$ continues to propagate as follows:

$$2\hat{I}_{1z}\hat{S}_{3x}$$

$$\downarrow\ \pi_x^I; \pi_x^S$$

$$-2\hat{I}_{1z}\hat{S}_{3x}$$

$$\downarrow\ \pi J_{13}\tau'$$

$$-2\hat{I}_{1z}\hat{S}_{3x}\cos\pi J_{13}\tau' - \hat{S}_{3y}\sin\pi J_{13}\tau'$$

$$\downarrow\ \pi J_{23}\tau'$$

$$-2\hat{I}_{1z}\hat{S}_{3x}\cos\pi J_{13}\tau'\cos\pi J_{23}\tau' - 4\hat{I}_{1z}\hat{I}_{2z}\hat{S}_{3y}\cos\pi J_{13}\tau'\sin\pi J_{23}\tau'$$
$$-\hat{S}_{3y}\sin\pi J_{13}\tau'\cos\pi J_{23}\tau' + 2\hat{I}_{2z}\hat{S}_{3x}\sin\pi J_{13}\tau'\sin\pi J_{23}\tau'$$

The propagation of the spin density operator through the entire sequence, therefore, may be written as

$$\hat{\rho}_{①} = \tfrac{1}{8}\mathbb{B}_I(\hat{I}_{1z} + \hat{I}_{2z}) + \ldots$$

$$\downarrow$$

$$\begin{aligned}\hat{\rho}_{⑥} &= -\tfrac{1}{8}\mathbb{B}_I\hat{S}_{3y}(2\sin\pi J_{13}\tau'\,\cos\pi J_{23}\tau') + \ldots \\ &= -\tfrac{1}{8}\mathbb{B}_I\hat{S}_{3y}\sin(2\pi J_{13}\tau') + \ldots\end{aligned}$$

The other terms have been dropped from the density operator because they generate antiphase S-spin signals that cancel out when a decoupling field is applied to the I-spins.

The transferred signal is maximized by adjusting the duration of the second spin echo sandwich to the value $\tau' = |(4J_{IS})^{-1}|$. The final density operator is then

$$\hat{\rho}_{⑦} = -\frac{1}{8}\mathbb{B}_I\hat{S}_{3y} + \ldots \tag{18.6}$$

This may be contrasted with the thermal equilibrium S-spin term in Equation 18.5, which has a factor $\frac{1}{8}\mathbb{B}_S$. When τ' is given by $\tau' = |(4J_{IS})^{-1}|$, the S-spin magnetization is enhanced by a factor γ_I/γ_S, compared with its thermal equilibrium value.

This shows that, in this idealized case, refocused INEPT leads to the same maximum enhancement of the S-spin signal for I_2S and IS spin systems, but that the optimal duration of the second spin echo is different in the two cases. The optimal duration τ' for an I_2S system is one-half of the optimal duration for an IS spin system (assuming equal coupling constants).

If the arguments are repeated for an idealized I_3S spin system, consisting of three chemically equivalent spins I_1, I_2, I_3 and a fourth spin S_4, we obtain a final spin density operator given by

$$\hat{\rho}_{⑦} = -\frac{1}{8}\mathbb{B}_I\hat{S}_{4y} \times 3\sin(\pi J_{13}\tau')\cos^2(\pi J_{13}\tau') + \ldots$$

The enhancement reaches a maximum value of $2\gamma_I/\sqrt{3}\gamma_S = 1.155\gamma_I/\gamma_S$ for the pulse sequence interval $\tau' = \left\{\cos^{-1}\sqrt{2/3}\right\}/(\pi J_{IS})$. Therefore, it is possible to enhance the S-spin magnetization by slightly more than the ratio γ_I/γ_S, in the case of an ideal I_3S spin system.

The refocused INEPT enhancement factors for IS, I_2S and I_3S spin systems are sketched below as a function of the interval τ':

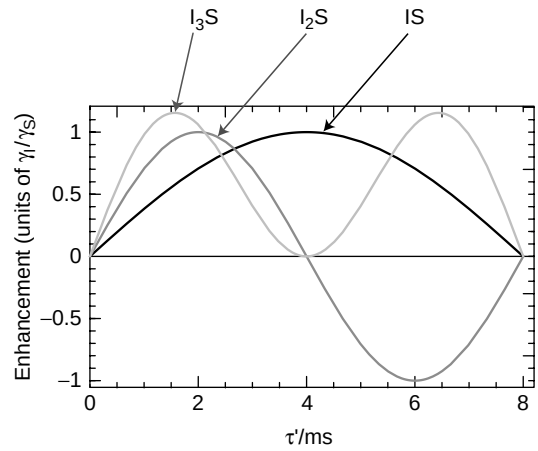

Figure 18.23
Enhancements of the S-spin magnetization by a refocused INEPT pulse sequence, for IS, I_2S and I_3S spin systems, with $J_{IS} = 125\,\text{Hz}$.

Note that the optimal value of τ' depends on the type of spin system.

In reality, most spin systems contain a distribution of J-couplings, and there are also relaxation effects. The optimum pulse sequence intervals and the enhancements achieved depend strongly on the practical spin system.

A variety of pulse sequences have been described which are less sensitive than INEPT to deviations of the J-couplings from the 'ideal' or expected values, and which are also less sensitive to the type of spin system (see *Further Reading*).

An interesting question is whether the enhancements achieved by refocused INEPT are the maximum possible, even in principle. Can one do better by using a different pulse sequence? For example, in an I_3S spin system, is it possible to transfer the sum magnetization of *all three* I-spins to the S-spin, leading to a very large enhancement? These deceptively simple questions lead into a lively field of research concerned with the *theoretical bounds on operator transformations*. See *Further Reading* for some references and the answer to the above question.

18.13 COSY in Multiple-Spin Systems

We now examine what happens when the COSY pulse sequence, described in Section 16.1, is applied to weakly coupled systems with more than two coupled spins-1/2. The product operator formalism is used to treat the two-dimensional spectrum.

The pulse sequence for COSY is given by:

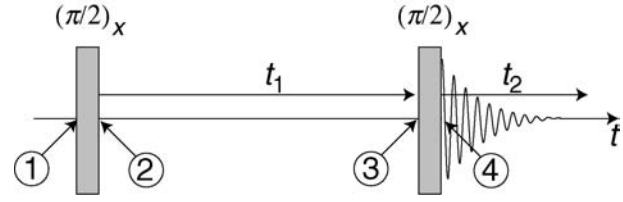

Figure 18.24
COSY pulse sequence.

This provides the 'cosine' signal in the States procedure (Section 5.9.4). The 'sine' signal is obtained by changing the phase of the first pulse to $\bar{y}$ (see Note 6).

18.13.1 AMX spectrum

Consider first an AMX spin system. The initial spin density operator is

$$\hat{\rho}_{①} \sim \hat{I}_z = \hat{I}_{1z} + \hat{I}_{2z} + \hat{I}_{3z} \tag{18.7}$$

omitting the unity operator and numerical factors. Consider the fate of the first term, under the 'cosine' pulse sequence (phase x for the first pulse):

$$\hat{\rho}_{①} = \hat{I}_{1z} + \ldots$$

$$\downarrow (\pi/2)_x$$

$$\hat{\rho}^{\cos}_{②} = -\hat{I}_{1y} + \ldots$$

$$\downarrow t_1$$

$$\begin{aligned}
\hat{\rho}^{\cos}_{③} = &-\hat{I}_{1y}\cos(\Omega_1^0 t_1)\cos(\pi J_{12} t_1)\cos(\pi J_{13} t_1) + \hat{I}_{1x}\sin(\Omega_1^0 t_1)\cos(\pi J_{12} t_1)\cos(\pi J_{13} t_1) \\
&+2\hat{I}_{1x}\hat{I}_{2z}\cos(\Omega_1^0 t_1)\sin(\pi J_{12} t_1)\cos(\pi J_{13} t_1) + 2\hat{I}_{1y}\hat{I}_{2z}\sin(\Omega_1^0 t_1)\sin(\pi J_{12} t_1)\cos(\pi J_{13} t_1) \\
&+2\hat{I}_{1x}\hat{I}_{3z}\cos(\Omega_1^0 t_1)\cos(\pi J_{12} t_1)\sin(\pi J_{13} t_1) + 2\hat{I}_{1y}\hat{I}_{3z}\sin(\Omega_1^0 t_1)\cos(\pi J_{12} t_1)\sin(\pi J_{13} t_1) \\
&+4\hat{I}_{1y}\hat{I}_{2z}\hat{I}_{3z}\cos(\Omega_1^0 t_1)\sin(\pi J_{12} t_1)\sin(\pi J_{13} t_1) - 4\hat{I}_{1x}\hat{I}_{2z}\hat{I}_{3z}\sin(\Omega_1^0 t_1)\sin(\pi J_{12} t_1)\sin(\pi J_{13} t_1) + \ldots
\end{aligned} \tag{18.8}$$

The second $(\pi/2)_x$ pulse transforms the product operators as follows:

$$\hat{\rho}^{\cos}_{③}$$

$$\downarrow (\pi/2)_x$$

$$\begin{aligned}
\hat{\rho}^{\cos}_{④} = &-\hat{I}_{1z}\cos(\Omega_1^0 t_1)\cos(\pi J_{12} t_1)\cos(\pi J_{13} t_1) + \hat{I}_{1x}\sin(\Omega_1^0 t_1)\cos(\pi J_{12} t_1)\cos(\pi J_{13} t_1) \\
&-2\hat{I}_{1x}\hat{I}_{2y}\cos(\Omega_1^0 t_1)\sin(\pi J_{12} t_1)\cos(\pi J_{13} t_1) - 2\hat{I}_{1z}\hat{I}_{2y}\sin(\Omega_1^0 t_1)\sin(\pi J_{12} t_1)\cos(\pi J_{13} t_1) \\
&-2\hat{I}_{1x}\hat{I}_{3y}\cos(\Omega_1^0 t_1)\cos(\pi J_{12} t_1)\sin(\pi J_{13} t_1) - 2\hat{I}_{1z}\hat{I}_{3y}\sin(\Omega_1^0 t_1)\cos(\pi J_{12} t_1)\sin(\pi J_{13} t_1) \\
&+4\hat{I}_{1z}\hat{I}_{2y}\hat{I}_{3y}\cos(\Omega_1^0 t_1)\sin(\pi J_{12} t_1)\sin(\pi J_{13} t_1) - 4\hat{I}_{1x}\hat{I}_{2y}\hat{I}_{3y}\sin(\Omega_1^0 t_1)\sin(\pi J_{12} t_1)\sin(\pi J_{13} t_1) + \ldots
\end{aligned}$$

For simplicity, suppress all terms that do not contain observable (simple) (-1)-quantum coherences:

$$\begin{aligned}
\hat{\rho}^{\cos}_{④} = &+\hat{I}_{1x}\sin(\Omega_1^0 t_1)\cos(\pi J_{12} t_1)\cos(\pi J_{13} t_1) \\
&-2\hat{I}_{1z}\hat{I}_{2y}\sin(\Omega_1^0 t_1)\sin(\pi J_{12} t_1)\cos(\pi J_{13} t_1) \\
&-2\hat{I}_{1z}\hat{I}_{3y}\sin(\Omega_1^0 t_1)\cos(\pi J_{12} t_1)\sin(\pi J_{13} t_1) + \ldots
\end{aligned} \tag{18.9}$$

These terms correspond to the following spectral features:

1. The *first* term in Equation 18.9 is proportional to $\hat{I}_{1x}$ and contains (-1)-quantum coherences of spin I_1. These coherences precess at frequencies close to Ω_1^0 during the detection interval t_2. Since this term is also modulated at frequencies close to Ω_1^0 during the evolution interval t_1, the first term generates a *diagonal peak* in the two-dimensional spectrum, with frequency coordinates around $(\Omega_1, \Omega_2) = (\Omega_1^0, \Omega_1^0)$.

2. The *second* term in Equation 18.9 is proportional to $-2\hat{I}_{1z}\hat{I}_{2y}$ and contains (-1)-quantum coherences of spin I_2. These coherences precess at frequencies close to Ω_2^0 during the detection interval t_2. Since this term is modulated at frequencies close to Ω_1^0 during the evolution interval t_1, the second term generates a *cross-peak* in the two-dimensional spectrum, with frequency coordinates around $(\Omega_1, \Omega_2) = (\Omega_1^0, \Omega_2^0)$.

3. The *third* term in Equation 18.9 is proportional to $-2\hat{I}_{1z}\hat{I}_{3y}$ and contains (-1)-quantum coherences of spin I_3. It resembles the second term and generates a *cross-peak* in the two-dimensional spectrum, with frequency coordinates around $(\Omega_1, \Omega_2) = (\Omega_1^0, \Omega_3^0)$.

The complete two-dimensional spectrum has the following schematic appearance:

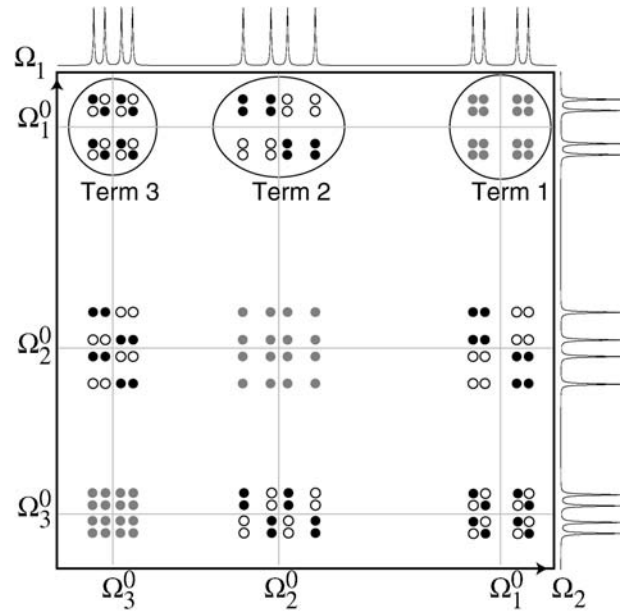

Figure 18.25
Form of the COSY spectrum for an AMX spin system.

This is shown for the case $\Omega_1^0/2\pi = 300\,\text{Hz}$, $\Omega_2^0/2\pi = 100\,\text{Hz}$, $\Omega_3^0/2\pi = -50\,\text{Hz}$, $J_{12} = 40\,\text{Hz}$, $J_{13} = 10\,\text{Hz}$ and $J_{23} = 25\,\text{Hz}$. Positive absorption peaks are indicated by black circles, negative absorption peaks are indicated by white circles, and dispersion peaks are indicated by grey circles. The multiplets generated by the three terms in Equation 18.9 are indicated by the ellipses. The remaining signals in the two-dimensional spectrum are generated by the $\hat{I}_{2z}$ and $\hat{I}_{3z}$ operators in Equation 18.7.

18.13.2 Active and passive spins

In Section 18.4, a definition of active and passive spins was given for *individual* coherences. For example, spin I_1 is active in coherence $\rho_{\boxed{-\alpha\alpha}}$, whereas spins I_2 and I_3 are passive in the same coherence.

The definition of active and passive spins will now be widened to encompass *coherence transfer processes*, i.e. the transfer of amplitude from one coherence into another. The expanded definition is as follows:

1. If a spin is active in *any* of the participating coherences, then that spin is said to be *active in the coherence transfer process.*

2. If a spin is passive in *both* of the participating coherences, then that spin is said to be *passive in the coherence transfer process*.

For example, spins I_1 and I_2 are active in the coherence transfer process $\rho_{\boxed{-\alpha\alpha}} \rightarrow \rho_{\boxed{\alpha-\alpha}}$, whereas spin I_3 is passive in the same process.

Consider now the second term in Equation 18.9, which is associated with the transformation of the density operator term $+2\hat{I}_{1y}\hat{I}_{2z}$ into $-2\hat{I}_{1z}\hat{I}_{2y}$ by the second $(\pi/2)_x$ pulse. Since spin I_1 is active in all coherences contained in $+2\hat{I}_{1y}\hat{I}_{2z}$, and spin I_2 is active in all terms contained in $-2\hat{I}_{1z}\hat{I}_{2y}$, one says that spins I_1 and I_2 are active in the transfer process $+2\hat{I}_{1y}\hat{I}_{2z} \rightarrow -2\hat{I}_{1z}\hat{I}_{2y}$. Since spin I_3 is passive for all coherences contained in both terms $+2\hat{I}_{1y}\hat{I}_{2z}$ and $-2\hat{I}_{1z}\hat{I}_{2y}$, one says that spin I_3 is passive in the same process $+2\hat{I}_{1y}\hat{I}_{2z} \rightarrow -2\hat{I}_{1z}\hat{I}_{2y}$.

The third term in Equation 18.9 is associated with the transformation of the density operator term $+2\hat{I}_{1y}\hat{I}_{3z}$ into $-2\hat{I}_{1z}\hat{I}_{3y}$ by the second $(\pi/2)_x$ pulse. In this case, spins I_1 and I_3 are active, while spin I_2 is passive.

18.13.3 Cross-peak multiplets

Examine the second term in Equation 18.9 more closely:

$$\hat{\rho}_{④}^{\cos} = -2\hat{I}_{1z}\hat{I}_{2y}\sin(\Omega_1^0 t_1)\sin(\pi J_{12}t_1)\cos(\pi J_{13}t_1) + \ldots \tag{18.10}$$

The form of this term (proportional to $-2\hat{I}_{1z}\hat{I}_{2y}$) indicates that the signal in the Ω_2 dimension corresponds to a spin I_2 multiplet, antiphase with respect to spin I_1. In the case $\Omega_1^0/2\pi = 300\,\text{Hz}$, $\Omega_2^0/2\pi = 100\,\text{Hz}$, $\Omega_3^0/2\pi = -50\,\text{Hz}$, $J_{12} = 40\,\text{Hz}$, $J_{13} = 10\,\text{Hz}$ and $J_{23} = 25\,\text{Hz}$, this multiplet has the following appearance *in the* Ω_2 *dimension*:

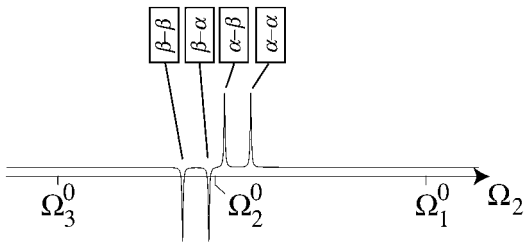

Figure 18.26
The Ω_2-multiplet generated by Equation 18.10.

Note that the sign of the peaks does not depend on the state label for the passive spin (I_3 in this case).

In order to understand the form of the two-dimensional multiplet, expand the trigonometric functions in Equation 18.10 as follows:

$$\begin{aligned}\hat{\rho}_{④}^{\cos} = {} & -2\hat{I}_{1z}\hat{I}_{2y} \times \\ & \left\{\frac{1}{4}\cos((\Omega_1^0 - \pi J_{12} - \pi J_{13})t_1) - \frac{1}{4}\cos((\Omega_1^0 + \pi J_{12} - \pi J_{13})t_1)\right. \\ & \left. + \frac{1}{4}\cos((\Omega_1^0 - \pi J_{12} + \pi J_{13})t_1) - \frac{1}{4}\cos((\Omega_1^0 + \pi J_{12} + \pi J_{13})t_1)\right\}\ldots\end{aligned} \tag{18.11}$$

If the calculation is repeated for the 'sine' pulse sequence (with the first pulse being $(\pi/2)_{\bar{y}}$ instead of $(\pi/2)_x$), we get

$$\hat{\rho}_{④}^{\sin} = -2\hat{I}_{1z}\hat{I}_{2y} \times$$
$$\left\{ \frac{1}{4}\sin\left((\Omega_1^0 - \pi J_{12} - \pi J_{13})t_1\right) - \frac{1}{4}\sin\left((\Omega_1^0 + \pi J_{12} - \pi J_{13})t_1\right) \right.$$
$$\left. + \frac{1}{4}\sin\left((\Omega_1^0 - \pi J_{12} + \pi J_{13})t_1\right) - \frac{1}{4}\sin\left((\Omega_1^0 + \pi J_{12} + \pi J_{13})t_1\right) \right\} \ldots \quad (18.12)$$

The 'cosine' pulse sequence only gives rise to cosine modulation terms in t_1, whereas the 'sine' experiment only gives rise to sine modulation terms. As a result, the States procedure gives pure absorption lineshapes for all spectral components generated by Equation 18.10.

Equations 18.11 and 18.12 show that the modulation components have different signs. The components with frequency $\Omega_1^0 - \pi J_{12} \pm \pi J_{13}$ are positive and the components with frequency $\Omega_1^0 + \pi J_{12} \pm \pi J_{13}$ are negative. This implies the following appearance for the multiplet *in the* Ω_1 *dimension*:

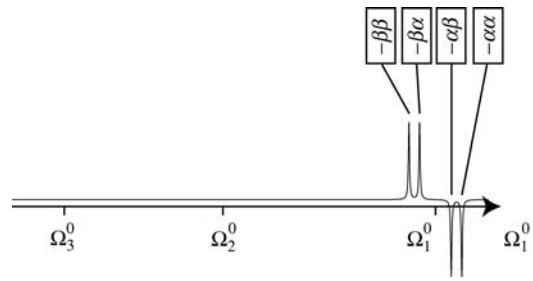

Figure 18.27
The Ω_1-multiplet generated by Equation 18.10.

The form of the multiplet in the Ω_1 dimension may be traced to its origin in the term proportional to $+2\hat{I}_{1y}\hat{I}_{2z}$ in Equation 18.8.

The two-dimensional cross-peak between spins I_1 and I_2, therefore, has the following appearance:

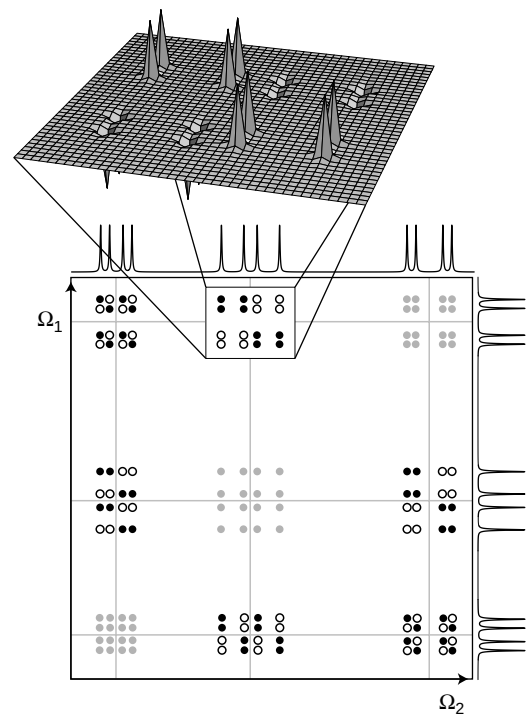

Figure 18.28
Form of the COSY multiplet between spins I_1 and I_2.

A similar calculation of the cross-peaks between spins I_1 and I_3 and between I_2 and I_3 shows that the multiplets have the following form:

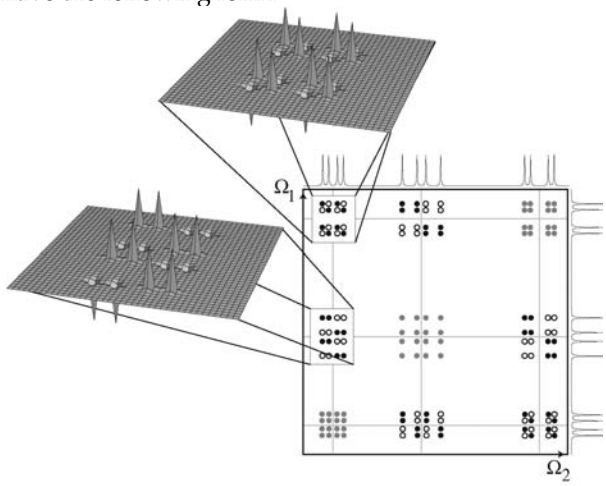

Figure 18.29
Form of the COSY multiplets between spins I_1 and I_3, and between spins I_2 and I_3.

In all cases, coherences with different state labels for the *active* spins have *opposite* sign, whereas coherences with different state labels for the *passive* spins have the *same* sign.

18.13.4 Diagonal peaks

The diagonal peaks in the COSY spectrum of an AMX system come out in pure dispersion when the data are acquired and processed according to the States scheme. If the calculation given in Section 16.1.4 is repeated for the AMX system, we get the following form for the diagonal peak multiplet of spin I_1:

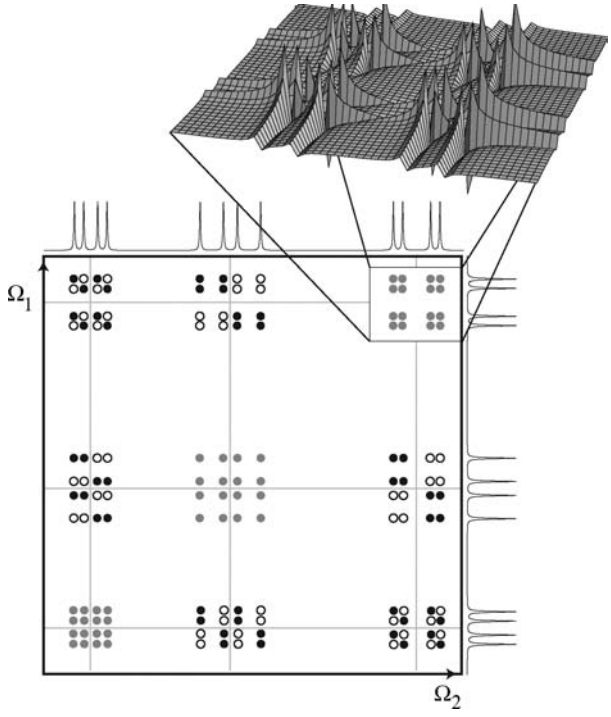

Figure 18.30
Form of the COSY diagonal peak multiplet for spin I_1.

The other diagonal peak multiplets have a similar appearance.

Such dispersion peakshapes are undesirable. The *double-quantum-filtered COSY* experiment is used to suppress the dispersion diagonal components (see *Further Reading* and Exercise 16.2).

18.13.5 Linear spin systems

If the coupling J_{13} vanishes, then the spin system is *linear* (see Section 17.9). In this case, the cross-peaks between spins I_1 and I_3 vanish, since the relevant antiphase terms $2\hat{I}_{1y}\hat{I}_{3z}$ and $2\hat{I}_{1z}\hat{I}_{3y}$ are never created during the evolution interval. In the frequency domain, we can imagine that the multiplet components with opposite sign have exactly the same frequency and cancel each other out. The two-dimensional COSY spectrum has the following form:

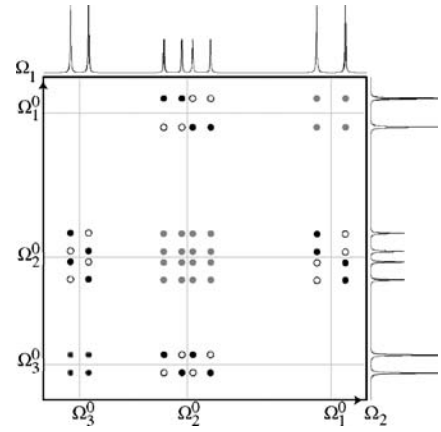

Figure 18.31
The COSY spectrum for a linear three-spin-1/2 system.

Note the two missing cross-peak multiplets.

This is a general property of COSY spectra. *The COSY cross-peak between two spins vanishes unless the two spins have a finite mutual J-coupling.*[4]

18.14 TOCSY

18.14.1 The ambiguity of COSY spectra

In many cases, one would like to identify two peaks as being generated by the same spin system, even if the corresponding spins do not have a finite J-coupling. For example, consider the case where the sample contains two independent linear three-spin systems A–M–X and A′–M′–X′. If all six chemical shifts are different, then the COSY spectrum has the following appearance (neglecting the multiplet structure):

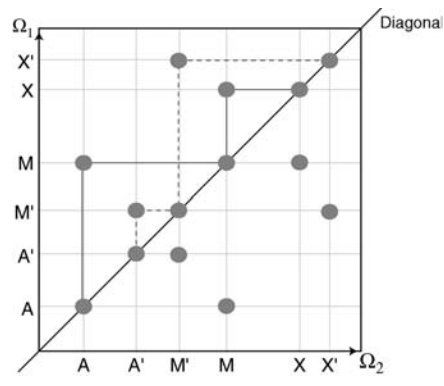

Figure 18.32
Form of the COSY spectrum for two linear AMX systems, with non-overlapping peaks.

If the spin systems are linear, then there are no cross-peaks between A and X spins, or between A′ and X′ spins. Nevertheless, it is possible to establish that the A and X spins belong to the spin system by following the connectivity through the M spin peak, as illustrated by the solid line. Similarly, the A′–M′–X′ connectivity may be established by following the dashed line through the M′ peak.

Now suppose that the chemical shifts of M and M′ are the same. The COSY spectrum has the following appearance:

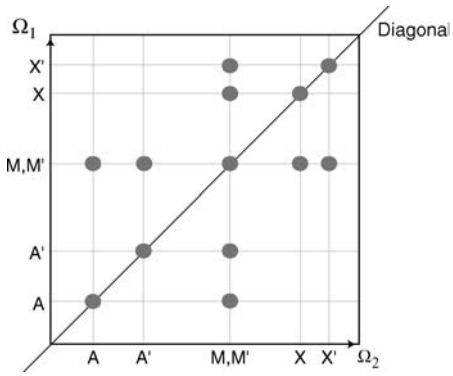

Figure 18.33
Form of the COSY spectrum for two linear AMX systems, in the case that the two M spins have the same chemical shifts.

The coincidence of the M and M′ resonances makes it impossible to disentangle the peaks from the two spin systems. The assignments become ambiguous, even though the A, A′, X and X′ peaks are all well resolved.

This simple example shows that the information content of COSY spectra is rapidly compromised when some peaks overlap, particularly in linear spin systems.

For this reason, NMR methods have been developed to allow the identification of resonances generated by the same spin system, even if they belong to spins that are not *directly* coupled with each other. One popular set of methods is called TOCSY (which stands for Total Correlation Spectroscopy).[7]

The basic aim of TOCSY is to produce cross-peaks between all spins that belong to the same spin system. An idealized TOCSY spectrum for a mixture of linear AMX and A′M′X′ spin systems, in which M and M′ have the same chemical shifts, appears as follows:

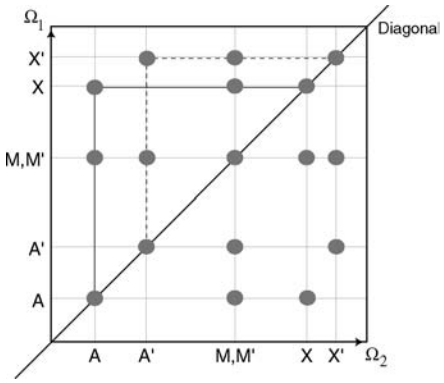

Figure 18.34
Form of the TOCSY spectrum for two linear AMX systems, in the case that the two M spins have the same chemical shifts.

This clearly establishes that the A and X peaks belong to one spin system, and that the A′ and X′ peaks belong to another.

18.14.2 TOCSY pulse sequence

There are many different variants of TOCSY pulse sequences. The simplest version (and the original one) is as follows:

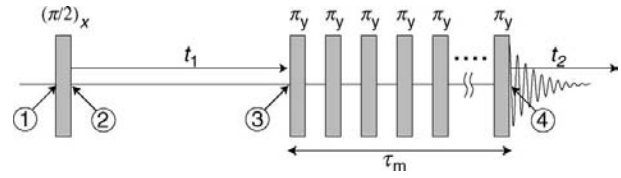

Figure 18.35
TOCSY pulse sequence.

This resembles the COSY pulse sequence, except that the second $(\pi/2)_x$ pulse is replaced by a train of many strong π pulses, spanning the *mixing interval* τ_m. In practice, the number of π pulses is large: I have only drawn six, for simplicity. If the interval between the pulses is denoted τ, and there are N equally spaced pulses, then the timings are related through

$$N\tau = \tau_m.$$

I assume here that the π pulses are infinitely strong and short, so that their duration may be neglected.

This pulse sequence requires that the π pulses are closely separated in time, so that there is little spin precession between the pulses (in the rotating frame). In general, the interval τ *between* pulses should be short enough to satisfy the condition

$$|(\Omega_j^0 - \Omega_k^0)\tau| << 1 \tag{18.13}$$

for all pairs of coupled spins j and k, where Ω_j^0 and Ω_k^0 are the resonance offsets in the rotating frame. At the same time, the *total* duration of the sequence τ_m should be long compared with the inverse of the J-couplings.

In practice, for proton systems, the spread in chemical shifts is around 10 ppm. If the proton Larmor frequency is around 500 MHz, and the reference frequency is placed in the centre of the spectrum, the resonance offsets $\Omega_j^0/2\pi$ lie in the range ± 2.5 kHz. The π pulses should, therefore, be separated by intervals of around 100 μs or less. At the same time, the total interval τ_m should be around 100 ms, to allow the J-couplings sufficient time to mix the coherences around. A typical TOCSY mixing sequence, therefore, consists of a train of several *hundred* π pulses.

This simple form of the TOCSY pulse sequence is quite sensitive to various sorts of experimental imperfections. A large number of alternative TOCSY pulse sequences have been developed which are more robust (see *Further Reading*). I only treat the simplest TOCSY sequence in this book.

18.14.3 Theory of TOCSY

The first part of the TOCSY pulse sequence is the same as for COSY. The initial spin density operator is

$$\hat{\rho}_{①} \sim \hat{I}_z = \hat{I}_{1z} + \hat{I}_{2z} + \hat{I}_{3z}$$

omitting the unity operator and numerical factors. The fate of the first term during the $(\pi/2)_x$ pulse and the t_1 interval is as follows:

$$\hat{\rho}_{①} = \hat{I}_{1z} + \ldots$$

$$\downarrow (\pi/2)_x$$

$$\downarrow t_1$$

$$\hat{\rho}_{③} = -\hat{I}_{1y}\cos(\Omega_1^0 t_1)\cos(\pi J_{12} t_1)\cos(\pi J_{13} t_1) + \ldots \tag{18.14}$$

There now follows the TOCSY mixing sequence of many closely spaced π pulses. Since the delay between the pulses satisfies Equation 18.13, the treatment given in Appendix A.10.1 is appropriate. The propagator for the mixing sequence is therefore

$$\widehat{U}_{\text{mix}} \cong \widehat{U}_J^{\text{strong}}(\tau_{\text{m}}) = \exp\{-\text{i}\widehat{\mathcal{H}}_J^{\text{strong}}\tau_{\text{m}}\} \tag{18.15}$$

where $\widehat{\mathcal{H}}_J^{\text{strong}}$ is given by:

$$\widehat{\mathcal{H}}_J^{\text{strong}} = \sum_{j<k}{}' 2\pi J_{jk}\hat{\mathbf{I}}_j \cdot \hat{\mathbf{I}}_k$$

For a three-spin system, the TOCSY mixing Hamiltonian is:

$$\begin{aligned}\widehat{\mathcal{H}}_J^{\text{strong}} = {} & 2\pi J_{12}(\hat{I}_{1x}\hat{I}_{2x} + \hat{I}_{1y}\hat{I}_{2y} + \hat{I}_{1z}\hat{I}_{2z}) \\ & +2\pi J_{13}(\hat{I}_{1x}\hat{I}_{3x} + \hat{I}_{1y}\hat{I}_{3y} + \hat{I}_{1z}\hat{I}_{3z}) \\ & +2\pi J_{23}(\hat{I}_{2x}\hat{I}_{3x} + \hat{I}_{2y}\hat{I}_{3y} + \hat{I}_{2z}\hat{I}_{3z})\end{aligned}$$

It is not easy to calculate the evolution of the spin density operator $\hat{\rho}_{③}$ in Equation 18.14 under this Hamiltonian. The product operator evolution rules given in Section 18.10 do not apply because the system is strongly coupled in the presence of the dense sequence of π pulses.

Nevertheless, some general conclusions about the evolution are readily drawn. The strongly coupled J-coupling Hamiltonian $\widehat{\mathcal{H}}_J^{\text{strong}}$ commutes with the *total* angular momentum operators along all three axes:

$$\begin{aligned}\left[\widehat{\mathcal{H}}_J^{\text{strong}}, \hat{I}_x\right] &= 0 \\ \left[\widehat{\mathcal{H}}_J^{\text{strong}}, \hat{I}_y\right] &= 0 \\ \left[\widehat{\mathcal{H}}_J^{\text{strong}}, \hat{I}_z\right] &= 0\end{aligned} \tag{18.16}$$

where

$$\hat{I}_x = \hat{I}_{1x} + \hat{I}_{2x} + \hat{I}_{3x}$$

and so on. As discussed in Section 7.5, these commutation properties imply that the total angular momentum along any axis is always preserved under the strongly coupled TOCSY evolution.

Consider, for example, the first term in Equation 18.14, representing angular momentum of spins I_1 along the $-y$-axis. During the mixing sequence, the angular momentum of spins I_1 along the $-y$-axis must decrease, since this term is converted into other terms. However, the commutation rules shown in

Equation 18.16 imply that this decrease must be accompanied by an increase in the polarization of spins I_2 and I_3 along the same axis. In other words, the total polarization along the $-y$-axis (or any other axis) may only be *transferred* between spins, never destroyed, as long as relaxation is neglected.

The idea of TOCSY mixing may be expressed in terms of magnetization vectors as follows:

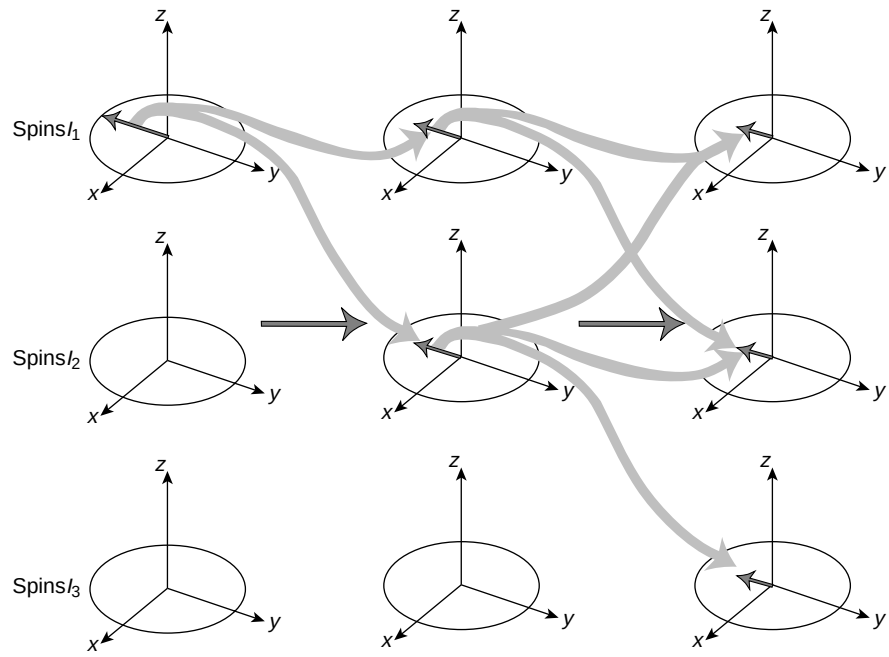

Figure 18.36
A qualitative picture of magnetization transfer between three spins under TOCSY.

The magnetization along a particular axis is transferred between the three spins through the network of J-couplings, keeping the total magnetization in any direction constant.

Note in particular that magnetization may be transferred from spins I_1 to spins I_3, even if the coupling constant J_{13} is vanishingly small. Given sufficient time, magnetization will get there, as long as the spins participate in the same coupling network.

Figure 18.37 shows accurate simulations of TOCSY dynamics in a linear four-spin system, with coupling constants $J_{12} = 10\,\text{Hz}$, $J_{23} = 5\,\text{Hz}$ and $J_{34} = -7\,\text{Hz}$: Magnetization starts on spin I_1 and oscillates rapidly between the two directly bonded spins I_1 and I_2. After a short delay, magnetization starts to develop on the next spin I_3, reaching a maximum on that spin after around 160 ms. Magnetization appears a little more slowly on the most distant spin I_4. Although the system never reaches a true equilibrium, the state at long times corresponds very roughly to an even distribution of magnetization throughout the whole spin system.

The calculation of a TOCSY spectrum for the AMX system may now be continued, based on the very rough assumption that the magnetization reaches an even distribution amongst the spins after a long TOCSY pulse sequence. With this assumption, we get[8] the following equation:

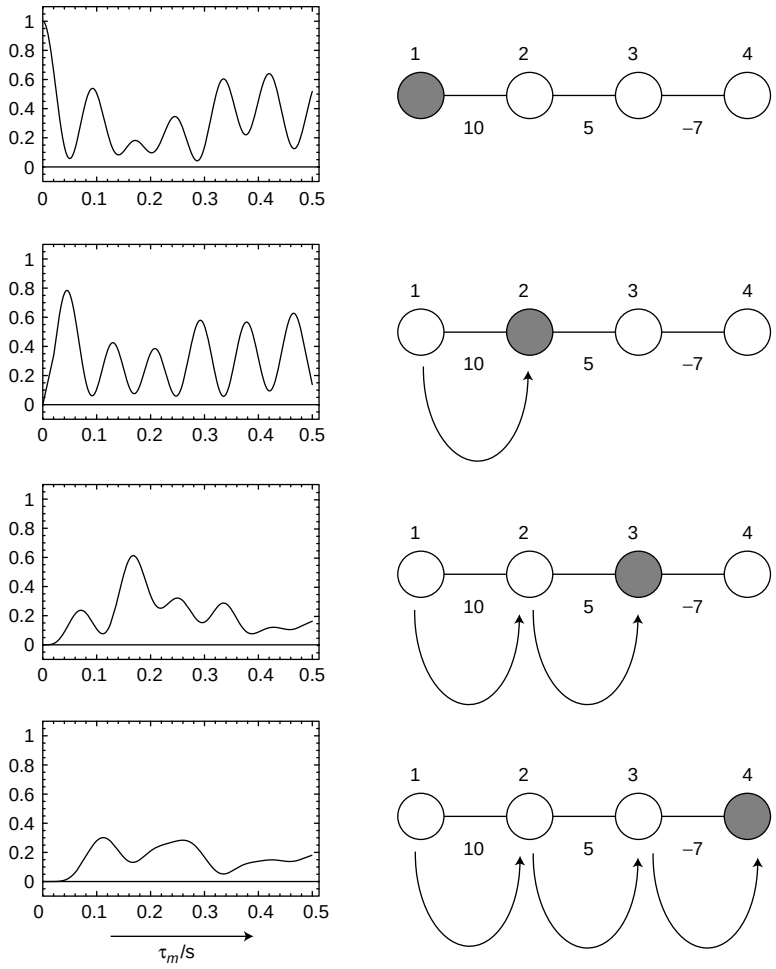

Figure 18.37
Accurate simulations of TOCSY spin dynamics, for a linear four-spin system, with the indicated J-couplings.

$$\hat{\rho}_{③} = -\hat{I}_{1y}\cos(\Omega_1^0 t_1)\cos(\pi J_{12} t_1)\cos(\pi J_{13} t_1) + \ldots$$

TOCSY mixing

$$\hat{\rho}_{④} \cong -\tfrac{1}{3}\hat{I}_{1y}\cos(\Omega_1^0 t_1)\cos(\pi J_{12} t_1)\cos(\pi J_{13} t_1)$$
$$-\tfrac{1}{3}\hat{I}_{2y}\cos(\Omega_1^0 t_1)\cos(\pi J_{12} t_1)\cos(\pi J_{13} t_1)$$
$$-\tfrac{1}{3}\hat{I}_{3y}\cos(\Omega_1^0 t_1)\cos(\pi J_{12} t_1)\cos(\pi J_{13} t_1) + \ldots$$

This corresponds to one diagonal peak and two cross-peaks, and it is readily shown that all multiplet components are in positive absorption after the States procedure.[8]

The idealized form of a TOCSY spectrum in an AMX system is therefore as follows:

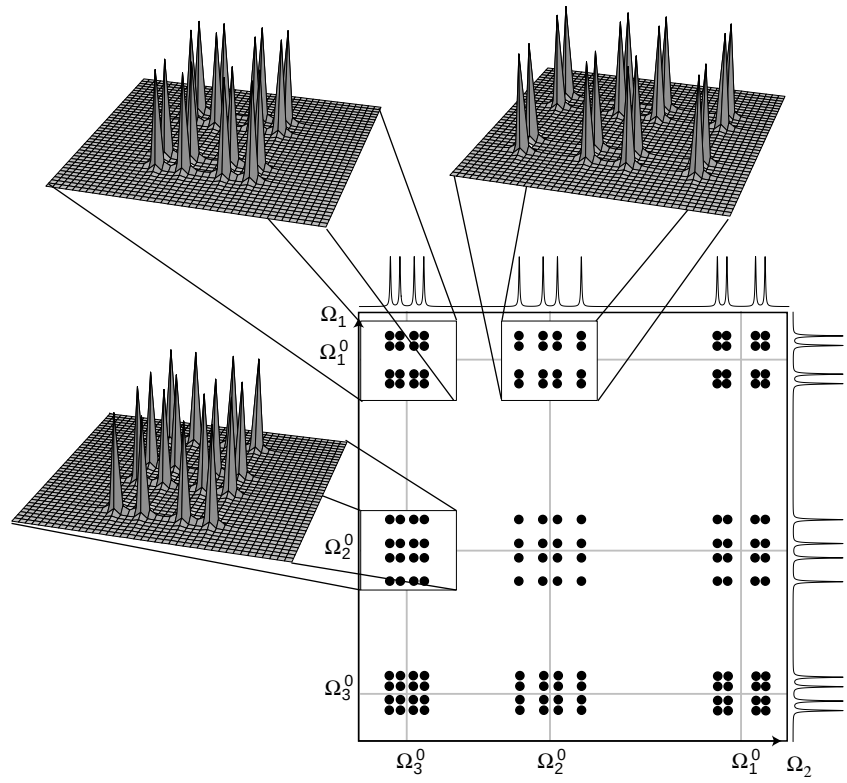

Figure 18.38
Ideal form of the TOCSY spectrum of an AMX spin system.

Notes

1. In favourable cases, many successive manipulations of coupled multiple-spin systems may be performed with great accuracy. It has been proposed to exploit such predictable spin manipulations as a way of performing certain algorithmic computations. In principle, the quantum-mechanical nature of the spin system allows certain computational tasks to be performed more rapidly than by using conventional sequential algorithms. Some primitive demonstrations of *NMR quantum computing* have actually been performed (see J. A. Jones, *Prog. NMR Spectrosc.* **38**, 325–360 (2001)). However, as of 2007, practical quantum computing by NMR appears to be a very long way off. For a critical view, see W. S. Warren *Science*, 277, 1688–1689 (1997).

2. The term *simple coherence* is new. There does seem to be a need for a term that is complementary to *combination coherence*.

3. An exception is when the liquid crystal phase is very weakly ordered, so that the secular dipole–dipole couplings are essentially finite only for neighbouring pairs of spins. This maintains a large degree of degeneracy, keeping such spectra interpretable (see Section 16.4).

4. The cancellation of opposite degenerate peaks is imperfect if the peaks have different widths. Typically, this occurs in the presence of cross-correlated relaxation mechanisms (see Section 20.8). For an example of unexpected coherence transfer caused by cross-correlated relaxation, see N. Müller, G. Bodenhausen, K. Wüthrich, R. R. Ernst, *J. Magn. Reson.*, **65**, 531 (1985).

5. This property has been used to design pulse sequences that select out signals generated by spin systems with a given coupling topology (see M. H. Levitt and R. R. Ernst, *J. Chem. Phys.*, **83**, 3297 (1985)).

6. The pulse sequence phases are consistent with the 'sign-corrected' version of the States procedure discussed in Section 5.9.4.

7. TOCSY is also known as *HOHAHA*, which stands for *Homonuclear Hartmann–Hahn*. This name comes from the close relationship between the TOCSY method and an older polarization transfer scheme originally invented for *heteronuclear* spin systems by Hartmann and Hahn. The Hartmann–Hahn method is best known in solid-state NMR, but the original paper does describe liquid-state applications as well (see S. R. Hartmann and E. L. Hahn, *Phys. Rev.* **128**, 2042 (1962)).

8. I have omitted the x-components of spin angular momentum in Equation 18.14, which are also preserved through the TOCSY mixing process and give rise to dispersion-mode peak components. In practice, these x-components tend to be destroyed by the accumulating effect of pulse imperfections (the phases of the π pulses are selected so as to rotate the magnetization components around the y-axis, so that all y-components are preserved, even if the pulses are imperfect). There are also many more sophisticated TOCSY pulse sequences in which the x-components are destroyed in a more exact way (see *Further Reading*).

Further Reading

- For a different angle on the material in this chapter, see J. Keeler, '*Understanding NMR Spectroscopy.*' Wiley, Chichester, 2005.
- For a detailed treatment of experiments on multiple-spin systems, including many applications, see J. Cavanagh, W. J. Fairbrother, A. G. Palmer and N. J. Skelton, *Protein NMR Spectroscopy. Principles and Practice*, Academic Press, New York, 1996.
- For deeper analysis of multiple spin-1/2 systems, see R. R. Ernst, G. Bodenhausen and A. Wokaun, *Principles of Nuclear Magnetic Resonance in One and Two Dimensions*, Clarendon Press, Oxford, 1987, and M. Goldman, *Quantum Description of High-Resolution NMR in Liquids*, Clarendon Press, Oxford, 1988.
- For reviews of polarization transfer pulse sequences, see O. W. Sørensen, *Prog. NMR Spectrosc.* 21, 503–569 (1989) and D. M. Doddrell, in the *Encyclopedia of Nuclear Magnetic Resonance*, vol. ***6***, D. M. Grant and R. K. Harris (eds), Wiley, 1996, pp. 3645–3654.
- For the subject of polarization transfer bounds, e.g. see S. J. Glaser, T. Schulte-Herbrüggen, M. Sieveking, O. Schedletzky, N. C. Nielsen, O. W. Sørensen and C. Griesinger, *Science* ***280***, 421–424 (1998) and references therein.
- For a review of more advanced TOCSY pulse sequences, see J. Sleucher, J. Quant, S. J. Glaser and C. Griesinger, in the *Encyclopedia of Nuclear Magnetic Resonance*, vol. 6, D. M. Grant and R. K. Harris (eds), Wiley, 1996, p. 4789.

Exercises

18.1 This exercise investigates the DEPT pulse sequence for polarization transfer between different spin species (see D. M. Doddrell, D. T. Pegg, and M. R. Bendall *J. Magn. Reson.*, **48**, 323 (1982)). One version of the DEPT pulse sequence is as follows:

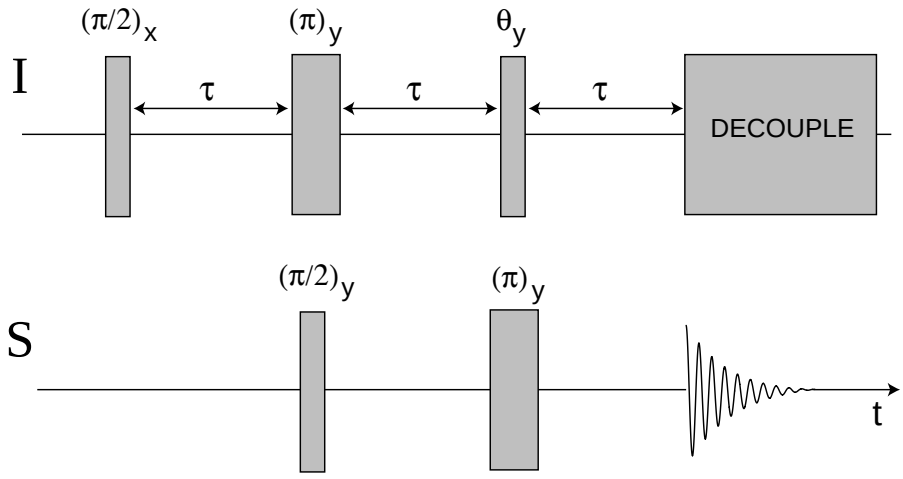

The flip angle θ of the last pulse on the I-spin channel is variable. Consider two spin species, I and S, with gyromagnetic ratios γ_I and γ_S. Assume that the delays are set to the value $\tau = (2J_{IS})^{-1}$, where J_{IS} is the J-coupling.

(i) Consider the case of an IS spin system. If the initial spin density operator is $\hat{\rho}_{①} \sim \hat{I}_z$, what is the spin density operator at the start of the signal detection period, for an arbitrary value of θ? What flip angle θ should be used to obtain the largest signal? By how much may the signal be enhanced compared with an experiment in which the signal is induced by a single $\pi/2$ pulse on the S-spin?

(ii) Repeat the calculation for an I_2S spin system. At the end of the calculation, only retain terms that give rise to observable signals. What flip angle θ should be used to obtain the largest signal? What is the maximum signal enhancement factor?

(iii) Repeat the calculation in (ii) for an I_3S spin system.